For Reference

NOT TO BE TAKEN FROM THIS ROOM

Ex libris
universitatis
albertaensis

QUAECUMQUE VERA

The University of Alberta
Printing Department
Edmonton, Alberta

THE UNIVERSITY OF ALBERTA

# MASS SPECTROMETRIC STUDIES OF ALKALI ION COMPLEXES IN THE GAS PHASE

BY

© WILLIAM ROBERT DAVIDSON

A THESIS

SUBMITTED TO THE FACULTY OF GRADUATE STUDIES AND RESEARCH
IN PARTIAL FULFILMENT OF THE REQUIREMENTS FOR THE DEGREE
OF
DOCTOR OF PHILOSOPHY

DEPARTMENT OF CHEMISTRY

EDMONTON, ALBERTA

SPRING, 1975

TO MY MOTHER

# ABSTRACT

A specially designed high pressure mass spectrometer equipped with a thermionic alkali ion source which could be pulsed for the study of the temporal behaviour of ions was used for the measurement of equilibrium constants for the complexing of alkali ions with various bases. The variation of these equilibrium constants with temperature permitted the evaluation of $\Delta G_{n-1,n}$, $\Delta S_{n-1,n}$, and $\Delta H_{n-1,n}$ for these reactions.

The reaction:

$$M^+(CH_3CN)_{n-1} + CH_3CN = M^+(CH_3CN)_n$$

where M = Na, K, Rb, Cs; was studied for values of n = 1 to 5. A comparison of the results with previous results for the gas phase hydration of alkali ions indicates that acetonitrile forms more stable clusters at low values of n than does water. A similar comparison with the gas phase solvation of halide ions by acetonitrile demonstrates that alkali ions are solvated much better in acetonitrile than their isoelectronic halide ion counterparts. With the use of proper thermodynamic cycles and the above results, the free energies of transfer of alkali and halide ions from liquid water to liquid acetonitrile can be obtained; the results being in good agreement with experimental liquid phase data.

A classical electrostatic potential calculation was made and found to correctly predict the experimental enthalpies for the clustering of alkali ions by one water or one

acetonitrile ligand. The same model correctly predicted the lower enthalpies of halide ion-acetonitrile complexes due to the diffuse positive charge in the acetonitrile dipole.

The gas phase Lewis basicities of various amines and ethers were studied by using the potassium ion as a Lewis acid and obtaining the thermodynamic functions for the reactions:

$$K^+ + B = K^+B$$

where B represents a host of amines and ethers. The order of gas phase Lewis basicities obtained at 600°K from the free energies is:

1,2-dimethoxyethane >> ethylenediamine >> pyridine > aniline > diethyl ether > dimethylamine > n-propylamine > methylamine > trimethylamine > dimethyl ether > ammonia.

This order is considerably different from basicity orders obtained when using the proton or trimethylboron as reference Lewis acids indicating that the nature of the acid-base interaction is extremely important in determining the strength of bases.

Gas phase stability constants were obtained for the reaction: $K^+(en)_{n-1} + en = K^+(en)_n$ ,where en represents ethylenediamine, for n = 1, 2, 3. The addition of the first two bidentate ligands is extremely favorable whereas the addition of the third ligand is not, indicating that the potassium ion is likely tetra- or penta-coordinated.

# ACKNOWLEDGEMENTS

I would like to express my sincere appreciation to Professor Paul Kebarle for his guidance and encouragement throughout the progress of this work.

The assistance of other members of the mass spectrometry group is gratefully acknowledged, in particular Yan Lau, who with the author performed the complexing of the potassium ion with methyl and ethyl ethers.

The author would like to thank the members of the Chemistry Department Machine and Electronics Shops. Special thanks are due to Mr. Ernie Young for his skill and patience in constructing the ion source assembly.

The author wishes to thank Ms. M. Nickolchuk for her care and devotion in typing the manuscript under the most difficult of circumstances.

The financial assistance provided by the University of Alberta and the National Research Council of Canada is acknowledged.

# TABLE OF CONTENTS

Page

ABSTRACT . . . . . . . . . . . . . . . . . . . . . . . . . v

ACKNOWLEDGEMENTS . . . . . . . . . . . . . . . . . . . . . . vii

LIST OF FIGURES. . . . . . . . . . . . . . . . . . . . . . xiii

LIST OF TABLES . . . . . . . . . . . . . . . . . . . . . . xviii

1. Introduction

1.1 The Present Study . . . . . . . . . . . . . . . . . . 1

1.2 Related Types of Ion-Molecule Reactions . . . . . 2

1.3 Thermodynamic Relationships Obtained from Gas Phase Clustering Reactions. . . . . . . . . . . . 7

1.4 The Nature of Solvation . . . . . . . . . . . . . 8

1.5 Acetonitrile as a Dipolar Aprotic Solvent . . . . 15

1.6 Related Studies in Liquid Acetonitrile. . . . . . 16

A. Methods Based on the Born Equation. . . . . . . . 18

B. Izmaylov Extrapolation Method . . . . . . . . . . 19

C. Solvent Independent Electrodes. . . . . . . . . . 20

D. Reference Electrolytes. . . . . . . . . . . . . . 21

E. Free Energies of Solvation from Volta Potentials. 21

1.7 Gas Phase Ion-Molecules Solvation Studies . . . . 24

A. Solvation Reactions Studied in the Present Laboratory. . . . . . . . . . . . . . . . . . . . . 25

B. Other Related Gas Phase Solvation Studies . . . . 28

1.8 Acid-Base Interactions. . . . . . . . . . . . . . 30

1.9 Related Gas Phase Basicity Studies. . . . . . . . 33

A. The Proton as the Reference Acid. . . . . . . . . 33

Page

B. Trimethylboron as a Reference Acid. . . . . . . . 34

2. Experimental

2.1 General . . . . . . . . . . . . . . . . . . . . . 37
2.2 The Vacuum Chamber. . . . . . . . . . . . . . . . 38
2.3 The Ion Source. . . . . . . . . . . . . . . . . . 39
2.4 The Thermionic Source . . . . . . . . . . . . . . 45
2.5 The Gas Handling Plant. . . . . . . . . . . . . . 48
2.6 Temperature Control . . . . . . . . . . . . . . . 55
2.7 Equilibrium Constants versus Field Strength . . . 58
2.8 Equilibrium Constants versus Pressure . . . . . . 61
2.9 The Detection System. . . . . . . . . . . . . . . 67
2.10 Comparison with Previous Data . . . . . . . . . . 71
2.11 Time Dependent Studies. . . . . . . . . . . . . . 71
A. Pulse Network . . . . . . . . . . . . . . . . . . 75
B. Pulsed versus Non-Pulsed Equilibrium Constants. . 79
C. Disadvantages to Pulsing. . . . . . . . . . . . . 79
2.12 The Drift Tube in Equilibrium Studies . . . . . . 83
A. Introduction. . . . . . . . . . . . . . . . . . . 83
B. Calibration of the Drift Tube . . . . . . . . . . 89
C. Equilibrium . . . . . . . . . . . . . . . . . . . 92
D. Equilibrium and Pressure. . . . . . . . . . . . . 101
E. Mobilities. . . . . . . . . . . . . . . . . . . . 101
F. Conclusion. . . . . . . . . . . . . . . . . . . . 104

Page

3. Results and Discussion of the Solvation of Alkali Metal Ions by Acetonitrile

3.1 Introduction. . . . . . . . . . . . . . . . . . . . 107

3.2 Presentation of Results . . . . . . . . . . . . . . 108

3.3 General Discussion. . . . . . . . . . . . . . . . . 133

3.4 A Comparison of the Gas Phase Solvation of Alkali Ions in Water and Acetonitrile. . . . . . . . . . 145

3.5 A Comparison Between the Gas Phase Solvation of Alkali Metal Ions and Halide Ions in Acetonitrile. . . . . . . . . . . . . . . . . . . . 151

3.6 A Comparison Between the Gas Phase Solvation and Liquid Phase Solvation of Alkali Cations in Acetonitrile. . . . . . . . . . . . . . . . . . . . 156

A. Consistency of Gas Phase Results. . . . . . . . . 156

B. Determination of Single Ion Free Energies of Solution in Acetonitrile from Gas Phase Data. . . 158

C. Calculation of the Free Energy of Transfer from Water to Acetonitrile . . . . . . . . . . . . . . . 165

3.7 Summary . . . . . . . . . . . . . . . . . . . . . 173

4. Ion-Solvent Electrostatic Calculations

4.1 Introduction. . . . . . . . . . . . . . . . . . . . 175

4.2 The Electronic and Physical Structure of Acetonitrile. . . . . . . . . . . . . . . . . . . . 176

4.3 Interaction Energies. . . . . . . . . . . . . . . . 179

A. Ion-Permanent Dipole Interactions . . . . . . . . 179

B. Ion-Induced Dipole Interactions . . . . . . . . . 182

C. Dispersion Energy . . . . . . . . . . . . . . . . 188

D. Repulsion Energy. . . . . . . . . . . . . . . . . 190

E. Total Energies. . . . . . . . . . . . . . . . . . 192

Page

4.4 Rotation of the Ion-Ligand Bond . . . . . . . . . 195

4.5 Electrostatic Calculations for Halide Ion-Acetonitrile Reactions. . . . . . . . . . . . . . 199

4.6 Consistency of the Present Calculations with Other Electrostatic and Quantum Mechanical Calculations. . . . . . . . . . . . . . . . . . 204

4.7 General Remarks on Electrostatic Calculations. . 207

5. Lewis Basicities with the Potassium Ion as a Reference Acid

5.1 Introduction. . . . . . . . . . . . . . . . . . 208

5.2 Some Special Problems Encountered in Lewis Basicities Determinations . . . . . . . . . . . 209

5.3 Presentation of Results -- Amines . . . . . . . . 215

5.4 Basicity Scales . . . . . . . . . . . . . . . . 228

5.5 Discussion of the Gas Phase Amine Basicity Order with $K^+$ as a Reference Acid . . . . . . . . . . 230

- A. Methyl Amines . . . . . . . . . . . . . . . . . 231
- B. Primary Aliphatic Amines. . . . . . . . . . . . 236
- C. Ethylenediamine -- Bidentate Ligands. . . . . . 240
- D. Aromatic Amines . . . . . . . . . . . . . . . . 240
  - (i) Pyridine. . . . . . . . . . . . . . . . . . 241
  - (ii) Aniline. . . . . . . . . . . . . . . . . 243

5.6 Correlation of the Gas Phase Lewis Acid-Base Reactions . . . . . . . . . . . . . . . . . . . 245

5.7 Limitations of the Drago Four Parameter Equation. 257

5.8 Gas Phase Basicity of Ethers with $K^+$ as a Reference Acid. . . . . . . . . . . . . . . . . . 258

5.9 Other Bases. . . . . . . . . . . . . . . . . . . 265

Page

A. Water . . . . . . . . . . . . . . . . . . . . . . 265

B. Acetonitrile. . . . . . . . . . . . . . . . . . . 266

6. Multidentate Ligands

6.1 Introduction. . . . . . . . . . . . . . . . . . . 268

6.2 Presentation of Results -- Ethylenediamine. . . . 269

6.3 General Discussion -- Ethylenediamine . . . . . . 274

6.4 Stability Constants -- The Chelation Effect . . . 280

6.5 1:1 Complex of Potassium and Dimethoxyethane. . . 285

6.6 Summary . . . . . . . . . . . . . . . . . . . . . 288

7. Suggestions for Further Research

7.1 Complexes Involving the Silver Ion. . . . . . . . 287

7.2 Alkali Ion Complexes with Crown Ethers. . . . . . 292

REFERENCES . . . . . . . . . . . . . . . . . . . . . . . . 301

# LIST OF FIGURES

| Figure | | Page |
|---|---|---|
| 1 | Bernal and Fowler--Eley and Evans Model of Ionic Solvation | 11 |
| 2 | Bockris and Saluja Solvation Cycle | 14 |
| 3 | Cross-Sectional View of Mass Spectrometer | 39 |
| 4 | The Ion Source | 41 |
| 5 | Normal Operating Voltages | 44 |
| 6 | The Gas Handling Plant | 49 |
| 7 | Calibration of Capillary demonstrating Viscous Flow | 52 |
| 8 | Pressure of Ethylenediamine in the Ion Source versus Bath Temperature. | 53 |
| 9 | Effect of a Third Body on Equilibrium for the Reaction: $K^+(en)_2 + en = K^+(en)_3$. | 54 |
| 10 | Thermocouple Assembly | 57 |
| 11 | Plot of $K^+(H_2O)_2/K^+(H_2O)$ versus Electric Field Used to Attract Potassium Ions to the Equilibrium Chamber. | 59 |
| 12 | Effect of Field Strength on Equilibrium at Very Low Pressures for the Reaction: $K^+(en) + en = K^+(en)_2$ . | 60 |
| 13 | Effect of Voltage Between the Filament and the Reaction Chamber at Low Pressure for the Reaction: $Rb^+(CH_3CN) + CH_3CN = Rb^+(CH_3CN)_2$ . | 62 |
| 14 | Variation of Equilibrium Constants with Pressure, at High Pressure. | 64 |
| 15 | Fraction of Cluster Dissociation in the Vacuum Chamber versus Pressure in the Reaction Chamber. | 66 |
| 16 | Percent Efficiency as a Function of Ion Mass for Two Spiraltron Electron Multipliers. | 69 |
| 17 | Counts per Second versus Voltage Across Spiraltron Electron Multiplier. | 70 |
| 18 | A Comparison of $K_{O,1}$ Obtained in this Study with that of Searles. | 72 |

| Figure | | Page |
|---|---|---|
| 19 | A Comparison of $K_{3,4}$ versus 1/T Obtained in This Study with Previous Results for the Hydration of the Potassium Ion. | 74 |
| 20 | Pulsing Sequence for the Study of the Temporal Behavior of Ions. | 76 |
| 21 | Time Dependent Output Demonstrating the Rapid Achievement of Equilibrium. | 77 |
| 22 | Time Dependent Output Showing Two Ions Approaching Equilibrium. | 78 |
| 23 and 24 | Time Dependent Outputs for the Hydration of the Potassium Ion. | 80 and 81 |
| 25 | Cross-Sectional View of the Drift Tube | 85 |
| 26 | Pulsing Scheme for Drift Tube Studies. | 86 |
| 27 | Drift Tube Output of the Potassium Ion in Argon at Various E/p. | 90 |
| 28 | Reduced Mobility versus E/p for the Potassium Ion in Argon. | 91 |
| 29 | Typical Drift Tube Output Showing Ions in Equilibrium. | 93 |
| 30 | Variation of Equilibrium Constants with E/p. | 95 |
| 31 | "Ion Temperature" versus E/p. | 98 |
| 32 | Equilibrium Constants at Low E/p. | 99 |
| 33 | Equilibrium Constants Obtained in a Drift Tube versus Pressure for the Reaction: $K^+(CH_3CN) + CH_3CN = K^+(CH_3CN)_2$ | 102 |
| 34 | Equilibrium Constants versus Pressure for the Reaction: $K^+ + H_2O = K^+(H_2O)$. | 103 |
| 35 | Determination of Ion Mobilities from Average Mobility Measurements. | 105 |
| 36 to 55 | Equilibrium Constants versus Pressure of Acetonitrile at Various Temperatures for the Gas Phase Solvation of Alkali Ions, $M^+$ (M = Na, K, Rb, Cs), by Acetonitrile. | 109 to 128 |

| Figure | | Page |
|---|---|---|
| 56 to 59 | Van't Hoff Type Plots of the Equilibrium Constants for the Gas Phase Solvation of Alkali Ions, $M^+$ (M = Na, K, Rb, Cs), by Acetonitrile | 129 to 132 |
| 60 | Enthalpies for the Clustering Reactions: $M^+(CH_3CN)_{n-1} + CH_3CN = M^+(CH_3CN)_n$. | 138 |
| 61 | Standard Free Energies at 298°C for the Clustering Reactions: $M^+(CH_3CN)_{n-1} + CH_3CN = M^+(CH_3CN)_n$. | 139 |
| 62 | Plot of Equilibrium Distribution of $Na^+(H_2O)_n$ and $Na^+(CH_3CN)_n$ as a Function of Pressure. | 144 |
| 63 | Van't Hoff Type Plots for the Gas Phase Solvation of the Sodium Ion by Acetonitrile and Water | 146 |
| 64 | A Comparison of the Enthalpies of the Gas Phase Solvation of $Na^+$ and $Cs^+$ in Water and Acetonitrile. | 148 |
| 65 | A Comparison of the Standard Free Energies of the Gas Phase Solvation of $Na^+$ and $Cs^+$ in Water and Acetonitrile. | 149 |
| 66 | A Comparison of the Total Standard Free Energy of the Gas Phase Solvation of $Na^+$ and $Cs^+$ versus the number of ligands in Water and Acetonitrile. | 150 |
| 67 | A Comparison of the Standard Free Energies of Gas Phase Solvation of Alkali and Halide Ions in Acetonitrile. | 152 |
| 68 | A Comparison of the Enthalpies of Gas Phase Solvation of Alkali and Halide Ions in Acetonitrile. | 153 |
| 69 | Comparison of Experimental Gas Phase Free Energies of Solvation with Total Single Ion Free Energies of Solvation in Acetonitrile Obtained by Case and Parsons. | 157 |
| 70 | Extrapolation of Free Energy versus n-1,n Plots for the Gas Phase Solvation of Halide Ions in Acetonitrile. | 159 |
| 71 | Comparison of the Experimental Differences in Gas Phase Free Energies of Solvation in Acetonitrile versus n to the Free Energy Differences of Case and Parsons. | 160 |
| 72 | Bond Distances, Angles, and Point Charge Distribution for Water and Acetonitrile. | 180 |
| 73 | Representation of Bond Polarizabilities. | 183 |

| Figure | | Page |
|---|---|---|
| 74 | Rotation of the Water Molecule | 196 |
| 75 | Time Dependence of Normalized Ion Intensities for the Determination of the Amount of Ethylamine Undergoing Thermal Decomposition. | 213 |
| 76 to 80 | Equilibrium Constants versus Pressure at Various Temperatures for the Interaction Between the Potassium Ion and Various Amines. | 216 to 220 |
| 81 | Switching Equilibrium Constants versus Pressure Ratio at Representative Temperatures for the Reaction: $K^+(H_2O) + CH_3NH_2 = K^+(CH_3NH_2) + H_2O$ . | 221 |
| 82 | Switching Equilibrium Constants versus Pressure Ratio at Representative Temperatures for the Reaction: $K^+(H_2O) + (CH_3)_3N = K^+((CH_3)_3N) + H_2O$ . | 222 |
| 83 | Van't Hoff Type Plots of Switching Equilibria | 224 |
| 84 | Van't Hoff Type Plots for Various Amines Reacting with the Potassium Ion. | 225 |
| 85 | Van't Hoff Type Plots for the Methyl Amines Reacting with the Potassium Ion. | 226 |
| 86 | Net Electron Populations on the Various Atoms in the Methyl Amines. | 232 |
| 87 | Equilibrium Constants versus Pressure at Various Temperatures for the Reaction: $K^+ + (CH_3)_2O = K^+((CH_3)_2O)$ . | 260 |
| 88 | Equilibrium Constants versus Pressure at Various Temperatures for the Reaction: $K^+ + (C_2H_5)_2O = K^+((C_2H_5)_2O)$ . | 261 |
| 89 | Van't Hoff Type Plots of the Interaction Between Dimethyl and Diethyl Ether and the Potassium Ion. | 262 |
| 90 to 92 | Equilibrium Constants versus Pressure at Various Temperatures for the Complexing of the Potassium Ion by Ethylenediamine. | 270 to 272 |
| 93 | Van't Hoff Type Plots for the Reactions: $K^+(en)_{n-1} + en = K^+(en)_n$. | 273 |
| 94 | Plot of $K_{0,1}$ for the Complexing of $K^+$ with Ethylenediamine, demonstrating Non-Equilibrium. | 276 |

| Figure | | Page |
|---|---|---|
| 95 | Van't Hoff Type Plots of the Various Complexing Reactions Reactions Between the Potassium Ion and Bases. | 279 |
| 96 | Equilibrium Constants versus Pressure at Various Temperatures for the Reaction: $K^+ + \text{glyme} = K^+(\text{glyme})$ . | 287 |
| 97 | Courtald and Structural Models of Dibenzo-18-crown-6. | 294 |
| 98 | Some Common Cyclic Polyethers. | 295 |
| 99 | Rough Approximation of Alkali Ion--Crown Ether Complexes. | 297 |

# LIST OF TABLES

| Table | | Page |
|---|---|---|
| 1 | Ion Currents at Various Plates | 46 |
| 2 | Comparison of Thermodynamic Functions Obtained in the Present Study with Previous Experimental and Theoretical Results. | 73 |
| 3 | A Comparison of Pulsed and Non-Pulsed Equilibrium Constants. | 82 |
| 4 | Effective and Ion Temperatures. | 96 |
| 5 | Sensitivity Dependence on Field Strength and Pressure. | 100 |
| 6 to 9 | Experimental Thermodynamic Values for the Gas Phase Solvation of Alkali Ions by Acetonitrile. | 134 to 137 |
| 10 | Ratio of Equilibrium Constants at Specific Temperatures. | 142 |
| 11 | Alkali-Halide Solvation Free Energies in Acetonitrile. | 162 |
| 12 | $\Delta G_s(X^-)$ and $\Delta G_s(M^+)$ from Gas Phase Data. | 163 |
| 13 | Free Energies of Transfer from Water To Acetonitrile. | 164 |
| 14 | Relevant Quantities to Predict Free Energies of Transfer. | 170 |
| 15 | Calculated Free Energies of Transfer. | 172 |
| 16 | Electron Population in Acetonitrile. | 178 |
| 17 | Location of Polarizability Centroids. | 186 |
| 18 | Bond and Molecular Polarizabilities. | 187 |
| 19 | Ionization Potentials and Polarizabilities of Alkali Ions. | 189 |
| 20 | Parameters for the Exponential Form of the Repulsion Potential for Alkali Ions. | 193 |
| 21 | Electrostatic Potential Energies for Alkali Ion Solvation in Acetonitrile and Water. | 194 |
| 22 | Effect of Rotation of the Solvent Molecule on Electrostatic Potential Energies. | 198 |

| Table | | Page |
|---|---|---|
| 23 | Ionization Potentials and Polarizabilities of Halide Ions. | 201 |
| 24 | Parameters for the Exponential Form of the Repulsion Potential for Halide Ions. | 202 |
| 25 | Electrostatic Potential Energies for Halide Ions. | 203 |
| 26 | Comparison of Electrostatic Potential Energies. | 205 |
| 27 | Comparison of Various Electrostatic Potential Energy Calculations. | 206 |
| 28 | Thermodynamic Functions for Amine--Potassium Ion Interactions. | 227 |
| 29 | A Comparison of Thermodynamic Properties of Amines Interacting with Various Lewis Acids. | 229 |
| 30 | Atomic and Molecular Polarizabilities and Ionization Potentials of the Methyl Amines. | 234 |
| 31 | Coordinates for Trimethylamine and Ammonia. | 237 |
| 32 | Calculated Electrostatic Potentials for $K^+$--Amine Interactions. | 239 |
| 33 | Dipole Moments, Total Polarization and Experimental Enthalpies of Amine--Potassium Ion Interactions. | 249 |
| 34 | Calculated and Experimental Enthalpies for Potassium Adducts with Methyl Amines. | 250 |
| 35 | Best Fit E and C Parameters. | 252 |
| 36 | Calculated and Experimental Enthalpies for Various Gas Phase Lewis Acid-Base Reactions. | 253 |
| 37 | E and C Parameters for Various Lewis Acids and Bases Using Drago's Amine Parameters. | 254 |
| 38 | Calculated and Experimental Enthalpies for Various Lewis Acid-Base Reactions Using Drago's Base Parameters. | 255 |
| 39 | Thermodynamic Functions for Potassium Ion--Ether Reactions. | 263 |
| 40 | Enthalpy and Free Energy at 298°K for Lewis Acid-Ether Reactions. | 264 |

Table Page

41 Standard Free Energies at 600°K and Enthalpies for Various Potassium Ion--Lewis Base Reactions. 267

42 Thermodynamic Functions for the Complexing of Ethylenediamine and the Potassium Ion. 275

43 Stability Constants for $K^+$-ethylenediamine Complexes. 280

44 A Comparison of Thermodynamic Properties for Bidentate Complexes with the Potassium Ion. 287

45 Stable Complexes Between Alkali Ions and Some Crown Ethers. 297

46 Melting Points of Some Crown Ethers. 299

CHAPTER 1

# INTRODUCTION

## 1.1 The Present Study

The present work may be broken down into two distinct areas: first, the gas phase solvation of alkali metal ions by acetonitrile and secondly, the relative solvation strengths of various amines using the potassium ion as a gas phase solute.

The solvation of alkali ions by acetonitrile is a follow-up on three studies performed in this laboratory (1 - 4). The first two studies dealt with the solvation of halide ions by water and acetonitrile, and the third dealt with the solvation of alkali metal ions by water. The results of the present study can be compared with the previous results to gain some understanding of the solvation differences between protic and aprotic solvents. Solvation thermodynamic functions for reactions 1.1 - 1.3 were determined from a variation of equilibrium constants as a function of temperature:

$$M^+ + CH_3CN \rightleftarrows M^+(CH_3CN) \qquad 1.1$$

$$M^+(CH_3CN) + CH_3CN \rightleftarrows M^+(CH_3CN)_2 \qquad 1.2$$

$$M^+(CH_3CN)_{n-1} + CH_3CN \rightleftarrows M^+(CH_3CN)_n \qquad 1.3$$

where $M^+$ represents the alkali metal ions, $Na^+$, $K^+$, $Rb^+$, and $Cs^+$.

The relative solvating strength of various amines is the foundation of a systematic study of the Lewis basicity of both amines and ethers. The gas phase Lewis basicity scale can be easily compared to gas phase Bronsted basicity scales as well as to liquid phase basicity scales.

Multidentate ligands such as ethylenediamine and dimethoxyethane were also used to solvate the potassium ion.

## 1.2 Related Types of Ion-Molecule Reactions

Only two types of ion-molecule reactions are significant in the present study. These can be classified as clustering or attachment reactions and ligand interchange or switching reactions. Due to the low ionization potentials of the alkali metal ions, charge transfer reactions between the ions and the solvating molecules will not occur unless the excess translational energy of the ion is significant. Consider the reaction 1.4:

$$Na^+ + S \rightarrow S^+ + Na \qquad 1.4$$

For this reaction to be exothermic requires that the ionization potential of S, the solvating neutral molecule, be less than that of sodium, i.e. less than 5.1 eV. Acetonitrile, for example has an ionization potential of 12.2 eV, and

therefore, the excess energy needed would be 7.1 eV. Such energy is not provided and charge transfer reactions do not occur.

Clustering reactions, demonstrated by 1.5, were the major type of reaction undertaken in this study.

$$M^+(S)_{n-1} + S \rightleftarrows M^+(S)_n \qquad 1.5$$

They are an attachment reaction, in which a molecule is bound to an ion by essentially electrostatic forces. The major attractive forces are those of ion-dipole and ion-polarizability interactions. Such reactions are usually third body stabilized, the third body being required to remove the excess energy due to the exothermicity of the reaction. When an ion and a neutral react an excited intermediate is formed (5):

$$M^+ + S \xrightarrow{k_c} [M^+S]^* \qquad \text{combination} \quad 1.6$$

Without a third body collision or collisions to deactivate this excited complex, it will simply dissociate:

$$[M^+S]^* \xrightarrow{k_d} M^+ + S \qquad \text{decomposition} \quad 1.7$$

However, in the presence of a third body, A, the excess energy is removed and a stable unexcited complex results:

$$[M^+S]^* + A \xrightarrow{k_s} M^+S + A \qquad \text{stabilization} \qquad 1.8$$

The overall reaction may then be written:

$$M^+ + S \underset{k_d}{\overset{k_c}{\rightleftarrows}} [M^+S]^* \xrightarrow[k_s]{A} M^+S \qquad 1.9$$

Under steady state conditions and at low pressure where the rate of decomposition is faster than the rate of deactivation, the forward rate constant of a clustering reaction, $k_f$, becomes

$$k_f = \frac{k_c k_s}{k_d} \qquad 1.10$$

Typical measured rate constants for clustering reactions are in the range $k_f = 10^{-28}$ to $10^{-31}$ cm$^6$ molecules$^{-2}$ sec$^{-1}$ (6).

The formed cluster can also dissociate upon collision with a neutral molecule. This leads to the clustering equilibrium:

$$M^+ + S \underset{k_r}{\overset{k_f}{\rightleftarrows}} M^+S \qquad 1.11$$

Under normal experimental conditions, the measured reverse reaction rate constant is usually in the range $k_r = 10^{-12}$ to $10^{-16}$ cm$^3$/sec.

A switching reaction is one in which a ligand attached

to an ion is replaced by another ligand of a different molecule.

$$M^{+}A + B \rightleftarrows M^{+}B + A \tag{1.12}$$

For the reaction 1.12 to be exothermic, the ion complex with the neutral ligand B would have to be more stable than the $M^{+}A$ cluster. From doing a series of experiments in this manner, it is then possible to set up a table of relative stabilities.

Exothermic switching reactions are very rapid and have rate constants in the order of $10^{-9}$ to $10^{-11}$ $cm^{3}$ $molec.^{-1}sec^{-1}$ (7,8). They are a useful tool in the study of equilibrium constants. The formation of a weakly bound cluster followed by a switching reaction may produce a more strongly bound ion cluster faster than the direct clustering reaction (9). Consider the reaction:

$$M^{+} + A \xrightarrow{k_1} M^{+}A \tag{1.13}$$

$$MA^{+} + B \xrightarrow{k_2} MB^{+} + A \tag{1.14}$$

If reaction 1.13 is relatively slow (i.e. $k_1 = 10^{-30}$ $cm^{6}$ $molecules^{-2}sec^{-1}$) and the pressures of A and B are 0.5 torr, the half life for the reaction will be about one millisecond. Assuming $k_2$ to be about $10^{-10}$ $cm^{3}$ $molecule^{-1}sec^{-1}$, the half

life of reaction 1.14 is approximately one microsecond. Thus if the switching reaction from $M^+(B)$ to $M^+(A)$ is of a similar rate, the two ions $MA^+$ and $MB^+$ will be in equilibrium long before either is in equilibrium with $M^+$.

If a clustering equilibrium constant for reaction 1.14 is known and it is desired to determine the similar constant for reaction 1.16 at pressures at which equilibrium will not readily be achieved, a switching reaction of the type 1.12 may be used.

$$M^+ + A \rightleftarrows M^+A \qquad 1.15$$

$$M^+ + B \rightleftarrows M^+B \qquad 1.16$$

Denoting $K_A$ and $K_B$ as the equilibrium constants of reactions 1.15 and 1.16 respectively and $K_S$ as the switching equilibrium constant, it is seen that:

$$K_B = K_A \times K_S \qquad 1.17$$

Thus from a knowledge of $K_A$ and the measurement of $K_S$, the desired equilibrium constant, $K_B$, may be obtained.

## 1.3 Thermodynamic Relationships Obtained from Gas Phase Clustering Reactions

The general clustering reaction for an alkali metal ion, $M^+$, with a solvent molecule, S, may be written:

$$M^+(S)_{n-1} + S \rightleftarrows M^+(S)_n \qquad 1.18$$

In the present study M represents the alkali metals: Na, K, Rb, and Cs. For alkali ion clusters, the interaction is mainly electrostatic and it is expected that there is little charge transfer. Thus the brackets are placed around the solvent molecule indicating the positive charge remains on the alkali metal ion.

The equilibrium constant for reaction 1.18 may be expressed as:

$$K_{n-1,n} = \frac{P_{M+(S)_n}}{P_{M+(S)_{n-1}} \times P_S} \qquad 1.19$$

The equilibrium concentrations of the two ionic species are measured with the high pressure ion source mass spectrometer described in the experimental chapter. Since the solvent pressure is also known the equilibrium constant can be determined.

Other thermodynamic functions can be obtained from the measured equilibrium constant. The free energy change, $\Delta G^o_{n-1,n}$ is given by equation 1.20:

$$\Delta G^{o}_{n-1,n} = -RT \ln K_{n-1,n} \qquad 1.20$$

From the well-known thermodynamic relationship:

$$\Delta G^{o} = \Delta H^{o} - T\Delta S^{o}$$

and equation 1.20 the Van't Hoff equation, 1.21, is obtained which allows one to determine $\Delta H^{o}_{n-1,n}$ and $\Delta S^{o}_{n-1,n}$.

$$\ln K_{n-1,n} = -\frac{\Delta H^{o}_{n-1,n}}{R}\left(\frac{1}{T}\right) + \frac{\Delta S^{o}_{n-1,n}}{R} \qquad 1.21$$

Thus by varying the temperature and measuring the corresponding equilibrium constants, values may be obtained for the enthalpy and entropy of reaction 1.18.

## 1.4 The Nature of Solvation

The solvation of an ion in a liquid solution is a complex matter. Many models have been used to explain solvation, but none have been able to describe all the phenomena which take place in solution. Most of these models deal with hydration, but some can be expanded to incorporate other polar solvents.

In general, all the acceptable models agree upon the idea that there are two types of solvation occurring when a gaseous ion is dissolved in a solvent. The first can be referred to as primary solvation. This is an interaction between the ion and the polar solvent molecules which are in

contact with it. These molecules will be immobilized and move as an entity with the ion. Naturally, the stronger the interactions, the larger the number of solvent molecules which are immobilized by the ion. One relationship predicting the size of this "solvation shell" is given by the Stokes-Einstein equation (10):

$$r_s = 0.819/\Lambda_o \eta$$

The radius $r_s$ is referred to as the Stokes radius of the ion, $\Lambda_o$ is the mobility of the ion in solution, and $\eta$ is the viscosity of the solvent. For example, the Stokes radius of $Na^+$ in tetrahydrofuran is 4.2 $A^o$ compared to a "bare" radius of $\sim$ 1.2 $A^o$, whereas $Cs^+$ has a Stokes radius of 2.4 $A^o$ with a corresponding "bare" radius of $\sim$ 1.9 $A^o$. From this it has been concluded that the sodium ion is solvated by tetrahydrofuran, but the cesium ion is not (11).

The second type of solvation can be referred to as secondary or distant solvation. This refers to the interactions between the ion with its intimate solvation shell and the bulk of the solvent. The Born equation, 1.22, is a classical electrostatic relationship, which predicts the free energy change of immersing an ion of charge Ze with radius, r, from a vacuum into a solvent of dielectric constant, D (12):

$$-\Delta G = Z^2e^2/2r(1-1/D) \qquad 1.22$$

This equation can be used to evaluate secondary solvation by replacing the radius of the ion with the radius of the first solvation shell. These two types of solvation, i.e. primary and secondary, lead to the "sphere in continuum" model of solvation (13).

One of the first useful solvation models was that of Bernal and Fowler (14) as modified by Eley and Evans (15). In this model, the monovalent alkali cations are all four-coordinated in an inner solvation shell. To determine the theoretical $\Delta H$ hydration, the authors used the cycle shown in Figure 1. It starts with an ion in the gas phase and liquid solvent. $\lambda$ represents the energy required to remove a cluster of five solvent molecules to the gas phase. (The cavity left in the solvent is later used to accommodate the tetra-solvated ion.) $\beta$ represents the energy to dissociate the five molecule solvent cluster into five separate molecules. $\pi$ is the energy released when four solvent molecules are tetra-coordinated to the ion. $\gamma$ is the energy released when the tetra-coordinated ion is put back into the solvent cavity. Finally, L is the energy released when the remaining solvent molecule is returned to the solvent, i.e. the free energy of condensation.

Various assumptions were made in order that the authors could evaluate the energy terms. A simple ion-dipole model was used to calculate $\pi$. Dispersion forces and electronic repulsion forces were considered to be small and to cancel each other out and thus were ignored. The lateral interactions

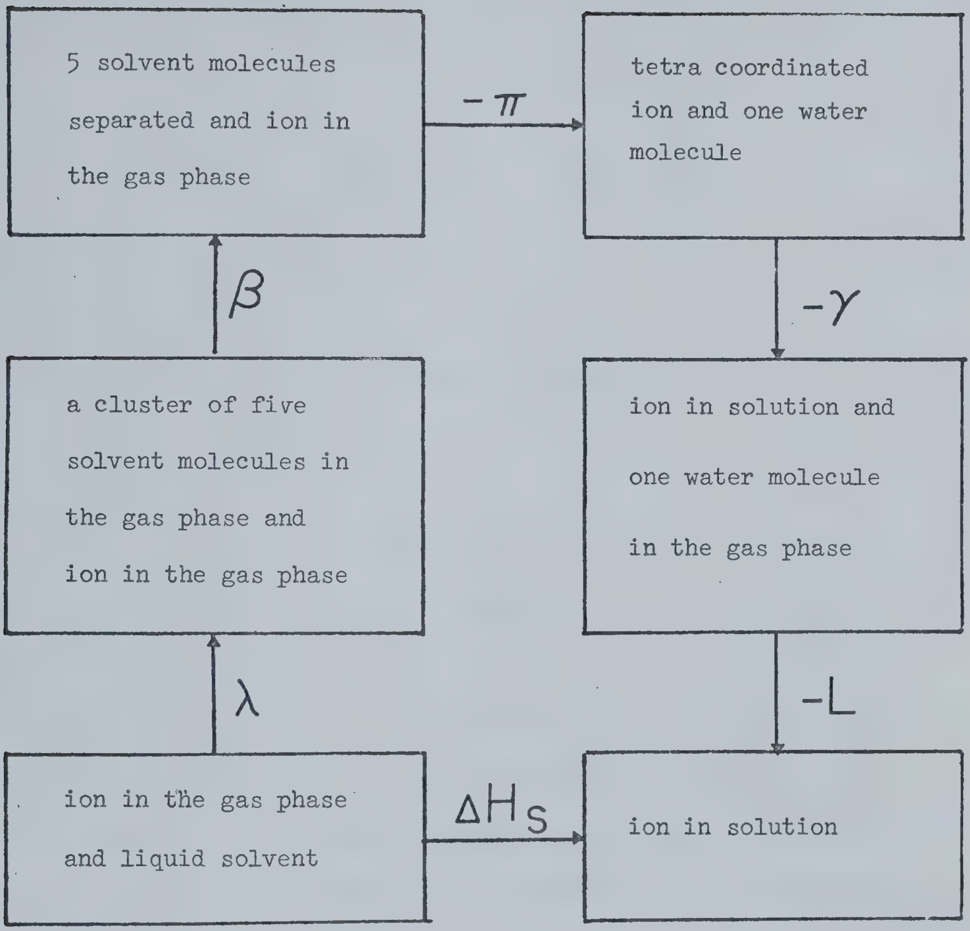
5 solvent molecules separated and ion in the gas phase
$-\pi$
tetra coordinated ion and one water molecule
$\beta$
$-\gamma$
a cluster of five solvent molecules in the gas phase and ion in the gas phase
ion in solution and one water molecule in the gas phase
$\lambda$
$-L$
ion in the gas phase and liquid solvent
$\Delta H_S$
ion in solution

$$\Delta H_S = \lambda + \beta - \pi - \gamma - L$$

FIGURE 1 Bernal and Fowler, Eley and Evans Model of Ionic Solvation.

between water molecules were also considered negligible and were neglected. The energy term, $\pi$, was then said to be:

$$\pi = 4 \times \Sigma \frac{Ze\,\alpha e}{r} \qquad 1.23$$

where Ze is the charge on the ion and $\alpha e$ is the fractional charge on the individual atoms of the solvent molecule.

The term $\beta$ was calculated in exactly the same way as $\pi$, except a water molecule, and not an ion, was the centre of the tetrahedron.

The terms $\lambda$ and $\gamma$ were determined as an entity by setting the difference $\lambda - \gamma$ equal to the sum of a structure reorientation term, $\Phi$, and a Born charging term given by equation 1.22. $\Phi$ was said to equal 8 kcal/mole for the reorientation of water molecules around a positive ion.

As primitive as this model was, it predicted fairly accurate heats of hydration for the various ions studied. Nearly all the ion-solvation cycles which have been proposed since 1940 are based on the Bernal and Fowler-Eley and Evans cycle.

In 1957, Frank and Wen (16) proposed a slightly more sophisticated model of solvation, and particularly hydration. Their model was similar to the Bernal-Fowler model except that a region between the solvation shell and the bulk solvent was introduced. This region, which was coined the "structure-breaking" region, consisted of solvent molecules which were more random in organization than the normal bulk

solution. The solvent molecules, in this case water molecules, were disorganized due to the competition between the forces of the electric field produced by the ion and forces present in the normal liquid structure.

One of the most recent models of ion solvation is due to Bockris and Reddy (17). In this model, the solvation shell of the ion is composed of solvent molecules bonded to the ion as well as non-coordinated ligands which are in turn bonded to the bulk solution. These non-coordinated ligands occur because their dipoles do not rotate into an attractive position. Bockris and Reddy also postulate that the structure-breaking region (in the case of water) will consist only of a monolayer of solvent molecules.

Bockris and Saluja (18) used a hypothetical cycle for determining the heats of ionic solvation (Figure 2) and found that the Bockris-Reddy model was most consistent with experimental data. The cycle involves the following steps: (1) evaporation of n solvent molecules, where n is the number of molecules in the solvation shell; (2) the gain on interaction of an ion with n solvent molecules; (3) a Born-charging term; and (4) the interaction among the molecules in the first shell with molecules in the bulk solution, i.e. a structure breaking term. Gas phase solvation studies such as those carried out in this laboratory give accurate experimental values for the second term.

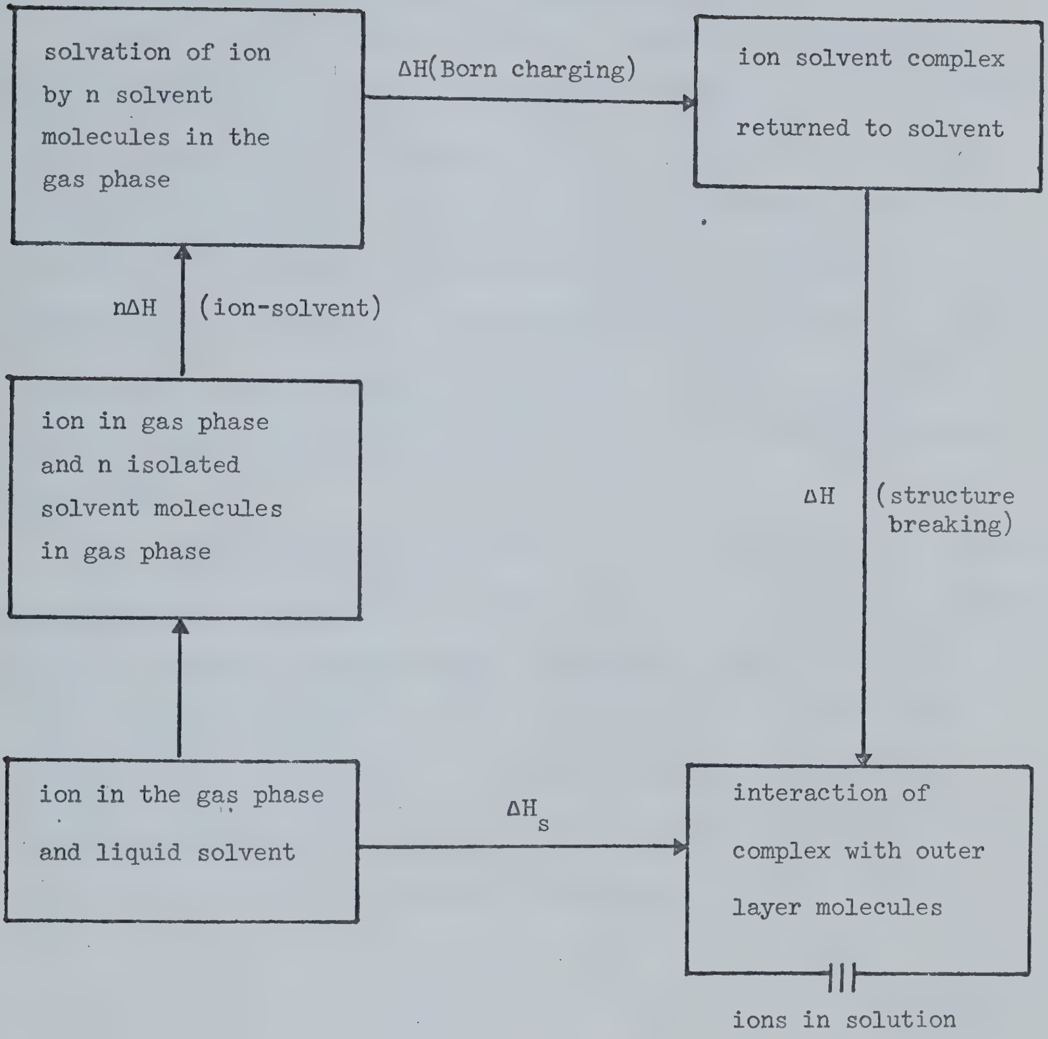
solvation of ion by n solvent molecules in the gas phase
ΔH(Born charging)
ion solvent complex returned to solvent
nΔH (ion-solvent)
ion in gas phase and n isolated solvent molecules in gas phase
ΔH (structure breaking)
ion in the gas phase and liquid solvent
ΔH s
interaction of complex with outer layer molecules
ions in solution

FIGURE 2 Bockris and Saluja Solvation Cycle.

## 1.5 Acetonitrile as a Dipolar Aprotic Solvent

Protic solvents, such as water, methanol, formamide, and hydrogen fluoride have a hydrogen atom which has partial positive charge and is suitable for the formation of fairly strong hydrogen bonds. Dipolar aprotic solvents, such as acetonitrile, acetone, dimethylformamide, dimethylsulphoxide and propylene carbonate, are defined as such since they have a dielectric constant greater than 15, as well as lacking polar hydrogen atoms capable of engaging in strong hydrogen bonds (19).

In a review article, Parker (19) has discussed at length how anions, especially those which form the strongest hydrogen bonds, are much less solvated in dipolar aprotic solvents than in protic solvents. This means that the anions are more "active" in aprotic solvents and chemical reactions involving anions are, as a result, much more efficient in aprotic solvents. For example, the $S_N2$ reaction (20):

$$CH_3I + Cl^- \rightarrow CH_3Cl + I^- \qquad 1.24$$

proceeds at a rate $10^6$ times greater in the aprotic solvent dimethylformamide than in the protic solvent methanol. Similarly, HCl is a strong acid in methanol (21) but a weak one in acetonitrile (22). This is because the solvation of $Cl^-$ in protic solvents assists the dissociation of the acid through the formation of hydrogen bonds (19).

Most dipolar aprotic solvents contain a nitrogen or an

oxygen atom with a lone pair or pairs of electrons. This means that there is a more distinct centre of the negative dipole and one would expect that cations would solvate better than anions in a given aprotic solvent. Thus, it is generally believed that dipolar aprotic solvent solvate negative ions poorly, but are fairly effective in positive ion solvation. The total solvation of a pair of ions like $Na^+$ and $Cl^-$ can be readily determined, however, the individual or single ion solvation energies are far more difficult to obtain. Some attempts to do so are described in the next section.

## 1.6 Related Solvation Studies in Liquid Acetonitrile

The evaluation of the thermodynamic functions involved in solvating a single ion (whether a cation or anion) in any solution, remains one of the classical problems in solution chemistry (23). Likewise, the determination of the change in these functions with a change in solvent for a particular ion remains equally as abstract. In this section, the various methods used in determining the alkali metal ion solvation energies in acetonitrile will be briefly discussed. A more detailed description is given in a review article by Popovych (24). All methods are based on an extra-thermodynamic assumption of some sort.

The partial molal free energy of a solute, i, in acetonitrile may be represented as:

$$G_i = G_i^o(an) + RT \ln a_i(an) \qquad 1.25$$

where $G_i^{\circ}(an)$ is the standard free energy of the solute in acetonitrile, and $a_i(an)$ is the activity of the solute in acetonitrile. For water as a solvent, the partial molal free energy will be:

$$G_i = G_i^{\circ}(w) + RT \ln a_i(w) \qquad 1.26$$

The difference between the standard free energies of the solute in water and acetonitrile, which is defined as the free energy of transfer, $\Delta G_t$, from water to acetonitrile, then becomes:

$$\Delta G_t = G_i^{\circ}(an) - G_i^{\circ}(w) = RT \ln \frac{a_i(w)}{a_i(an)} \qquad 1.27$$

At infinite dilution:

$$\frac{a_i(w)}{a_i(an)} = \frac{\gamma_i(w)}{\gamma_i(an)} = {}_m\gamma_i \qquad 1.28$$

${}_m\gamma_i$ is referred to as the medium effect (24) or the solvent activity coefficient (19). The medium effect, rather than the standard free energy of transfer, is the term most often quoted in literature, but it is a relatively simple matter to transform ${}_m\gamma_i$ into $\Delta G_t$. Thus from taking acceptable values for the free energy of an ion in water and determining the free energy of transfer, the free energy of the ion in acetonitrile can be obtained.

## A Methods Based on the Born Equation

The Born equation is the simplest expression for estimating the solvation energy of an ion (12). The free energy change, $\Delta G$, represents the difference between the electrostatic free energy of a spherical ion in vacuo ($D=1$) and the energy in a continuum of uniform dielectric. The Born equation (1.22) has many drawbacks. The parameters usually used are the crystallographic radius of the ion and the bulk dielectric constant of the solvent. This means that it unreasonably assumes that the ionic radius is not affected by solvation and that the dielectric constant in the vicinity of the ion remains the same as in the bulk. Also, it ignores the short range electrostatic interactions between the ion and solvent molecules, as well as all non-electrostatic contributions to the solvation energy of an ion.

Latimer, Pitzer and Slanski (25) offered a modification to the Born equation in which the radius of the ions were corrected to fit experimental data:

$$-\Delta G_{\pm}^{o} = \frac{Ne^2z^2}{2}(1 - 1/D)\left(\frac{1}{r^+ + R^+} + \frac{1}{r^- + R^-}\right) \tag{1.29}$$

where $R^+$ and $R^-$ are empirical corrections to the cation and anion crystallographic radii, $r^+$ and $r^-$ respectively. Using this method, Strehlow and his co-workers (26) determined a correction term $R^+$ of 0.72 A for rubidium in acetonitrile. This led to a value of $\Delta G_t$ which showed that

rubidium was more strongly solvated in water than in acetonitrile. This conclusion was reached since rubidium was reduced at a less negative potential in acetonitrile than in water. This meant that rubidium was likely more solvated in water, and thus not as "available" for reduction. In order to obtain single ion thermodynamic functions for the solvation of the alkali ions in acetonitrile, they imposed another restriction on the Born equation. Rather than just comparing the differences in single ions in the two solvents as Strehlow did, they compared the difference between ion pairs (eg. $Li^+$-$K^+$, $Na^+$-$Rb^+$, etc.) in both acetonitrile and water. Their value of $R^+$ became 0.81 A for the alkali metal ion in acetonitrile and the modified Born equation then predicted a more favorable solvation of alkali ions by water than by acetonitrile.

## B Izmaylov Extrapolation Method

Izmaylov (28) interpreted the solvation of ions as a process in which the ion accepts unshared electron pairs of the solvent molecule into its vacant orbitals. He assumed that the solvation energy differences for isoelectronic alkali and halide ions would approach zero with increasing $1/n^2$, where n is the principle quantum number of the lowest vacant orbital of the ion (for $Na^+$, $F^-$, n=3; $K^+$, $Cl^-$, n=4; and so on). Therefore, by plotting the experimentally determined function $\left[-\Delta G_i^{\circ} + \left\{\frac{\Delta G_M - \Delta G_X}{2}\right\}\right]_n$

vs. $1/n^2$ and extrapolating to $1/n^2=0$, the solvation energy of an ion, $\Delta G_i^o$, could be determined. Once the $\Delta G^o$ of any ion was estimated in a solvent, it was possible to determine the $\Delta G$'s of all the other ions through their electrically neutral combinations. His results predicted a slight solvation preference for alkali metal ions in water compared to acetonitrile.

## C Solvent Independent Electrodes

The difference in solvation energies of an ion can be directly related to the difference in the standard potentials of an electrode in two solutions. Thus if a reference electrode could be found in which the ion had the same solvation energies in all solvents, it could act as a reference in determining the solvation energies of other ions in a variety of solutions. Pleskov (29) postulated that the rubidium ion, with its large radius and low polarizability should have approximately the same solvation energies in all solvents and that the rubidium electrode could serve as a solvent-independent reference electrode. One would feel that cesium would be even more solvent independent due to its larger radius, but Strehlow (30) has pointed out that the difference in standard potentials of $Rb^+$ and $Cs^+$ is nearly independent of solvent, and thus $Rb^+$ fulfills all the qualifications of cesium. Although the rubidium method is plausible for comparisons of very similar solvents, its major importance is that it paved the way to more sophisti-

cated empirical approaches.

## D Reference Electrolytes

The most commonly used and most widely accepted extrathermodynamic method of determining single ion solvation energies (via free energies of transfer) is the use of a reference electrolyte, in which the cation and anion supposedly have equal medium effects. This method requires that the cation and anion have similar size and structure and that the atom which has the charge be "buried" under similar groups. Common reference electrolytes are tetraphenylarsonium-tetraphenylborate (31), tetraphenylphosphonium-tetraphenylborate (32) and triisoamyl-n-butylammonium tetraphenylborate (33). Thus in the case of $Ph_4As\text{-}BPh_4$, it is assumed $\Delta G_t(Ph_4As^+) = \Delta G_t(BPh_4^-)$. It has been suggested (24) that the solvent-solute interactions of these large ions may be determined primarily by the four neutral phenyl groups and no specific solvent interactions with the central ion takes place to any extent.

This method has been applied to acetonitrile (24,31) and free energies of transfer were determined which demonstrated that water solvates alkali ions slightly better than acetonitrile does.

## E Free Energies of Solvation from Volta Potentials

The only technique that seems to have been developed to evaluate absolute solvation energies of single ions

without any assumptions about the dimensions of the ions are those based on the measurement of the Volta potential between an electrolyte solution and another surface separated from the solution by a vacuum or inert gas (35). Randles (36) has applied this method to the determination of the absolute energy of hydration of alkali and halide ions.

The experimental setup used by Randles consists of a glass tube through the centre of which flows a small jet of mercury. A solution of KCl flows along the inner surface of the glass tube. An inert gas such as nitrogen or argon insulates the solution and the mercury jet. If the outer, or Volta potentials, of the two liquids are different, an electric field is created in the gap. However, the charge on the surface of the mercury is carried away when the jet breaks up into droplets. Eventually, the jet will reach a state of equilibrium when the outer potentials of the two liquids are equal. The emf of the cell:

$$\mathrm{Hg\ jet}|N_2|\mathrm{KCl}(a = 1)|Hg_2Cl_2|\mathrm{Hg}$$

which can be called $F\Psi^o$, corresponds to the first reaction given below:

$$\begin{array}{lll}
1) & Hg + Cl^{-}_{aq} \rightarrow \frac{1}{2}Hg_2Cl_2(s) + e_{Hg} & F\psi^{o} \\
2) & e_{Hg} \rightarrow e_{g} & W \\
3) & K_{s} + \frac{1}{2}Hg_2Cl_2(s) \rightarrow K^{+}_{aq} + Cl^{-}_{aq} + Hg & FE^{o}_{K,Cl} \\
4) & K^{+}_{g} + e_{g} \rightarrow K_{s} & -(\Delta G_{subl} + \\
 & & \Delta G_{ioniz.}) \\
\hline
5) & K^{+}_{g} \rightarrow K^{+}_{aq} & \Delta G^{o}_{h}\ (K^{+})
\end{array}$$

By considering the cell $K|Hg|Hg_2Cl_2|KCl(a = 1)|K$ along with the electron work function of mercury W and the sublimation and ionization energies of solid potassium, the free energy of solvation of $K^+$ is obtained following the above sequence of equations.

From Randles' value of the absolute free energy of hydration of the potassium ion and available thermodynamic data, an absolute scale of free energies of hydration can therefore be set up.

Case and Parsons (37) determined the value $\Delta G_{Ag^+}$ (acetonitrile) by measuring the difference in the free energy of solvation of the silver ion in acetonitrile and water (i.e., the free energy of transfer), by the Volta potential technique. Since the free energy of silver ion hydration was known from Randles, the free energy in acetonitrile could be obtained from the free energy of transfer.

In the Case and Parson setup (38), an aqueous $AgNO_3$ solution flowed down the surface of a glass tube, while a jet of acetonitrile solution of $AgNO_3$ was directed down the axis of the tube in a stream of nitrogen. The compensation potential, E, of the system:

$$\underset{\text{water}}{Ag|AgNO_3(M)}|N_2|\underset{\text{acetonitrile}}{AgNO_3(M')|Ag}$$

was measured. (M) is the molarity of $AgNO_3$ in aqueous solution and (M') is the molarity in acetonitrile.

The free energy of transfer was calculated from the relationship:

$$\Delta G_t = -EF + RT \ln\left[\frac{a_{Ag^+(w)}}{a_{Ag^+(an)}}\right] \qquad 1.30$$

where F represents the Faraday.

It is felt that this method is the best manner of determining single ion solvation energies and, therefore, in the present work the Case and Parsons values for the solvation of alkali and halide ions by acetonitrile are considered the most accurate.

## 1.7 Gas Phase Ion-Molecule Solvation Studies

Single ion solvation thermodynamic functions in the gas phase are quite readily determined by the use of high pressure mass spectrometers or related instruments. Unlike the liquid phase, the complication of having both cations and anions solvating at the same time is removed. Intrinsic thermodynamic

values for the ion-solvent interactions in the solvation shell can then be obtained experimentally. A general history of ion-molecule clustering reactions is given by Dzidic (39) and will not be dealt with here.

## A Solvation Reactions Studied in the Present Laboratory

In the past few years, the following ion-molecule solvation reactions have been carried out in this laboratory:

### $H^+(H_2O)_n$

The $H^+(H_2O)_n$ system has been extensively studied in this laboratory. Equilibrium constants and thermodynamic relationships were determined up to n = 8 (40) for the reaction:

$$H_3O^+(H_2O)_{n-1} + H_2O \rightleftarrows H_3O^+(H_2O)_n \qquad 1.31$$

and the values obtained (to n = 4) were reproduced more recently (41) within experimental error using a slightly different experimental technique.

The kinetics of the above reaction have also been studied extensively (42, 43) under various experimental conditions, and the temperature dependence of the forward and reverse reactions have been determined.

## $NH_4^+(NH_3)_n$, $NH_4^+(H_2O)_n$ and Mixed Clusters

As was the case with the $H^+(H_2O)_n$ system, the $NH_4^+(NH_3)_n$ system has undergone a great deal of research in this laboratory (43 - 46). Thermodynamic values for the reaction:

$$NH_4^+(NH_3)_{n-1} + NH_3 \rightleftarrows NH_4^+(NH_3)_n \qquad 1.32$$

have been determined for values of n up to 5.

By using a large water to ammonia ratio, it was possible to study the solvation of the ammonium ion by water (44). By increasing the ammonia concentration mixed cluster equilibrium constants and thermodynamic values for the reaction:

$$NH_4^+(NH_3)_{n-1}(H_2O)_w + NH_3 \rightleftarrows NH_4^+(NH_3)_n(H_2O)_w \qquad 1.33$$

were determined (43, 46).

## $H^+(CH_3OH)_n$ and $H^+(CH_3OCH_3)_n$

The importance of hydrogen bonding in solvation reactions has been shown (47) by comparing the following reactions:

$$H^+(H_2O)_{n-1} + H_2O \rightleftarrows H^+(H_2O)_n \qquad 1.34$$

$$H^+(CH_3OH)_{n-1} + CH_3OH \rightleftarrows H^+(CH_3OH)_n \qquad 1.35$$

$$H^+(CH_3OCH_3)_{n-1} + CH_3OCH_3 \rightleftarrows H^+(CH_3OCH_3)_n \qquad 1.36$$

The protonated water and methanol species easily formed clusters containing more than two ligands. However, the dimethyl ether clusters with n equal to or greater than 3 were very unstable. This is thought to be due to the lack of available hydrogens for hydrogen bonding.

This work was continued (48) in the determination of ion equilibria for protonated mixed water-dimethyl ether clusters and for protonated mixed methanol-dimethyl ether clusters. This study again showed the importance of hydrogen bonding in cluster stability.

### $X^-(H_2O)$ and $M^+(H_2O)$

The gas phase hydration of halide negative ions (1) and of alkali metal positive ions (3, 4) has been studied in this laboratory. The thermodynamic quantities $\Delta H$, $\Delta G$, and $\Delta S$ have been determined for the general reactions:

$$X^-(H_2O)_{n-1} + H_2O \rightleftarrows X^-(H_2O)_n \qquad 1.37$$

$$M^+(H_2O)_{n-1} + H_2O \rightleftarrows M^+(H_2O)_n \qquad 1.38$$

where $X^- = F^-$, $Cl^-$, $Br^-$, $I^-$ and $M^+ = Li^+$, $Na^+$, $K^+$, $Rb^+$, $Cs^+$. The values obtained from the alkali ion hydration studies are very valuable in comparing the solvation properties of the ions in water and acetonitrile, which is done in the present study.

### $X^-(CH_3CN)$

The temperature dependence on the equilibrium constant of the reaction:

$$X^-(CH_3CN)_{n-1} + (CH_3CN) \rightleftarrows X^-(CH_3CN)_n \qquad 1.39$$

has been studied for values of n from 1 to 4 or 5 in this laboratory, where $X^-$ is a halide negative ion. The thermodynamic quantities so obtained have also been compared to those determined from the halide solvation in water (1). The data obtained from this solvation sequence provide an opportunity to compare alkali metal ion solvation in acetonitrile with that of halide ions.

## B Other Related Gas Phase Solvation Studies

Gas phase solvation studies of alkali metal ions undertaken in laboratories other than this one have been mainly concerned with atmospheric reactions and not directly concerned with a comparison to liquid solution. No research done on the solvation of alkali metal ions in dipolar aprotic solvents in the gas phase could be found in the literature.

McKnight and Sawina (49) have used a drift tube to study the clustering of $Cs^+$ with water:

$$Cs^+(H_2O)_{n-1} + H_2O \rightleftarrows Cs^+(H_2O)_n \qquad 1.40$$

for values of n up to three. The determined values of $-\Delta H^o$

and $-\Delta S^o$ are considerably lower than those observed by Dzidic and Kebarle (3). McKnight and Sawina also determined the $-\Delta H^o_{0,1}$ and $-\Delta S^o_{0,1}$ for the clustering of $Cs^+$ with $SO_2$ as well as the rate of the reaction. They found that the forward rate of this reaction was greater than that with water ($3 \times 10^{-29}$ $cm^6$ $molec.^{-2}$ $sec^{-1}$ in $SO_2$ compared to $9 \times 10^{-30}$ $cm^6 molec.^{-2} sec^{-1}$ in water), yet the $-\Delta H$ of the water cesium reaction is larger by over a kilocalorie/mole.

Tang and Castleman (50) using a high pressure mass spectrometer have demonstrated by the gas phase hydration of $Pb^+$, that the electronic structure of the ion plays a role in cluster stability. The alkali metal ions are isoelectronic, and it is expected and has been found (3) that the size of the central ion is the dominant factor in the stability of the ion-water cluster. The monovalent lead ion, however, has a ($6s^2 6p^1$) valence configuration and these remaining electrons appear to influence the bonding of the ion with water. The lead monovalent ion bonds almost as strongly to water as does the sodium ion for the first water molecule, which would not be expected from their comparative sizes. However, as the number of water molecules increases, the reaction enthalpies tend toward the values obtained for the hydration of $Cs^+$, an ion of approximately the same size as $Pb^+$.

## 1.8 Acid-Base Interactions

The second part of the present study is concerned with the gas phase basicity of some amines and ethers, using $K^+$ as a reference Lewis acid. G. N. Lewis has postulated (51) that all chemical complexing reactions can be attributed to acid-base interactions. In his definition, an acid is any species which can accept electrons, whereas a base is any species which can donate electrons. To avoid confusion with Bronsted acids, which are defined as proton donors, these generalized acids are usually referred to as Lewis acids, or electron acceptors. Bronsted bases are defined as proton acceptors and Lewis bases as electron donors.

All metal atoms and ions are Lewis acids. However, it has been demonstrated (52) that they interact with different bases in different ways. That is, a certain base may interact strongly with one acid and very weakly with another acid, whereas a second base may interact with the two acids in the opposite way. This difference in acid-base interactions has been studied in detail by Pearson (53 - 55), who has described these peculiarities under the "Principle of Hard and Soft Acids and Bases" (HSAB). In this theory all Lewis acids and bases can be classified as "hard", "soft", or "borderline". The terms "hard" and "soft" stem from the inability or ability of the acid or base to be polarized. "Hard" acids in general are small in size, have high positive charge and do not contain unshared pairs of electrons in their valence shell, whereas

"soft" acids are large in size, of low positive charge and often contain pairs of d or p electrons in their valence shell. "Hard" bases have in general a donor atom of high electronegativity and low polarizability such as F, O, or N. The term "hard" describes how the donor atoms hold on to their electrons tightly. Donor atoms which hold on to their electrons loosely due to low electronegativity and high polarizability are thus referred to as "soft" bases.

Due to the presence of nitrogen or oxygen, aliphatic amines and ethers are classified (53) as "hard" bases. The presence of an aromatic ring tends to "soften" the donor atom and compounds such as aniline and pyridine are thus placed in the borderline category. Of the alkali metal ions, $Li^+$, $Na^+$, and $K^+$ have been classified by Pearson as "hard" acids (53) with the degree of hardness decreasing with an increase in ionic size. $Cs^+$ has been classified as "soft" and it seems reasonable to assume $Rb^+$ would be "borderline".

Mulliken has offered a very detailed classification of donors and acceptors involved in complexing reactions (56). Alkali cations in his system are classified as vacant-orbital acceptors or more simply v-acceptors. The amines and ethers used in this study are classified as onium donors or n-donors. Onium donors are described as systems containing relatively easily ionized atomic lone pairs. Thus, it would seem that an onium donor could be a "hard" or "soft" base under Pearson's definition. Likewise, Mulliken's

v-acceptors contain both "hard" and "soft" Lewis acids, since there is no criterion for polarizability in his classification. According to Mulliken, n-donors and v-acceptors should form fairly stable n→v complexes (56), the degree of interaction being related to the donating and accepting powers of the two species.

In the present study, the potassium ion is used as a reference Lewis Acid. It is classified as a "hard" acid and v-acceptor and thus it is expected to interact mainly with "hard" bases and n-donors. From studying the standard free energy or enthalpy of a series of reactions:

$$K^{+} + B \rightarrow K^{+}B \qquad 1.41$$

a relative scale of basicities may be set up.

In recent years a great deal of attention has been placed on the Bronsted gas phase basicities of amines and ethers. The relative proton affinities of many bases have been studied by various authors (57 - 65) and a fairly consistent Bronsted basicity order has been determined. This gives us an opportunity to compare the two basicity scales using different reference acids. Also, it is of interest to compare the basicity order determined for the potassium ion with that of a well studied neutral Lewis acid such as $B(CH_3)_3$.

## 1.9 Related Gas Phase Basicity Studies

### A The Proton as a Reference Acid

Recently, a great deal of research has been done on the gas phase protolysis of various bases. The experimental techniques vary, but all are interested in determining the proton affinity, i.e. the enthalpy change for the deprotonation reaction 1.42, for various organic bases, B.

$$BH^+ \rightleftarrows B + H^+ \qquad 1.42$$

Due to the strong interaction between the proton and organic bases, in order to determine the proton affinity it is necessary to measure equilibrium constants for proton exchange reactions for two bases, $B_1$ and $B_2$, such as 1.43:

$$B_1H^+ + B_2 \rightleftarrows B_2H^+ + B_1 \qquad 1.43$$

Using this technique, and assuming that the proton affinity of a reference base such as ammonia is known, and that entropy changes in the proton transfer reactions are so small that it can be said: $\Delta H \approx \Delta G = -RT \ln K_{eq}$. A more precise method would be to measure the temperature dependence of reaction 1.43 and thus determine ΔH directly. However, it has been found (59) that the entropy values were usually less than 3 e.u. and thus $\Delta G \approx \Delta H$ to within 1 kcal/mole.

The major experimental techniques used to set up a "Bronsted" basicity scale are high pressure mass spectrometry

(57 - 60) and ion cyclotron resonance (ICR) spectrometry (61 - 65).

The original qualitative gas phase basicity scale was determined by Munson (58) in a high pressure mass spectrometer. By utilizing equilibrium conditions, Kebarle and his co-workers in this laboratory (57, 59) have obtained a more quantitative order of amine basicity. They demonstrated by varying the ratio of the components in the proton transfer reaction, 1.43, by up to a factor of 100, that the equilibrium constant is independent of the pressure ratio. From these equilibrium constants, the proton affinities of various bases were determined using the proton affinity of ammonia (64) as a standard. This work was continued to diamines, and the results demonstrated that there was a large entropy effect, accounted for by the cyclization of the proton bound diamine (57).

Brauman, Riveros and Blair (61) obtained a qualitative basicity order in the gas phase by using ion cyclotron resonance spectrometry. With this technique, ions are forced into a circular orbit by a strong magnetic field. By maintaining the ions in this orbit for several hundred milliseconds, they undergo many ion-molecule collisions. Pressures must be kept very low, $10^{-5}$ torr (61), so the long time spent in orbit by the ion is essential for the achievement of equilibrium. Quantitative data (62 - 65) provided by this method for the gas phase basicity of amines are in good agreement with high pressure techniques.

## B Trimethyl Boron as a Reference Acid

Trimethyl boron has been described by Pearson (53) as a "borderline" Lewis acid, and by Mulliken (56) as a vacant orbital acceptor. In these respects it is very similar to the potassium ion, in that the potassium ion is supposedly nearly "borderline", although classified "hard", and it too is a vacant orbital acceptor. However, the interaction between trimethyl boron and a base cannot be expected to be similar to the interaction between the potassium ion and the same base. Whereas $K^+$ is charged and spherical, $B(CH_3)_3$ is a neutral acid and interaction with a base would be stereospecific due to the methyl groups. Also, when boron complexes are formed, the donated electron pair completes the valence octet, and boron becomes approximately $sp^3$ hybridized (66). That is, the geometry of the trimethyl boron changes from trigonal ($sp^2$ hybridized) to tetrahedral. Such rehybridization will not occur with the potassium ion.

Trimethyl boron readily forms complexes with amines. These complexes are stable enough in the gas phase that the thermodynamic functions of the dissociative reaction 1.44, where A represents an amine, can be studied.

$$AB(CH_3)_3 \rightleftarrows A + B(CH_3)_3 \qquad 1.44$$

In the 1940's and early 1950's, H. C. Brown and his co-workers studied these gas phase dissociative reactions in great detail with the hopes of explaining steric strains

(67 - 71). The data obtained by this group was summarized in a centenary lecture delivered by Brown and later published (72). From this data, a basicity scale using $B(CH_3)_3$ as the reference acid can easily be set up, and compared to the scales using $K^+$ or $H^+$ as the reference acids.

## CHAPTER 2

## EXPERIMENTAL

### 2.1 General

For the study of alkali ion-molecule reactions at high pressure, considerable modifications to a conventional mass spectrometer must be made. The primary alkali ions are generated by thermionic emission from a platinum gauze filament, coated with an appropriate alkali-alumina-silicate. An electric drift field is applied between the filament and the field free equilibrium chamber. The ions undergo several collisions with the neutral gas and equilibrium is achieved. The thermalized ions diffuse and many escape from the reaction chamber through a low conductance slit. A pressure differential is maintained between the high pressure ion source and the vacuum chamber by a high capacity pumping system. The pressure in the vacuum chamber is kept below $10^{-4}$ torr in order that the mean free path be greater than the dimensions of the apparatus.

The ions are accelerated and focussed by a modified Nier type electrode system and mass separated by a 15 cm radius, $60^{\circ}$ magnetic sector mass analyzer. A Bendix spiraltron electron multiplier is used as a detector with the output signal being fed into an electrometer or ratemeter. The apparatus can be operated in a pulsed beam or static mode.

The mass spectrometer was designed and assembled by

J. G. Collins (73) and modified for the study of gas phase hydration of alkali ions by S. K. Searles (74). Further modifications and features of the instrument of particular importance to gas phase solvation work are described in the subsequent sections of this chapter.

## 2.2 The Vacuum Chamber

A schematic diagram of the overall mass spectrometer is shown in Figure 3. The basic apparatus was built by the University of Alberta Machine Shops and assembled by J. G. Collins (73). The main vacuum chamber consists of a six-inch diameter tube supporting four ports at right angles to each other. One port in the plane of Figure 3 carries the ion source and the ion acceleration system, while the other is used for removal of the ion source from the vacuum chamber. The ports at right angles to the plane of the diagram carry various electrical feedthroughs, gas inlet and outlet tubes, as well as coolant tubes for temperature control of the ion source.

The vacuum system of the mass spectrometer consists of a 1400 l/sec 6" diffusion pump backed by a 425 liter/second forepump. Above the diffusion pump is mounted a 6" diameter gate valve and a 6" liquid nitrogen cooled baffle. Using ammonia, Searles (74) measured the pumping speed as 350 l/sec with the liquid nitrogen baffle uncooled and as 1900 l/sec when liquid nitrogen was added to the baffle. This difference was due to condensation of ammonia on the baffle. The pumping speed was calculated from the pressure

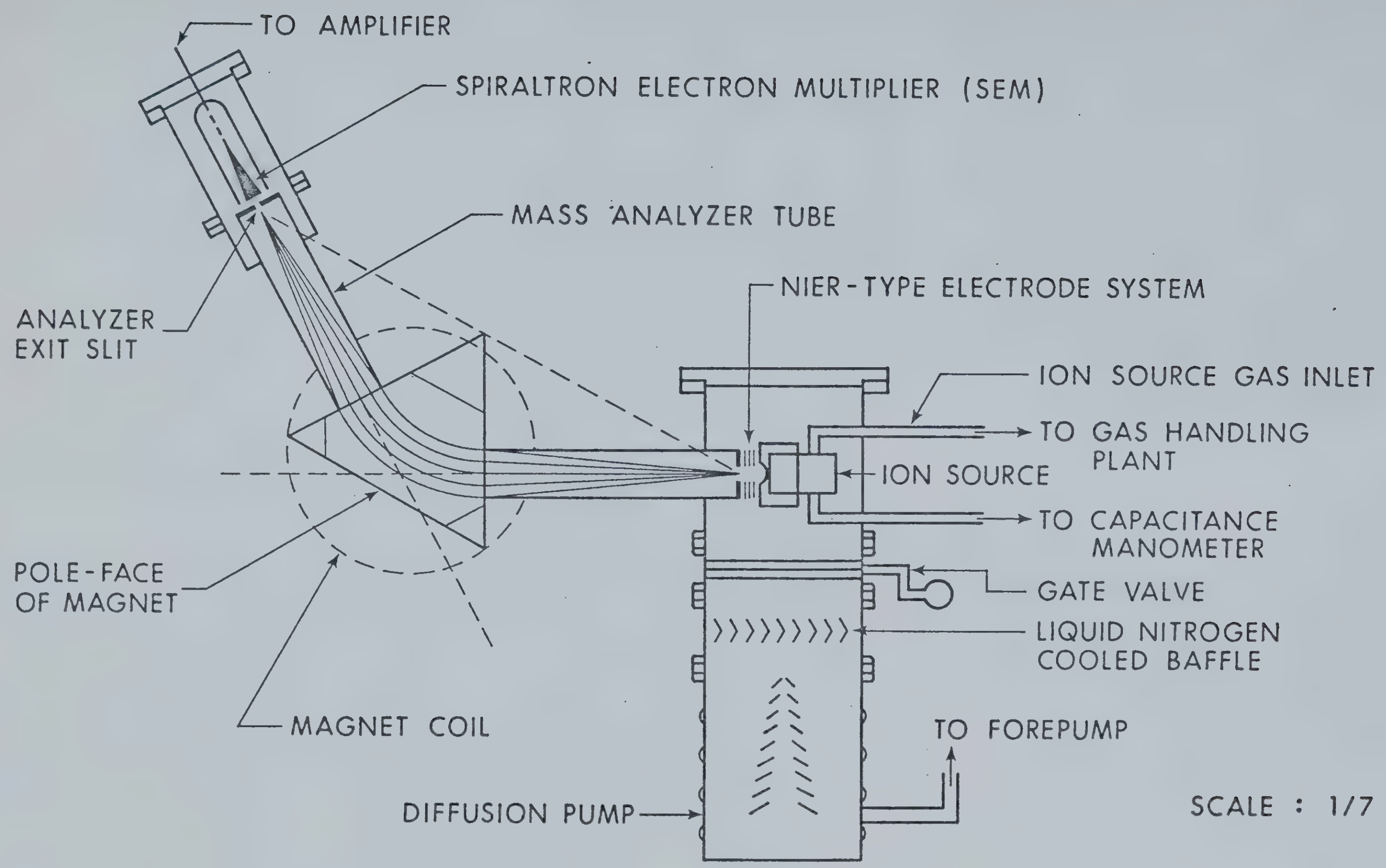
TO AMPLIFIER
SPIRALTRON ELECTRON MULTIPLIER (SEM)
MASS ANALYZER TUBE
NIER-TYPE ELECTRODE SYSTEM
ANALYZER EXIT SLIT
ION SOURCE GAS INLET
TO GAS HANDLING PLANT
ION SOURCE
TO CAPACITANCE MANOMETER
POLE-FACE OF MAGNET
GATE VALVE
LIQUID NITROGEN COOLED BAFFLE
MAGNET COIL
TO FOREPUMP
DIFFUSION PUMP
SCALE : 1/7

FIGURE 3 Cross-sectional View of Mass Spectrometer

drop in the gas handling plant reservoir with respect to time and from the pressure in the vacuum housing measured by an ionization gauge.

The mass spectrometer tube and electron multiplier housing were not differentially pumped. The pressure in the tube was typically $10^{-5}$ torr for water at an ion source pressure of one torr. Ultimate vacuum in the system was $2 \times 10^{-7}$ torr.

## 2.3 The Ion Source

For the study of the solvation of alkali ions in acetonitrile, a new ion source was designed and constructed (Figure 4). The major reason for changing from the source used by Searles (74) and Dzidic (39) was the accurate determination of ion source pressure. In the Searles-Dzidic source, the filament housing was separated from the reaction chamber by a ceramic insulator. Although this insulator was a tight fit between the housing and the reaction chamber, it certainly was a source of gas leakage to the vacuum chamber. In the new ion source, gas can only leak out through the exit slit.

The ion source consists of a heavy-walled cylinder of stainless steel. A plate, which holds the filament and two electrodes, is bolted to the top of the ion source and another plate holding the exit slit is screwed onto the bottom of the cylinder. Two tiny channels were bored into the cylinder to allow the reactant gas to enter the ion source

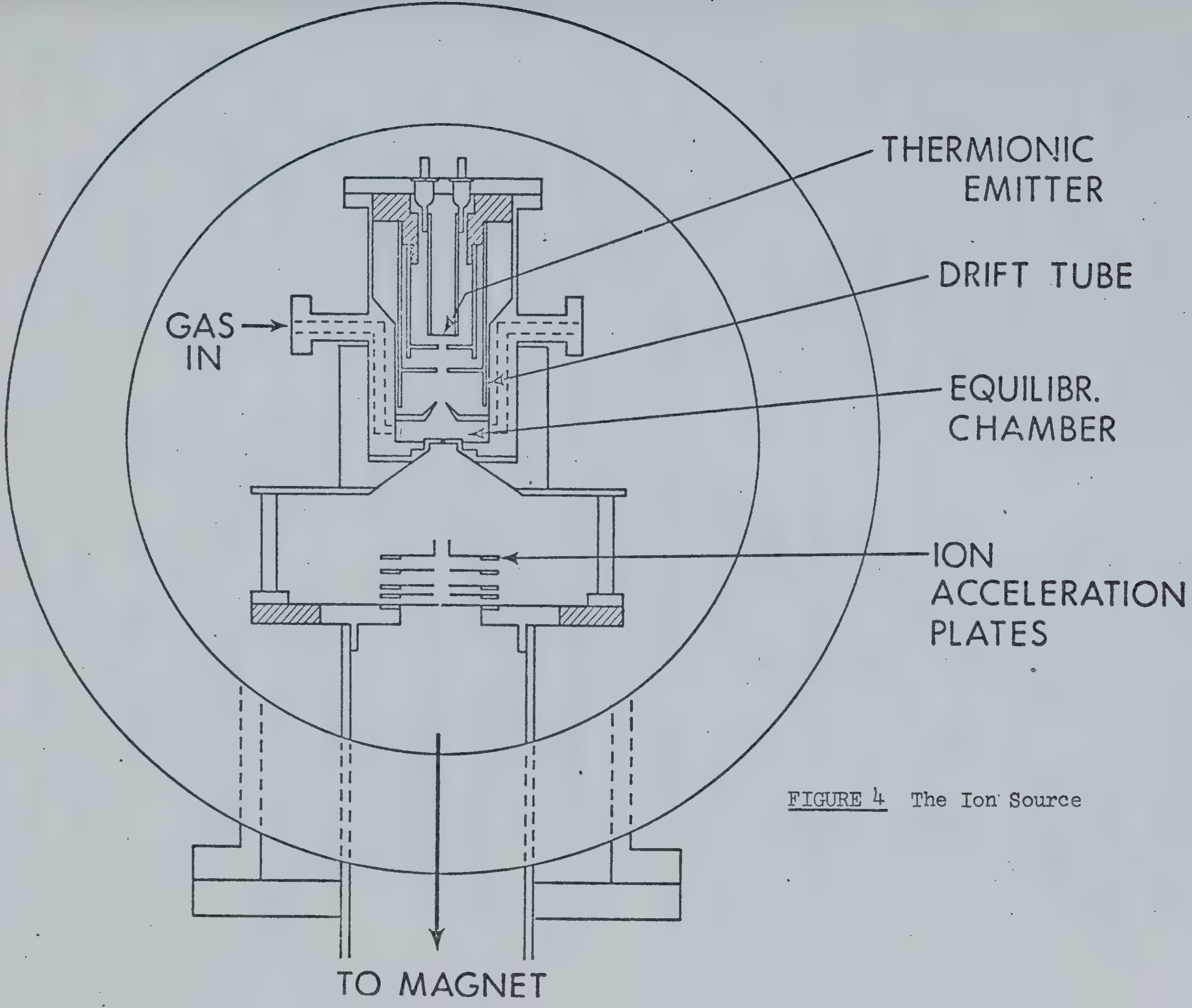
THERMIONIC EMITTER
DRIFT TUBE
GAS IN
EQUILIBR. CHAMBER
ION ACCELERATION PLATES
TO MAGNET

FIGURE 4 The Ion Source

and to measure the ion source pressure. These two channels end in flanges which can be bolted to the exterior gas and manometer lines. To ensure that there will be no gas leakage to the vacuum chamber, except through the exit slit, gold "O"-rings are placed around the plates and flanges.

The plate which houses the filament contains four electrical feedthroughs - two for the filament and one for each of the electrodes. Two nichrome studs, 3/32" in diameter are silver soldered to the filament feedthroughs. These studs were made as wide as possible to cut down on their resistance and prevent them from adding to the heat of the system. The filament consists of a strip of platinum gauze coated with an alkali-alumina-silicate spotwelded between the studs. Typical filament dimensions were 7 mm by 2 mm. The filament was normally kept at a current of 5 amps, with a 2 volt RMS drop across it. The wattage requirement of the filament was then 10 watts (compared to 20 in the Searles-Dzidic system).

Two cylindrical electrodes are also attached to the plate. They are isolated from one another and the ion source by a ceramic block, which is bolted to the plate. The electrodes not only can be used to focus the alkali ion beam into the reaction chamber, but also cut down on the direct radiation of the reaction chamber by the filament. Three mm holes were bored into the top of each of the electrodes in order that the direct heat of the filament be kept away from the reaction chamber. The electrodes are

evenly spaced: the first being .75 cm from the second, and 1.5 cm from the reaction chamber.

The reaction chamber is approximately 9 mm in depth. Ions enter the chamber through a 2 mm hole. To ensure that it is a field free region, it is snugly fitted to the inside of the ion source cylinder. Two ports were bored into the chamber to allow the reactant gas to enter and to allow the pressure of the gas to be measured. The exit slit consists of two parallel razor blades spotwelded over a 1 mm hole in the exit slit plate. The slits used in the acetonitrile and amine experiments were 10 to 15 microns in width.

All metal parts of the ion source were constructed of stainless steel.

The reaction chamber and ion source block are kept at a constant voltage of 2000 volts. To focus the alkali ion beam into the ion source, the filament and the two electrodes are kept at a more positive voltage. The filament is normally kept at 2200 volts, the additional voltage being supplied from a 0-400 volt regulated power supply. The voltages on the two electrodes are varied using potentiometers until a maximum signal is recorded. Common operating voltages are shown in Figure 5. Different filaments required slightly different voltages.

The intensity of the ion beam at various electrodes can be measured by attaching a vacuum tube voltmeter to the electrodes. This was done in vacuum and with one torr water pressure to determine the efficiency of the electrode system

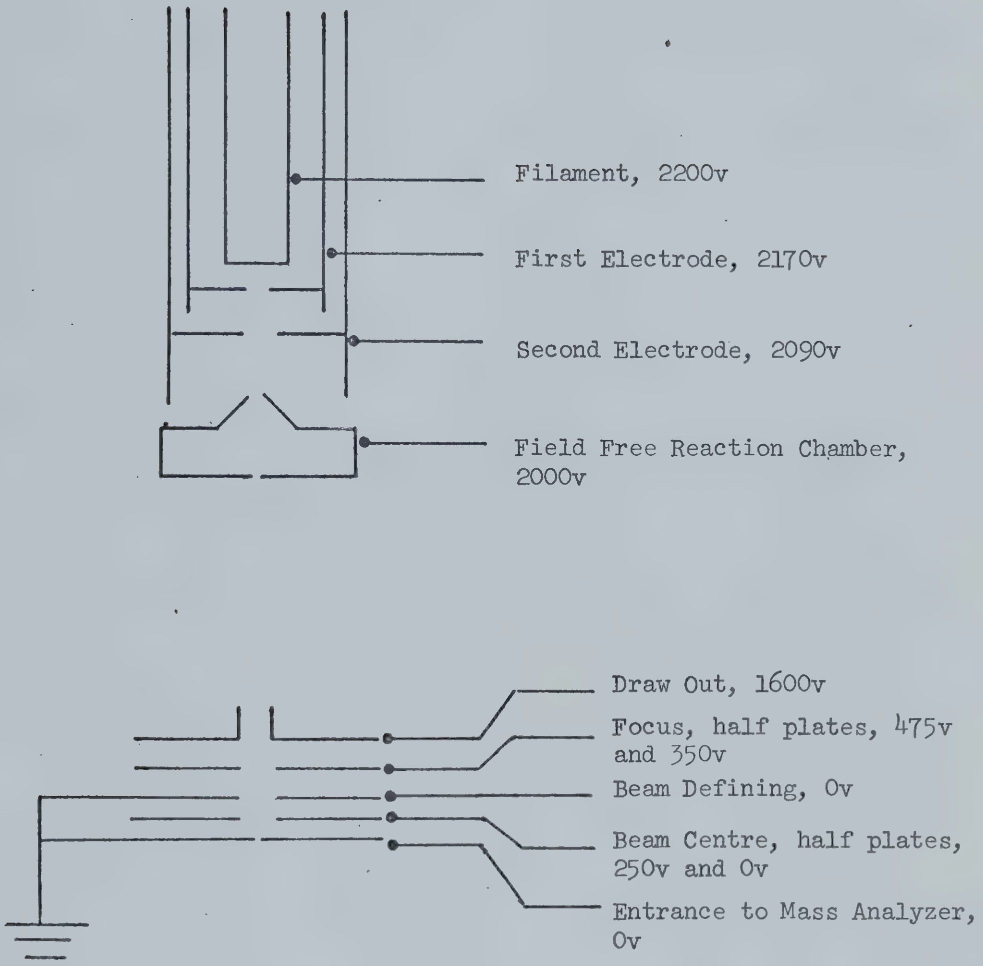
Filament, 2200v
First Electrode, 2170v
Second Electrode, 2090v
Field Free Reaction Chamber, 2000v
Draw Out, 1600v
Focus, half plates, 475v and 350v
Beam Defining, 0v
Beam Centre, half plates, 250v and 0v
Entrance to Mass Analyzer, 0v

FIGURE 5 Normal Operating Voltages

and the effect of reactant gases on the ion beam. The addition of water cooled the filament and more power was required to obtain the same ion emission. Table 1 shows the currents measured at the entrance to the reaction chamber and after the exit slit for both the vacuum case and with one torr water. When the current was being measured on the first acceleration plate, the focus plates (Figure 5) were kept at a more positive voltage in order that ions did not penetrate the first plate. Table 1 demonstrates that the loss of ion signal in the field free region is a factor of $5 \times 10^6$ with one torr water pressure compared to a factor of 300 in vacuum where there is no diffusion but just spreading of the beam. Geometrically, the area of the entrance hole to the field free region is 3.14 $mm^2$ and the area of the slit is $1.5 \times 10^{-2}$ $mm^2$, the ratio of the two being a factor of 200.

## 2.4 The Thermionic Source

The alkali-alumina-silicate filament used as a source of alkali ions has many advantages over the Kunsman source previously used for alkali ion-water solvation studies. Because the filament is enclosed in the same housing as the reaction chamber, it tends to heat the chamber. The alumina-silicate filament can be operated at lower wattages than the Kunsman source and this heating effect can then be reduced. Also, it was found that the filament would have to be turned on several hours before an experimental run in order that the temperature of the reaction chamber reach equilibrium. In order to make more than one run a day, it

## TABLE 1

## Ion Currents at Various Plates

| | Vacuum | One Torr Water | Current in Vacuo / Current with 1 Torr Water |
|---|---|---|---|
| Emission | $4.4 \times 10^{-6}$ amps | $4.6 \times 10^{-6}$ amps | 1.0 |
| Current at reaction chamber | $4.5 \times 10^{-7}$ | $1.5 \times 10^{-8}$ | 3.0 |
| Current at first acceleration plate | $1.5 \times 10^{-9}$ | $<3 \times 10^{-14}$ | $>5 \times 10^{4}$ |
| Loss to reaction chamber | factor of 10 | 30 | |
| Loss to first acceleration plate | 3,000 | $>1.5 \times 10^{8}$ | |
| Loss in reaction chamber | 300 | $>5 \times 10^{6}$ | |

was necessary to leave the filament on continuously. The Kunsman filament has an effective lifetime of 100 hours (75), whereas the alkali-alumina-silicate filament has a lifetime of over 300 hours in most cases. This meant the filament had to be changed less often. In the Kunsman case, the salts were fused on a platinum ribbon. This required great care, since the melting point of the salt mixture is just below that of platinum. The filament then had to be reduced in hydrogen, which made the whole procedure time-consuming. The manufacturing of the alumina-silicate filament is a much more simple process. In this case, the alkali-alumina-silicate is just painted on platinum gauze using water as a base. It was also found that the interior of the ion source was kept much cleaner when using the alumina-silicate source.

The alkali-alumina-silicate was prepared following the method of Blewett and Jones (76). The final salt has the formula $1R_2O : 1\ Al_2O_3 : 2SiO_2$, where R is the appropriate alkali ion. It is prepared by fusing the alkali carbonate, aluminum nitrate and pure powdered fused silica with a flame. The melts are powdered and re-melted twice. The final melt is again powdered and is ready for use. No attempts were made to find the salt composition having optimum emission properties.

As stated before, the major disadvantage of the ion source is the heating of the reaction chamber by the filament. When the filament is the only source of heat, the temperature of the chamber varies with the wattage of the filament. At

the normal operating current, i.e. 5 amps, the temperature of the reaction chamber is 107° C when only the filament acts as a source of heat. With a Kunsman filament, the reaction chamber heated up to about 130°.

## 2.5 The Gas Handling Plant

The gas handling plant used in this work was re-designed in order that it could be baked out. The new plant is shown in Figure 6. It consists of an inlet to which a needle valve is attached to control the pressure of reactant gas, a two-liter bulb which can be used to stabilize pressures, a cold finger, vacuum lines, lines to the ion source and the manometer, and various Hoke valves which can valve off certain sections of the plant when not in use. All these are contained in a marinite box which can be heated to 150° C for the purpose of baking out. The lines to the manometer and to the ion source are covered with heating tape so they can also be baked out.

An Atlas-Breman capacitance manometer was installed to replace the dibutyl-phthalate manometer used in previous studies. It was calibrated by using a dibutyl-phthalate manometer and a catheometer. The calibration was checked from time to time to ensure the accuracy of the pressure measurement. The reference side of the manometer is attached to the vacuum line and continuously pumped through a mercury diffusion pump.

In the ethylenediamine complexing experiments (Chapter 6), the pressures of ethylenediamine (abbreviated en) had to be

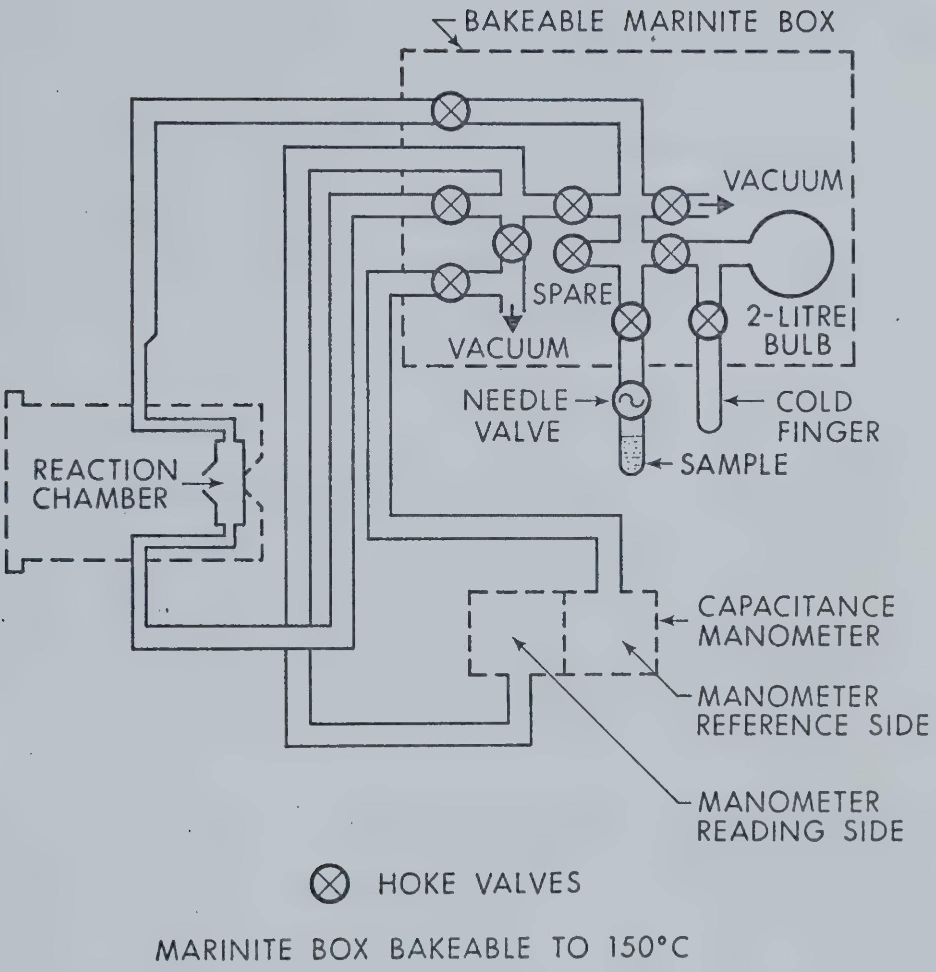
BAKEABLE MARINITE BOX
VACUUM
2-LITRE BULB
SPARE
VACUUM
NEEDLE VALVE
COLD FINGER
SAMPLE
REACTION CHAMBER
CAPACITANCE MANOMETER
MANOMETER REFERENCE SIDE
MANOMETER READING SIDE
⊗ HOKE VALVES
MARINITE BOX BAKEABLE TO 150°C

FIGURE 6 Gas Handling Plant

kept very low (20 - 150 microns) in order that the "stripping" phenomenon (section 2.8) did not affect the results. This required a special gas inlet system.

The pressure was controlled by heating (or cooling) a bulb containing ethylenediamine by means of a thermostatic bath. The bulb was separated from the ion source by a stainless steel capillary, 6/100" in diameter and 10 cm in length. The capillary, and the tubing between the capillary and the bath were heated to about 70 degrees C to prevent condensation of the vapors when the temperature of the bulb was greater than room temperature.

The flow through the capillary was viscous. This was shown by expanding air through the capillary from a known volume into another volume. In viscous flow, the number of moles flowing through a tube is (77):

$$n_M = \frac{\pi}{16\eta_T} \times \frac{a^4}{l} \times \frac{P_2^{\,2} - P_1^{\,2}}{RT} \qquad 2.1$$

where $n_M$ is the rate of flow through the tube in moles per second, $\eta_T$ is the viscosity of the gas at temperature T, a is the radius of the capillary in centimeters, l is the length of the tube in centimeters, $P_2$ and $P_1$ are the pressures at the two ends of the tube. By using high pressures of air and expanding into a vacuum $P_2 \gg P_1$ and the following equation will result:

$$\frac{dP_1}{dt} \propto P_2^{\,2} \qquad 2.2$$

Since $P_2$ will change negligibly, the pressure in the second bulb ($P_1$) will be:

$$P_1 = C \times t \qquad 2.3$$

where C is a constant taking into account the physical dimensions of the capillary, viscosity of air, temperature and the initial value of $P_2$. That the above relationship holds for the capillary can be shown by measuring the pressure in the second bulb as a function of time and obtaining a straight line. For the capillary in question, this is indeed the case as is shown in Figure 7.

Since the capillary is said to have viscous flow, and since the vapor pressure of ethylenediamine is known at various temperatures of the bath, $T_B$, the pressure of en in the ion source, P(en), will then be:

$$P(en) \propto P_V^2 \propto [\exp(-\Delta H_V/RT_B)]^2 \qquad 2.4$$

The proportionality constant was determined at high values of P(en) which could be read directly from the capacitance manometer. Figure 8 gives the variation of P(en) with the temperature of the bath.

In order that equilibrium be achieved, the carrier gas ($N_2$) was maintained at a pressure of two torr. The effect of the pressure of the third body is demonstrated in Figure 9. The pressure of ethylenediamine (20.7μ) was as low as usually used, so 2 torr was considered an adequate total

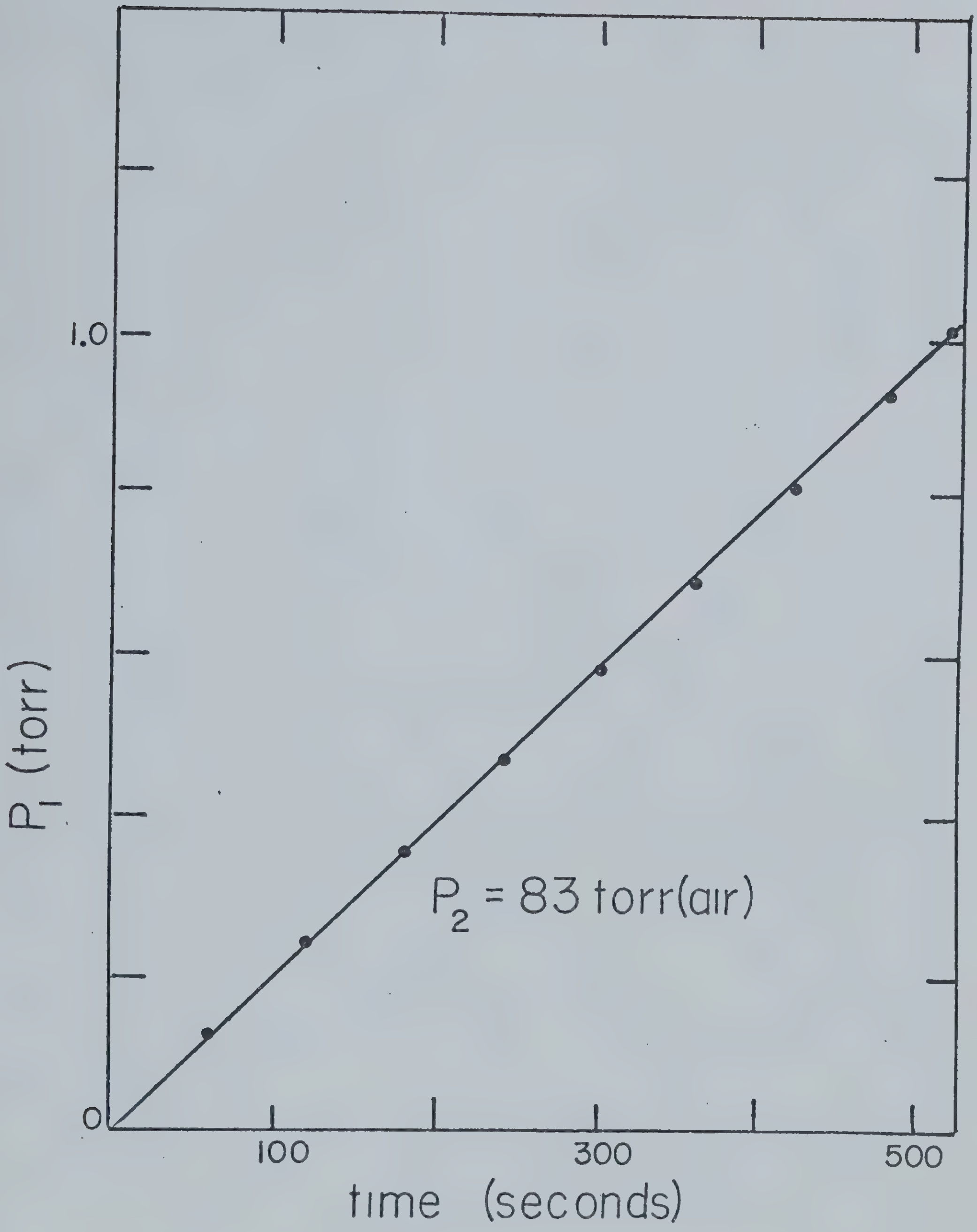

FIGURE 7 Calibration of Capillary Demonstrating Viscous Flow (see text).

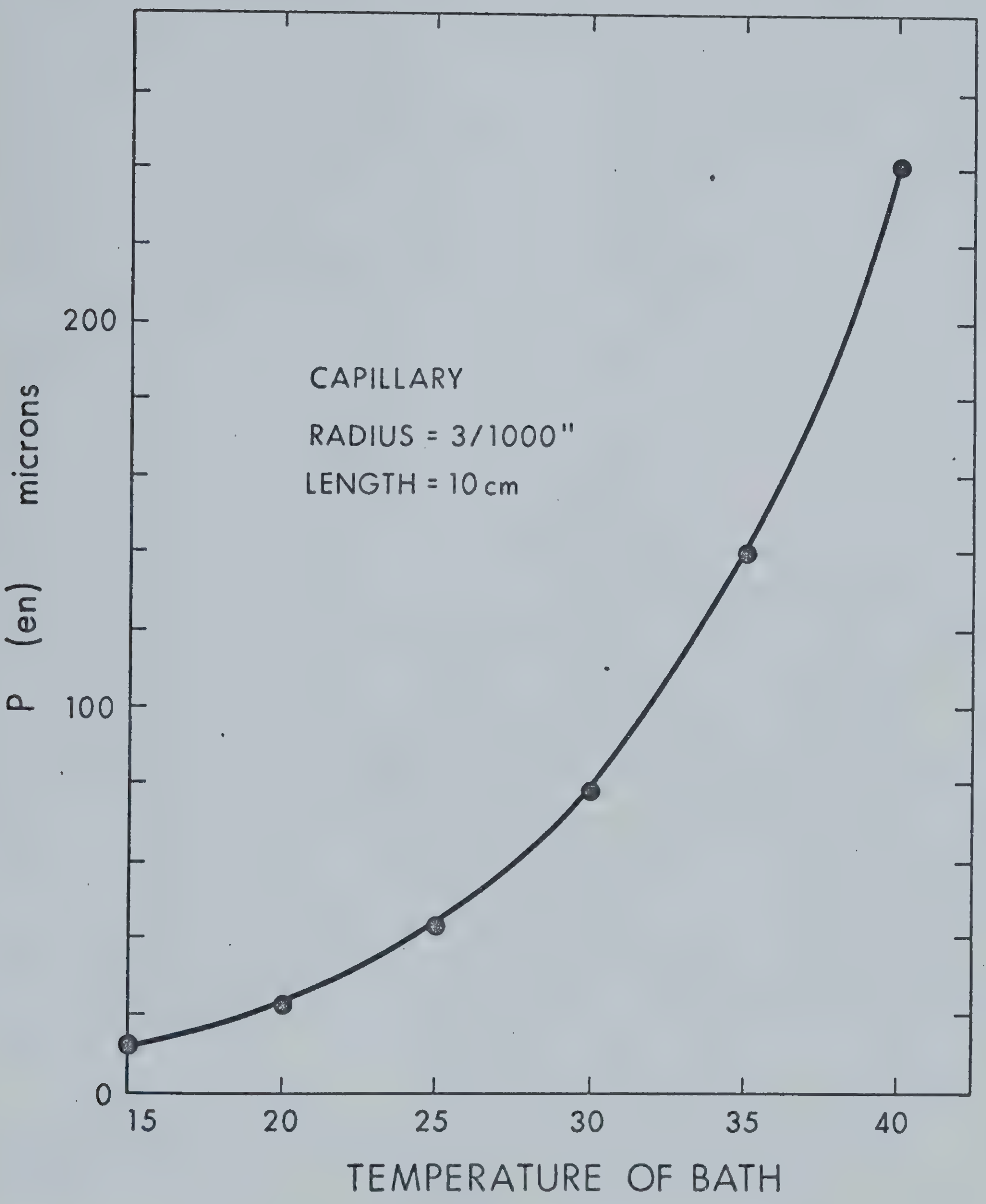

FIGURE 8 Pressure of Ethylenediamine in the Ion Source versus Bath Temperature.

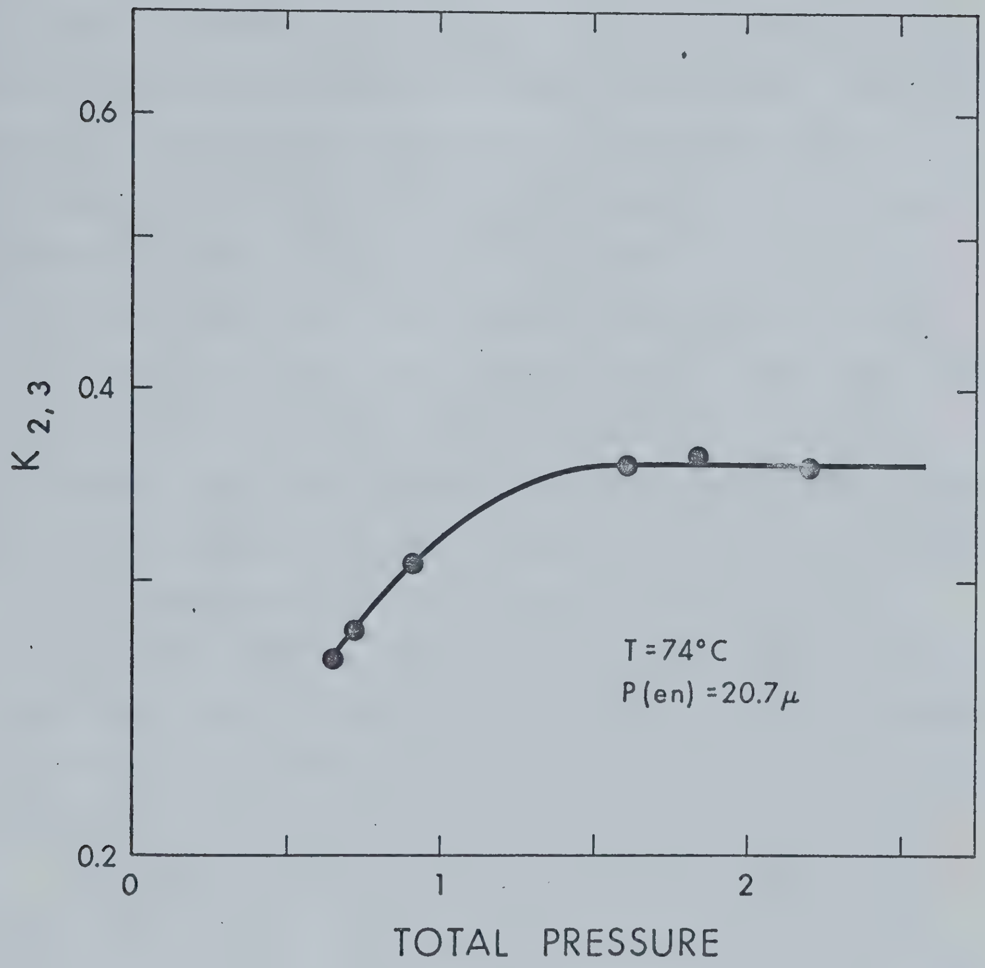

FIGURE 9 Effect of a Third Body on Equilibrium for the Reaction:

$$K^+(en)_2 + en \underset{N_2}{\rightleftarrows} K^+(en)_3 \quad .$$

pressure to maintain since signal intensities were too low at higher pressures, yet equilibrium appeared to be achieved.

## 2.6 Temperature Control

The reaction chamber temperatures above 100° C are achieved by using a stainless steel heat cylinder which fits around the ion source (Figure 4). The cylinder contains 12 holes and into each a two-holed ceramic rod is placed. Molybdenum wire, 0.010 inches in diameter is threaded through the rods with care being taken to assure that the wire is not in contact with the ion source. With this system, temperatures up to 450° C can be obtained with little difficulty. Above 450° alkali ions, mostly $K^+$, are formed from sources other than the filament. Probably this is due to direct emission from the ion source into the vacuum region. Ions created in vacuo and near the accelerating electrodes (Figure 4) are collected with greater efficiency. Therefore, even though the extraneous emission might be low, its effect is large and upsets equilibrium measurements.

For reaction chamber temperatures below 100° C, the heating cylinder is replaced with a copper/brass cooling system. The coolant, either water or methanol, circulates uniformly through the cylinder by a network of tubes bored into the block. For temperature regulation and circulation, a Calora-Ultra-Thermostat bath is used. To achieve temperatures from 30 - 100°, water is used as the coolant and for reaction chamber temperatures below 30 degrees, the bath is filled with methanol and cooled with a 4-liter

stainless steel beaker filled with dry ice. The greatest depth of beaker immersion in the bath allowed reaction chamber temperatures as low as -23° C. Because the filament always acts as a source of heat, the temperature of the reaction chamber is always greater than the temperature of the bath. For example, at a bath temperature of -53°, the coolest temperature which could be obtained by this method was -23 degrees. This difference becomes less as the temperature of the bath is raised.

The temperature of the reaction chamber is measured with an iron-constantan thermocouple. Since it was felt that one of the greatest experimental errors would be in temperature measurement, great care was taken in the construction of the thermocouple assembly. A 2 mm hole was drilled through the ion source and the inner part of the hole was plugged with silver to give the best possible thermal conduction. The thermocouple is made out of very fine wires, in order that there be no conductance of heat along the wires, and is threaded through a ceramic rod. The junction is sandwiched between the silver plug and a silver cap at the end of the tube holding the ceramic rod. A swagelok-type fitting can be hand-turned to make sure that the thermocouple is tightly sandwiched. The assembly is shown in Figure 10.

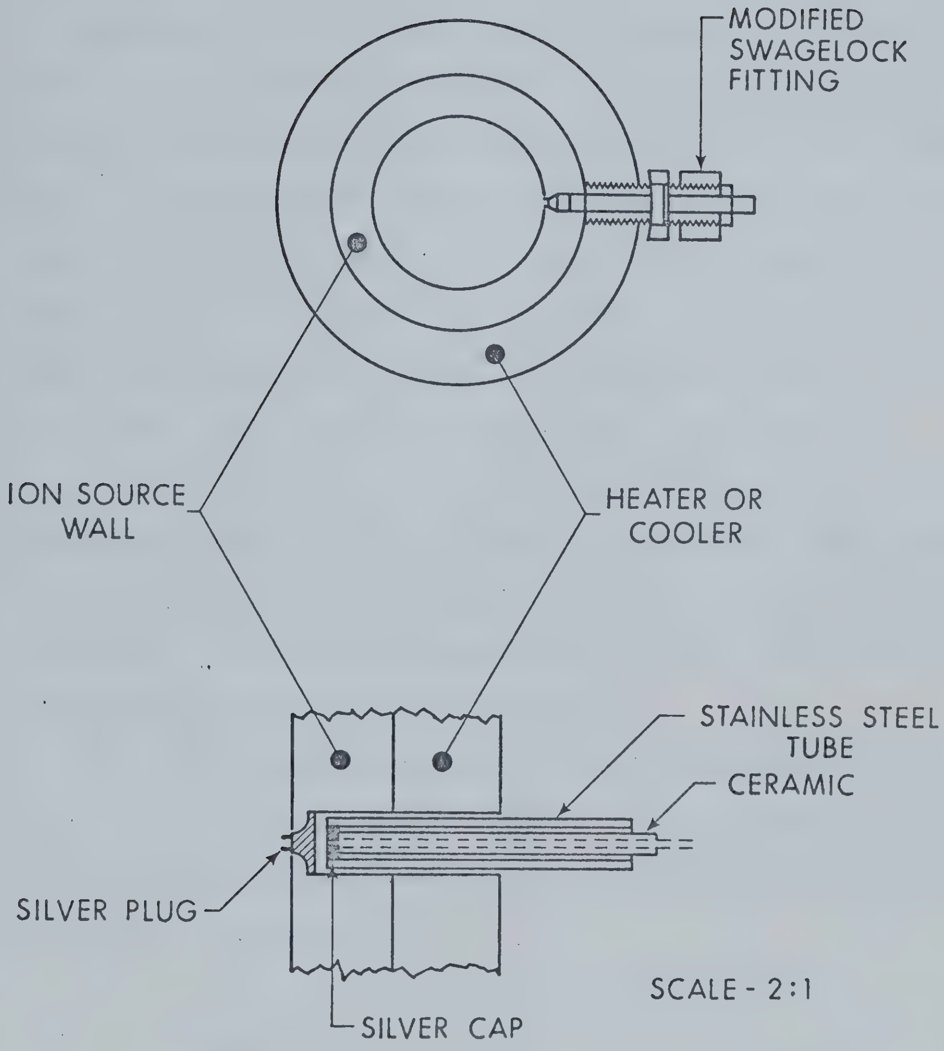
MODIFIED SWAGELOCK FITTING
ION SOURCE WALL
HEATER OR COOLER
STAINLESS STEEL TUBE
CERAMIC
SILVER PLUG
SCALE - 2:1
SILVER CAP

FIGURE 10 Thermocouple Assembly

## 2.7 Equilibrium Constants Versus Field Strength

After having been ejected from the filament, the ions come under the influence of an electric field which accelerates and focusses them into the reaction chamber. It was found in doing the drift studies that at the high electric field strength used between the filament and the reaction chamber (up to 200 volts/cm), most of the ions entering the reaction chamber are unclustered. The translational energy of these ions increases as the voltage increases, and in order to assure that this does not affect the equilibrium, checks were made by varying the field strength and seeing whether this affected the equilibrium constant. Figure 11 shows the result of such a check for 1.97 torr water pressure. The equilibrium constant remains constant over the total range and it therefore appears that there is no field effect on the equilibrium at these pressures.

However, when equilibrium is not being achieved, the field strength does have an effect. For example, at very low pressures of ethylenediamine (en), the equilibrium constant of the reaction:

$$K^+(en) + en \rightleftarrows K^+(en)_2 \qquad 2.5$$

is very dependent on the field, or more accurately, on the field strength divided by the pressure (E/p). Figure 12 demonstrates this for pressure of ethylenediamine of 30 microns and a total pressure of $N_2$ varying from 1 to 1.9 torr.

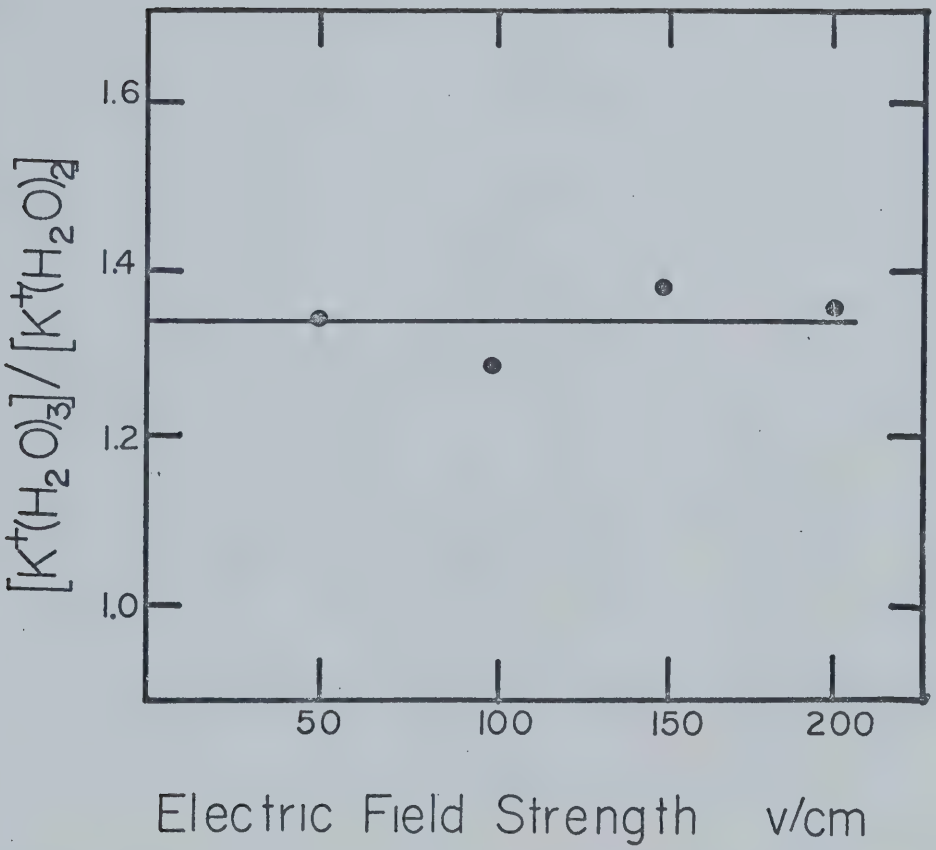

FIGURE 11 Plot of $K^+(H_2O)_2/K^+H_2O)$ versus Electric Field Used to Attract $K^+$ ions to the Equilibrium Chamber. Water pressure--1.97 torr, temperature -- 170 °C.

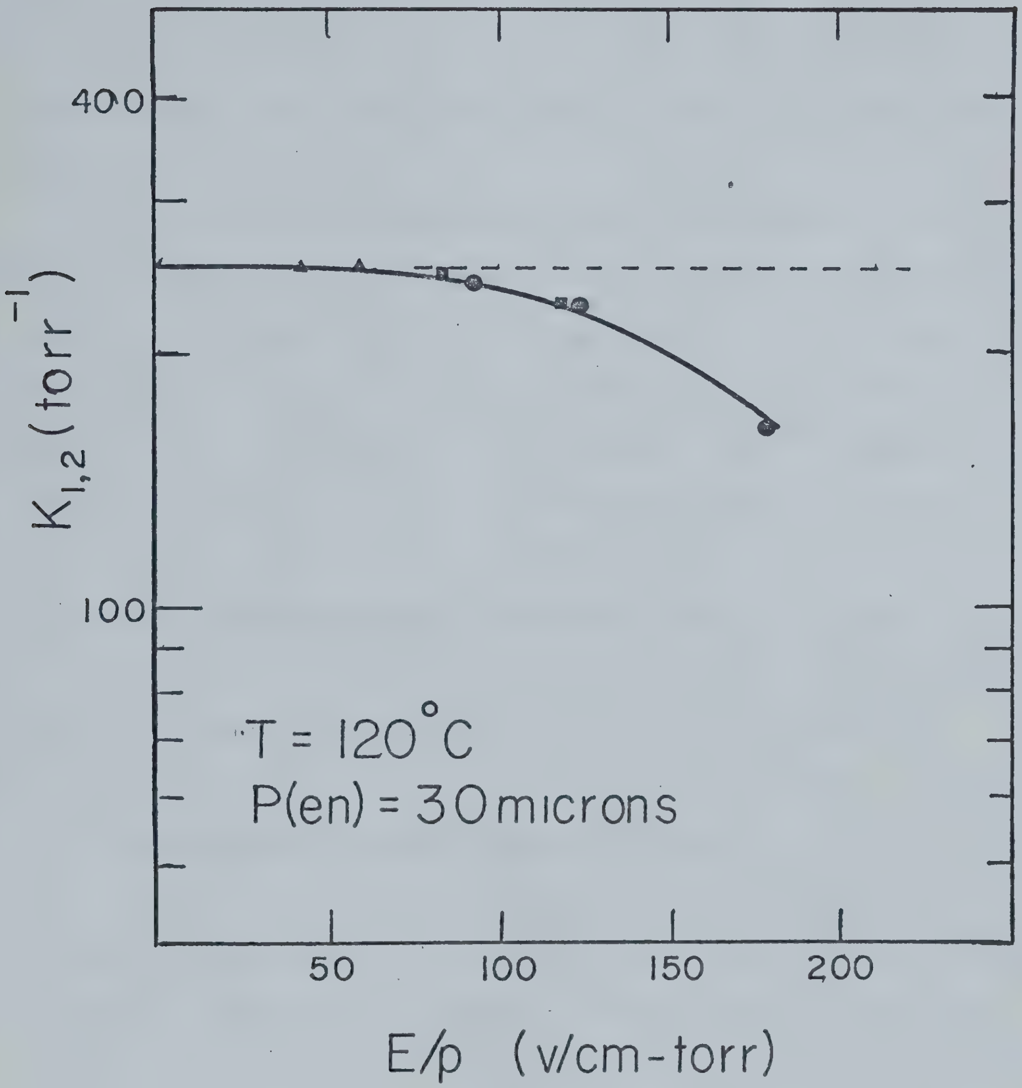

FIGURE 12 Effect of Field Strength on Equilibrium at Very Low Pressures for the Reaction:

$$K^+(en)_1 + en \underset{N_2}{\rightleftarrows} K^+(en)_2 .$$

● Voltage filament to reaction chamber = 270v

■ = 180v

▲ = 90v.

Dashed line indicates actual $K_{1,2}$ from Van't Hoff plot.

In such cases, the field strength was lowered or the total pressure raised until a constant ratio of ions occurred. If equilibrium was in doubt, a temporal study (Section 2.11)of the reaction was made. The total pressure was maintained at about 2 torr.

When doing the experiments with acetonitrile, pressures as low as 0.2 torr were often used. In these low pressure cases, the danger of field strength upsetting the equilibrium existed, but the equilibrium constant did not appear to be bothered by the strength of the field. This is shown in Figure 13 for the $Rb^+$-acetonitrile 1,2-reaction. However, when low pressures of any reactant gas were used, such a check was always made and in certain cases the field strength had to be lowered at low pressures to extend the pressure range at which equilibrium could be measured.

## 2.8 Equilibrium Constants Versus Pressure

If the reaction being studied is at equilibrium, a change in pressure should not affect the equilibrium constant. At every temperature at which a reaction was studied, the pressure was varied and it was found to be constant over a certain pressure range. Acetonitrile was found to cluster quite readily and for the $K_{1,2}$, $K_{2,3}$, etc., equilibrium was achieved at pressures as low as 0.16 torr. Pressures below this were difficult to determine accurately. For the $K_{0,1}$ reactions, the lowest pressures at which equilibrium appeared to be achieved was 0.3 torr. As the pressures became larger, however, the equilibrium constants began to

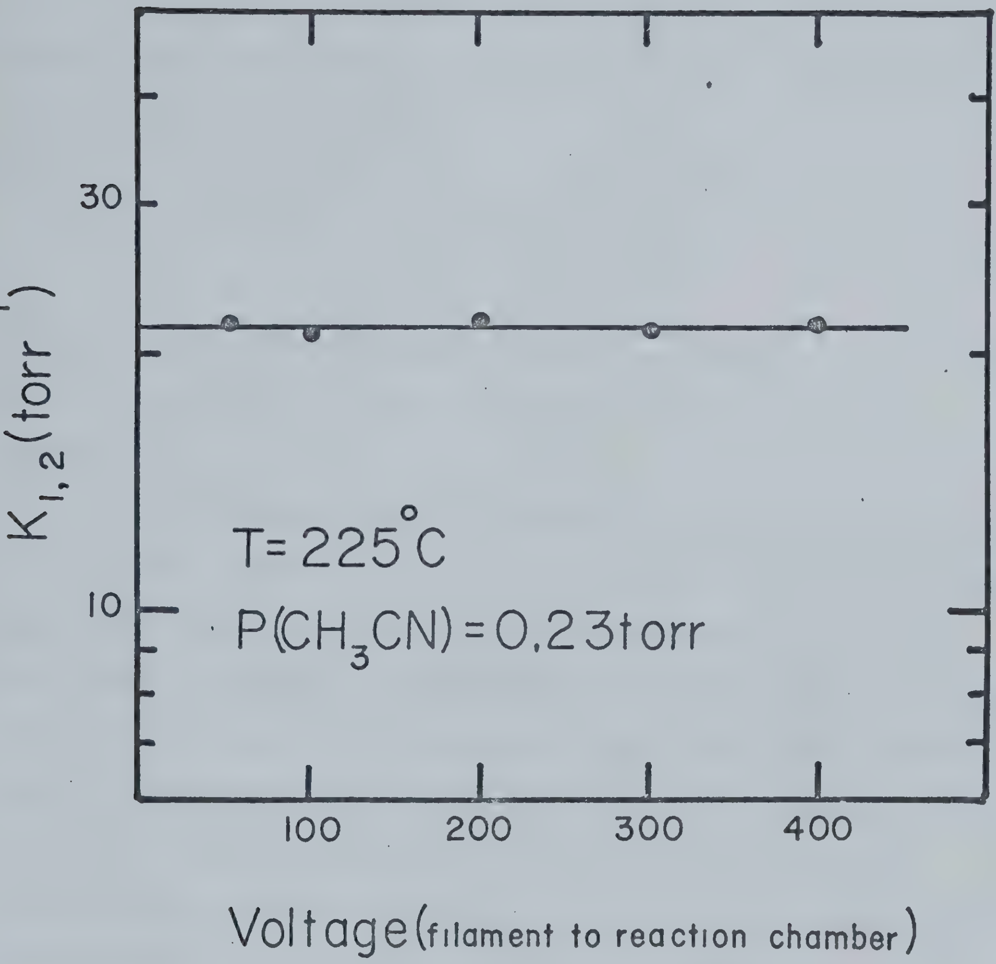

FIGURE 13 Effect of Voltage Between the Filament and the Reaction Chamber at Low Pressure for the Reaction:

$$Rb^+(CH_3CN) + CH_3CN \rightleftharpoons Rb^+(CH_3CN)_2 \ .$$

drop off quite rapidly. This had also been the case in the water-alkali ion studies, but the drop occurred at higher reaction chamber pressures and was not as rapid. Figure 14 shows the variation of the equilibrium constant with pressure beyond the range used to determine the "true" equilibrium constant for the reaction:

$$K^+(CH_3CN)_1 + CH_3CN \rightleftarrows K^+(CH_3CN)_2 \qquad 2.6$$

All the clustering reactions studied showed this effect but the rate of drop off varied widely, depending upon the reactant gas.

It was thought that this decrease was due to collisions taking place outside the reaction chamber in the area around the exit slit. It would have to occur quite close to the slit, since no shift in the peak location was noted, and the peak did not appear to be skewed to one side. This would occur if the collision took place in the acceleration region, since the lower mass ions would have varying energies. (Metastable peaks were noticed, but their intensities were much too small to account for the difference.)

If such a phenomenon is occuring, the equilibrium constant measured, K', will be:

$$K' = \frac{n_2 - \alpha n_2}{n_1 + \alpha n_2} \times \frac{1}{p} \qquad 2.7$$

where $n_1$ refers to the number of ions of lower mass, $n_2$ the number of ions at higher mass, p the pressure in the reaction

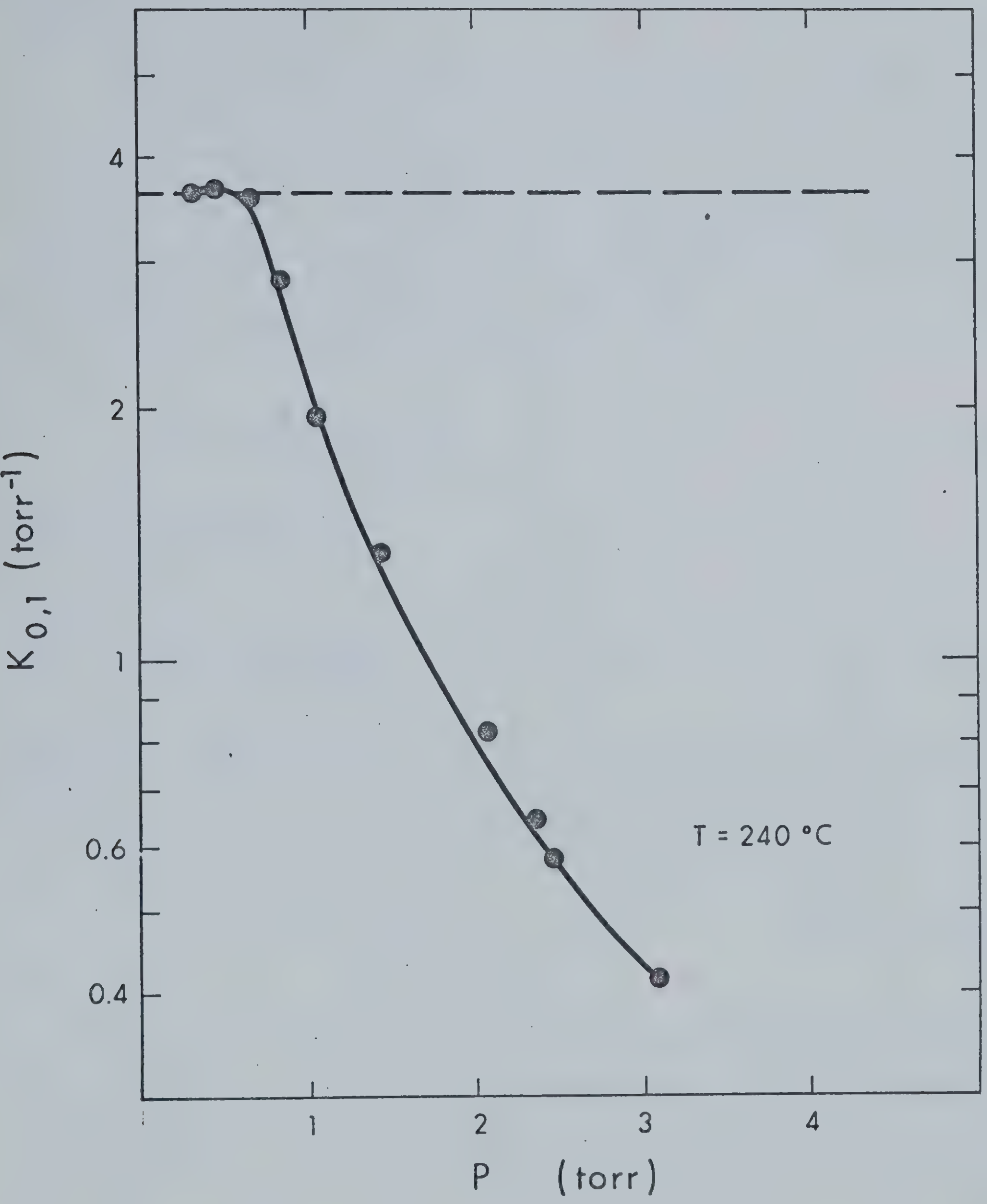

FIGURE 14 Variation of Equilibrium Constants with Pressure, at High Pressure, for the Reaction:

$$K^+(CH_3CN) + CH_3CN \rightleftarrows K^+(CH_3CN)_2 .$$

chamber and $\alpha$ is the fraction of the higher mass species which dissociates.

It can be shown that $\alpha$ is proportional to pressure. This is reasonable since the mean free path of the ion will be proportional to the pressure. This is done by using equation 2.7 and substituting the true equilibrium constant, K, into it. Thus, replacing $n_2$ with $n_1Kp$:

$$K' = \frac{n_1Kp\ (1 - \alpha)}{n_1(1 + \alpha Kp)} \qquad 2.8$$

which rearranges to:

$$\alpha = \frac{K - K'}{K + KK'p} \qquad 2.9$$

Setting $\alpha$ equal to S x p, where S is the "stripping coefficient":

$$S = \alpha/p = \frac{K - K'}{Kp + KK'p^2} \qquad 2.10$$

Using the data in Figure 14, and assuming K to be the value shown by the low pressure data, i.e. 3.6 (ss = 1 torr), the values of $\alpha$ at higher pressures may be determined. These are shown in Figure 15 as a function of pressure. There is a bit of scatter, but to a first approximation it would appear that $\alpha$ will indeed be proportional to pressure. The coefficient S, which in this case has the value 0.136 $\text{torr}^{-1}$, is a function of such things as collision cross sections, and bond strengths.

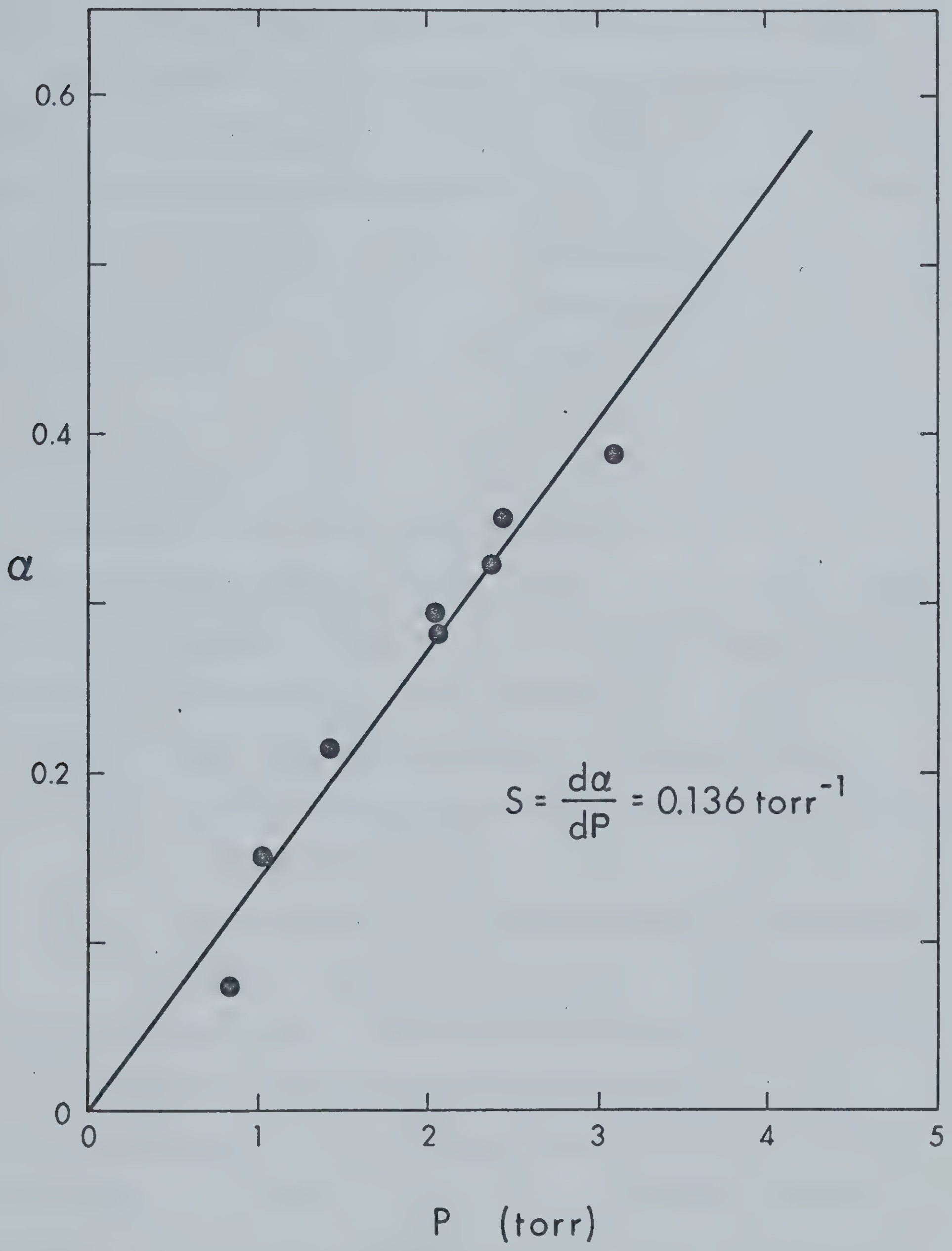

FIGURE 15 Fraction of Cluster Dissociation in the Vacuum Chamber versus Pressure in the Reaction Chamber for the Reaction:

$$K^+(CH_3CN) + CH_3CN \rightleftarrows K^+(CH_3CN)_2$$

at 240° C.

If $\alpha$ is proportional to pressure, the lower the pressure the smaller the fraction of the higher mass ion lost. This coupled with the lower relative intensity of the upper mass at lower pressures means that the measured equilibrium constant will be close to the true constants. However, even these low pressure readings will be in error at high values of K, or more precisely, at high $n_2/n_1$. For example, the 0.29 torr point in Figure 14, if corrected by the determined value of S, will be in error by 9%.

## 2.9 The Detection System

The ions, after mass analysis, were detected by a Bendix Spiraltron Electron Multiplier. The 17 stage copper-beryillium secondary electron multiplier used in the water studies was replaced for three reasons:

1) to allow the system to be pulsed,
2) to increase intensity due to the higher multiplication of the Spiraltron,
3) the Spiraltron is not affected by air as was the 17 stage multiplier and thus when replacing the filament, the multiplication capability of the electron multiplier is not affected.

The efficiency of the multiplier can be measured by determining the number of electrons striking it when no voltage is applied, and comparing that value to the number of ions counted when voltage is applied across the multiplier. Unfortunately, the ion intensities in the present study were too low to measure with no multiplication and such a comparison

could not be made. However, Potter and Mauersberger (78) did such a study with the Spiraltron electron multiplier and found that the efficiency asymtotically approaches 90% above a m/e of 40 (Figure 16). This means that in the present study, mass discrimination due to the electron multiplier was negligible since the lowest mass studied was $K^+$ (m/e = 39).

The electron multiplier is normally operated at -3000 volts according to the manufacturer's specifications. Further increase in this voltage does not affect the number of counts recorded, as shown in Figure 17. However, as the Spiraltron becomes older, the voltage has to be increased to keep it in a plateau region. When a voltage of -4000 v was applied and no plateau was reached, the electron multiplier was replaced with a new one.

The pulse amplifier is an EG&G model AN201/N quad amplifier which amplifies the negative output pulses of the electron multiplier by 64. The amplified signal is fed into an EG&G model T101 discriminator which rejects low level noise signals. The threshold of the discriminator is varied until the maximum signal to noise ratio is achieved. This varies with different electron multipliers but it was normally set at -200 to -300 millivolts. The noise level varied but was usually around 1 to 5 counts per second. The discriminated pulses are then fed into an Ortec model 441 ratemeter and model 431 scaler where they can be counted. The scaler is of tremendous value, since it allows small

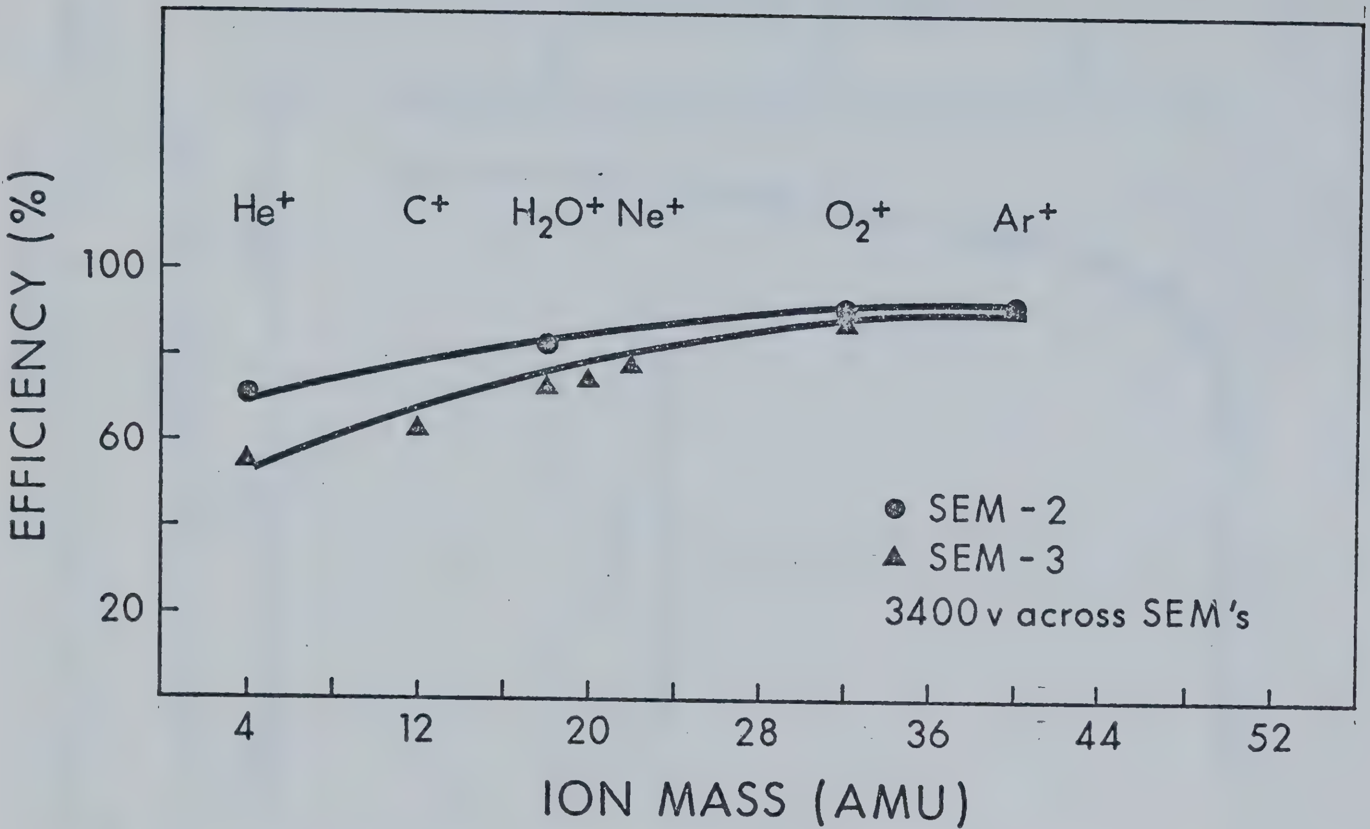

FIGURE 16 Percent Efficiency as a Function of Ion Mass for Two Spiraltron Electron Multipliers (from reference 78).

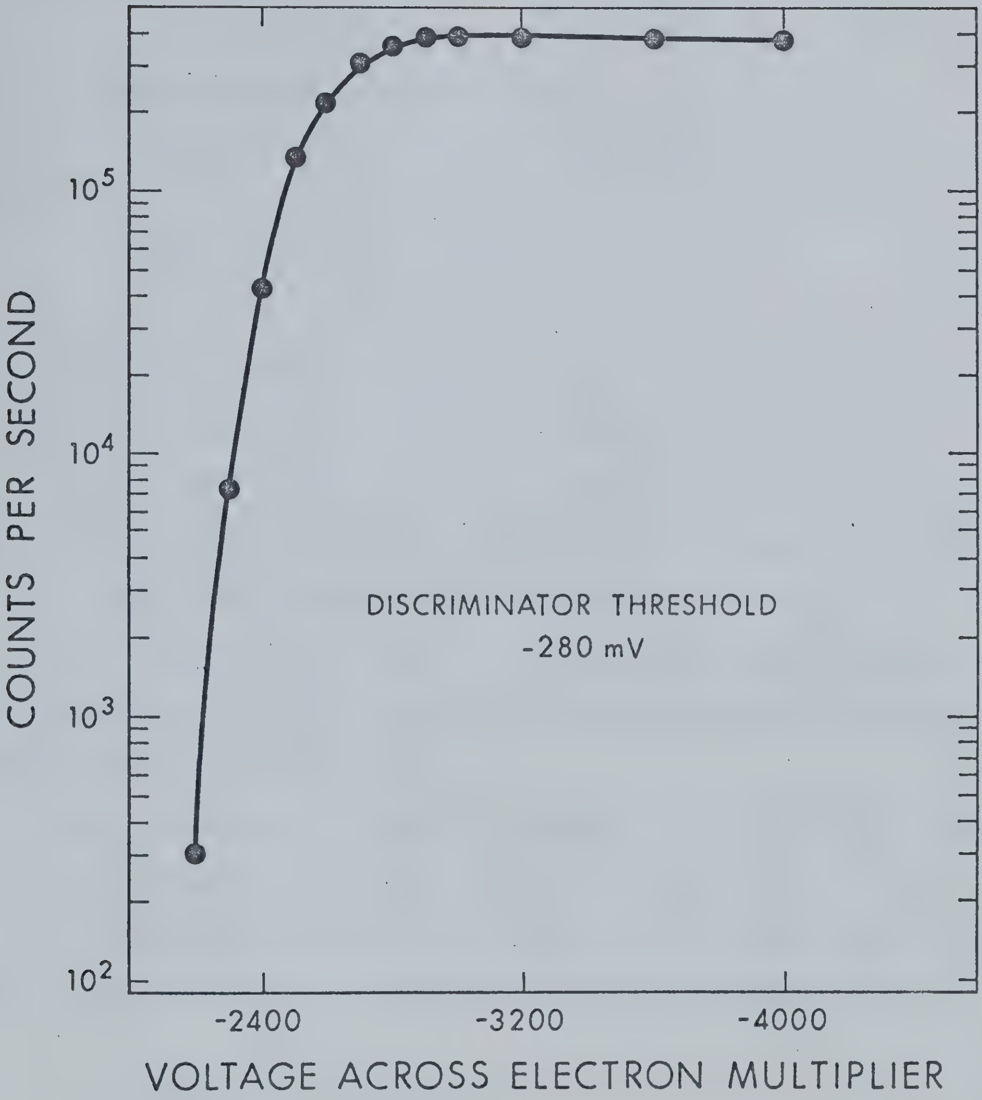

FIGURE 17 Counts per second versus Voltage Across Spiraltron Electron Multiplier.

signals to be counted for long periods of time. The noise level, if significant, is always subtracted from the total number of counts.

## 2.10 Comparison with Previous Data

The equilibrium constant for the reaction:

$$K^+ + (H_2O) \rightleftarrows K^+(H_2O) \qquad 2.12$$

was measured at various temperatures to see how the new ion source performed relative to the one used by Searles (74) and Dzidic (39). Figure 18 is a comparison of the Van't Hoff plot obtained with the new ion source compared to that of Searles. The thermodynamic properties are compared in Table 2. Theoretical calculations by Kistenmacher, Popkie, and Clementi (79) give the $\Delta H,_{0,1}$ for the potassium water reaction as -15.7 kcal/mole.

When the cooling jacket was placed around the ion source, another comparison was made at lower temperatures. Only two values were determined and they agreed within experimental error with the $K_{3,4}$'s obtained by Searles (Figure 19).

## 2.11 Time Dependent Studies

In order to ascertain whether or not two ions are in equilibrium, time dependent studies of a pulsed ion beam can be made.

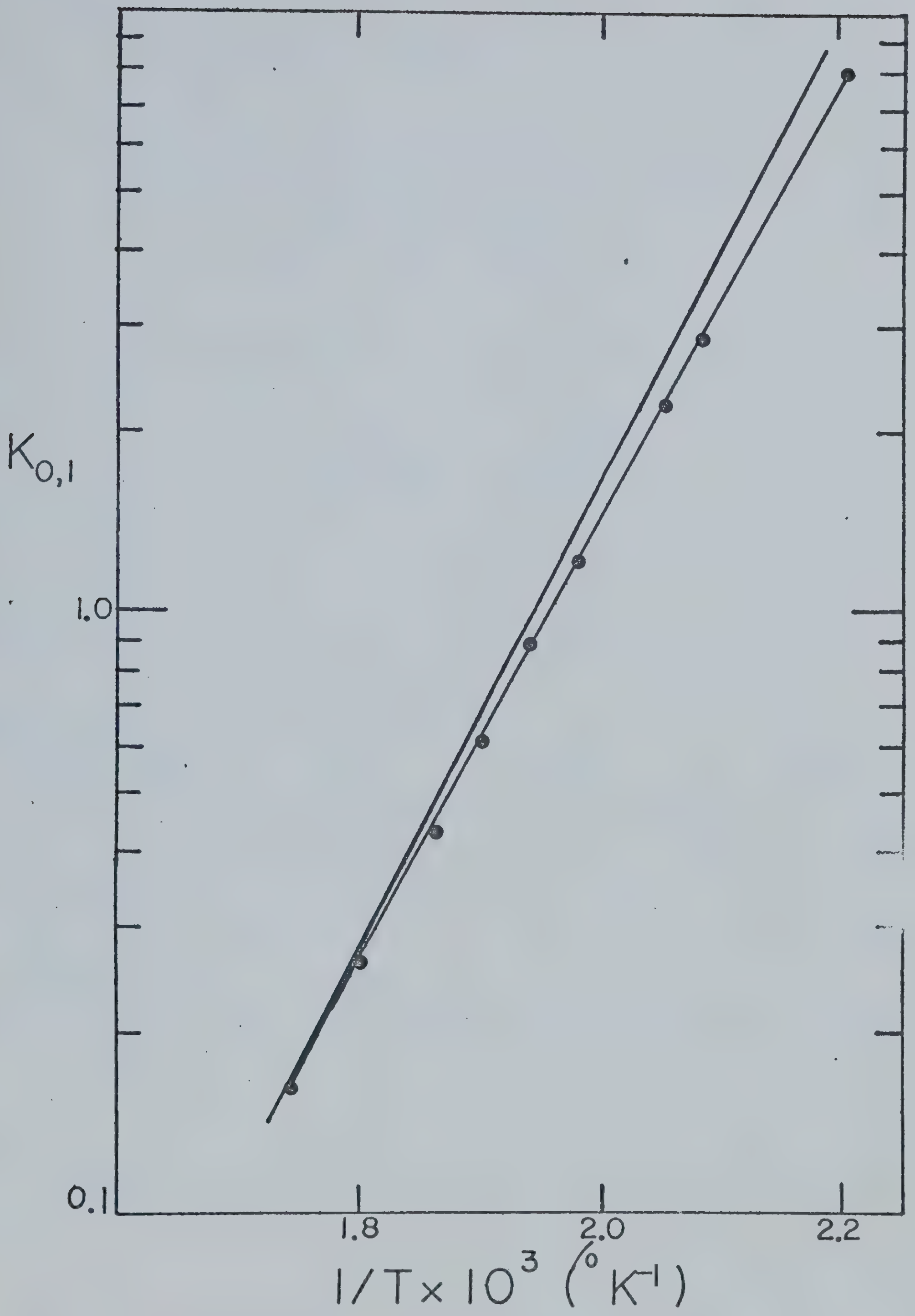

FIGURE 18 A Comparison of $K_{0,1}$ Obtained in this Study(line with points) with that of Searles (solid line) versus 1/T for the Reaction:

$$K^+ + H_2O = K^+(H_2O) \cdot$$

# TABLE 2

## A Comparison of the Thermodynamic Properties for the Reaction:

$$K^+ + H_2O \rightleftarrows K^+(H_2O)$$

| | $-\Delta H^o$ (kcal/mole) | $-\Delta G^o_{298}$ [a] (kcal/mole) | $-\Delta S^o$ [a] (kcal/mole) |
|---|---|---|---|
| This work | 16.9 | 11.0 | 19.9 |
| Searles and Kebarle (4) | 17.9 | 11.4 | 21.6 |
| Kistenmacher, Popkie and Clementi (79) | 15.7 | | |

[a] SS = 1 atm

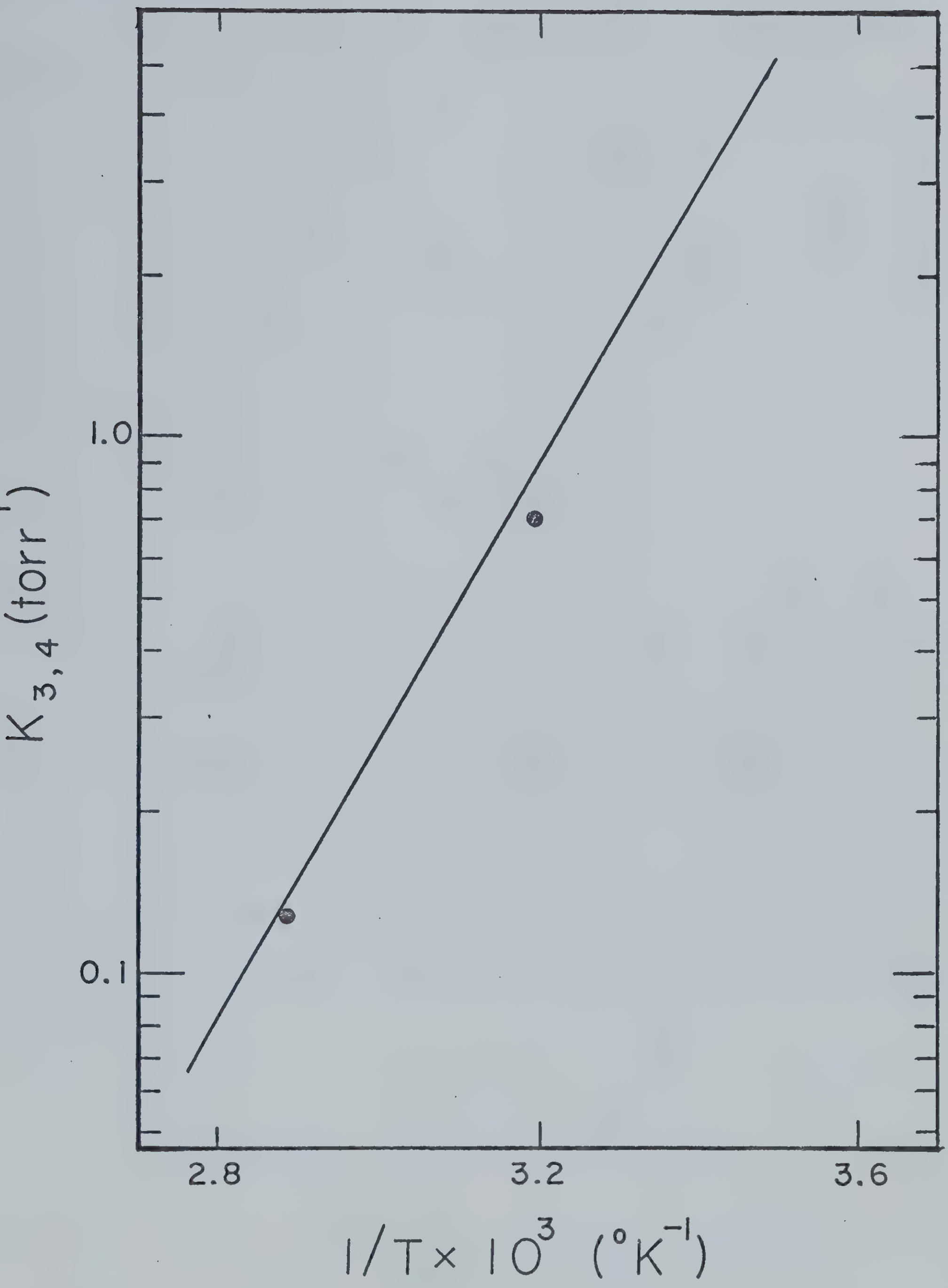

FIGURE 19 A Comparison of $K_{3,4}$ versus 1/T Obtained in This Study (circles) with Previous Results (solid line).

## A Pulse Network

Either of the two electrodes in the ion source can be pulsed to achieve a pulsed ion beam. In general, the electrode closest to the filament was pulsed so that a more uniform field would be set up in the "off" mode. Figure 20 shows the "on" and "off" voltages on the various electrodes in the ion source. The electrode was pulsed from 17 to 140 microseconds with a repetition time of from 1.3 to 3 milliseconds. In most studies, the ion intensities were so small that the widest pulse (140 microseconds) had to be used. Also, the repetition rate was increased to a maximum value such that the next pulse was set off very soon after the ion signal of the former pulse had decayed to a low value.

After mass analysis and detection, the output signal was fed into a multichannel scaler where a time dependent profile appeared. If two ions were in equilibrium in the nonpulsed mode, the ratio of their intensities at all times in the pulsed mode should remain the same, or the logs of their intensities should be parallel. Figure 21 shows a case in which the two ions are at all times in equilibrium for the reaction:

$$K^+(CH_3CN)_1 + CH_3CN \rightleftarrows K^+(CH_3CN)_2 \qquad 2.13$$

Figure 22 shows a case in which ions reach equilibrium only after the peak maximum for the reaction:

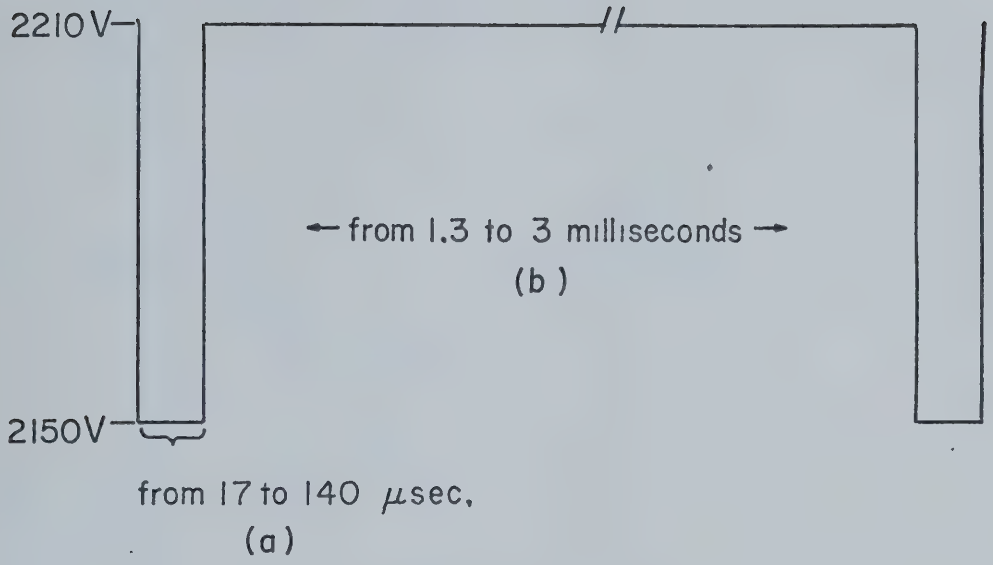
2210 V
2150 V
from 1.3 to 3 milliseconds
(b)
from 17 to 140 μsec.
(a)

(a) ions enter drift area and reaction chamber

(b) ions cannot pass first electrode

Voltages on Various Electrodes in Pulsing Experiments

| | during pulse (a) | after pulse (b) |
|---|---|---|
| Filament | 2200 v | 2200 v |
| First Elec. | 2150 | 2210 |
| Second Elec. | 2100 | 2100 |
| Reaction Chamb. | 2000 | 2000 |

FIGURE 20 Pulsing Sequence for the Study of the Temporal Behavior of Ions.

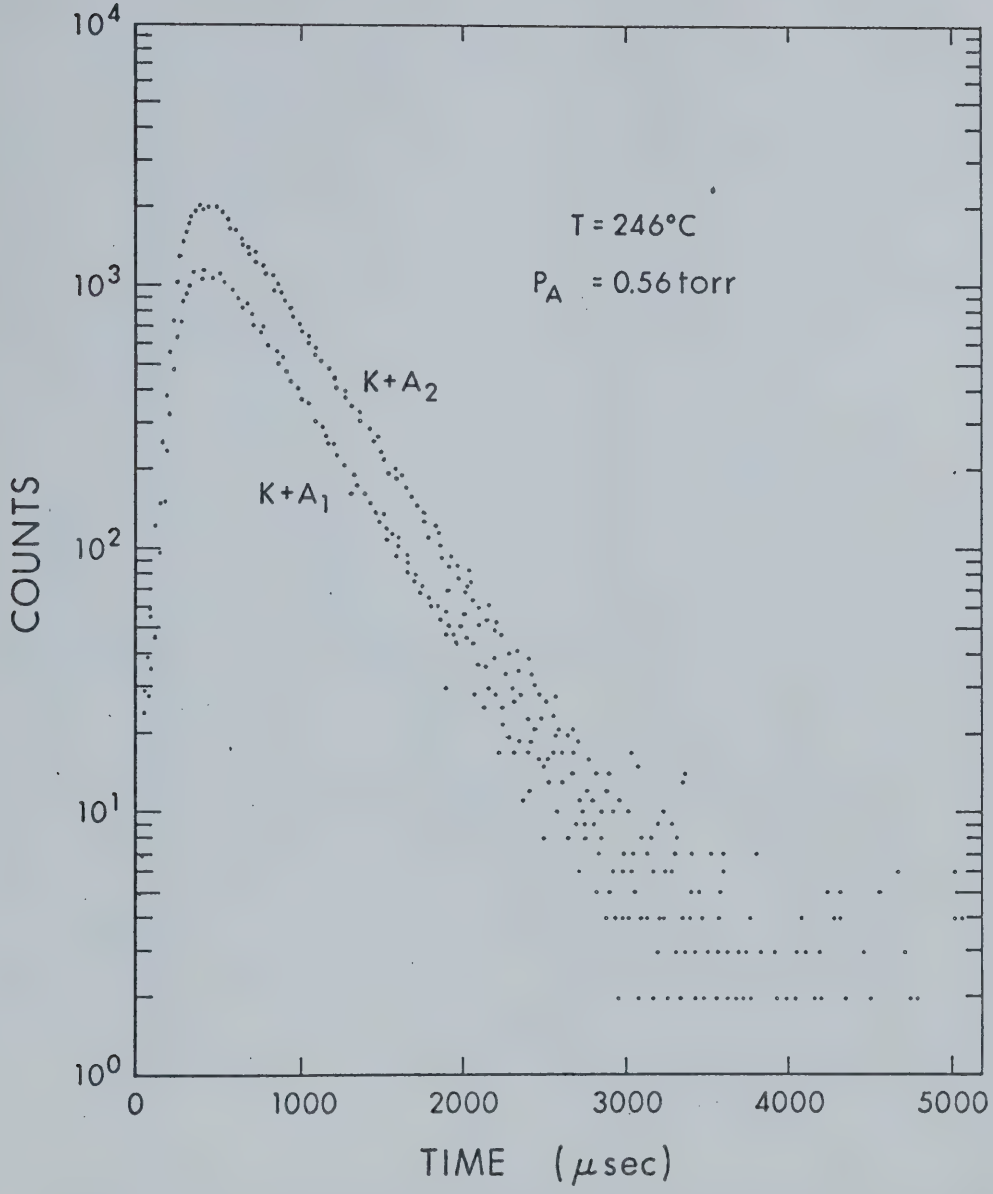

FIGURE 21 Time Dependent Output for the Reaction:

$$K^+(CH_3CN) + CH_3CN = K^+(CH_3CN)_2$$

Demonstrating the Rapid Achievement of Equilibrium at Low Pressure.

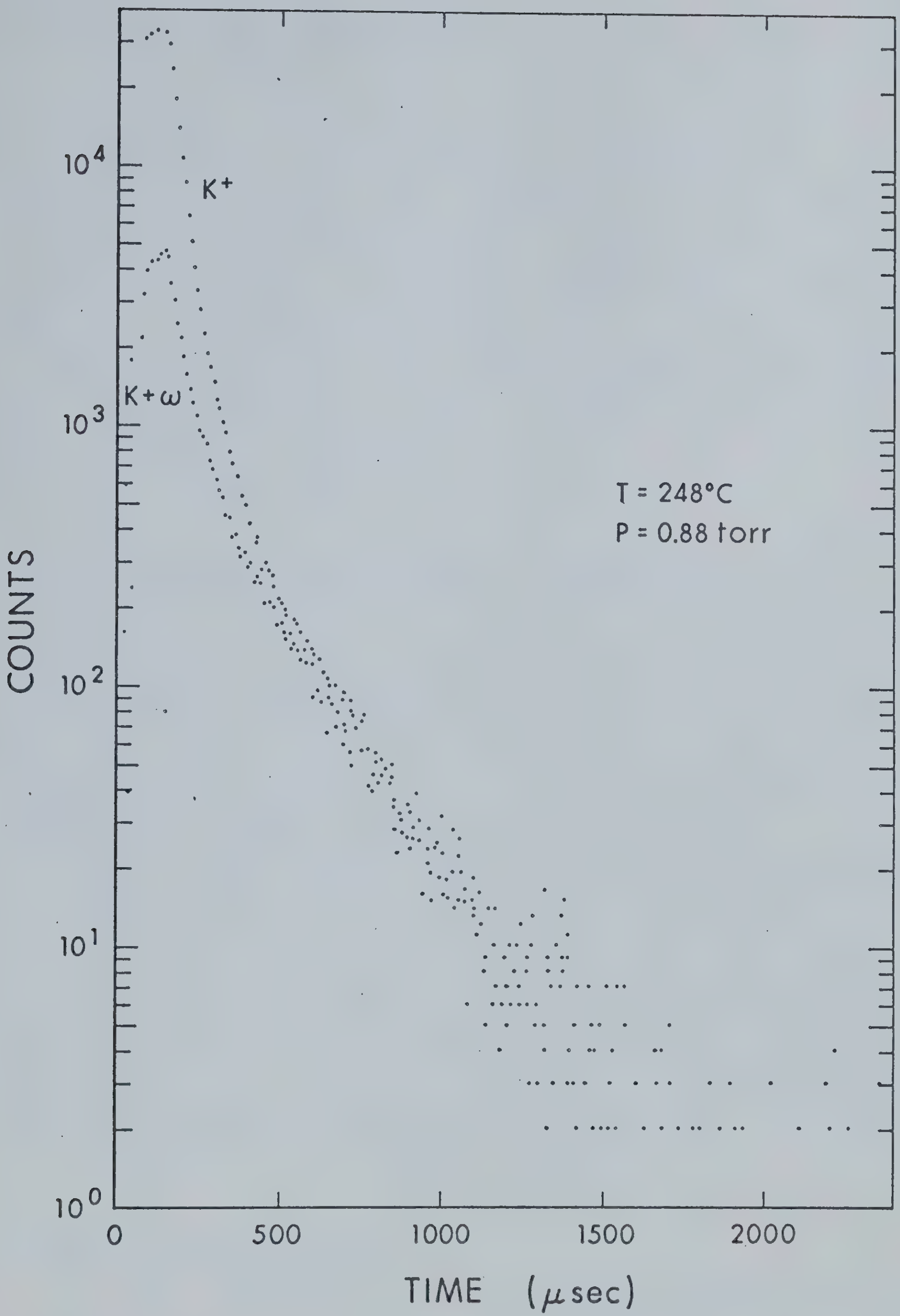

FIGURE 22 Time Dependent Output for the Reaction:

$$K^+ + H_2O = K^+(H_2O)$$

Showing Two Ions Approaching Equilibrium.

$$K^+ + H_2O \rightleftarrows K^+(H_2O) \qquad 2.14$$

The clustering of a water molecule on potassium is a relatively slow reaction (80) and thus equilibrium is not achieved rapidly at low pressures. A non-pulsed study of Figure 22 would give an equilibrium constant much lower than the true one. Thus by using a pulsed system, a wider pressure range can be used since it is not required that the ions reach equilibrium immediately.

### B Pulsed Versus Non-pulsed Equilibrium Constants

Figures 23 and 24 show the time dependent output signal for the reaction 2.14 at pressures of 1.66 and 3.0 torr. Both yield equilibrium constants of 0.85 torr$^{-1}$ at 250$^{o}$ C. The equilibrium constant for the non-pulsed case for reaction 2.14 was 0.76, which is within experimental error.

The agreement between pulsed and non-pulsed experiments was even better for reaction 2.13 as is shown in Table 3. From this table it can also be seen that the equilibrium constant is decreasing with pressure in both the pulsed and non-pulsed cases. Figure 21 shows the time dependent output for reaction 2.13 at 0.56 torr and 246$^{o}$ C.

### C Disadvantages to Pulsing

The major disadvantage to using a pulsing technique for all experiments is the low intensity of signal. Since the maximum pulse used was 140 microseconds and the repetition

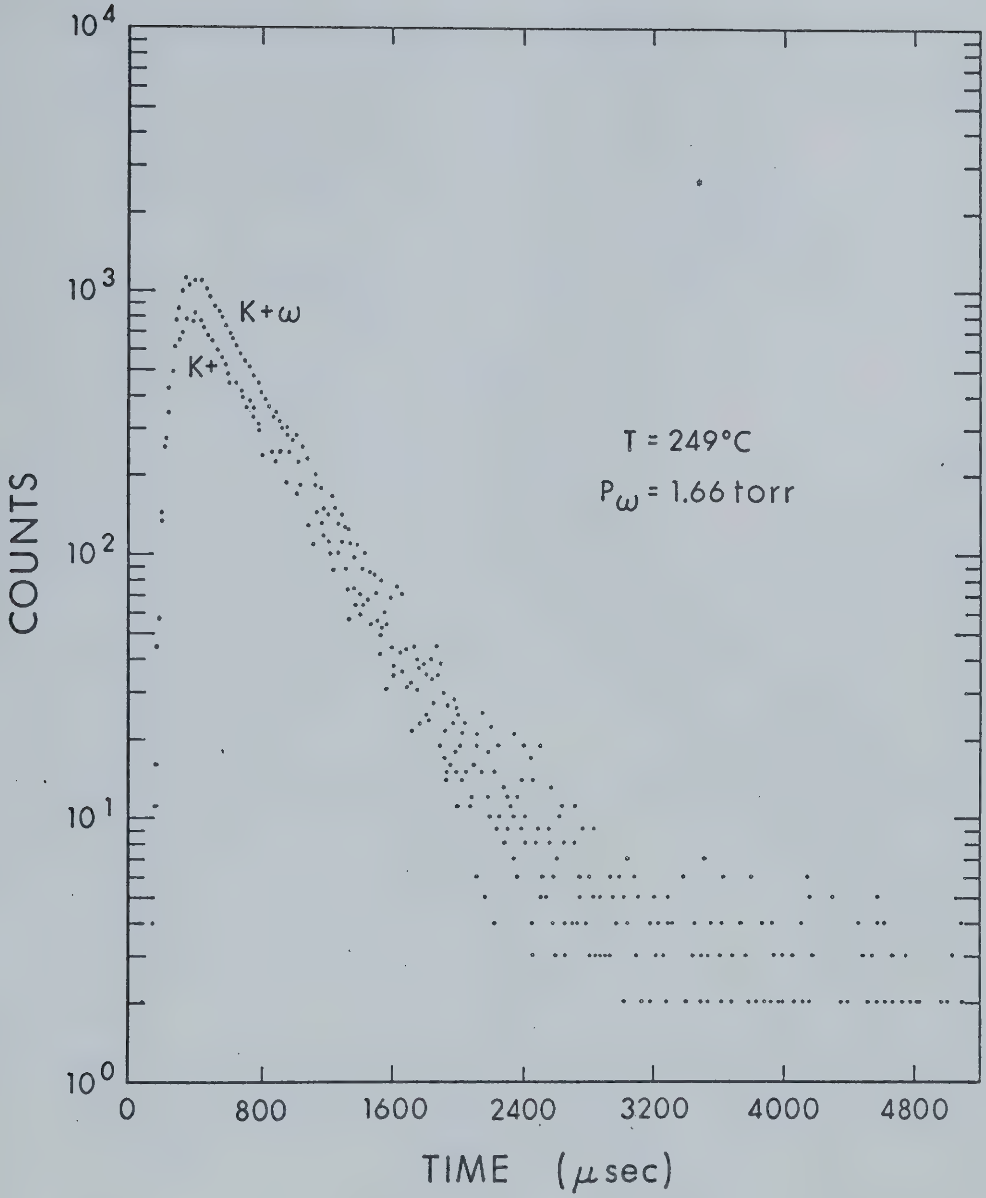

FIGURE 23 Time Dependent Output for the Reaction:

$$K^+ + H_2O = K^+(H_2O) .$$

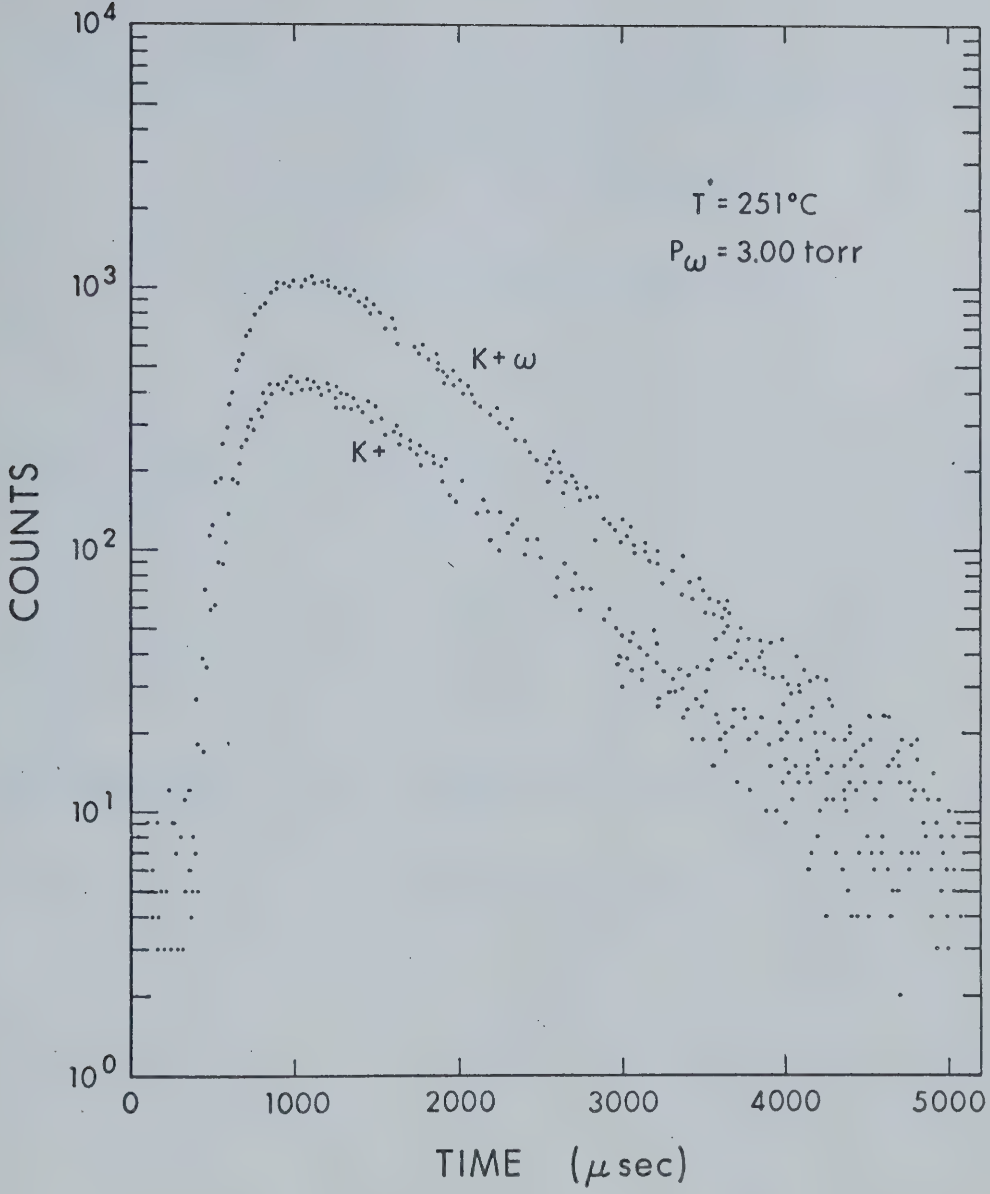

FIGURE 24 Time Dependent Output for the Reaction:

$$K^+ + H_2O = K^+(H_2O) .$$

## TABLE 3

## A Comparison of Pulsed and Non-Pulsed Equilibrium Constants for the Reaction:

$$K^+(CH_3CN) + CH_3CN \rightleftarrows K^+(CH_3CN)_2{}^{a}$$

## At Various Pressures of Acetonitrile

| Press (torr) | $K_{1,2}$ Pulsed[b] | $K_{1,2}$ Non-pulsed[b] |
|---|---|---|
| 1.16 | 2.32 | 2.29 |
| 1.18 | 2.10 | 2.29 |
| 0.56 | 3.17 | 3.15 |
| 0.56+0.64 Ar. | 2.55 | 2.78 |

[a] T = 246° C

[b] SS = 1 torr

time was normally 20 times that, the signal was cut down by at least a factor of 20. Also, this signal was distributed over many channels of the multichannel scaler which also lowered the intensity. Since the signal intensity was not large in the non-pulsed case, it was often negligible in the pulsed setup.

At the high temperatures needed for the potassium ion-acetonitrile $K_{0,1}$ study, the pulse system broke down due to shorting in the ion source. Because the $K_{0,1}$ was the only case in which equilibrium wasn't immediately reached at low pressures (0.2 torr), the pulsing technique was not necessary in the acetonitrile study.

In general, pulsed experiments were only undertaken if the achievement of equilibrium was in doubt.

## 2.11 The Drift Tube in Equilibrium Studies

### A Introduction

One manner of increasing signal intensity is to remove the field free region in the ion source, thus lowering the free diffusion of ions; (as pointed out earlier, the loss of signal in the field free region is approximately a factor of $10^5$ at one torr water pressure). The ion source then acts as a drift tube. Equilibrium studies have recently been carried out in drift tube mass spectrometers with success (81, 49).

In the present system, the lid of the reaction chamber

(Figure 4) was removed and the second electrode was extended as shown in Figure 25. This arrangement leads to a fairly uniform drift field. The first electrode was used as a gate which prevented ions from entering the drift space after an initial pulse. The second electrode was placed half way (1.25 cm) between the first electrode and the ion exit slit. The voltage difference between the exit slit and the first electrode could be varied, thus leading to different field strengths. The second electrode was maintained at a voltage of one-half the total drift voltage in order to keep the field uniform.

The basic pulse system is shown in Figure 26. In the "off" position, the ion burst is created and reaches the first electrode which is kept at the same voltage as the filament. The second electrode is at a more positive potential and the ions will not likely penetrate the drift space. However, the "location" of the ion burst at this time (i.e. during the "off" pulse) isn't known, and in this respect the gate is inadequate.

In the "on" position the first electrode is raised to a higher potential than the second electrode and the exit slit, creating a uniform drift field. The ions will then drift towards the exit slit. No other ions will pass the gate since it is now at a much higher potential than the filament. During drift tube experiments, no stray ions were observed - in this respect the gate was adequate.

After mass analysis the ion signal was detected,

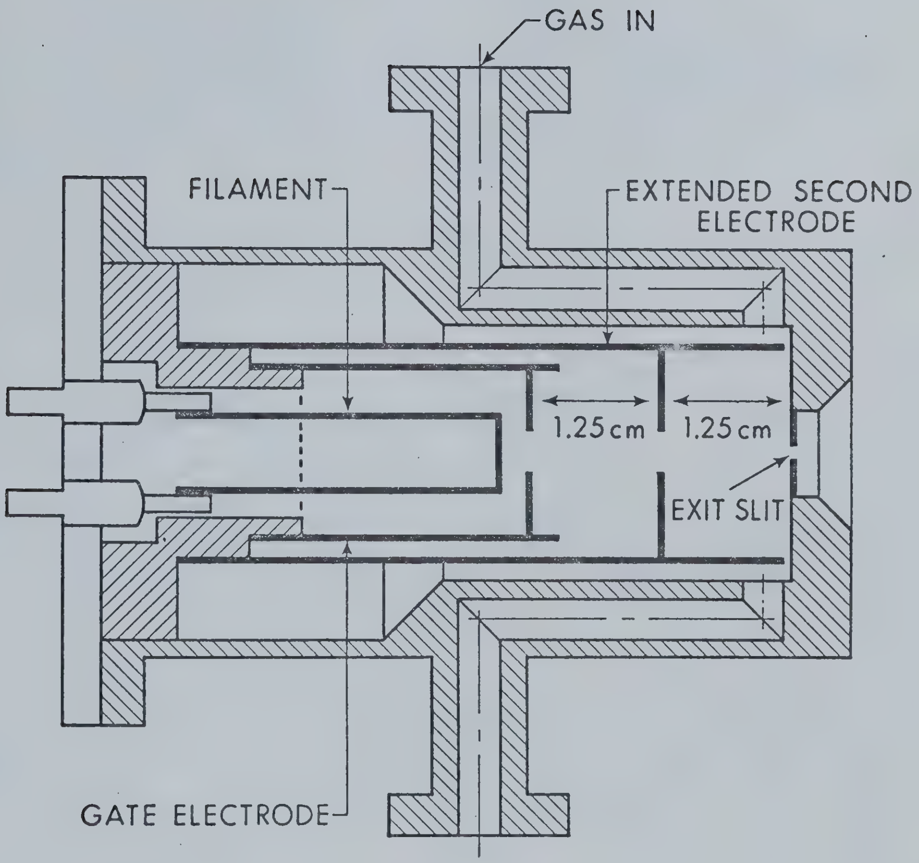
GAS IN
FILAMENT
EXTENDED SECOND ELECTRODE
1.25 cm
1.25 cm
EXIT SLIT
GATE ELECTRODE

FIGURE 25 . Cross-sectional View of the Drift Tube.

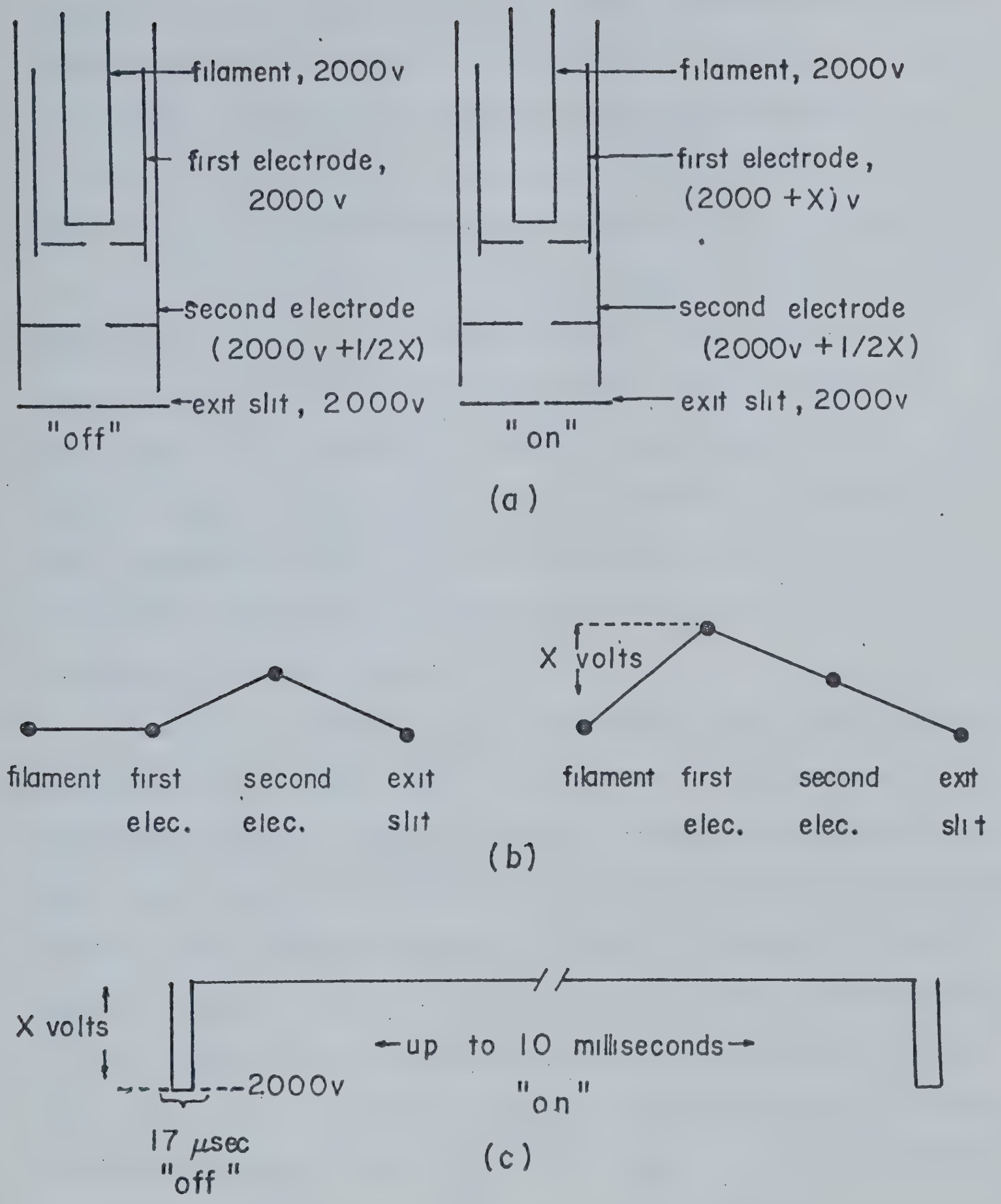
filament, 2000 v
first electrode, 2000 v
second electrode (2000 v + 1/2X)
exit slit, 2000v
"off"
filament, 2000 v
first electrode, (2000 + X) v
second electrode (2000v + 1/2X)
exit slit, 2000v
"on"
(a)
filament
first elec.
second elec.
exit slit
X volts
filament
first elec.
second elec.
exit slit
(b)
X volts
2000v
17 μsec
"off"
up to 10 milliseconds
"on"
(c)

FIGURE 26 Pulsing Scheme for Drift Tube Studies.

(a) voltages on the various electrodes in "off" and "on" positions

(b) electric field at various electrodes in "off" and "on" positions

(c) Pulse on first electrode in "off" position

amplified and fed into a Nuclear Data multichannel scaler, where the time dependent signal could be monitored. The peak could be integrated by also feeding the signal into a single channel scaler and the total ion intensity could be measured. It can be calculated that the time of flight of the ions in the low pressure mass analysis section corresponds to some 10 - 20 microseconds or less. Since the time the ions spend in the drift tube is much longer in most cases (milliseconds), the time that the ions spent in the ion source could be accurately assessed. For ions which spend less than 100 microseconds in the drift tube, there would be some error due to this time of flight through the mass analysis section.

The drift velocity, $v_d$, of the ions can be determined by dividing the time spent in the drift tube, by the distance the ions travel in the ion source, 2.50 cm. When in a drift tube, ions are accelerated by the field and thus gain kinetic energy. The electric force on an ion of charge e, is eE, where E is the electric field intensity. If it is assumed an ion loses all the energy acquired from the field in a collision with a neutral molecule, the velocity it obtains between collisions will be $eE\tau/m$, where $\tau$ is the mean free time (82). Since $\tau$ is inversely proportional to pressure, the velocity of an ion in the drift space is then proportional to E/p. The resultant energy gained by the ion due to the field is referred to as the "field energy" of the ion. When the field energy of the ion is small compared to thermal

energy, the drift velocity of the ion in the field direction is proportional to the field intensity. The field energy is said to be low (82) when

$$\left[\frac{M}{m} + \frac{m}{M}\right] eE\lambda \ll kT \qquad 2.15$$

where M and m are the molecular and ionic masses and $eE\lambda$ is the energy gained by the ion moving a distance $\lambda$ in the field direction. For an ion-neutral collision cross section of about 50 $\text{Å}^2$, the field energy is negligible compared to thermal energy if E/p is less than 2 volts/cm-torr (82).

At low field then:

$$Vd = \mu E \qquad 2.16$$

where the proportionality constant, $\mu$, is referred to as the mobility of the ion. $\mu$ varies inversely with the gas density and thus is a function of pressure and temperature, i.e., $\mu \propto T/p$. To standardize mobility data, a reduced mobility, $\mu_o$, is determined by reducing the experimentally obtained mobility to the standard conditions of $0^o$ C and one atmosphere pressure. Thus

$$\mu_o = \mu \times \frac{P}{760} \times \frac{273}{T} \qquad 2.17$$

where the pressure is in torr and the temperature in degrees Kelvin. If the drift velocity is measured in cm/second and the field strength is volts/cm, the mobility has units of $cm^2$/volt-sec.

## B Calibration of the Drift Tube

The mobilities of alkali ions in various gases are well known and in order to check that the drift tube was reliable, the mobility of potassium ions in argon was determined. This was done by pulsing the $K^+$ beam in the manner described above and collecting the output on the multichannel scaler (MCS). The average time an ion spent in the ion source was taken as the time of peak maximum minus the "off" pulse width (in most cases 18 microns). This was necessary since the MCS was triggered at the beginning of the "off" pulse, yet the drift tube was not operational until the "off" pulse was over, i.e. when the first electrode became more positive than the second electrode. Figure 27 shows typical output signals for $K^+$ in argon.

To determine the reduced mobility, the field strength, E, and the pressure, p, were varied. Since the drift velocity is proportional to only E/p at low E/p (82), at a constant temperature, the reduced mobility should remain constant. A plot of $\mu_o$ for $K^+$ in argon versus E/p is shown in Figure 28. The reduced mobility did indeed remain constant over the range of E/p covered. The average value of $\mu_o$ was 2.90 $cm^2$/volt-sec. compared to a value of 2.73 obtained recently by Keller (83) and 2.81 obtained by Tyndall (84). The slightly higher mobility is likely due to the lack of knowledge of the "location" of the ion burst, or to slight errors in the measurement of the drift tube length (.1 or .2 mm would account for the difference).

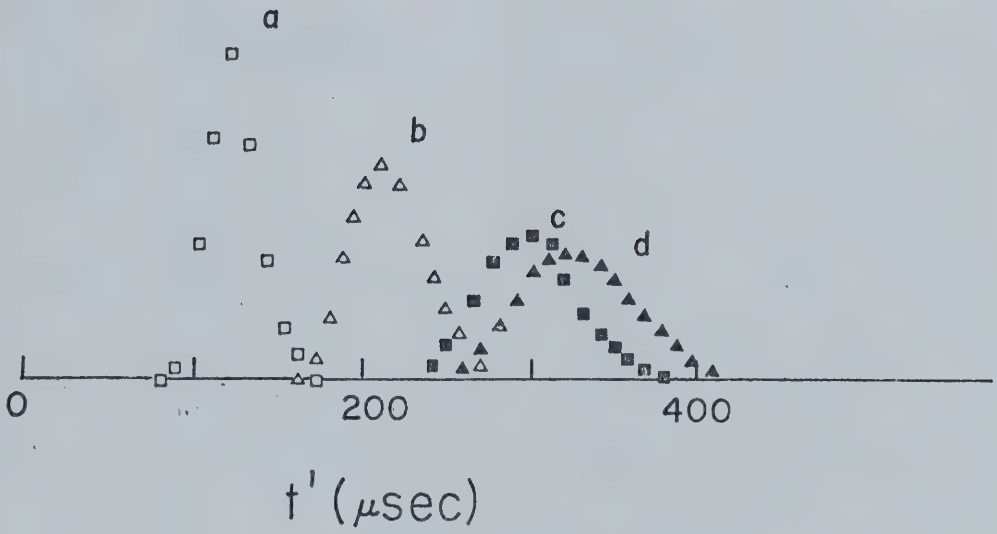

FIGURE 27 Drift Tube Output of the Potassium Ion in Argon at Various E/p.

| | p(torr) | t(μsec) | E/p(v/cm-torr) | $\mu_0$($cm^2$/v-sec) |
|---|---|---|---|---|
| a) | 0.75 | 103 | 8.37 | 2.74 |
| b) | 1.45 | 192 | 4.33 | 2.84 |
| c) | 2.13 | 277 | 2.94 | 2.90 |
| d) | 2.35 | 300 | 2.67 | 2.95 |

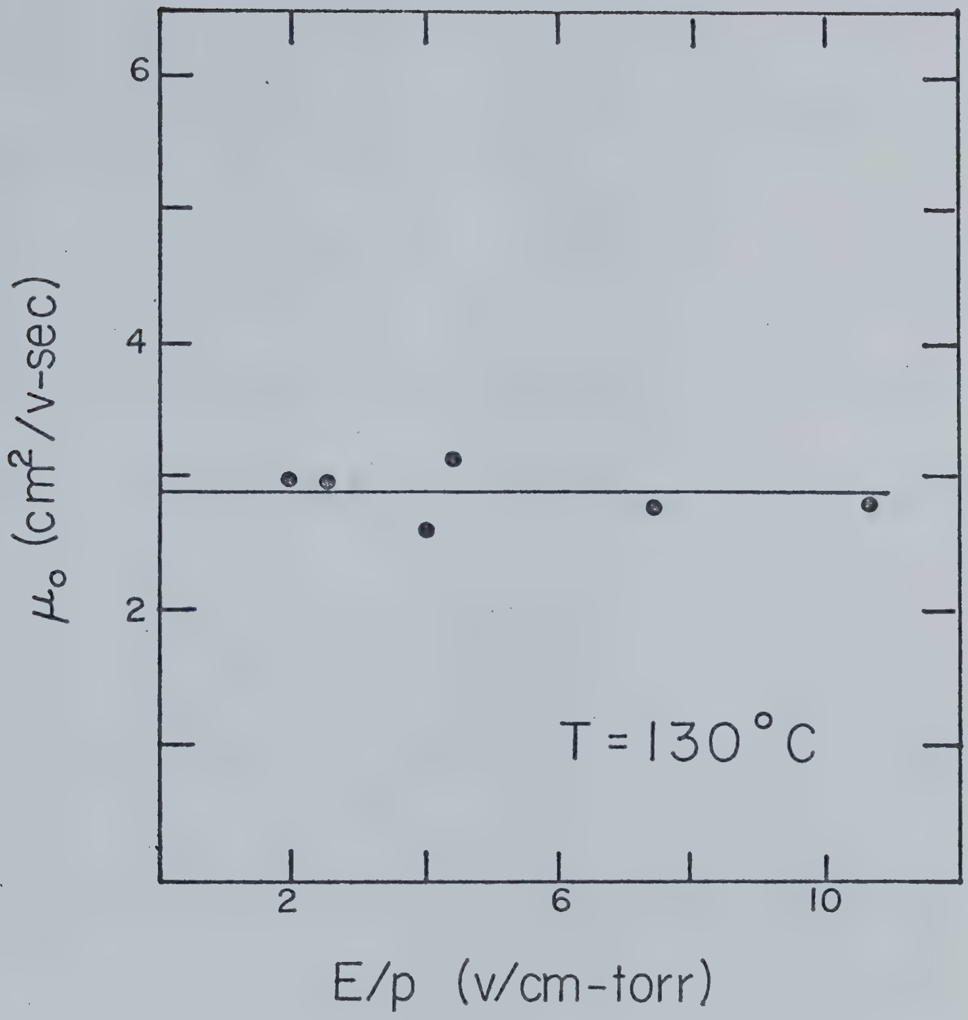

FIGURE 28 Reduced Mobility versus E/p for the Potassium Ion in Argon.

## C Equilibrium

The equilibrium constants for three reactions were determined by using the drift tube:

$$K^+ + H_2O \rightleftarrows K^+(H_2O) \qquad 2.18$$

$$K^+(CH_3CN) + CH_3CN \rightleftarrows K^+(CH_3CN)_2 \qquad 2.19$$

$$K^+(CH_3CN)_2 + CH_3CN \rightleftarrows K^+(CH_3CN)_3 \qquad 2.20$$

If two ions are in equilibrium, it is expected that their arrival times will be the same, even though they have different mobilities. This was found to be the case as is shown in Figure 29 for reaction 2.20. However, the measured equilibrium constant is not necessarily the "true" constant for the reaction since energy is also supplied from the field. For the extreme case, when the energy supplied by the field is much larger than thermal energy, Wannier (85) developed a formula for the total energy of a drifting ion:

$$E = \frac{mv_d^2}{2} + \frac{Mv_d^2}{2} + \frac{3kT}{2}$$

where m and M are the ionic and molecular masses, $v_d$ the drift velocity and 3kT/2 the thermal energy. The first term on the right-hand side of the formula is the field energy associated with the drift motion of the ion, whereas the second term is the random part of the field energy. This

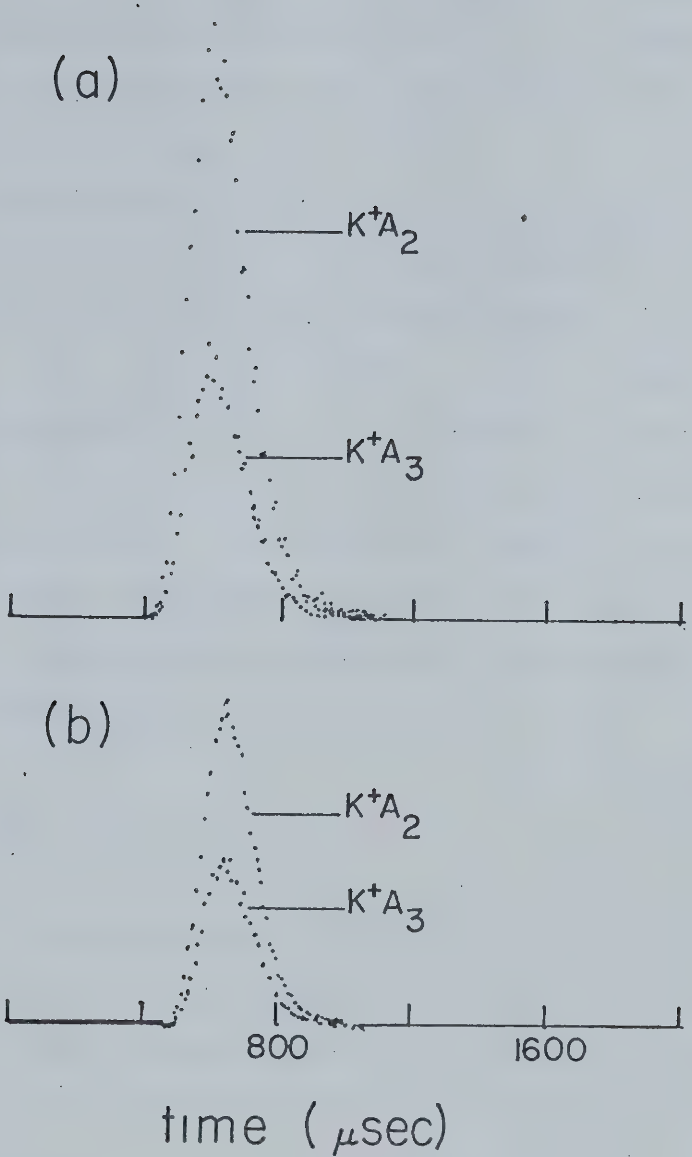

FIGURE 29 Typical Drift Tube Output Showing Ions in Equilibrium for the Reaction:

$$K^+(CH_3CN)_2 + CH_3CN \rightleftharpoons K^+(CH_3CN)_3 \quad .$$

Field Strength in both cases = 14 v/cm
Temperature in both cases = 175° C

a) Pressure = 0.58 torr
$K_{2,3}$ = 0.715

b) Pressure = 0.84 torr
$K_{2,3}$ = 0.645

random or "invisible" part is described (82) as the energy the ion stores in the gas through which it is drifting. Thus the energy supplied by the field will be represented by the first two terms.

The variation of K with E/p is shown in Figure 30 for reaction 2.20. The value of the equilibrium constant determined in the field free reaction chamber mode is 6.6 torr$^{-1}$, at this temperature, 130° C. From the equilibrium constants measured in Figure 30, an effective temperature, $T_e$, may be calculated from the Van't Hoff plot obtained in the field free mode. This effective temperature can then be equal to the temperature of the gas, $T_g$, plus the theoretical temperature created by the field referred to as the "ion temperature", $T_i$, (86), i.e.:

$$T_e = T_i + T_g \qquad 2.21$$

For the various equilibrium constants in Figure 30, the values of $T_i$ and $T_e$ are presented in Table 4. If the Wannier formula is valid for these values of E/p, then the first two terms may be set equal to a term incorporating the "ion temperature":

$$\frac{(m + M)v_d^2}{2} = \frac{3kT_i}{2} \qquad 2.22$$

From the measured drift velocities for the data in Figure 30, the "ion temperature" as calculated from the Wannier formula

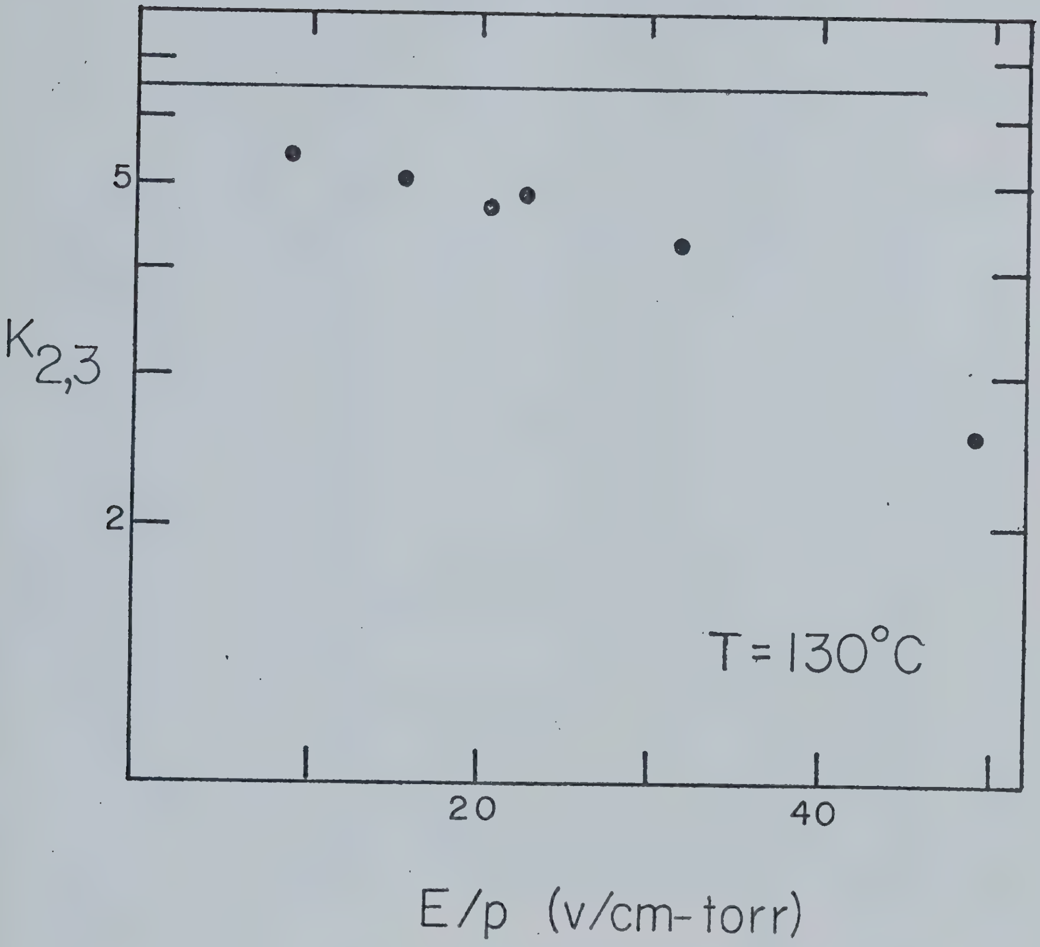

FIGURE 30 Variation of Equilibrium Constants with E/p for the Reaction:

$$K^+(CH_3CN)_2 + CH_3CN = K^+(CH_3CN)_3$$

at $CH_3CN$ pressures below 0.5 torr. The solid line indicates the value obtained in a field free reaction chamber.

## TABLE 4

### Effective and Ion Temperatures for the Reaction:

### $K^+(CH_3CN)_2 + CH_3CN \rightleftharpoons K^+(CH_3CN)_3$ at 130° C

| K | E/P (v/cm-torr) | $V_d \times 10^{-4}$ (cm/sec) | Effective Temp., $T_e$(°K) | Ion Temp.,[a] $T_i$(°K) | Wannier $T_i$(°K) |
|---|---|---|---|---|---|
| 6.60[c] | 0 | 0 | 403 | 0 | 0 |
| 5.44 | 8.9 | .368 | 406.3 | 3.3 | 10.1 |
| 5.04 | 15.5 | .610 | 407.7 | 4.7 | 27.9 |
| 4.76 | 20.5 | .782 | 408.8 | 5.8 | 45.1 |
| 4.90 | 22.4 | .862 | 408.2 | 5.2 | 55.6 |
| 4.37 | 31.8 | 1.119 | 410.3 | 7.3 | 93.8 |
| 2.58 | 49.0 | 1.925 | 420.2 | 17.2 | 264.1 |

[a] $T_i = T_e - T_g (403^\circ K)$

[b] $T_i = \frac{(m + M)V_d}{3k}$ ; m = ion mass, M = gas mass, k = boltzman constant

[c] From field free mode

can be determined. These are compared with the values obtained from the Van't Hoff plot in Table 4. This demonstrates that the Wannier formula cannot be used to determine "ion temperature". So even though the energy supplied by the field is not negligible, it appears that is is not high enough to make the Wannier equation valid.

Varney (86) has stated that the "ion temperature" will be proportional to E/p, (in the Wannier formula it was proportional to $(E/p)^2$). If the data from Figure 30 is taken and the "ion temperature" is plotted against E/p, the result should be a straight line. This is done in Figure 31. It is difficult to say from this figure whether or not the slope will be a constant due to the high scatter of the data.

Experimentally then, the only way to determine the equilibrium constant at a particular temperature is to lower E/p until a constant value of K is obtained (49). This was done for reaction 2.18 and the results are plotted in Figure 32. Below an E/p of 2 volts/cm-torr the equilibrium constants are extremely close to the ones determined in the field free mode.

Lowering E/p requires that either the field strength be lowered or the pressure increased. If the field strength is lowered, the signal intensity decreases, as shown in Table 5. If the pressure is raised, collisions outside the ion source occur and the measured intensities will be in error. This will be discussed in more detail in the next sub-section.

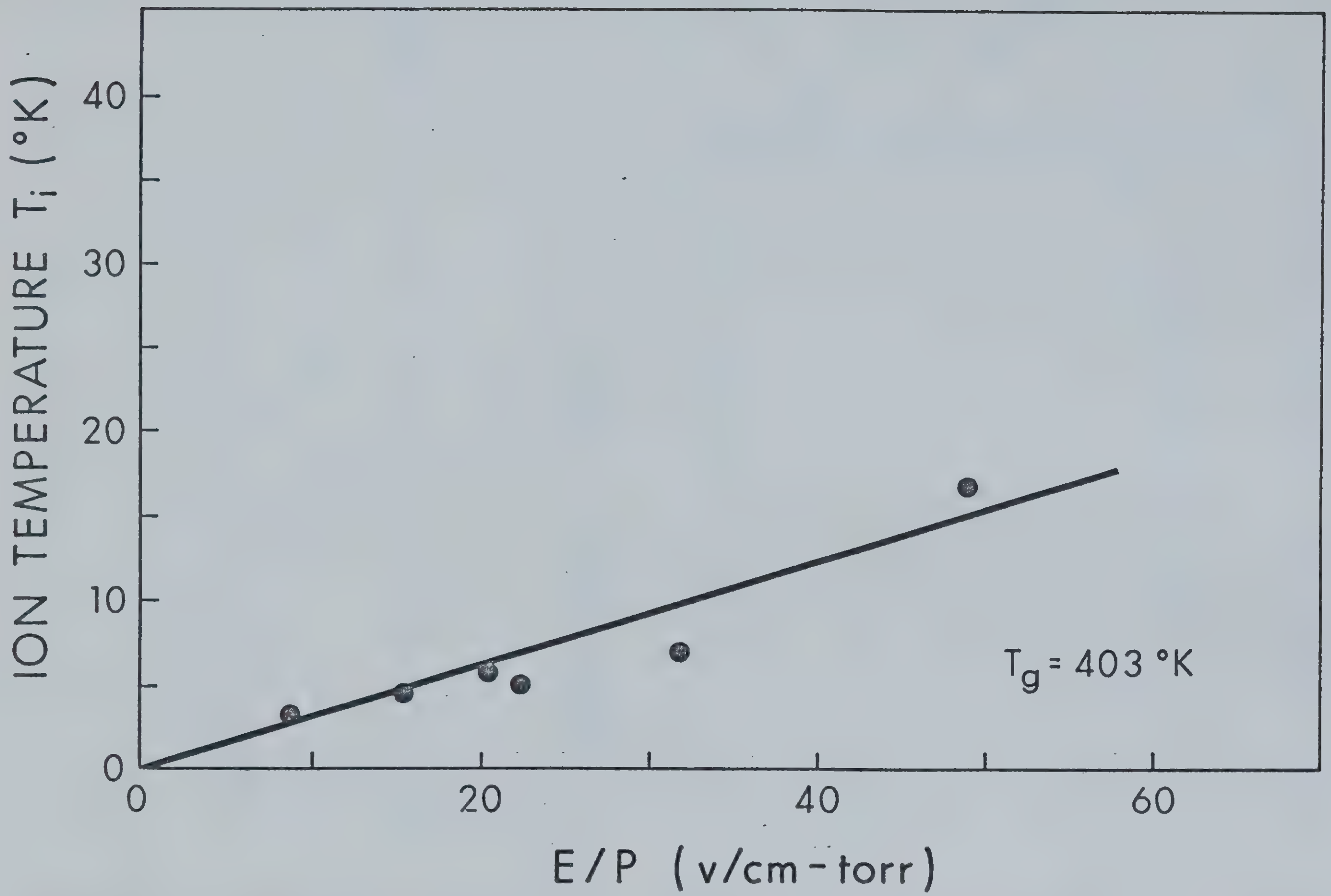

FIGURE 31 "Ion Temperature" versus E/p for the Reaction: $K^+(CH_3CN)_2 + CH_3CN = K^+(CH_3CN)_3$ .

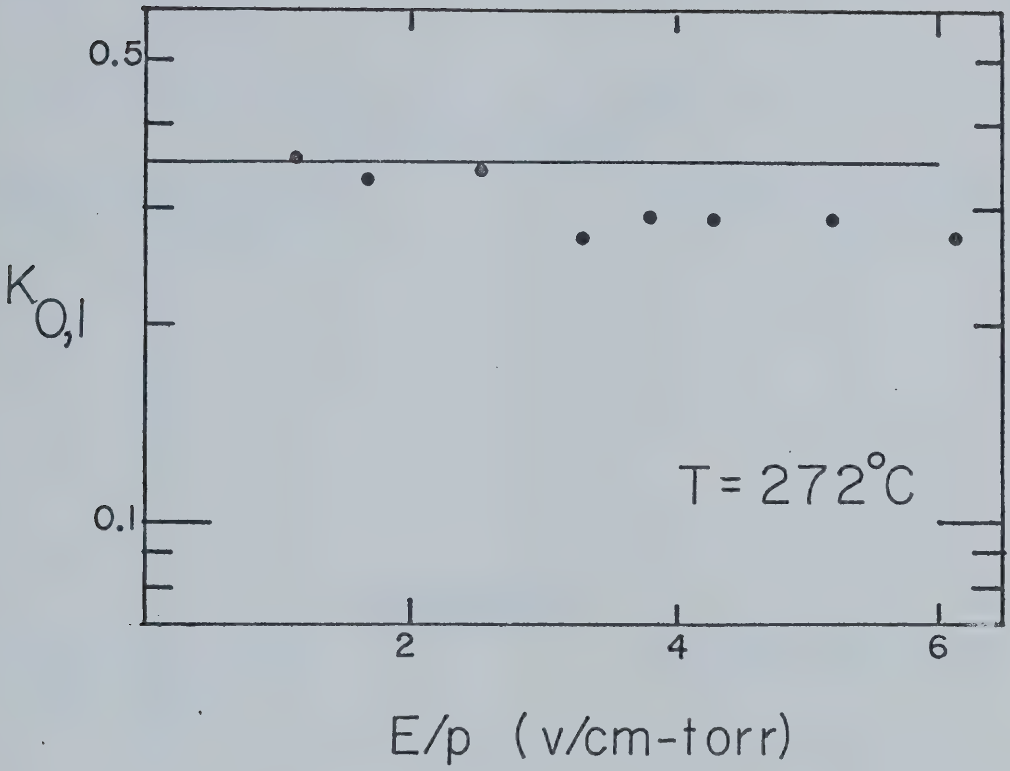

FIGURE 32 Equilibrium Constants at Low E/p for the Reaction:

$$K^+ + H_2O = K^+(H_2O) .$$

The solid line indicates the equilibrium constant obtained with a field free reaction chamber.

## TABLE 5

## Sensitivity Dependence on Field Strength and on Pressure

### A. Field Strength[a]

| Field Strength (V/cm) | Relative Intensity[b] |
|---|---|
| 42 | 100 |
| 31 | 59 |
| 21 | 29 |
| 11 | 10 |
| 3 | 1.1 |

### B. Pressure[c]

| Pressure $H_2O$[c] (torr) | Relative Intensity[b] |
|---|---|
| 2.8 | 31 |
| 3.7 | 46 |
| 4.5 | 62 |
| 5.6 | 93 |
| 7.3 | 100 |
| 8.3 | 91 |

[a] Pressure constant - 3.0 torr $H_2O$

[b] Total ion intensities normalized to maximum intensity = 100

[c] Field strength constant - 19.6 V/cm

## D Equilibrium and Pressure

Figure 33 shows the effect pressure has on the equilibrium constant of reaction 2.19. This is thought to be due to collisions outside the ion exit slit in which the larger $K^+(CH_3CN)_2$ ion dissociates into the smaller $K^+(CH_3CN)$ ion. One method of getting around this problem would be to work at lower pressures. However, the signal intensities decrease with a decrease in pressure to a point where they become unreliable (Table 5). The field energy would also have to be lowered to keep a relatively low E/p, which again would result in a smaller signal.

For the potassium ion-water reaction, the "stripping" effect was less pronounced as shown in Figure 34.

## E Mobilities

Due to the inhomogeneous field and inadequate gate, measured mobilities of ions would be only approximate. When two ions are in equilibrium, the average drift velocity can be expressed as:

$$V_{ave} = \frac{v_1 n_1 + v_2 n_2}{n_1 + n_2} \qquad 2.23$$

where $v_1$ is the drift velocity of ion (1), $v_2$ the drift velocity of ion (2), and $n_1$ and $n_2$ represent the relative intensities of each ion. Since the drift velocity is proportional to the mobility and since the field strength, pressure, and temperature are the same for each ion,

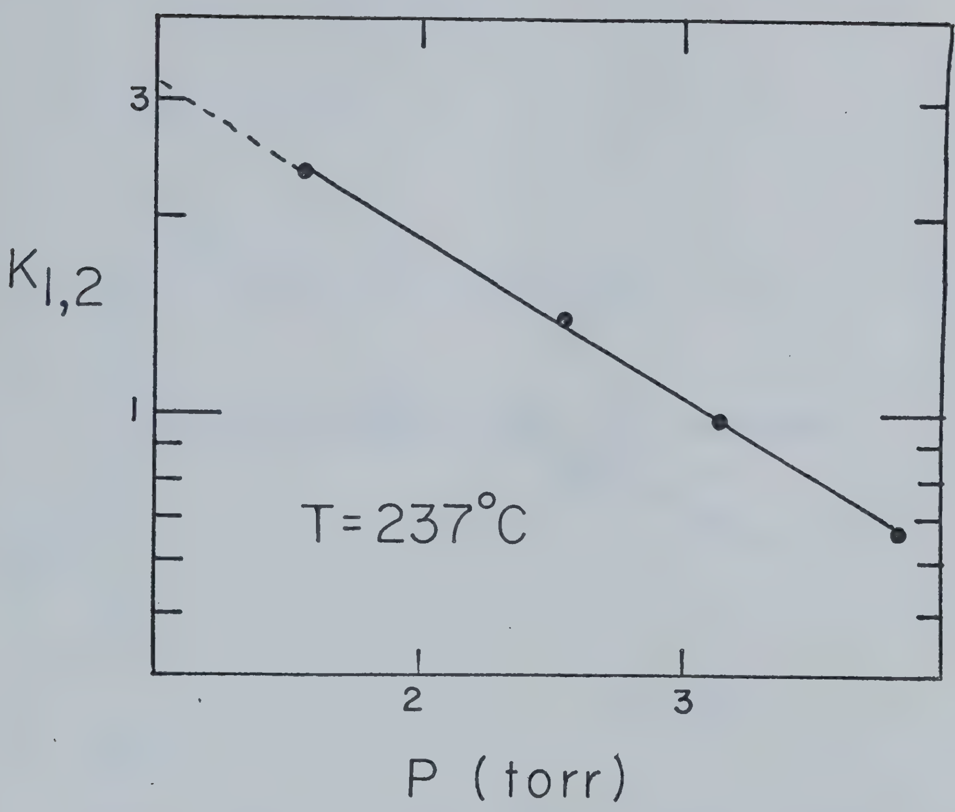

FIGURE 33 Equilibrium Constants Obtained in a Drift Tube versus Pressure for the Reaction:

$$K^+(CH_3CN) + CH_3CN = K^+(CH_3CN)_2 .$$

The $K_{1,2}$ measured in a field free reaction chamber at 237° C is 4.0.

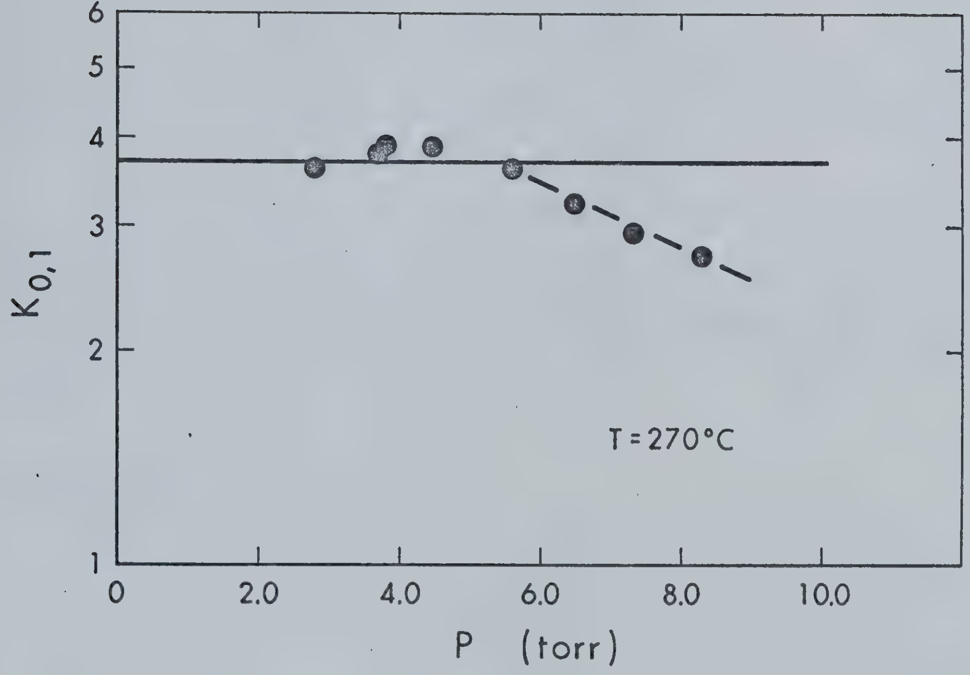

FIGURE 34 Equilibrium Constants versus Pressure for the Reaction:

$$K^+ + H_2O = K^+(H_2O) .$$

The solid line indicates the $K_{0,1}$ measured in a field free ion source at 270° C.

reduced mobilities may be substituted into equation 2.24:

$$\mu_{o_{ave}} = \frac{\mu_{o_1} n_1 + \mu_{o_2} n_2}{n_1 + n_2} \qquad 2.24$$

which rearranges to:

$$\frac{\mu_{o_{ave}} (n_1 + n_2)}{n_1} = \mu_{o_1} + \mu_{o_2} \frac{n_2}{n_1} \qquad 2.25$$

and a plot of $\frac{\mu_{o_{ave}} (n_1 + n_2)}{n_1}$ versus $\frac{n_2}{n_1}$ will give a slope, $\mu_{o_2}$, and intercept, $\mu_{o_1}$. An example is shown in Figure 35 for the ions $K^+(CH_3CN)_3$ and $K^+(CH_3CN)_2$. Their reduced mobilities turn out to be 0.30 and 0.34 $cm^2$/volt-sec respectively.

## F Conclusion

Drift tubes can be used for the study of equilibrium. However, the increase in intensity that was hoped for was never realized in the acetonitrile case, since runs had to be done at low pressure and low field strength, conditions which gave the lowest possible intensities. In the water-potassium ion case, however, higher pressures could be used and the intensities were fairly high. The equilibrium constants remained constant over a large pressure range and they agreed fairly well with the results from the field free source.

Another disadvantage to the present drift setup is that

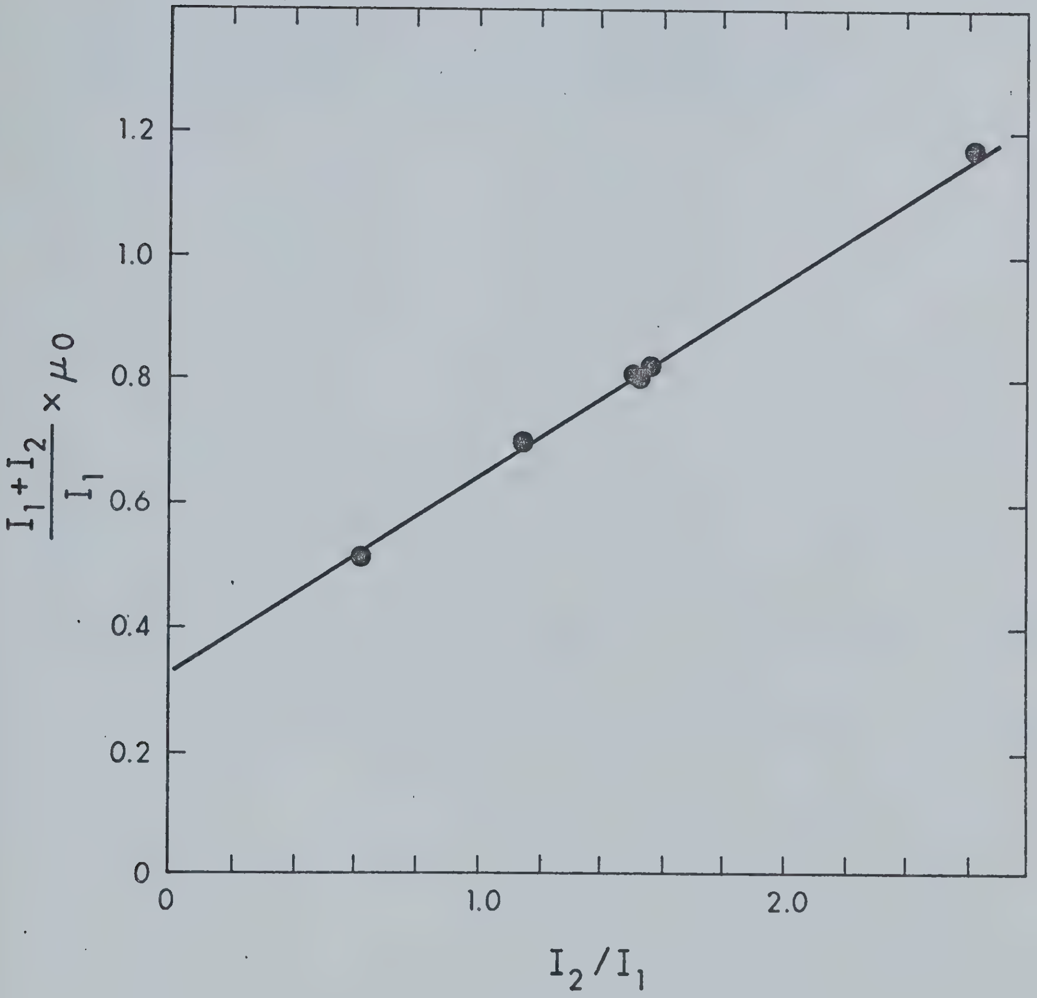

FIGURE 35 Determination of Ion Mobilities From an Average Mobility Measurement. $I_2$ represents the intensity of the ion $K^+(CH_3CN)_3$ and $I_1$ represents the intensity of the ion $K^+(CH_3CN)_2$. The slope yields a mobility of 0.30 for $K^+(CH_3CN)_3$, whereas the intercept yields a mobility of 0.34 for the ion $K^+(CH_3CN)_2$.

there is a temperature gradient along the drift tube due to the heating from the filament. This could not be measured accurately and could lead to somewhat erroneous results.

If the mobilities of the ions were important to study, a much more sophisticated drift arrangement would be necessary, complete with guard rings and a much better gate.

CHAPTER 3

## RESULTS AND DISCUSSION OF THE SOLVATION OF ALKALI METAL IONS BY ACETONITRILE

### 3.1 Introduction

As discussed in Chapter 1, high pressure mass spectrometry provides an efficient method for determining the gas phase thermodynamic constants for the solvation of ions. When alkali ions collide with a neutral such as acetonitrile in a field free region, a complex is formed:

$$M^{+} + CH_3CN \rightleftarrows M^{+}(CH_3CN)_1 \qquad 3.1$$

Upon further collisions, this complex can continue to grow, resulting in larger clusters:

$$M^{+}(CH_3CN)_{n-1} + CH_3CN \rightleftarrows M^{+}(CH_3CN)_n \qquad 3.2$$

By varying the temperature of the reaction chamber in the mass spectrometer and measuring the equilibrium constants for the reaction 3.2 at various values of n, thermodynamic values for the step-by-step clustering reactions are obtained.

In this chapter, the experimental results obtained by this method are presented for the alkali metal ions: $Na^{+}$, $K^{+}$, $Rb^{+}$, and $Cs^{+}$. The gas phase solvation of alkali metal ions in acetonitrile can then be compared with the gas phase

solvation of alkali ions in water, halide ions in acetonitrile, in order to provide information regarding the differences in the solvation of ions by protic or aprotic solvents.

## 3.2 Presentation of Results

The equilibrium constants for the solvation of sodium, potassium, rubidium and cesium ions by acetonitrile are shown as a function of pressure in Figures 36-55. At a given temperature over the pressure range covered, the equilibrium constants remain relatively constant indicating that the reaction being studied indeed has reached equilibrium.

These equilibrium constants are plotted as a function of 1/T in a Van't Hoff type plot in order to determine the enthalpy and entropy of the reactions from the slope and intercept respectively. These plots are shown in Figures 56-59. The equilibrium constants presented in these Figures are $K_{0,1}$ to $K_{4,5}$ for potassium, rubidium and cesium, and $K_{1,2}$ to $K_{4,5}$ for sodium. The $K_{0,1}$ values for sodium could not be measured directly since the ion source was not capable of operating at temperatures above 700°K, and at this temperature no unclustered $Na^+$ was observed. For similar reasons, lithium was not studied since it was expected that the interaction with this ion would be even stronger, and that the $K_{0,1}$ and $K_{1,2}$ could probably not be determined. The higher equilibrium constants were also difficult to measure since the $Li^+$ source in general led

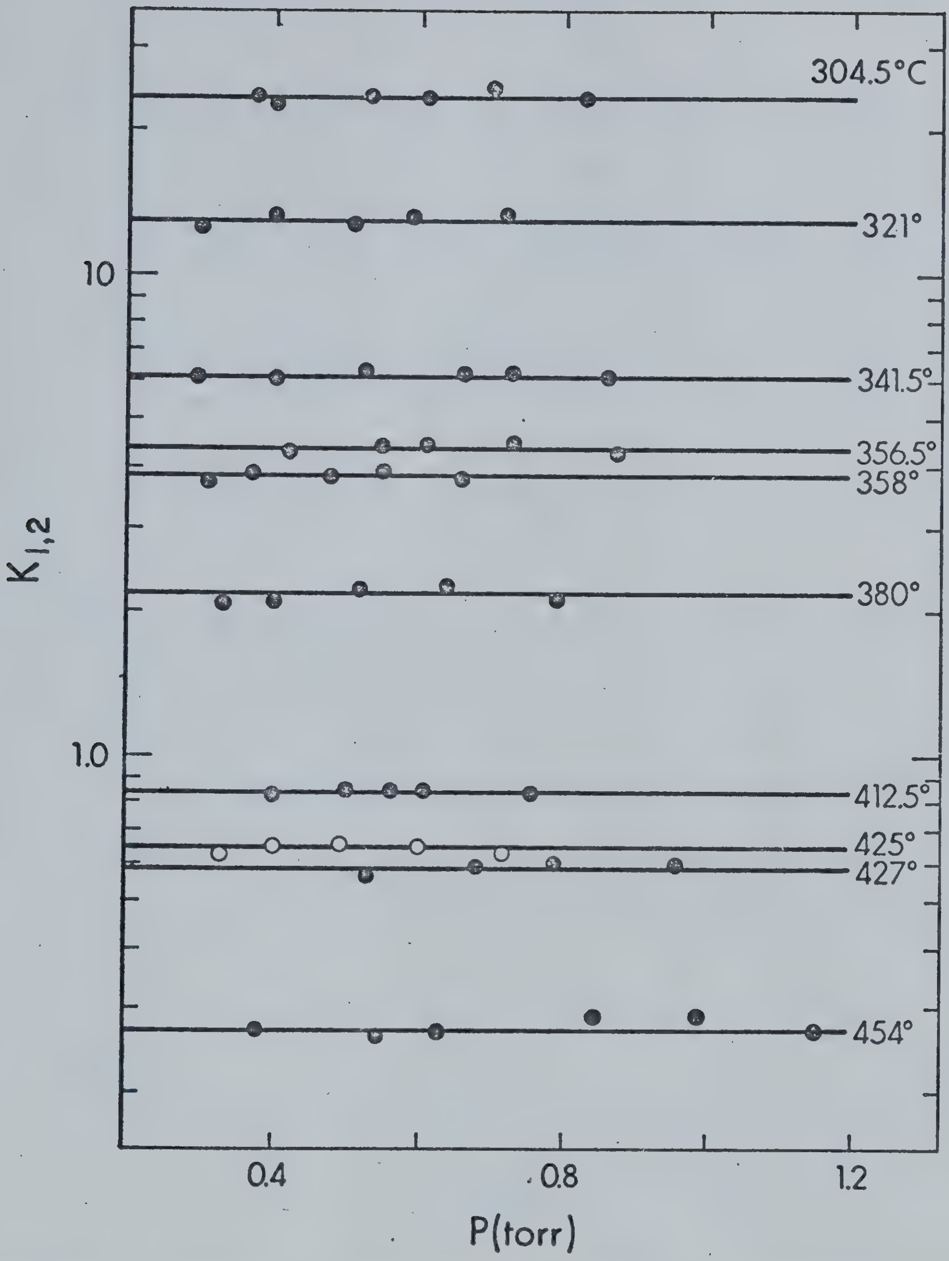

FIGURE 36 Equilibrium Constants versus Pressure of Acetonitrile at Various Temperatures for the Reaction:

$$Na^+(CH_3CN) + CH_3CN = Na^+(CH_3CN)_2 .$$

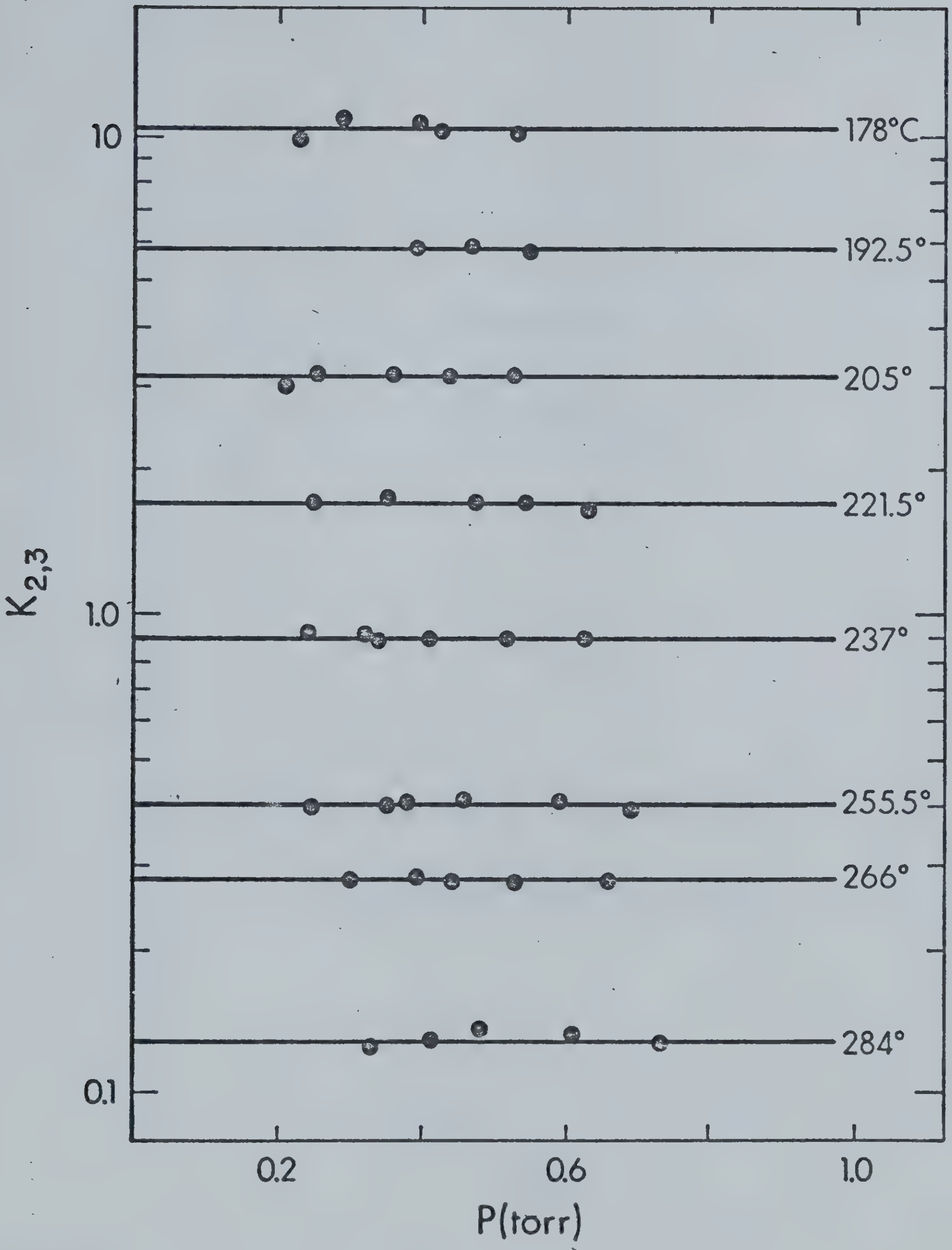

FIGURE 37 Equilibrium Constants versus Pressure of Acetonitrile at Various Temperatures for the Reaction:

$$Na^+(CH_3CN)_2 + CH_3CN = Na^+(CH_3CN)_3 \quad .$$

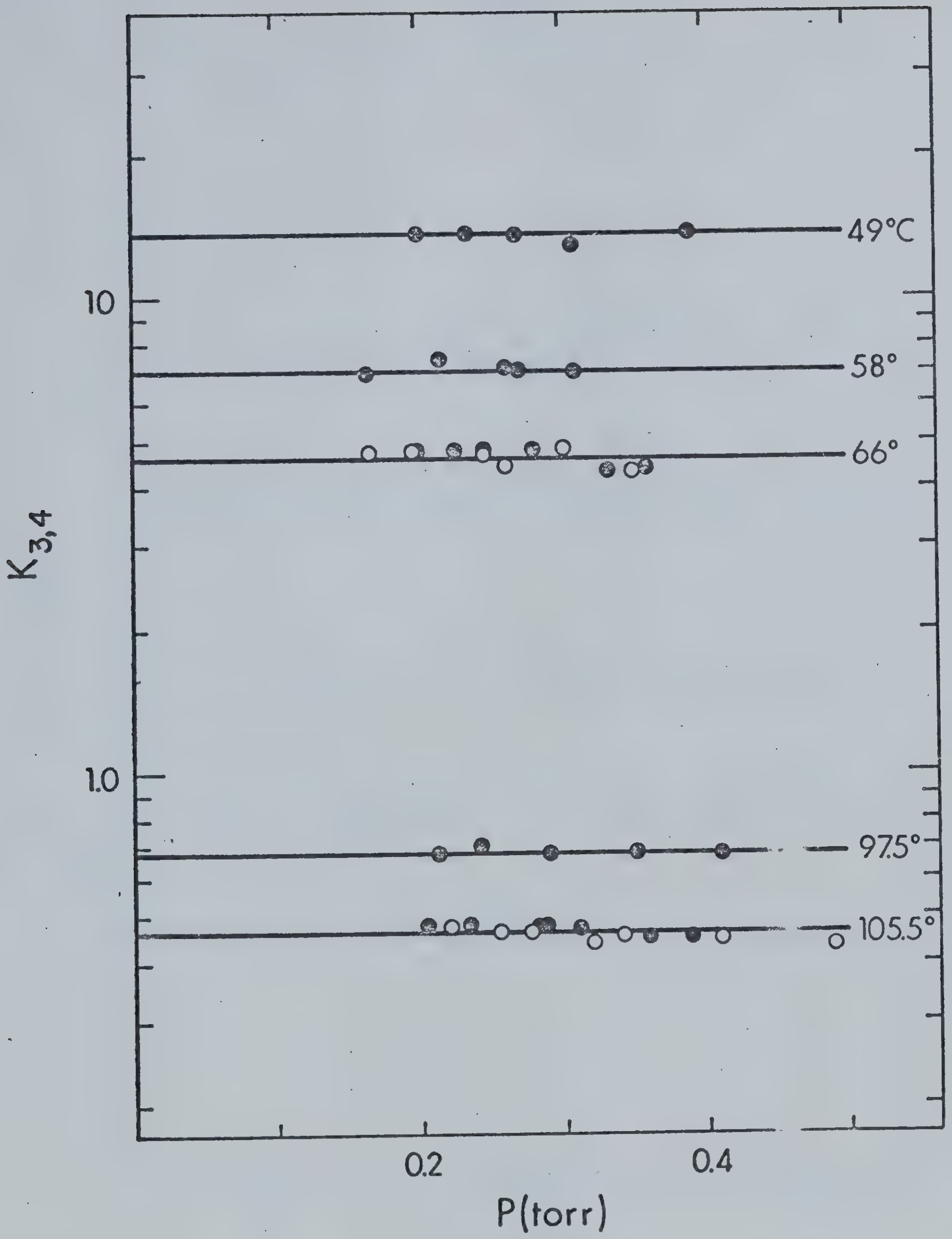

FIGURE 38 Equilibrium Constants versus Pressure of Acetonitrile at Various Temperatures for the Reaction:

$$Na^+(CH_3CN)_3 + CH_3CN = Na^+(CH_3CN)_4 .$$

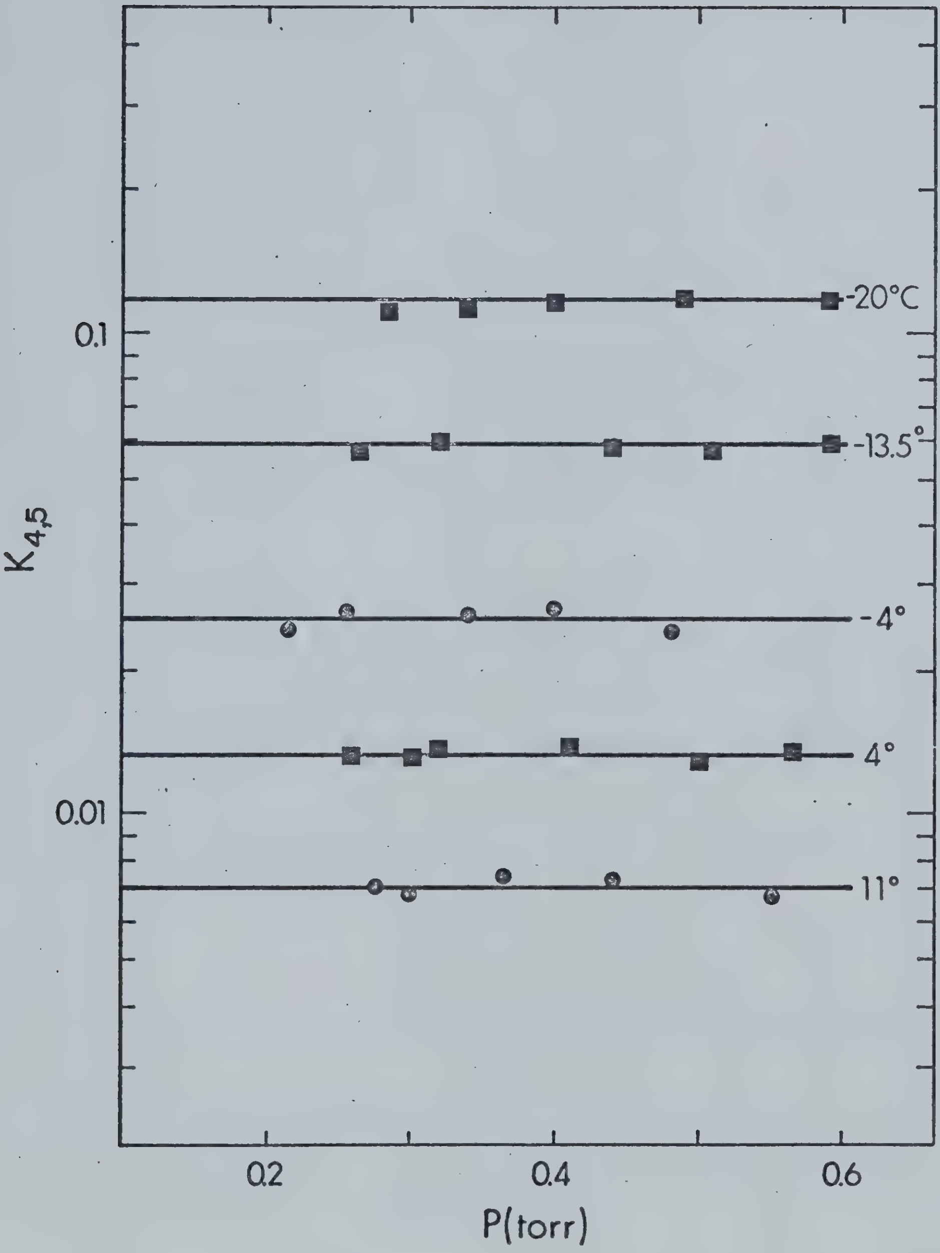

FIGURE 39 Equilibrium Constants versus Pressure of Acetonitrile at Various Temperatures for the Reaction:

$$Na^+(CH_3CN)_4 + CH_3CN = Na^+(CH_3CN)_5 .$$

■ Points from potassium-sodium source.

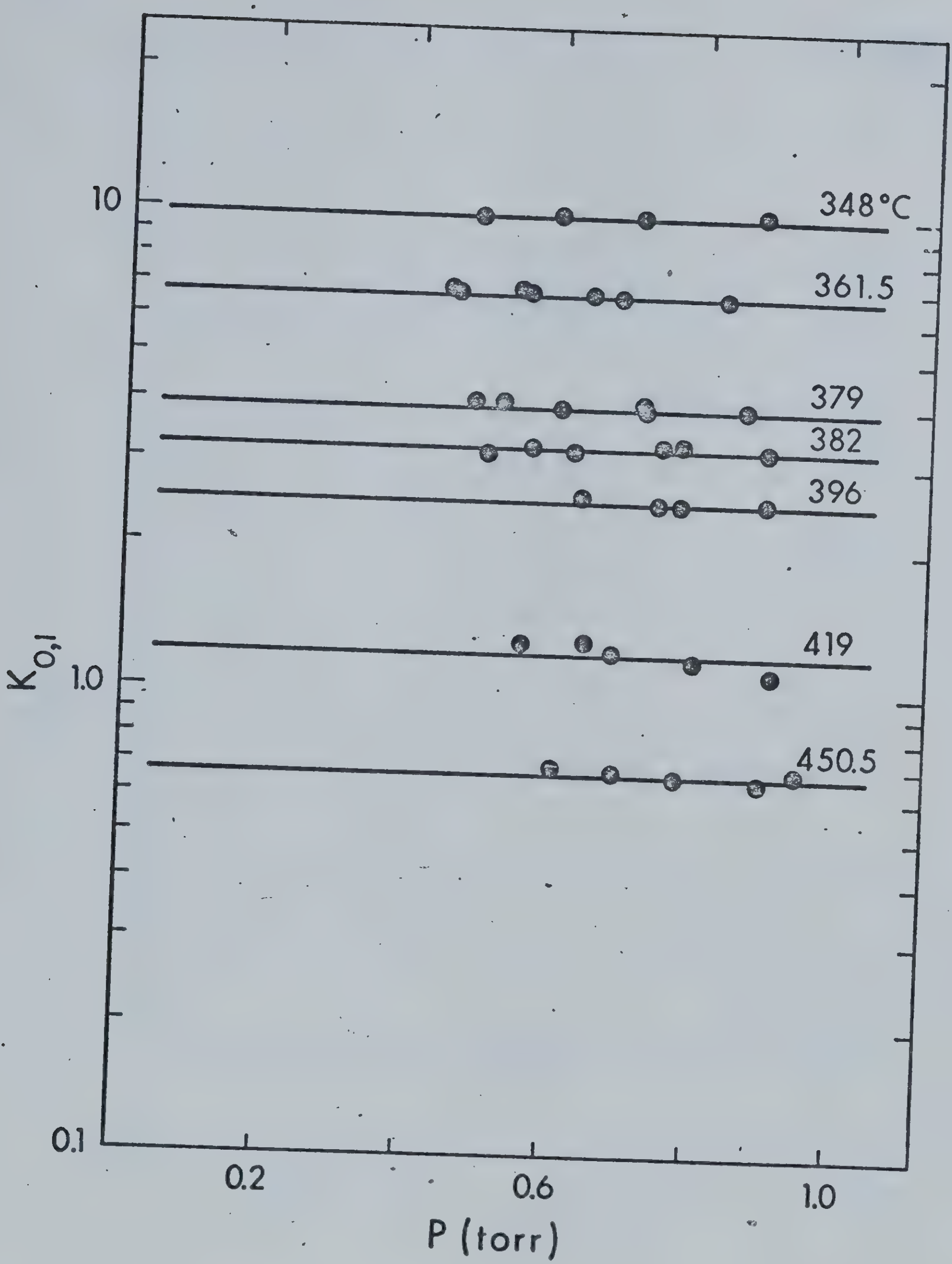

FIGURE 40 Equilibrium Constants versus Pressure of Acetonitrile at Various Temperatures for the Reaction:

$$K^+ + CH_3CN = K^+(CH_3CN) .$$

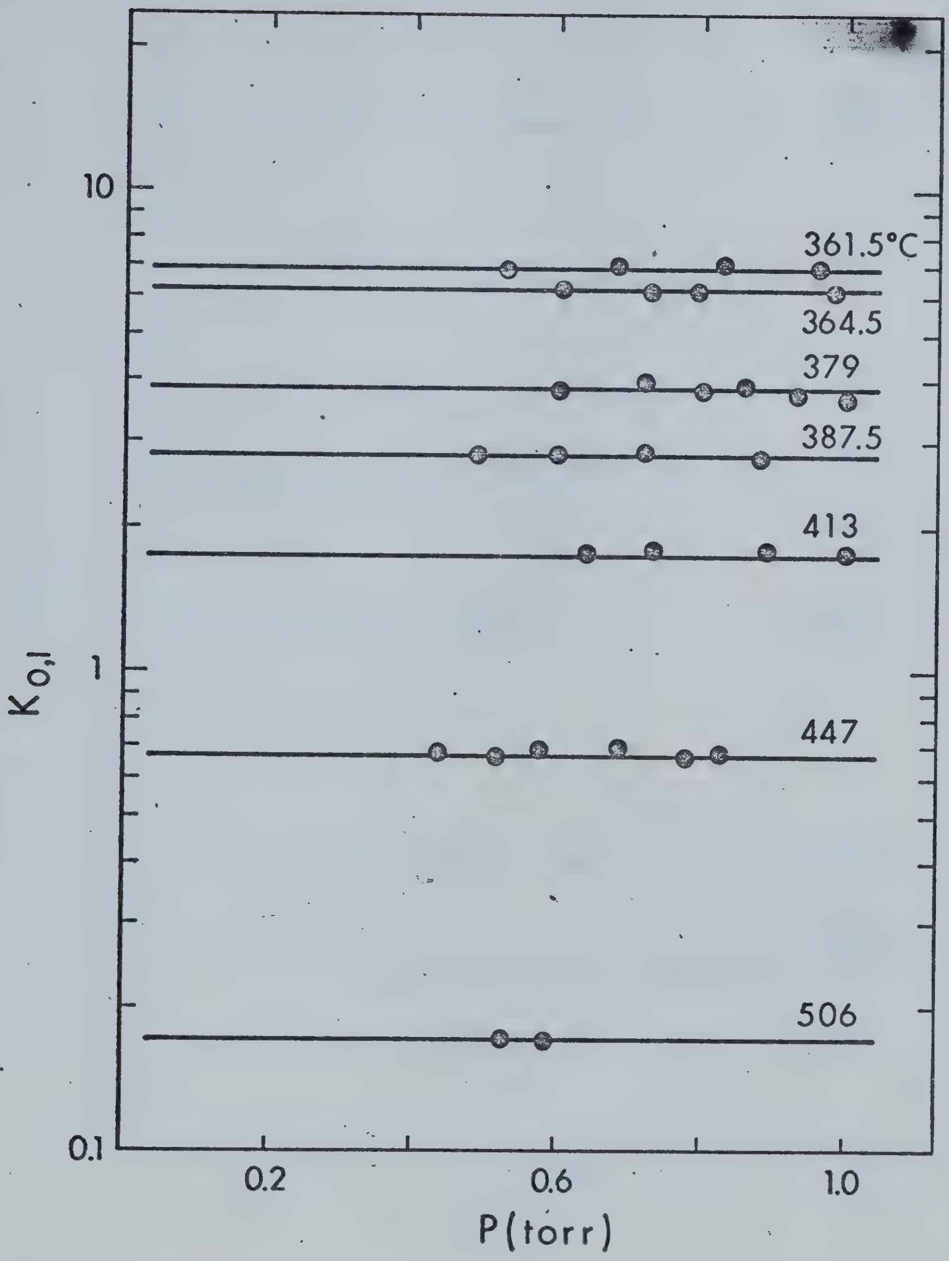

FIGURE 41 Equilibrium Constants versus Pressure of Acetonitrile at Various Temperatures for the Reaction:

$$K^+ + CH_3CN = K^+(CH_3CN) \ .$$

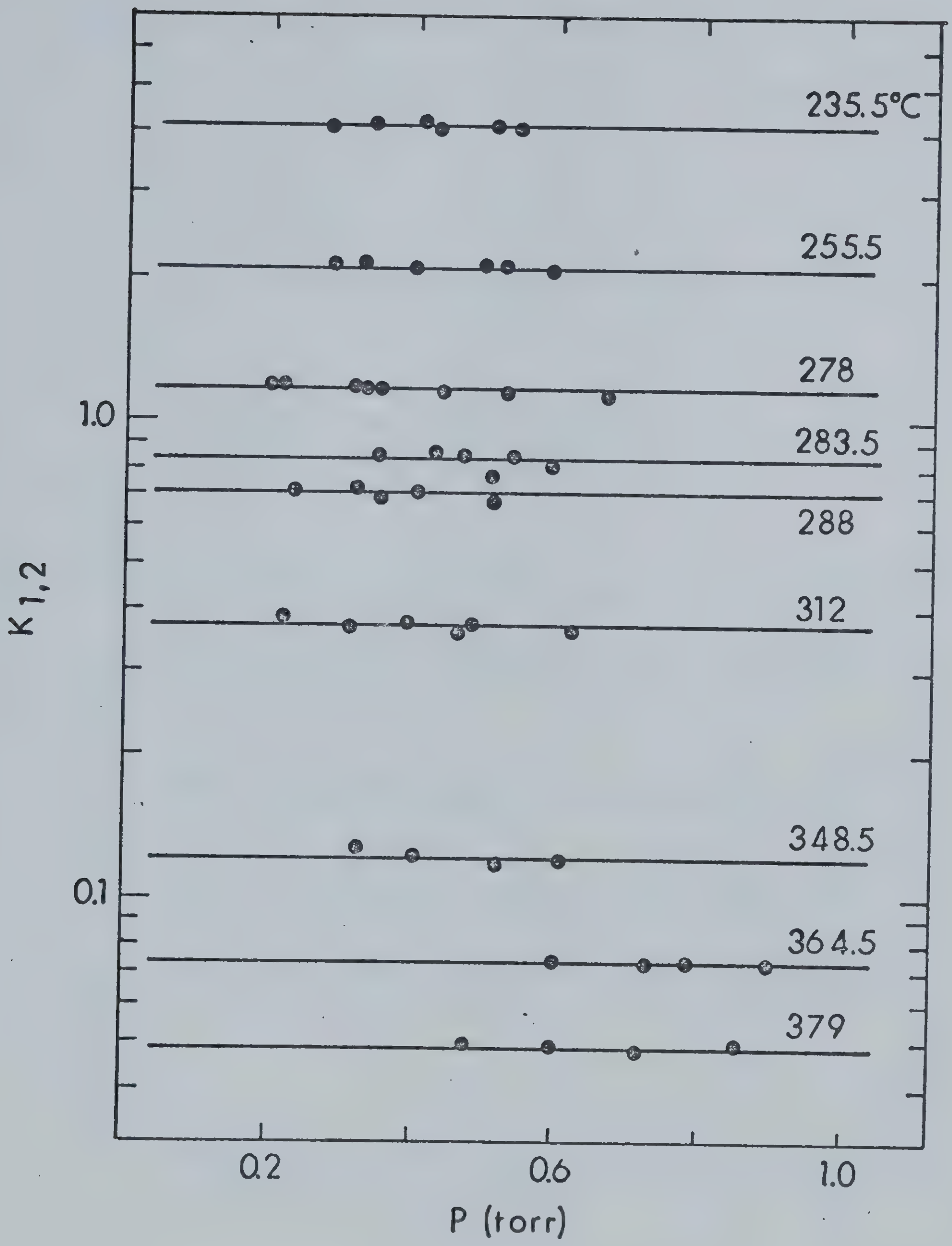

FIGURE 42 Equilibrium Constants versus Pressure of Acetonitrile at Various Temperatures for the Reaction:

$$K^+(CH_3CN) + CH_3CN = K^+(CH_3CN)_2 \ .$$

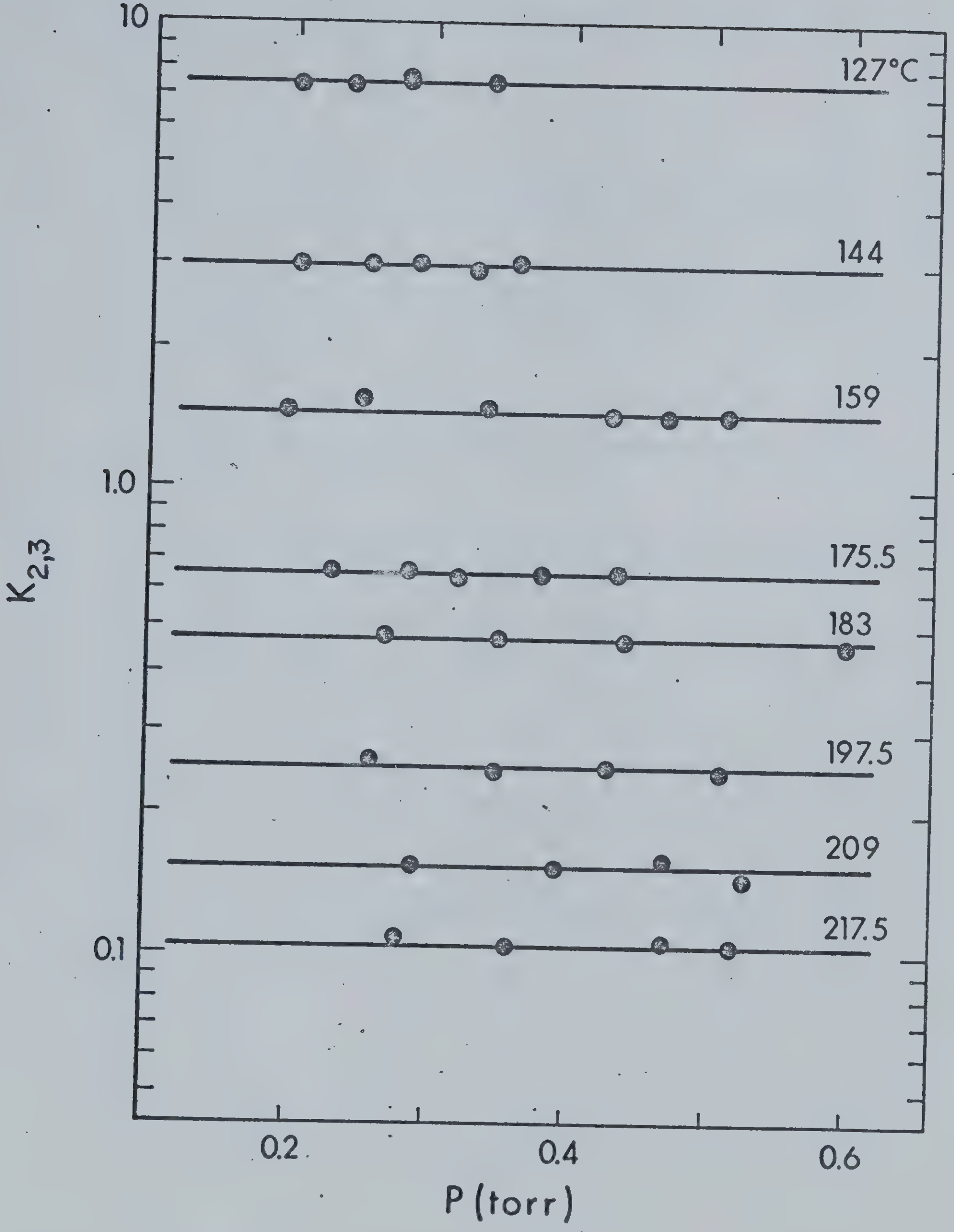

FIGURE 43 Equilibrium Constants versus Pressure of Acetonitrile at Various Temperatures for the Reaction:

$$K^+(CH_3CN)_2 \ + \ CH_3CN \ = \ K^+(CH_3CN)_3 \ .$$

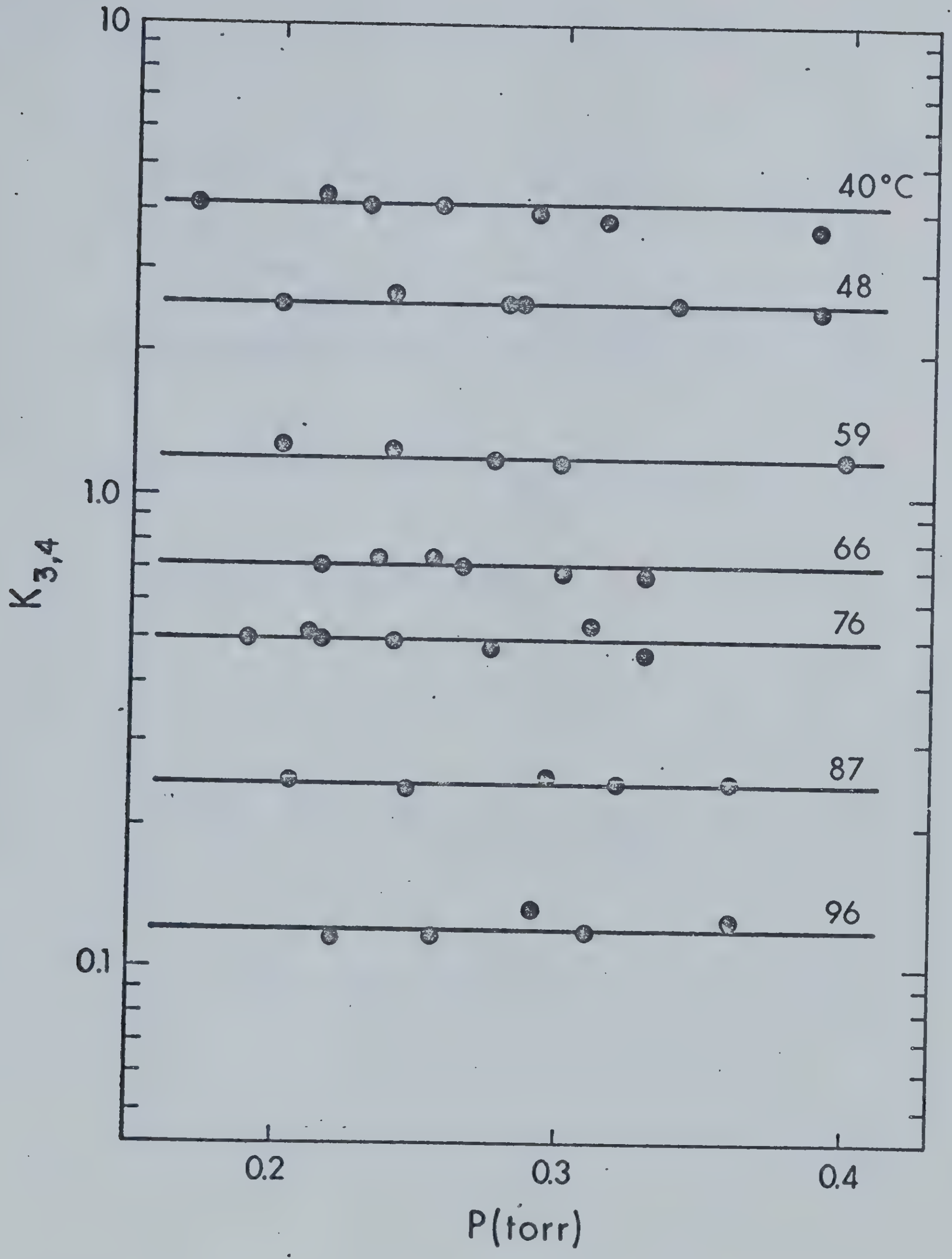

FIGURE 44 Equilibrium Constants versus Pressure of Acetonitrile at Various Temperatures for the Reaction:

$$K^+(CH_3CN)_3 + CH_3CN = K^+(CH_3CN)_4 .$$

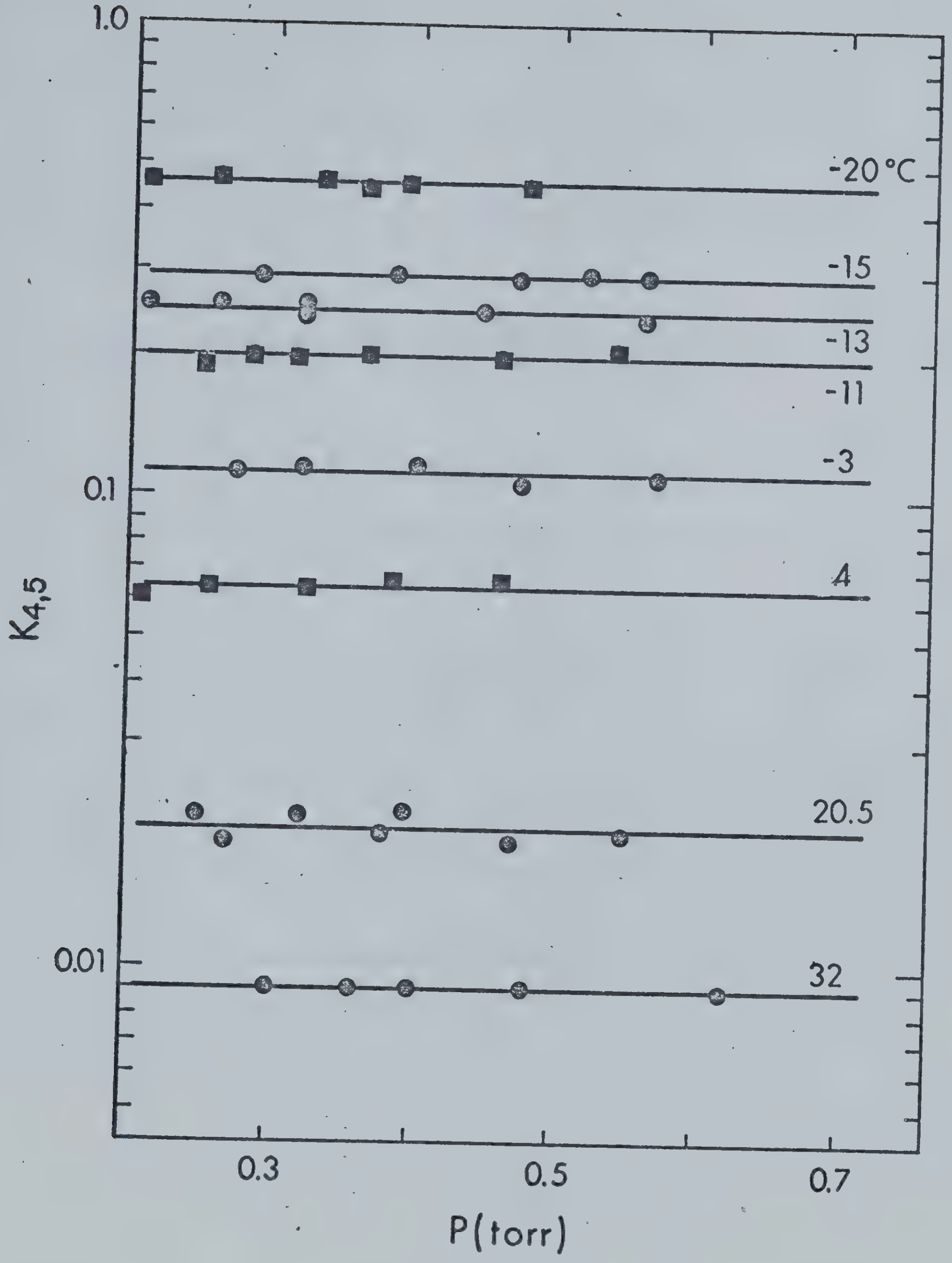

FIGURE 45 Equilibrium Constants versus Pressure of Acetonitrile at Various Temperatures for the Reaction:

$$K^{+}(CH_3CN)_4 + CH_3CN = K^{+}(CH_3CN)_5 .$$

■ Points from potassium-sodium source.

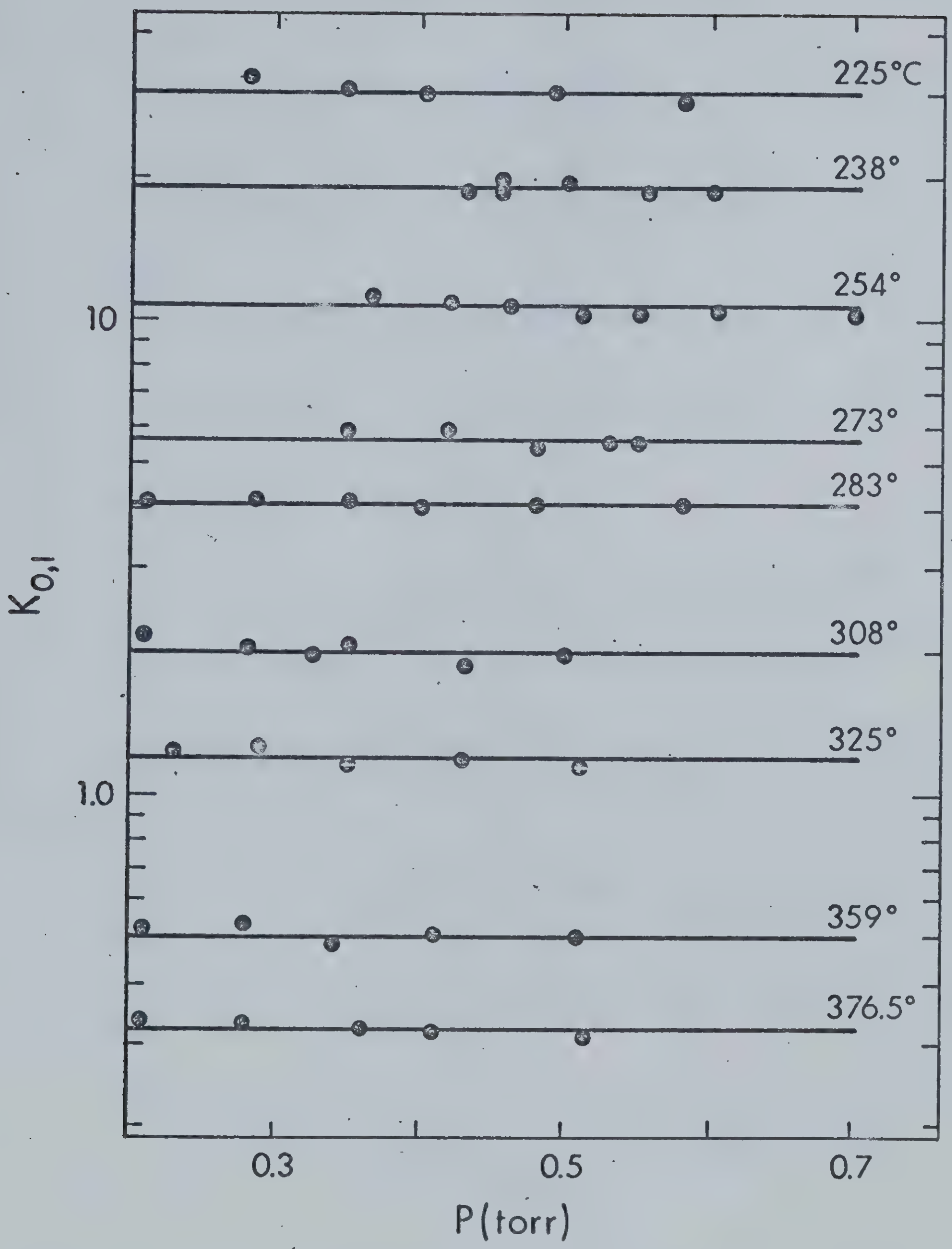

FIGURE 46 Equilibrium Constants versus Pressure of Acetonitrile at Various Temperatures for the Reaction:

$$Rb^+ + CH_3CN = Rb^+(CH_3CN) .$$

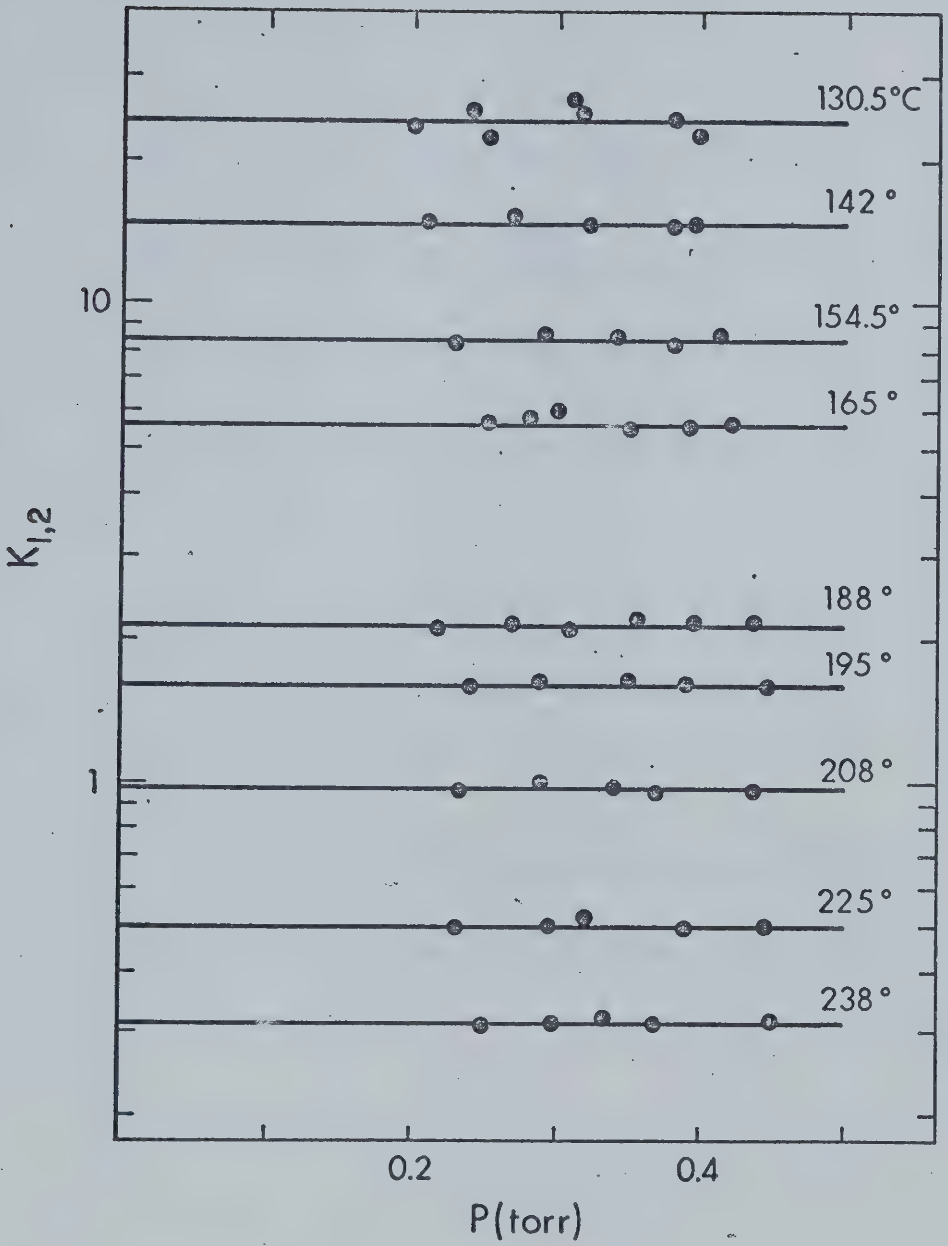

FIGURE 47 Equilibrium Constants versus Pressure of Acetonitrile at Various Temperatures for the Reaction:

$$Rb^+(CH_3CN) + CH_3CN = Rb^+(CH_3CN)_2 .$$

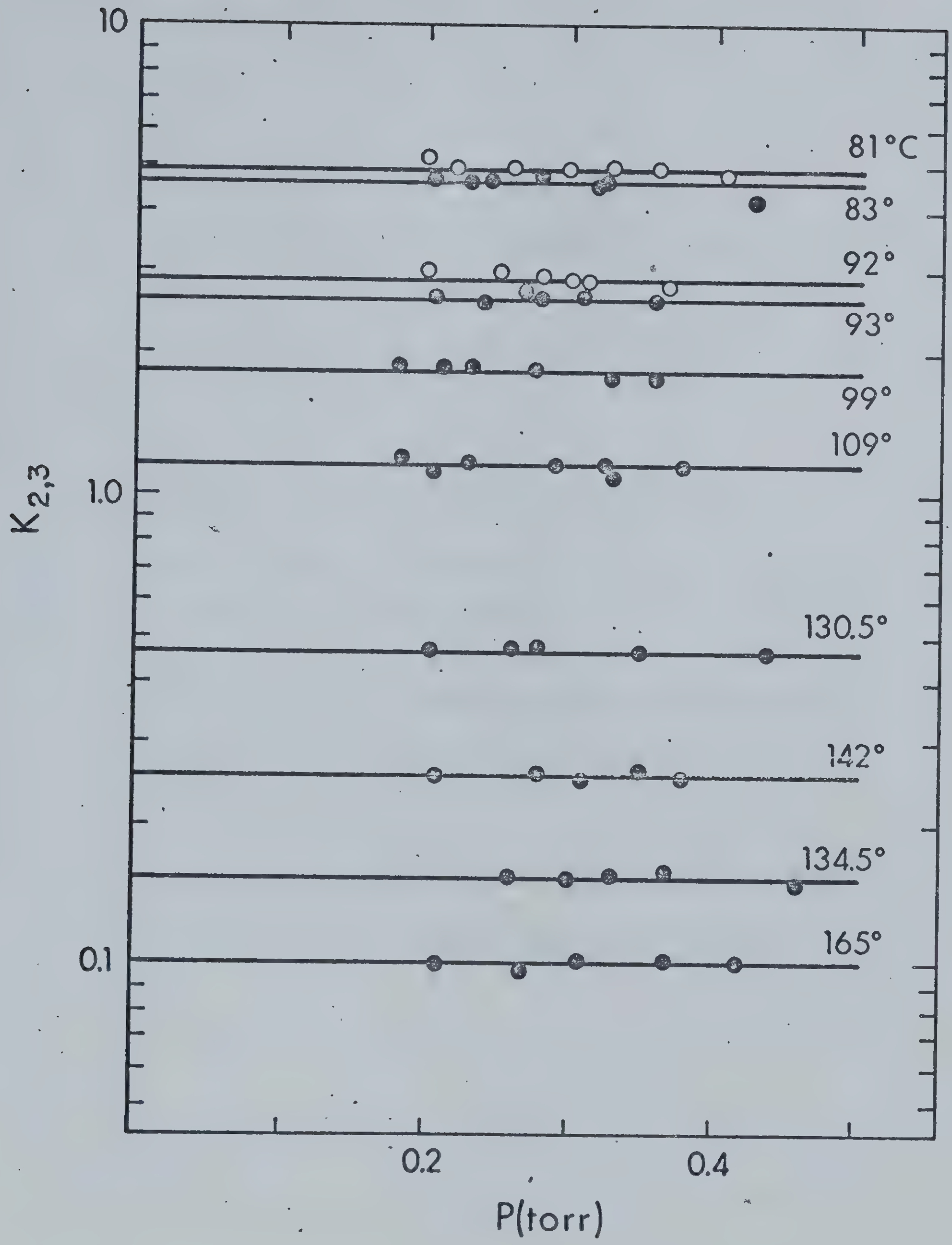

FIGURE 48 Equilibrium Constants versus Pressure of Acetonitrile at Various Temperatures for the Reaction:

$$Rb^+(CH_3CN)_2 + CH_3CN = Rb^+(CH_3CN)_3 \quad .$$

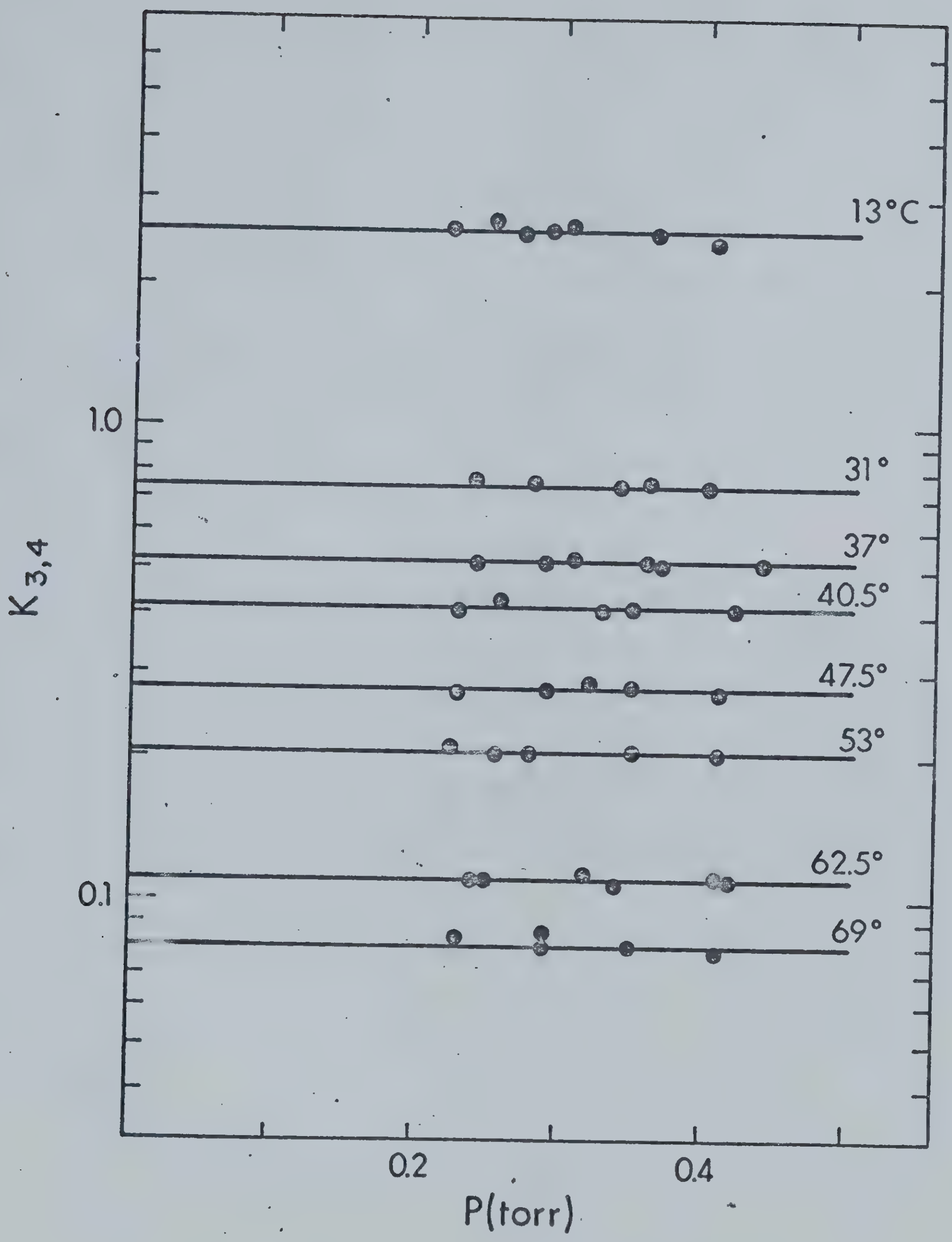

FIGURE 49 Equilibrium Constants versus Pressure of Acetonitrile at Various Temperatures for the Reaction:

$$Rb^+(CH_3CN)_3 + CH_3CN = Rb^+(CH_3CN)_4 .$$

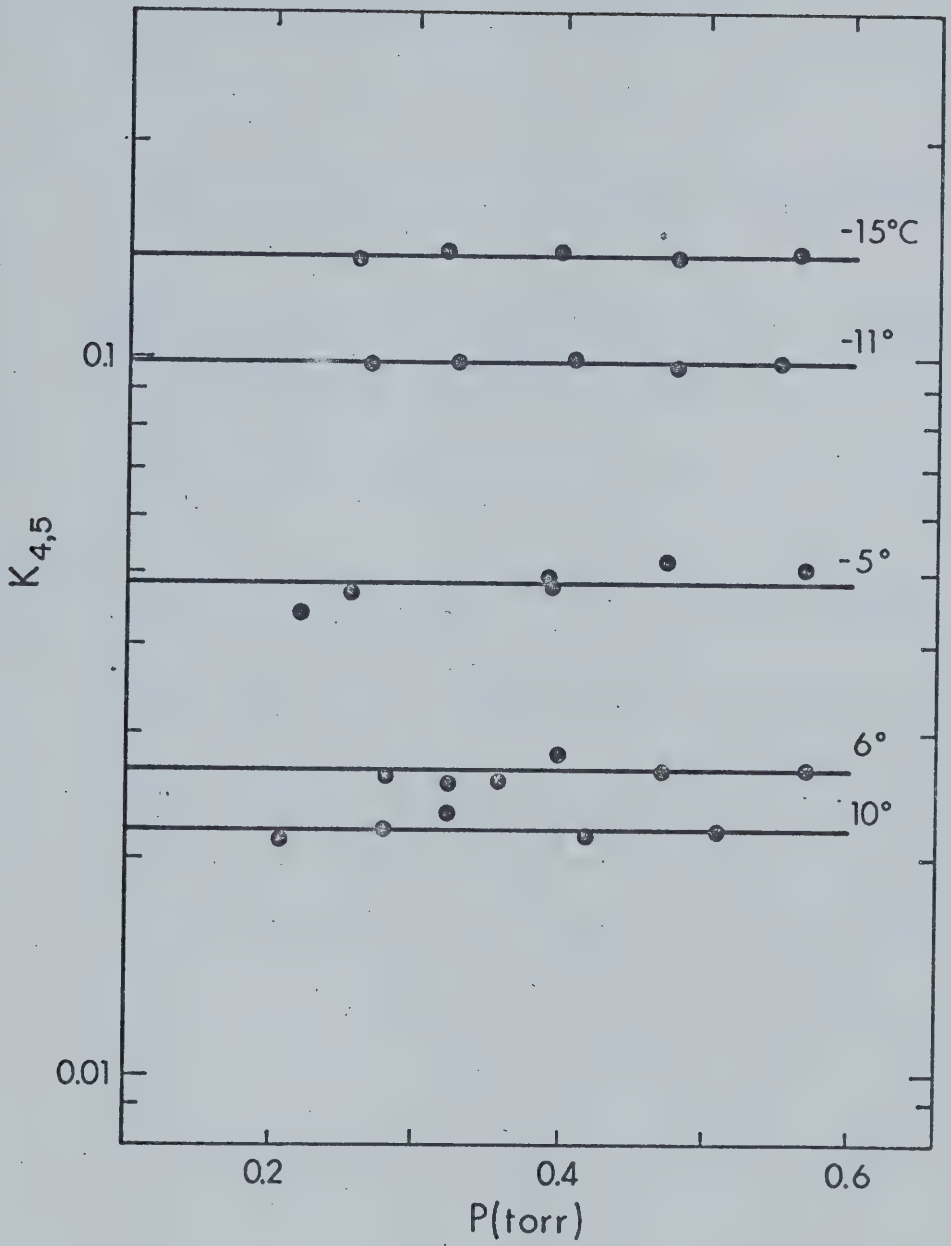

FIGURE 50 Equilibrium Constants versus Pressure of Acetonitrile at Various Temperatures for the Reaction:

$$Rb^+(CH_3CN)_4 + CH_3CN = Rb^+(CH_3CN)_5 .$$

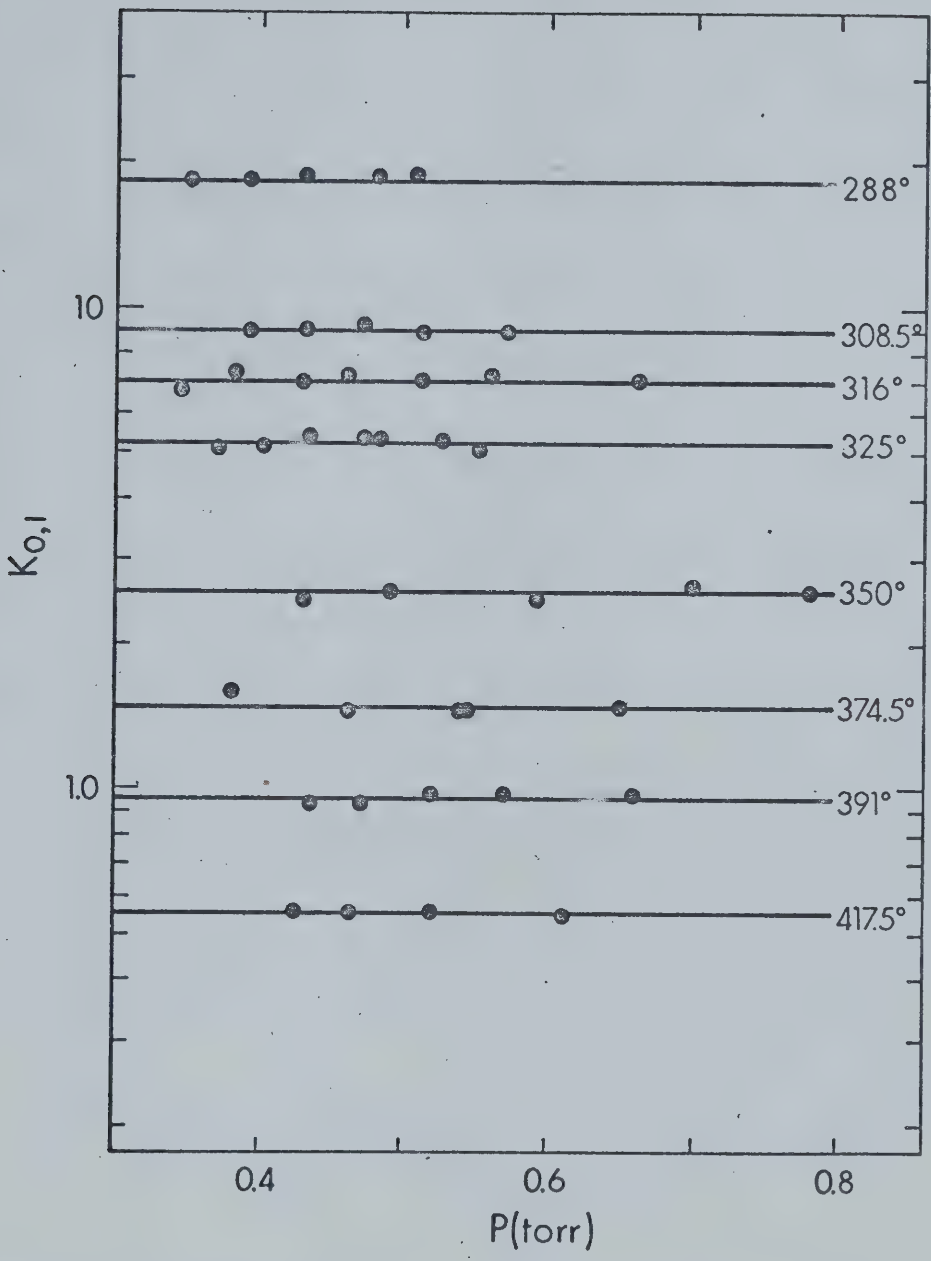

FIGURE 51 Equilibrium Constants versus Pressure of Acetonitrile at Various Temperatures for the Reaction :

$$Cs^+ + CH_3CN = Cs^+(CH_3CN) .$$

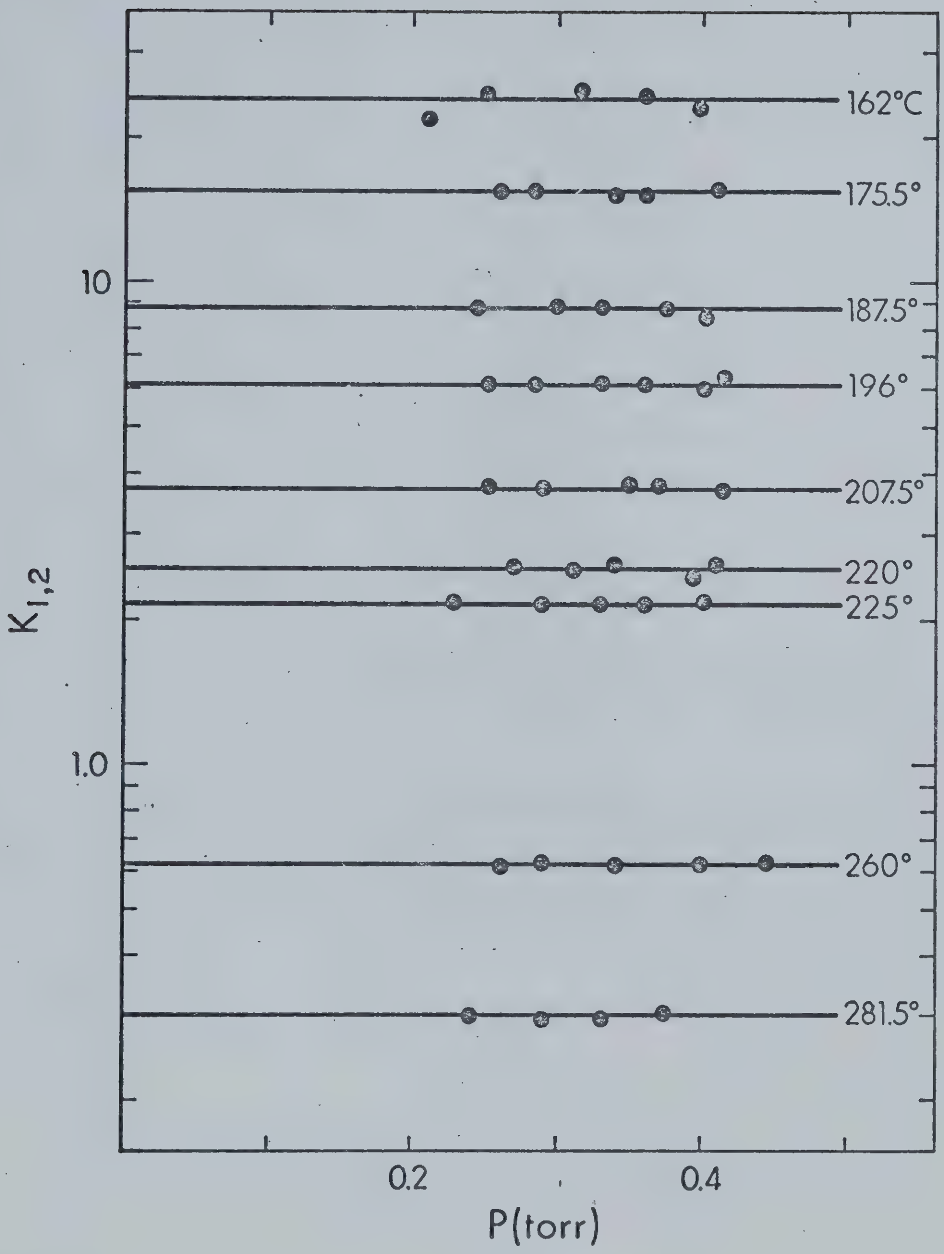

FIGURE 52 Equilibrium Constants versus Pressure of Acetonitrile at Various Temperatures for the Reaction:

$$Cs^+(CH_3CN) + CH_3CN = Cs^+(CH_3CN)_2 .$$

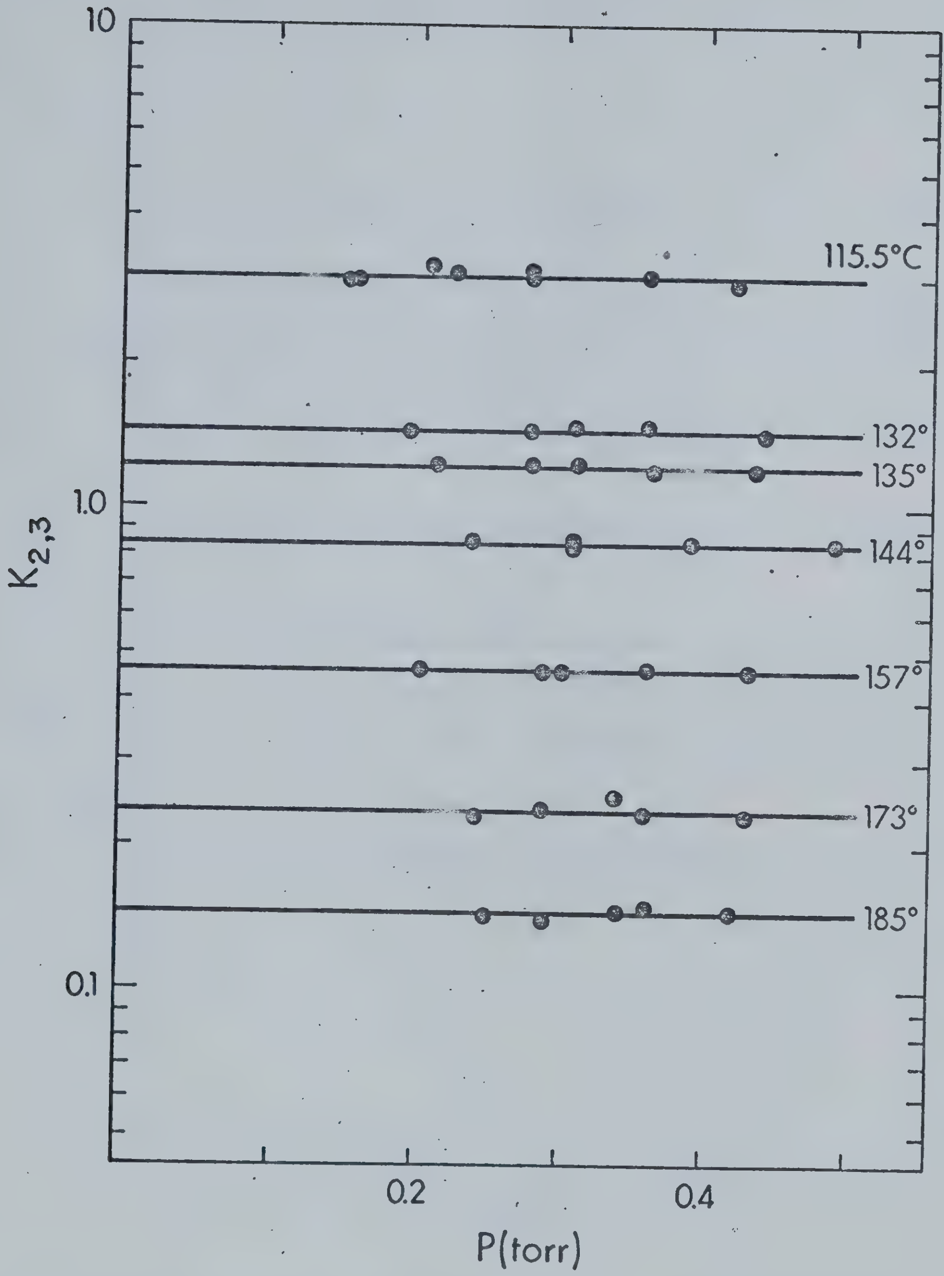

FIGURE 53 Equilibrium Constants versus Pressure Of Acetonitrile at Various Temperatures for the Reaction:

$$Cs^+(CH_3CN)_2 + CH_3CN = Cs^+(CH_3CN)_3 .$$

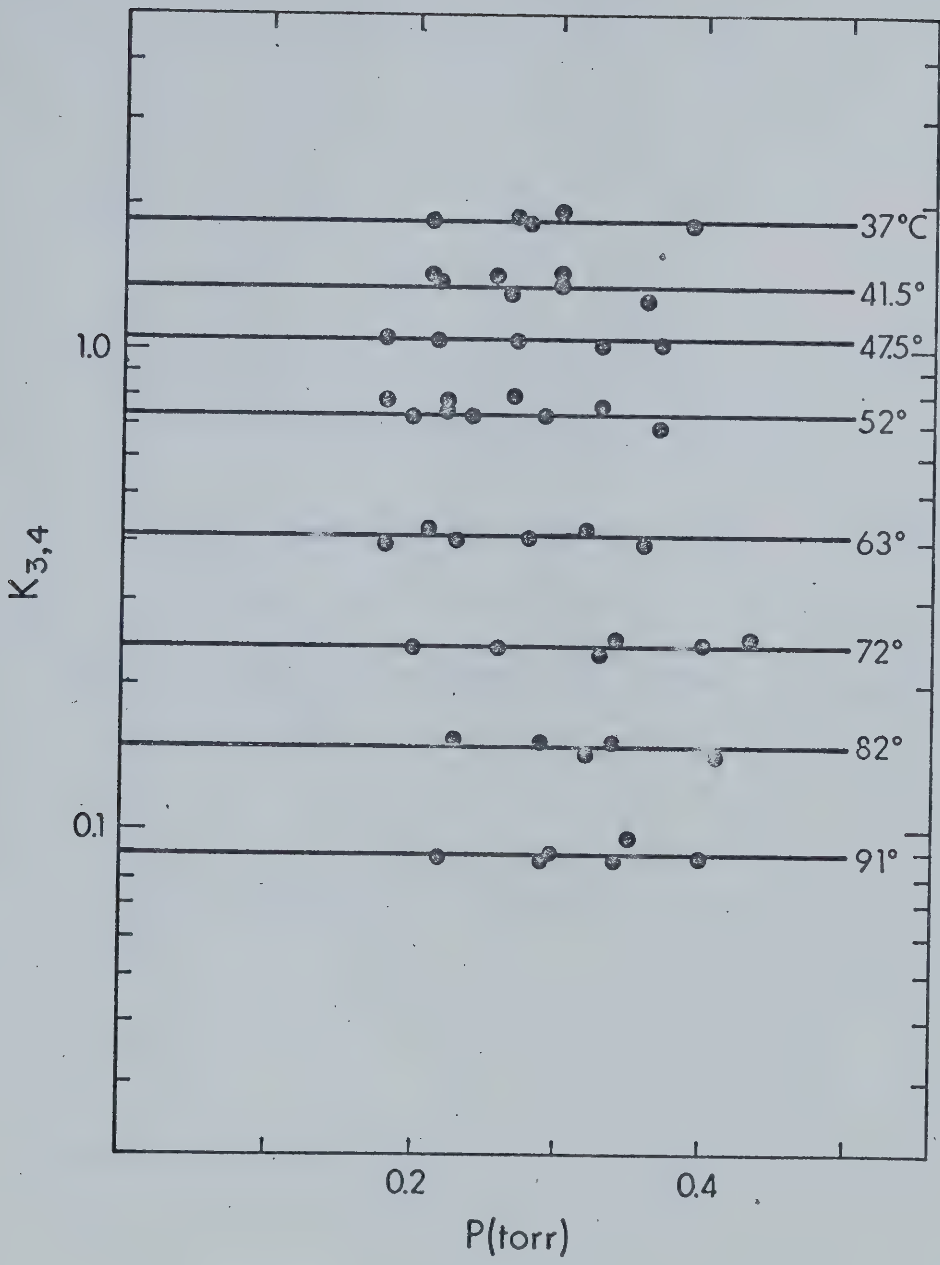

FIGURE 54 Equilibrium Constants versus Pressure of Acetonitrile at Various Temperatures for the Reaction:

$$Cs^+(CH_3CN)_3 + CH_3CN = Cs^+(CH_3CN)_4 .$$

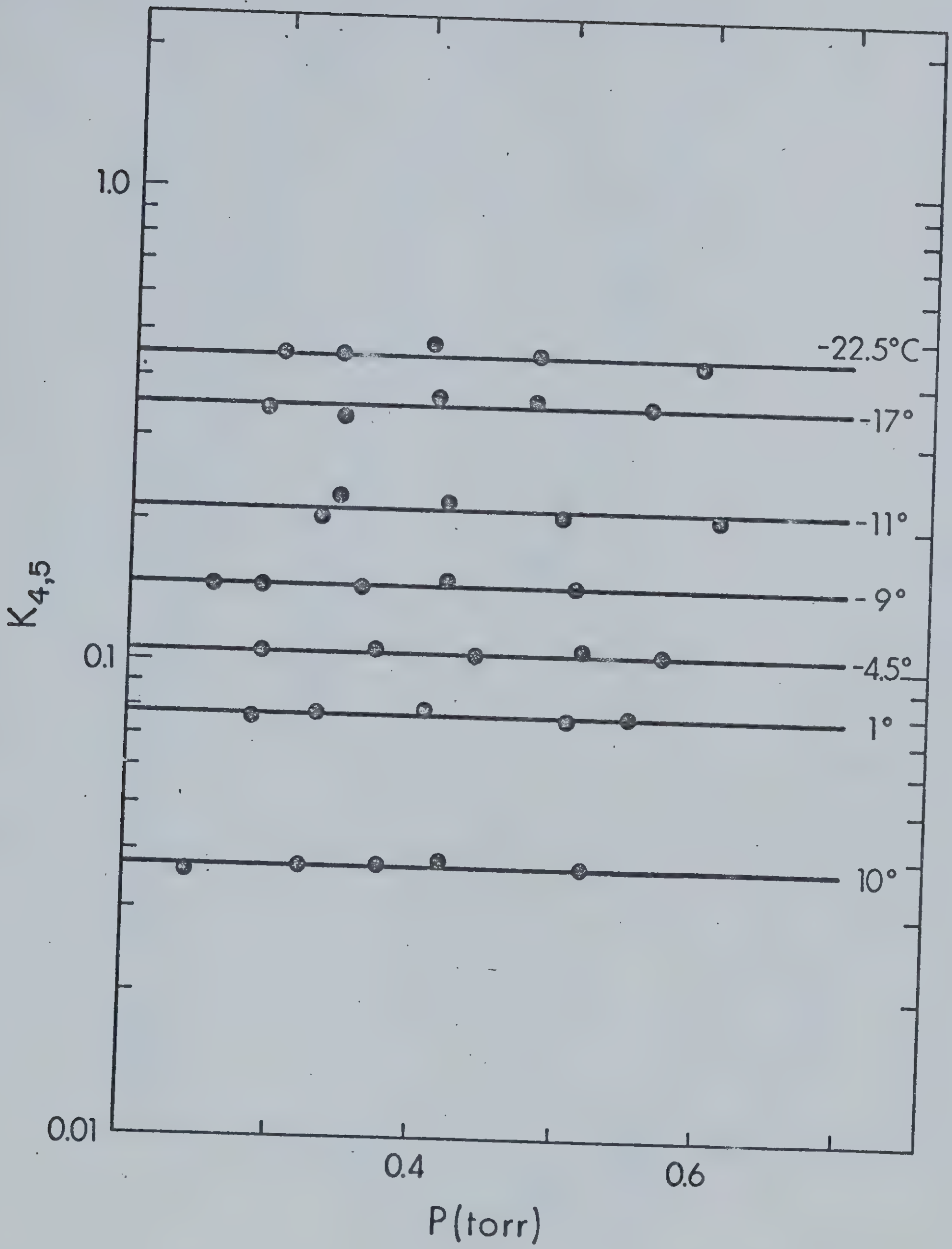

FIGURE 55 Equilibrium Constants versus Pressure of Acetonitrile at Various Temperatures for the Reaction:

$$Cs^+(CH_3CN)_4 + CH_3CN = Cs^+(CH_3CN)_5 .$$

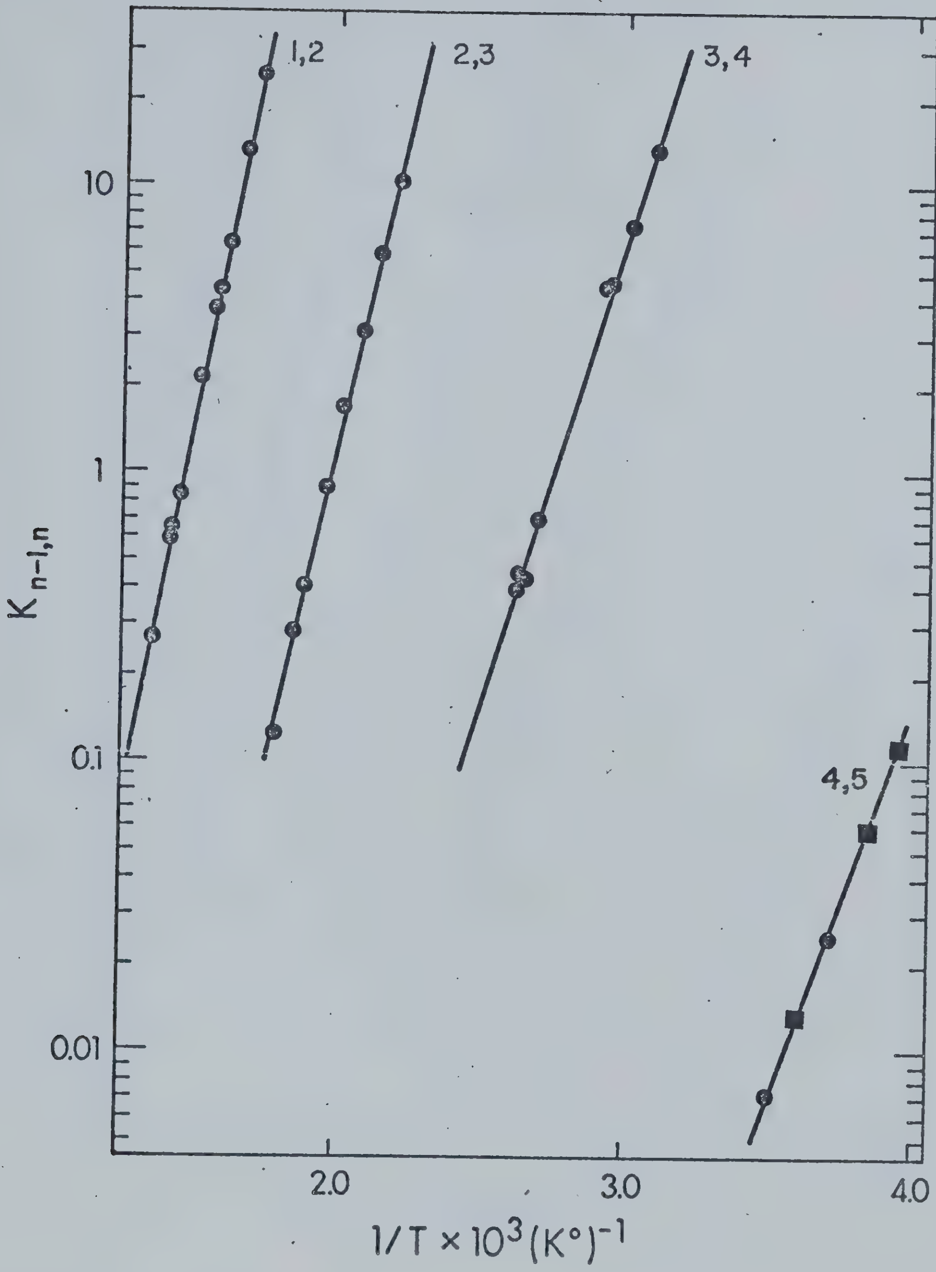

FIGURE 56 Van't Hoff Type Plots of the Equilibrium Constants for the Gas Phase Solvation of the Sodium Ion by Acetonitrile.

■ Points from Potassium-Sodium source.

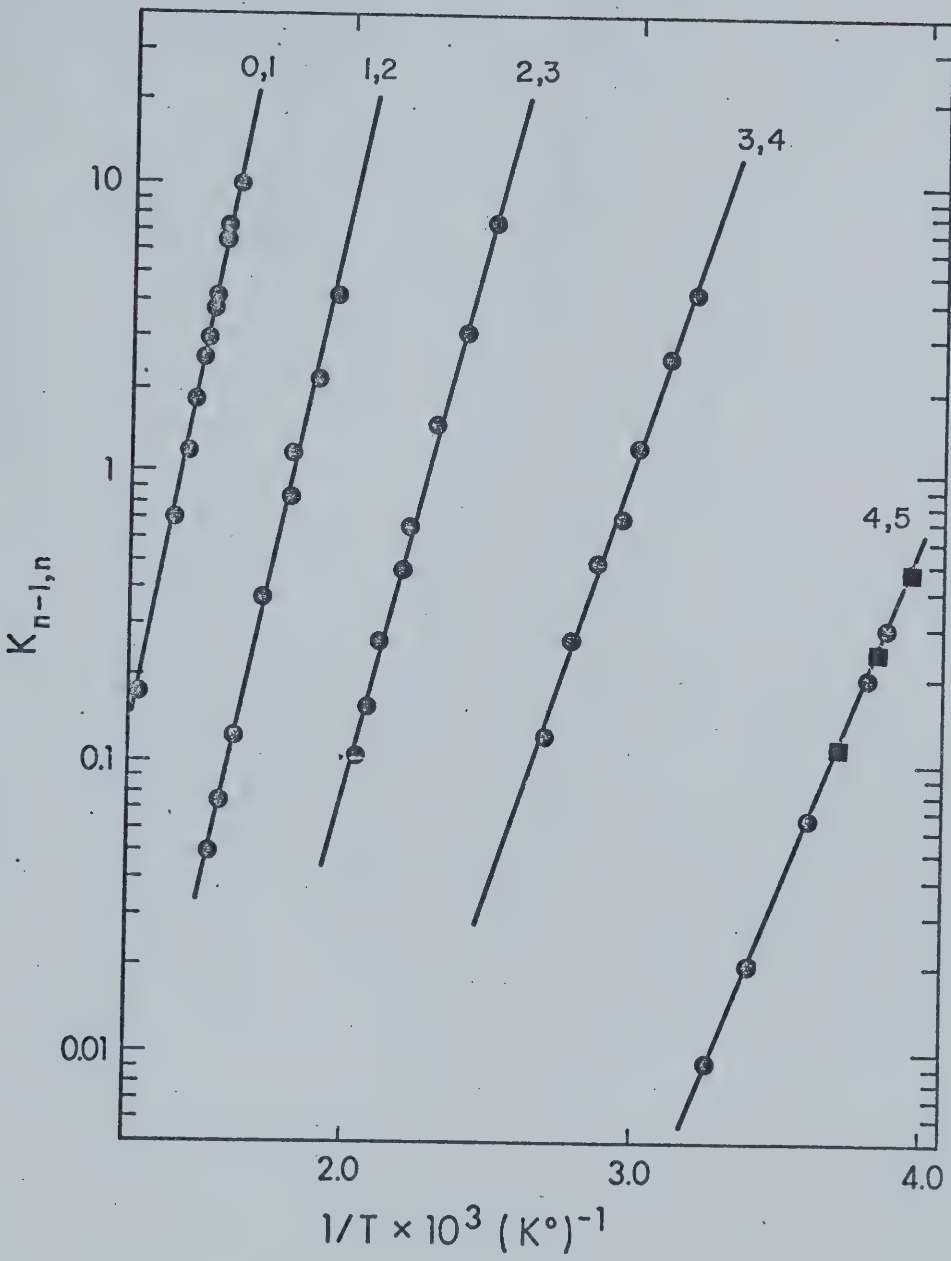

FIGURE 57 Van't Hoff Type Plots of the Equilibrium Constants for the Gas Phase Solvation of the Potassium Ion by Acetonitrile.

■ Points from potassium-sodium source.

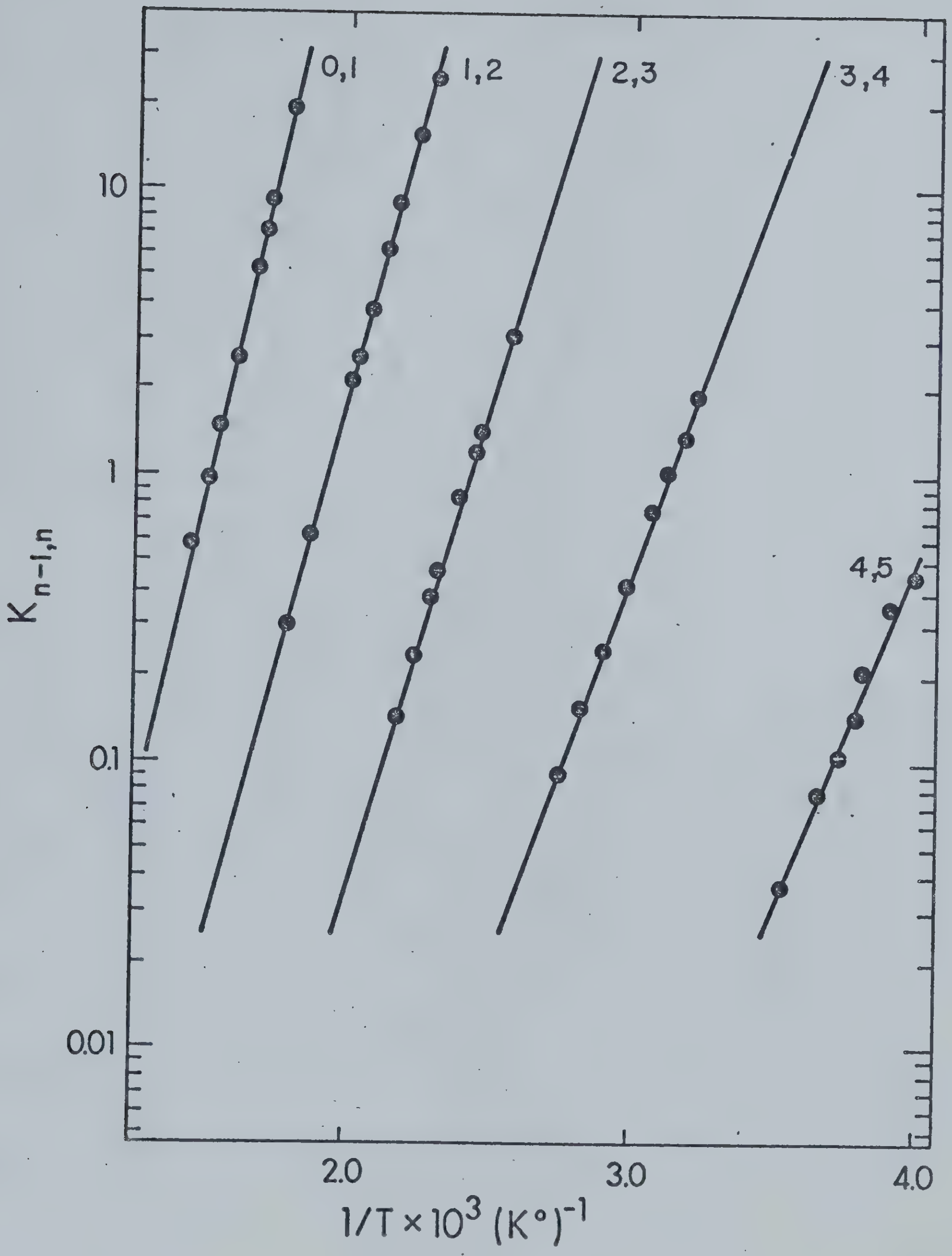

FIGURE 58 Van't Hoff Type Plots of the Equilibrium Constants for the Gas Phase Solvation of the Rubidium Ion by Acetonitrile.

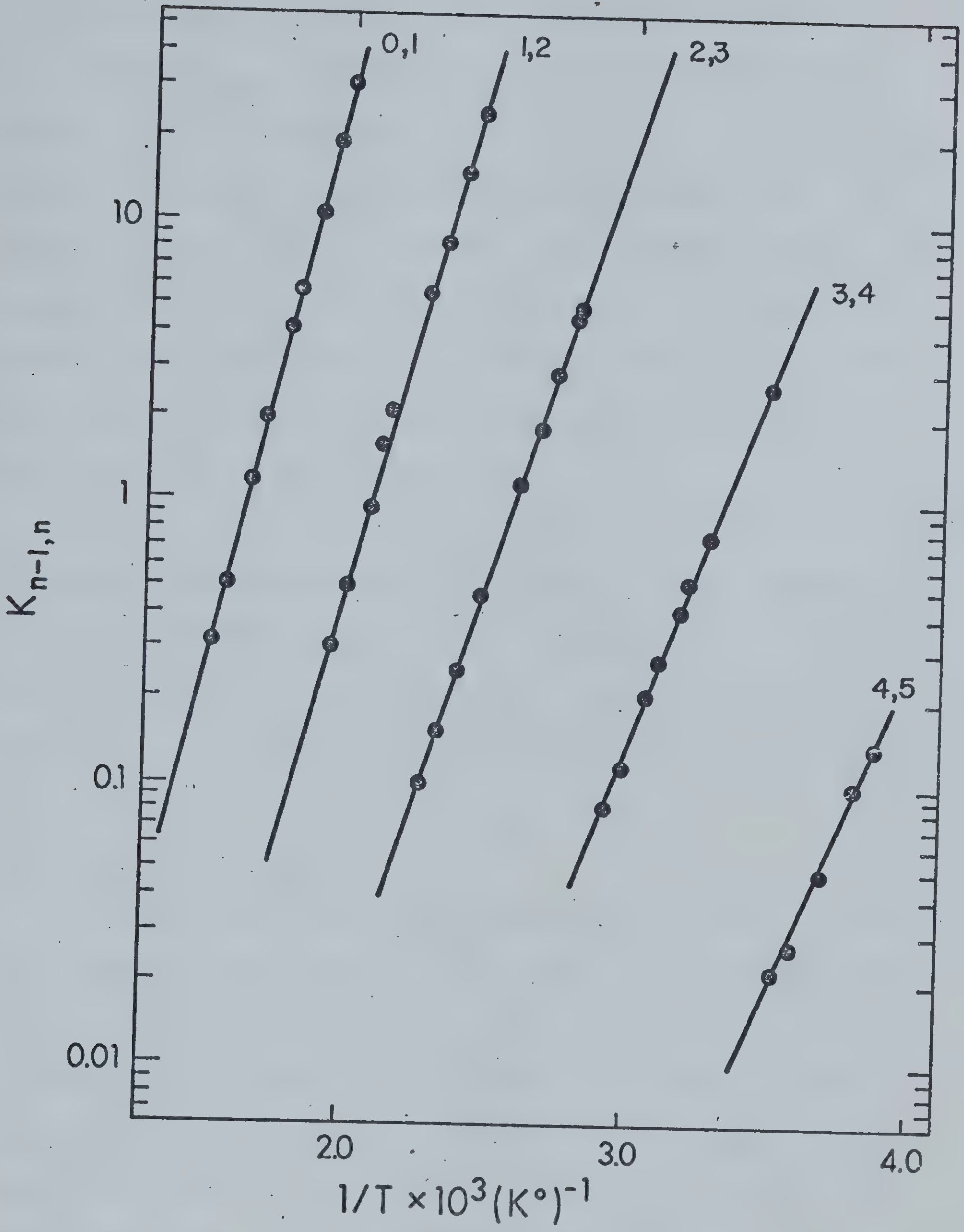

FIGURE 59 Van't Hoff Type Plots of the Equilibrium Constants for the Gas Phase Solvation of the Cesium Ion by Acetonitrile.

to low intensities. Thus no $Li^+$ data are presented.

The $\Delta G^o_{n-1,n}$ values at 298° K were determined by extrapolation of the Van't Hoff plots to room temperature. The values obtained for the enthalpy, entropy and free energy at room temperature for the reactions studied are presented in Tables 6 to 9. The values are obtained by a least square treatment of the data. The standard deviation, determined as well from the least square treatment, is also given for the various reactions.

The enthalpies for the various n-1,n clustering reactions are plotted as a function of n, the number of ligands, in Figure 60. Likewise, the free energy change at 298° K is plotted versus n in Figure 61. The values of $\Delta H^o_{0,1}$ and $\Delta G^o_{0,1}$ for the sodium ion are obtained by extrapolation.

## 3.3 General Discussion

For gas phase solvation studies, it has been found (3) that the values of $-\Delta H_{n-1,n}$ and $-\Delta G^o_{n-1,n}$ at 298° K decrease with the value of n. This is to be expected from the increase in dipole-dipole interactions between ligand molecules as the number of ligands is increased. From Tables 6-9 and from Figures 60 and 61, this can be seen to be the case with the solvation of alkali ions in acetonitrile. Likewise, it has been found (3) that the values of $-\Delta G^o$ and $-\Delta H^o$ decrease for a given value of n as the radius of the alkali ion increases. That is, sodium is expected to have a larger $-\Delta H^o$ and $-\Delta G^o$ than cesium due

## TABLE 6

### Experimental Thermodynamic Values for the Gas Phase Reactions:

$$Na^{+}(CH_3CN)_{n-1} + CH_3CN \rightleftarrows Na^{+}(CH_3CN)_{n} \qquad (n-1,n)$$

| Reaction (n-1,n) | $-\Delta H_{n-1,n}$ (kcal/mole) | $-\Delta G_{n-1,n}$[a] (kcal/mole) | $-\Delta S_{n-1,n}$[a] (e.u.) |
|---|---|---|---|
| 1,2 | 24.4 ±0.3 | 17.6 ± 0.4 | 22.7 ± 0.5 |
| 2,3 | 20.6 ±0.5 | 12.3 ± 0.5 | 27.5 ± 0.9 |
| 3,4 | 14.9 ±0.2 | 6.61 ± 0.3 | 27.9 ± 0.6 |
| 4,5 | 12.7 ±0.2 | 0.39 ± 0.3 | 41.2 ± 0.7 |

[a] Standard state 1 atm and 298°K

The errors quoted in this and subsequent tables are indeterminent errors obtained from least square fitting.

## TABLE 7

### Experimental Thermodynamic Values for the Gas Phase Reactions:

$$K^+(CH_3CN)_{n-1} + CH_3CN \rightleftarrows K^+(CH_3CN)_n \qquad (n-1,n)$$

| Reaction $n-1,n$ | $-\Delta H^o_{n-1,n}$ (kcal/mole) | $-\Delta G^o_{n-1,n}$ $^a$ (kcal/mole) | $-\Delta S^o_{n-1,n}$ $^a$ (e.u.) |
|---|---|---|---|
| 0,1 | 24.4 ± 0.4 | 18,0 ± 0.5 | 21.5 ± 0.7 |
| 1,2 | 20.6 ± 0.5 | 13.4 ± 0.5 | 24.2 ± 0.5 |
| 2,3 | 18.2 ± 0.3 | 9.8 ± 0.3 | 28.3 ± 0.6 |
| 3,4 | 13.6 ± 0.4 | 5.44 ± 0.5 | 27.5 ± 1.2 |
| 4,5 | 11.5 ± 0.1 | 1.43 ± 0.1 | 33.7 ± 0.3 |

[a] Standard state 1 atm and 298° K

# TABLE 8

## Experimental Thermodynamic Functions for the Gas Phase Reactions:

$$Rb^{+}(CH_3CN)_{n-1} + CH_3CN \rightleftarrows Rb^{+}(CH_3CN)_n \qquad (n-1,n)$$

| Reaction n-1,n | $-\Delta H^{o}_{n-1,n}$ (kcal/mole) | $-\Delta G^{o\,a}_{n-1,n}$ (kcal/mole) | $-\Delta S^{a}_{n-1,n}$ (e.u.) |
|---|---|---|---|
| 0,0 | 20.7 ± 0.3 | 15.3 ± 0.3 | 18.1 ± 0.5 |
| 1,2 | 17.7 ± 0.2 | 11.4 ± 0.3 | 20.9 ± 0.5 |
| 2,3 | 15.7 ± 0.2 | 8.30 ± 0.3 | 24.8 ± 0.5 |
| 3,4 | 12.5 ± 0.2 | 4.80 ± 0.3 | 25.7 ± 0.5 |
| 4,5 | 11.1 ± 0.6 | 1.42 ± 0.8 | 32.5 ± 2.1 |

[a] Standard state 1 atm and 298° K

# TABLE 9

## Experimental Thermodynamic Functions for the Gas Phase Reactions:

$Cs^{+}(CH_3CN)_{n-1} + CH_3CN \rightleftarrows Cs^{+}(CH_3CN)_n$ (n-1,n)

| Reaction n-1,n | $-\Delta H^{o}_{n-1,n}$ (kcal/mole) | $-\Delta G^{o}_{n-1,n}$ [a] (kcal/mole) | $-\Delta S^{o}_{n-1,n}$ [a] (e.u.) |
|---|---|---|---|
| 0,1 | 19.2 ± 0.1 | 13.7 ± 0.1 | 18.6 ± 0.2 |
| 1,2 | 16.7 ± 0.3 | 10.2 ± 0.3 | 21.6 ± 0.6 |
| 2,3 | 14.3 ± 0.1 | 7.2 ± 0.2 | 24.0 ± 0.4 |
| 3,4 | 12.1 ± 0.1 | 4.01 ± 0.2 | 27.0 ± 0.4 |
| 4,5 | 10.9 ± 0.3 | 1.06 ± 0.5 | 32.9 ± 1.2 |

[a] Standard state 1 atm and 298° K

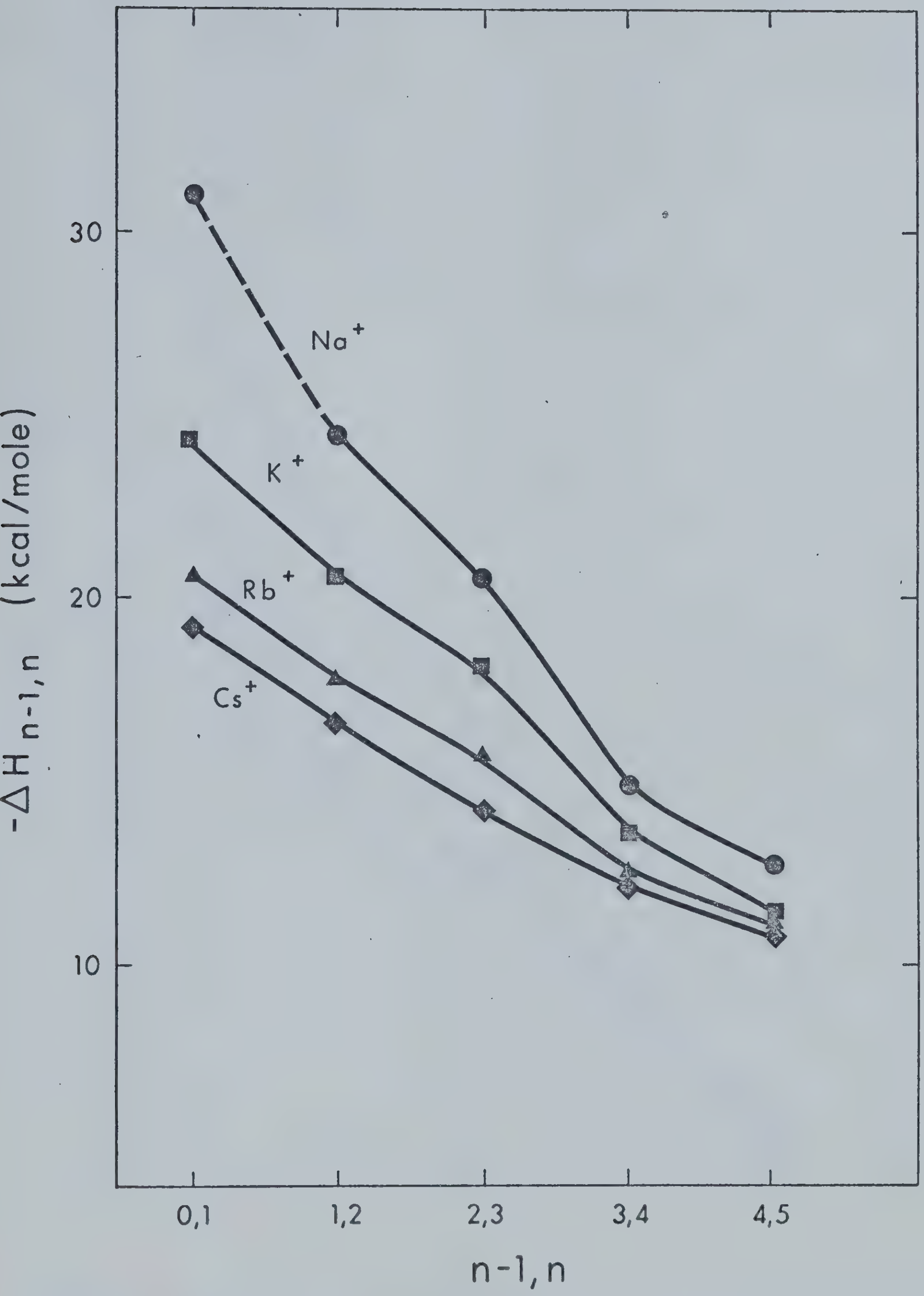

FIGURE 60 Enthalpies for the Clustering Reactions:

$$M^+(CH_3CN)_{n-1} + CH_3CN = M^+(CH_3CN)_n \ .$$

M = Na, K, Rb, Cs. The dashed line indicates an extrapolated value.

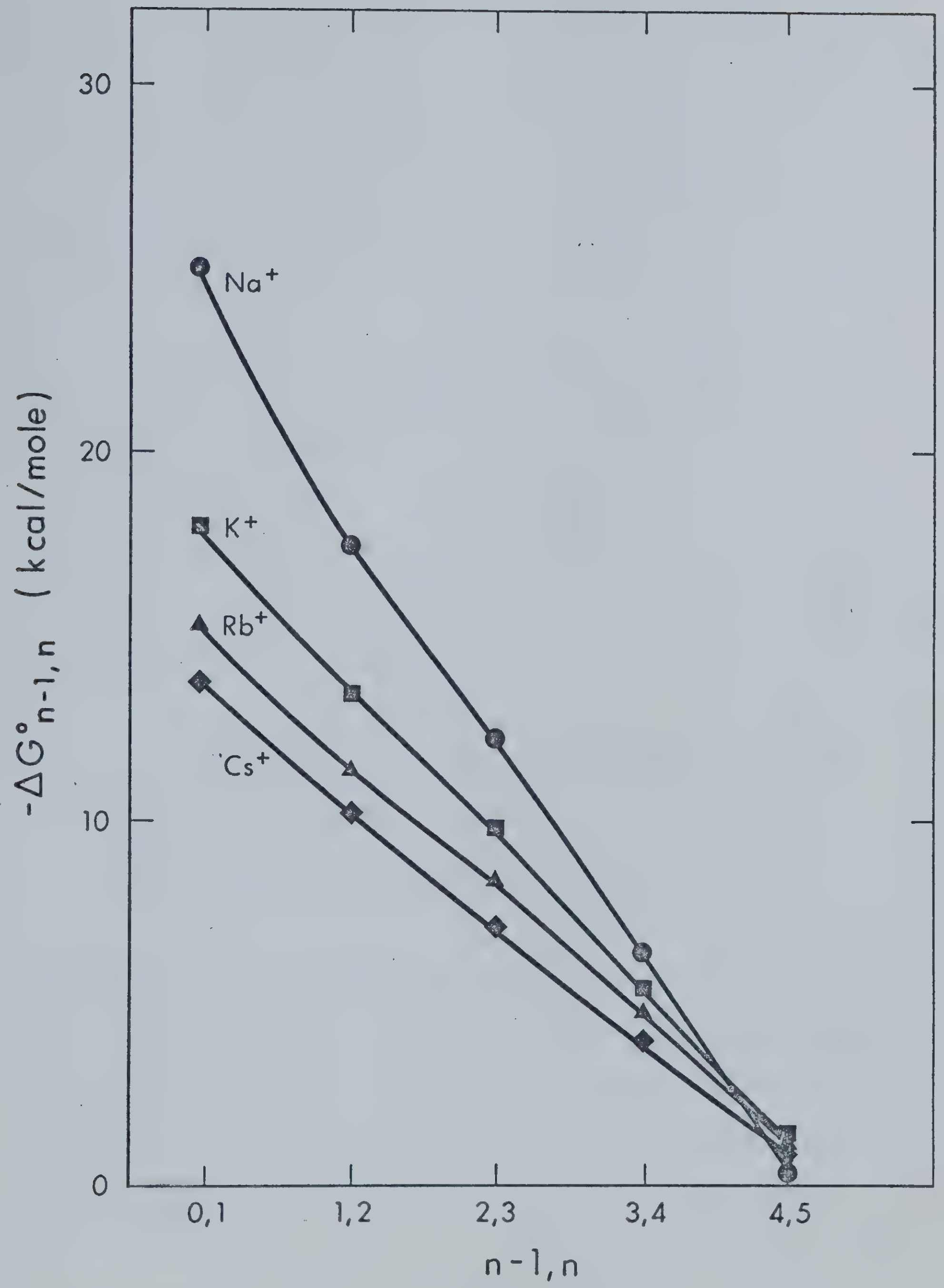

FIGURE 61 Standard Free Energies at 298° K for the Clustering Reactions:

$$M^+(CH_3CN)_{n-1} + CH_3CN = M^+(CH_3CN) .$$

M= Na,K,Rb,Cs. Standard State = 1 atm.

$\Delta G_{0,1}$ for $Na^+$ obtained by extrapolation.

to the greater charge density of the sodium ion. With acetonitrile as the solvent, this is the case for clusters with up to four acetonitrile ligands, but the value of $-\Delta G^{o}_{4,5}$ for sodium is lower than the corresponding values for potassium, rubidium, and even cesium. The $-\Delta H_{4,5}$ value for sodium is still slightly greater than the corresponding enthalpies for $K^+$, $Rb^+$, and $Cs^+$ - the difference being attributed to the abnormally unfavourable entropy of the $Na^+$-$CH_3CN$, 4-5 reaction.

To ensure that this phenomenon was not due to some instrumental defect, a filament containing both sodium and potassium ion was constructed and the equilibrium constants of the reactions:

$$Na^+(CH_3CN)_4 + CH_3CN \rightleftarrows Na^+(CH_3CN)_5 \qquad 3.3$$

$$K^+(CH_3CN)_4 + CH_3CN \rightleftarrows K^+(CH_3CN)_5 \qquad 3.4$$

were studied at the same temperatures and pressures. These equilibrium constants are in good agreement with those obtained when using a filament containing only one ion (Figures 39, 45, 56 and 57). In all cases, the potassium ion-acetonitrile reaction was more favourable than the sodium-acetonitrile reaction; (that is, the equilibrium constant for reaction 3.4 was greater than the corresponding constant for reaction 3.3). When n is less than 5, the sodium equilibrium constant is always greater than the

potassium equilibrium constant at a given temperature, as shown in Table 10. The temperatures used in this Table are taken from the centre of the experimental range for the sodium clustering reaction. Rubidium and cesium are included in this Table as well.

In previous solvation studies (40, 41, 45), it was found that the Van't Hoff plots tend to become closer to each other as the size of the cluster increases. In the case of acetonitrile with alkali metal ions this occurs until the 4,5 plot. The spacing between the 4,5 and 3,4 plots (as can be seen from Figures 56-59) is greater than that between the 3,4 and 2,3 plots, with the greatest abnormality in the $Na^+$ case. From the values of $-\Delta H$ and $-\Delta S$ (Tables 6-9) this would appear to be due to the high entropy term, rather than the enthalpy term which is decreasing rather steadily.

It was found in the alkali ion-water studies (3) that the $-\Delta S_{n-1,n}$ increased steadily as the number of ligands increased, and there were no distinct changes as is the case with acetonitrile. This abrupt change in the entropy upon the addition of the fifth acetonitrile molecule can be attributed to the restriction of motion with the increased crowding of the acetonitrile ligands in the first solvation shell. In the $NH_4^+(H_2O)$, $NH_4^+(NH_3)$, and halide ion-acetonitrile studies done in this laboratory (45, 2, 41) it was found that the $-\Delta S_{n-1,n}$ of the larger clusters took an abrupt decrease. This was attributed to the formation

## TABLE 10

### Ratio of Equilibrium Constants at Specific Temperatures[a] for the Reactions:

$$Na^+(CH_3CN)_{n-1} + CH_3CN \rightleftarrows Na^+(CH_3CN)_n \qquad (n-1,n)$$

Compared to:

$$M^+(CH_3CN)_{n-1}{}^{b} + CH_3CN \rightleftarrows M^+(CH_3CN)_n \qquad (n-1,n)$$

| Reaction (n-1,n) | Temperature[a] ($^oK$) | $\frac{K_{n-1,n}(Na^+)}{K_{n-1,n}(K^+)}$ | $\frac{K_{n-1,n}(Na^+)}{K_{n-1,n}(Rb^+)}$ | $\frac{K_{n-1,n}(Na^+)}{K_{n-1,n}(Cs^+)}$ |
|---|---|---|---|---|
| 0,1[c] | 931 | 71 | 95 | 275 |
| 1,2 | 680 | 35 | 58 | 171 |
| 2,3 | 506 | 16 | 33 | 89 |
| 3,4 | 363 | 5 | 9 | 31 |
| 4,5 | 234 | 0.3 | 0.4 | 0.8 |

[a] Temperature at which $K_{n-1,n}(Na^+) = 1$ torr$^{-1}$

[b] $M^+ = K^+$, $Rb^+$ and $Cs^+$

[c] Extrapolated values of thermodynamic functions used for $K_{0,1}(Na^+)$

of an outer solvation shell (41). Clearly from the present data on alkali ion solvation in acetonitrile, no outer shell is readily formed.

The weighted average number of ligands per ion at 298° K may be readily determined at a given acetonitrile pressure with a knowledge of the various values of $K_{n-1,n}$ obtained from the Van't Hoff plots. For example, the concentration of the species $Na^+(CH_3CN)_n$ at a pressure, p, will be:

$$[Na^+(CH_3CN)_n] = p^n \times \prod_{i=1}^{n} K_{i-1,i} \qquad 3.5$$

By setting the total concentrations of all the ionic species to unity at various pressures ($10^{-4}$ to 10 torr), a plot of the relative concentrations of the ions versus pressure may be obtained, as shown in Figure 62. In this figure, the data obtained for the hydration of sodium are also included.

In the case of the $Na^+(CH_3CN)$ system, only two ions of significant intensity occur in this large pressure range - $Na^+(CH_3CN)_3$ and $Na^+(CH_3CN)_4$. Between 0.2 and 10 torr, the normal working range in high pressure mass spectrometry, the $Na^+(CH_3CN)_4$ species accounts for over 90% of the total ionization. With water, however, five separate ions exist in this range and at about 2 torr water pressure, the four, five and six hydrated ions are of similar intensities. This same effect was noted to even a larger degree in the case of $H^+(H_2O)_n$. (40)

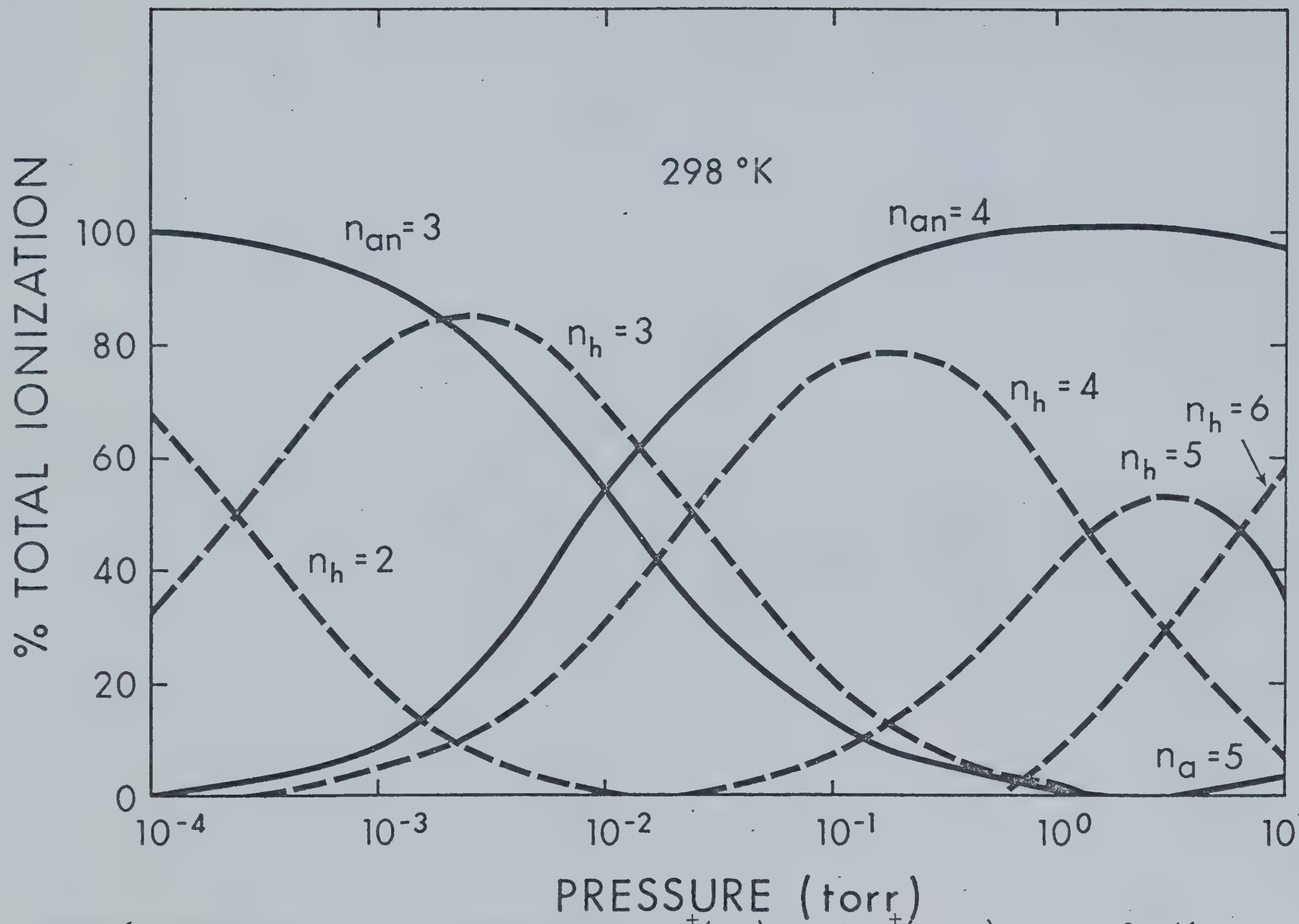

FIGURE 62 Plot of equilibrium distribution of $Na^+(H_2O)_{n_h}$ and $Na^+(CH_3CN)_{n_{an}}$ as a function of pressure.

Figure 62 demonstrates that stability differences between successive acetonitrile clusters are much larger than between the hydrates. A practical consequence of this is that the certainty with which equilibrium constants may be determined is much lower than in the case of a system such as $Na^+(H_2O)_n$.

## 3.4 A Comparison of the Gas Phase Solvation of Alkali Metal Ions in Water and Acetonitrile

In the gas phase, where ion-dipole and ion-induced dipole interactions play such an important part in solvation energies, it is expected that acetonitrile with its large dipole moment (3.97 D) and high polarizability (4.3 $A^3$) will solvate ions to a different degree than water with its much lower dipole moment of 1.85 D and lower polarizability (1.48 $A^3$). The data collected in this study can easily be compared to the thermodynamic functions obtained for the alkali metal ion-water solvation studies (3, 4).

The most direct method of comparing the relative solvating strengths of water and acetonitrile is to look at their Van't Hoff plots. This is done for sodium in Figure 63. The acetonitrile plots (solid lines) at low values of n-1,n are further to the high temperature (i.e. low 1/T) side of the figure than the water plots (dashed lines) of comparable n-1,n. This corresponds to more favourable solvation of acetonitrile at a given temperature at low n.

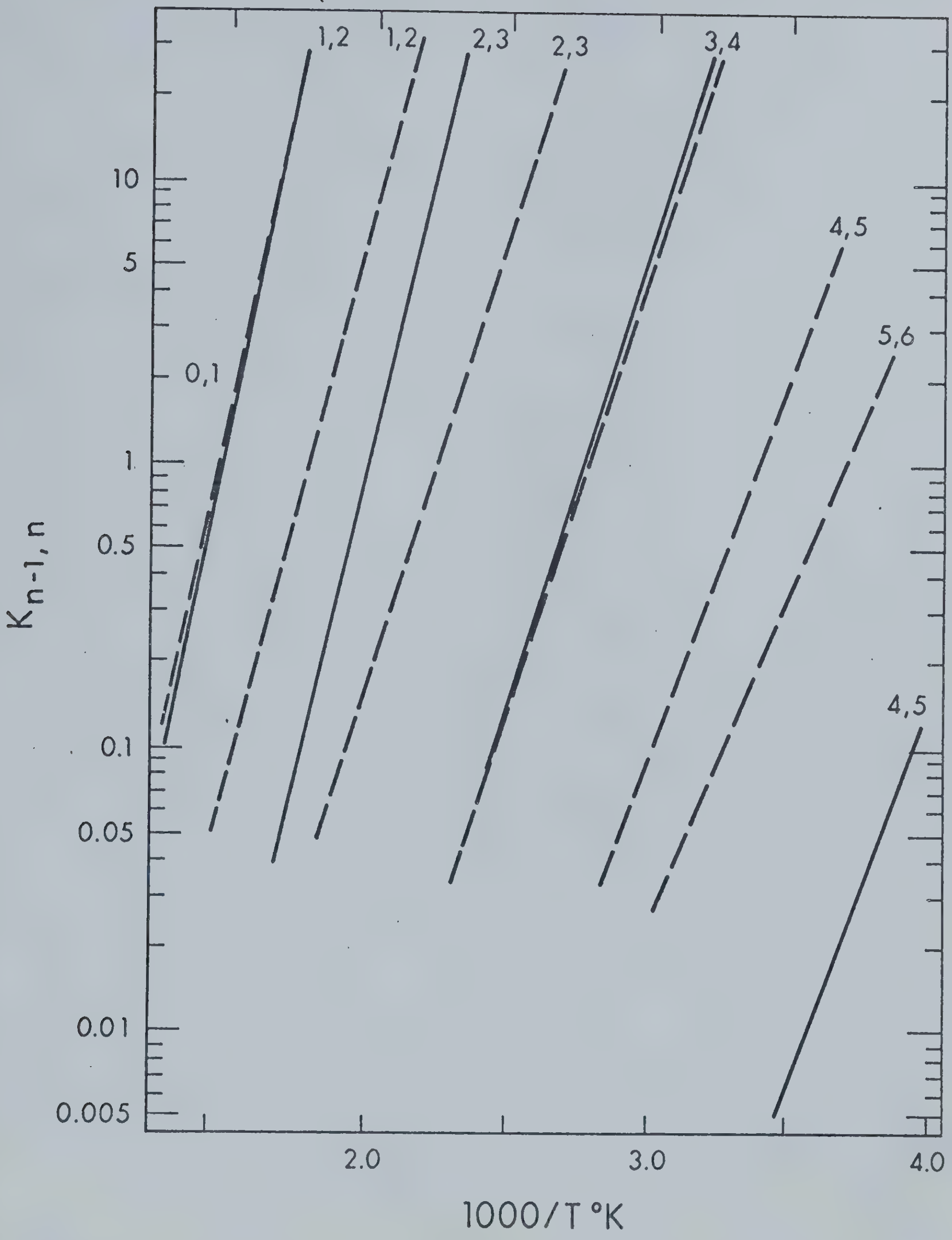

FIGURE 63 Van't Hoff Type Plots for the Gas Phase Solvation of the Sodium Ion by Acetonitrile (solid lines) and Water (dashed lines).

At (n-1,n) = 3,4 the plots are almost identical and then for higher values of n, the trend reverses. The $K_{4,5}$ values for $Na^+$-$CH_3CN$ are even lower at a corresponding temperature than the $K_{5,6}$ values for $Na^+$ and water. This implies that as the number of ligand increases, the water clusters become relatively more stable than the sodium-acetonitrile clusters.

The enthalpy and standard free energy functions of sodium and cesium clustering with both acetonitrile and water are shown in Figures 64 and 65 respectively. From both plots it is obvious that at low values of n, acetonitrile solvates the ions much more readily. As the cluster size reaches n=5, the enthalpies become almost equal, but there is a crossover in the free energy, indicating that free energy-wise water forms the more stable cluster. (To prevent cluttering the figures, solvation data involving the potassium and rubidium ions were not included.)

The difference in the $-\Delta G$ and $-\Delta H$ plots versus n-1,n can be attributed to the entropy values. For acetonitrile with sodium for example, $-\Delta S_{4,5}$ = 41.2 e.u. compared to the much lower value of 28.8 e.u. for water. This indicates a much more restricted solvation of the ion by the fifth acetonitrile molecule compared with the fifth water molecule.

The total free energy of solvation in the gas phase from 0 to n ($\Delta G_{0,n}$) is shown in Figure 66 plotted against n, the number of ligands. Again data from $Na^+$ and $Cs^+$ with both water and acetonitrile are shown. From the diagram, it

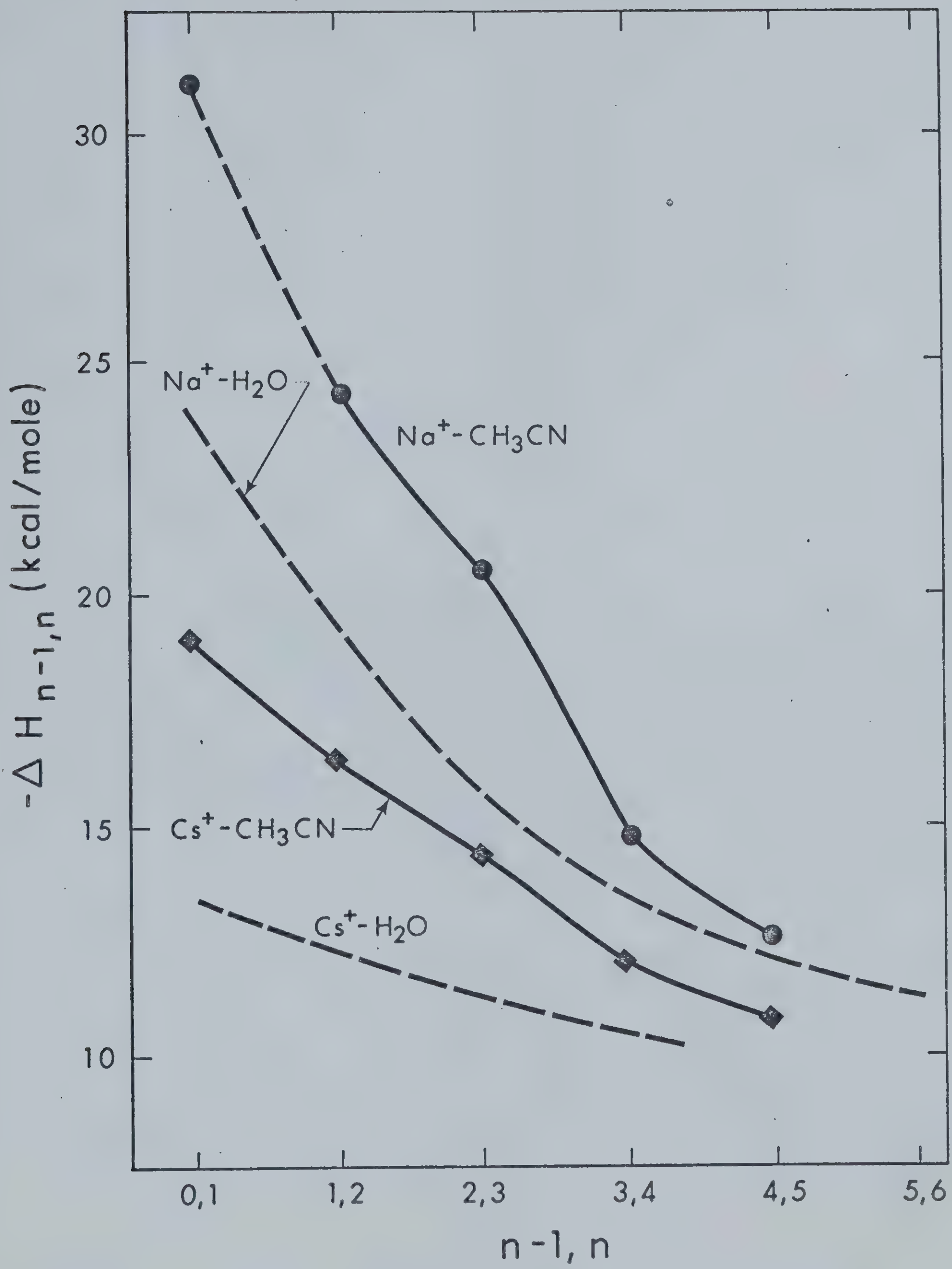

FIGURE 64 A Comparison of the Enthalpies of the Gas Phase Solvation of $Na^+$ and $Cs^+$ in Water and Acetonitrile.

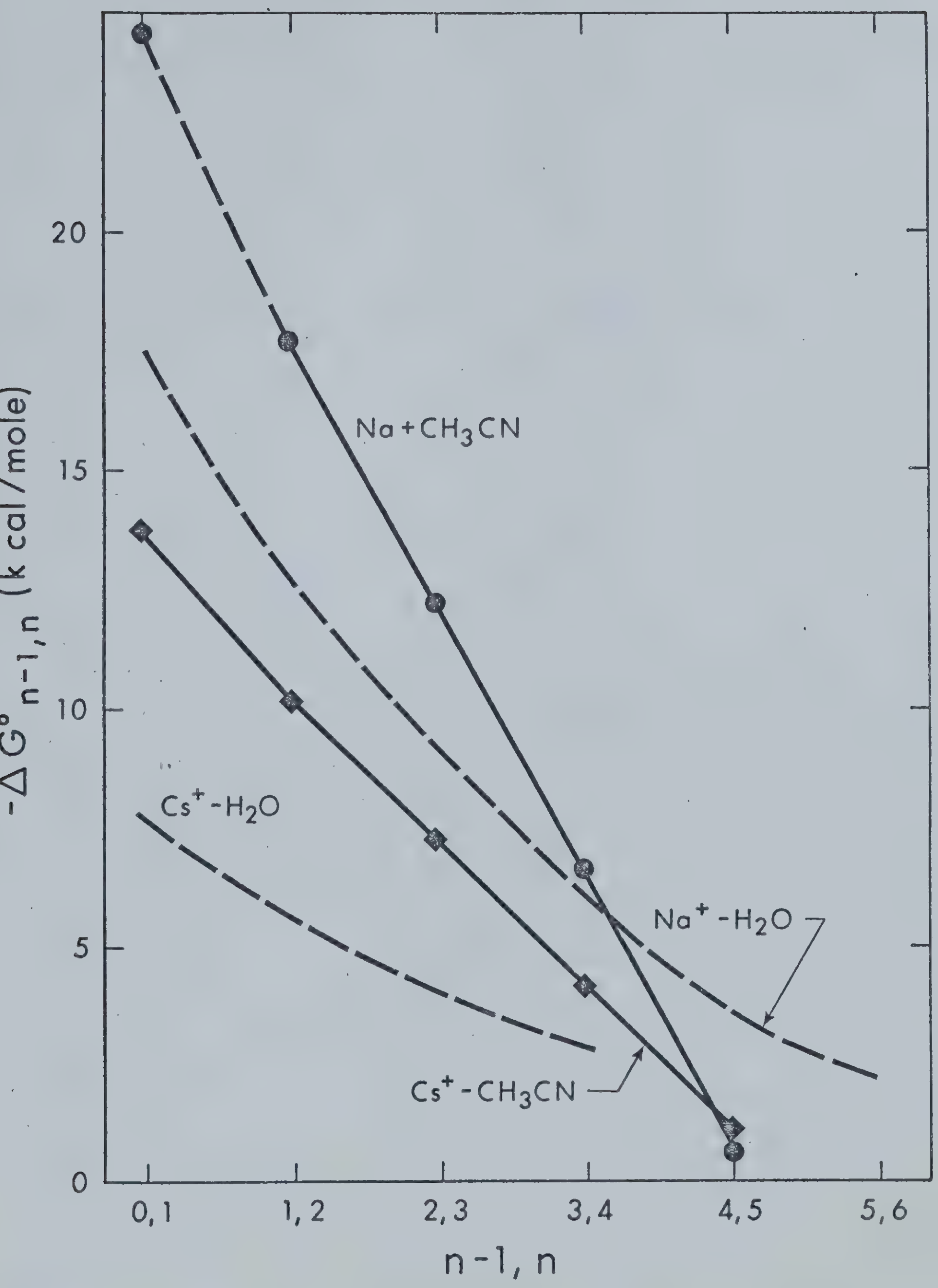

FIGURE 65 A Comparison of the Standard Free Energies of the Gas Phase Solvation of $Na^+$ and $Cs^+$ in Water and Acetonitrile. Standard state = 1 atm. and 298° K .

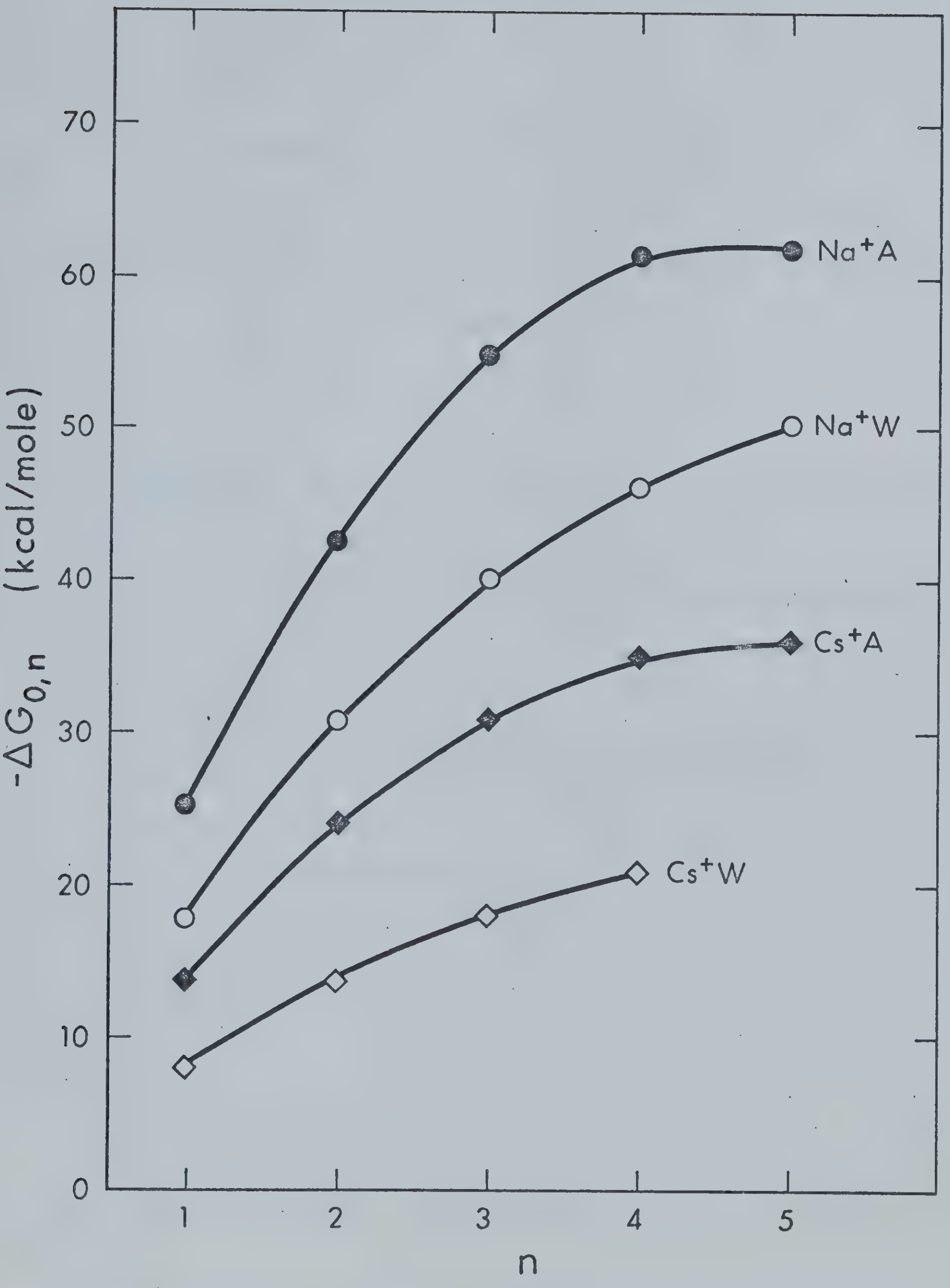

FIGURE 66 A Comparison of the Total Standard Free Energy of the Gas Phase Solvation of $Na^+$ and $Cs^+$ in Water and Acetonitrile versus the Number of Ligands. Standard State: 1 atm. and 298° K .

does not appear that the total water cluster will become more favourable than the acetonitrile cluster, or even approach it at high n. This is in direct conflict with solution chemists (Section 3.6) who have demonstrated that water solvates both sodium and cesium as well as, or better than, acetonitrile does. Therefore, one can conclude that the difference between the solvation energies of acetonitrile and water in solution are based on more than the close electrostatic interactions observed in the gas phase.

## 3.5 A Comparison between the Gas Phase Solvation of Alkali Metal Ions and Halide Ions in Acetonitrile

The strong preference for the solvation of cations over anions in acetonitrile which occurs in the liquid phase is also demonstrated in the gas phase. In Figure 67 the $\Delta G^{o}_{n-1,n}$ of the alkali and halide ions versus n-1,n are compared and in Figure 68 the enthalpies are similarly compared. To avoid confusion only $Na^+$, $Cs^+$, and their isoelectronic counterparts $F^-$ and $I^-$ are plotted. The other alkali and halide ions follow similar trends. The thermodynamic values for the halide ions are taken from Yamdagni and Kebarle (2).

At low values of n, the free energy of cation solvation is much more favourable than the free energy of anion solvation.

As the number of ligands increases this preference diminishes and in the case of the isoelectronic pair $Na^+$ and

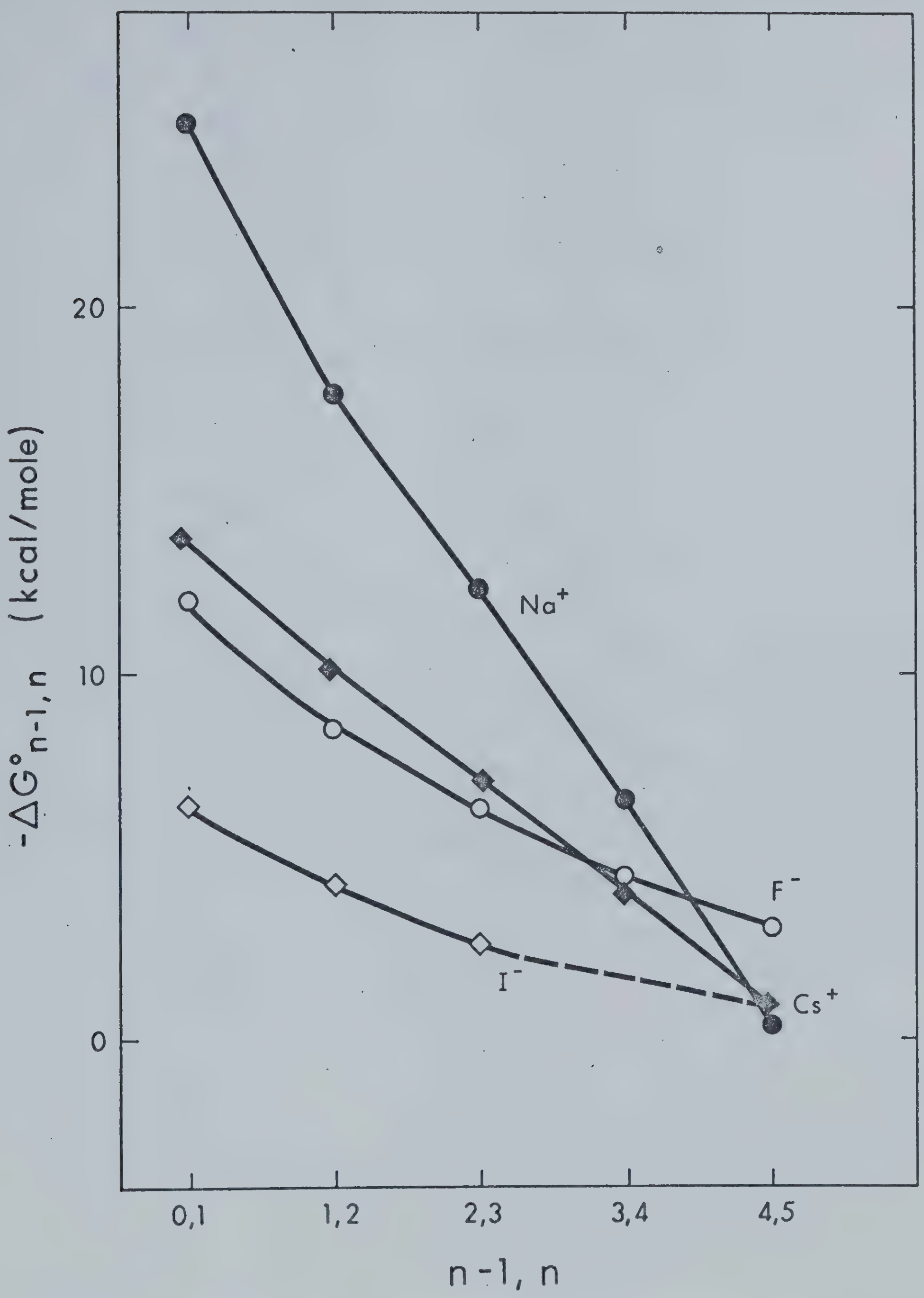

FIGURE 67 A Comparison of the Standard Free Energies of Gas Phase Solvation of Alkali and Halide Ions in Acetonitrile. Standard State: 1 atm. and 298° K.

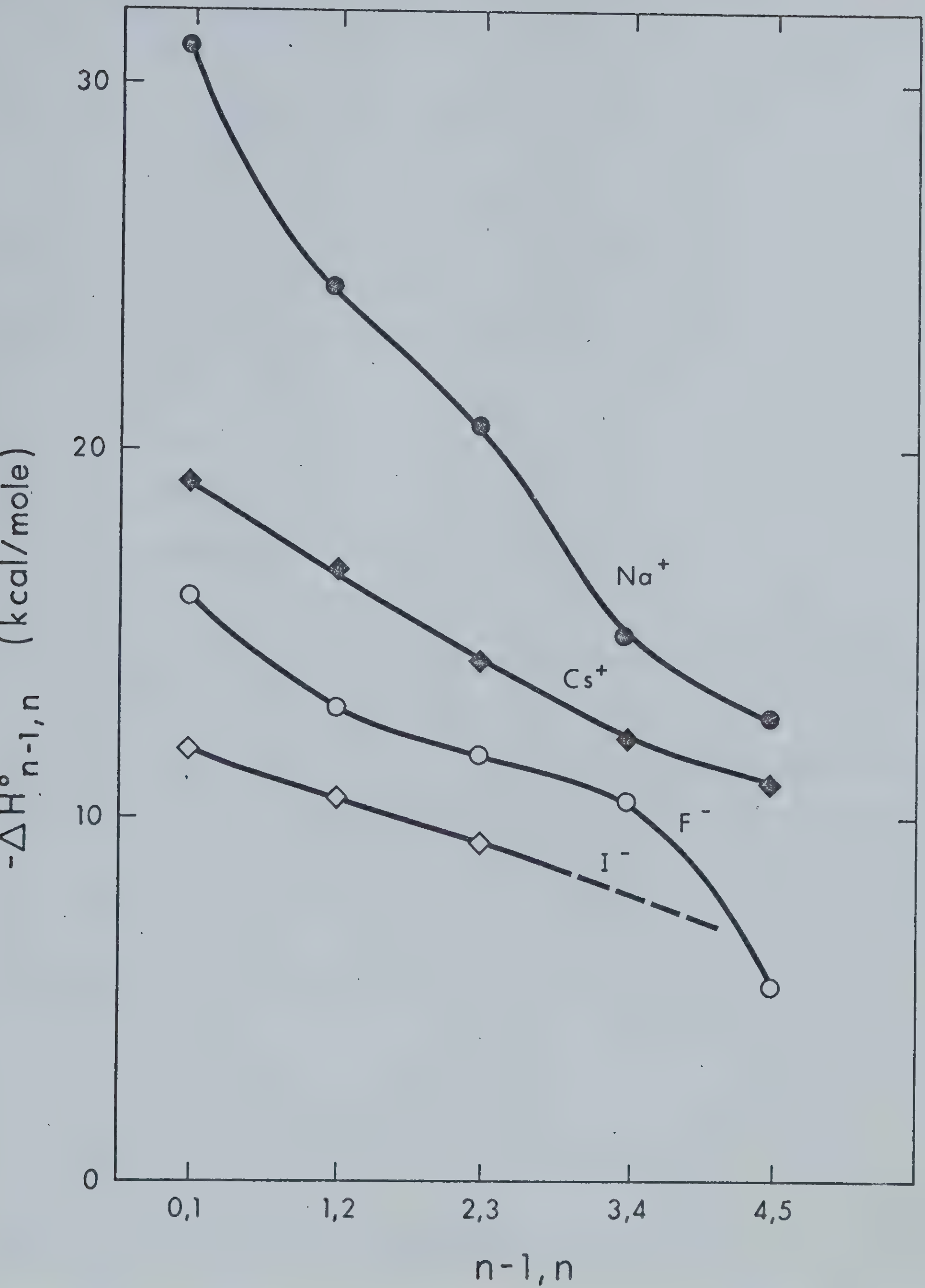

FIGURE 68 A Comparison of the Enthalpies of Gas Phase Solvation of Alkali and Halide Ions in Acetonitrile.

$F^-$ the trend reverses, that is the reaction:

$$F^-(CH_3CN)_4 + CH_3CN \rightleftarrows F^-(CH_3CN)_5 \qquad 3.6$$

becomes more favourable than its sodium counterpart. The $\Delta H_{n-1,n}$ plot is much more difficult to interpret. For the $Na^+$, $F^-$ pair, the two curves appear to be approaching until n=4, but at n=5 the enthalpy of the $F^-$-acetonitrile reaction takes a plunge and the two curves diverge. The enthalpies of the $Cs^+$, $I^-$ pair are slowly converging.

One explanation of the $Na^+$, $F^-$ situation can be attributed to the geometry of the two complexes and the possibility of shell formation. In the fluoride ion case, the ion-molecule bond probably occurs through the methyl hydrogens (87). This leaves the cyano group available for association with another acetonitrile molecule. In pure liquids it is well known that acetonitrile self-associates. Two models have been proposed for the dimer: one, an antiparallel dipole pair (88)

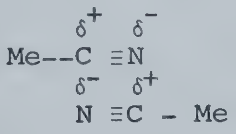

$$\begin{array}{lll} & \delta^+ & \delta^- \\ Me{-}{-} & C & \equiv N \\ & \delta^- & \delta^+ \\ & N & \equiv C - Me \end{array}$$

and the second, a skewed configuration (89)

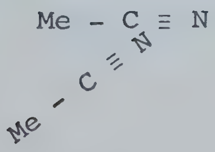

If the antiparallel configuration occurs, then it could be responsible in part for shell formation in negative ions. For positive ions it would geometrically be impossible, since the cyano group is oriented towards the cation. The heat of dissociation of the acetonitrile dimer has been determined between 3.8 (90) and 5.2 (88) kcal/mole. The tendency towards the antiparallel dimerization will lead to an opposing dipole interaction with the negative ion, as well as steric crowding so the low value of $-\Delta H_{4,5}$ for reaction 3.6 (-5.2 kcal/mole) can be expected.

The entropy also demonstrates the possibility of shell formation with negative ions. For the fluoride ion, the $-\Delta S$ changes from 19.6 for the 3,4 reaction to a much lower value of 7.4 e.u. for the 4,5 reaction. This is indicative of the greater freedom in the outer shell. The sodium ion, as pointed out earlier, has a substantial increase in entropy between the 3,4 and 4,5 reaction - indicative of greater restriction and thus the lack of shell formation.

The difference between the solvation enthalpies of halide and alkali ions at low n would be expected from the electronic structure of acetonitrile. (For a detailed view at the electronic structure see Chapter 4.) The positive part of the acetonitrile dipole is diffusely spread out over the hydrogen atoms in the methyl group, whereas the nitrogen atom contains the major negative part of the dipole, with a well-directed lone pair of electrons (87). From a purely electrostatic point of view, it then seems reasonable that

the ion-molecule bond between the cation and the nitrogen of the cyano group would be stronger than the bond between the anion and the methyl hydrogens.

## 3.6 A Comparison between the Gas Phase Solvation and Liquid Phase Solvation of Alkali Cations in Acetonitrile

### A Consistency of Gas Phase Results

The consistency of the $\Delta G_{o,n}$ values for the different alkali ions with available solution thermodynamic data is shown in Figure 69, which gives a plot of $\Delta G_{o,n}(Cs^+) - \Delta G_{o,n}(M^+)$ versus n. As n increases, it would be expected that the above difference would approach the difference between the free energy of solution $\Delta G_s(Cs^+) - \Delta G_s(M^+)$. Case and Parsons' values obtained from Volta potential measurements (37) are used for the liquid phase free energies. Comparing the differences in free energies between ions is advantageous, since it eliminates to some extent interactions with the bulk liquid. That is, after the primary solvation sphere is complete, the charge density of the ion becomes less important in ion-solvent interactions.

From Figure 69, it can be seen that as n increases the difference in the free energy, $\Delta G_{o,n}$, of an ion and cesium approaches the Case and Parson value. For potassium the agreement is especially good. However, for rubidium and sodium, it is unlikely further extrapolation of the plot

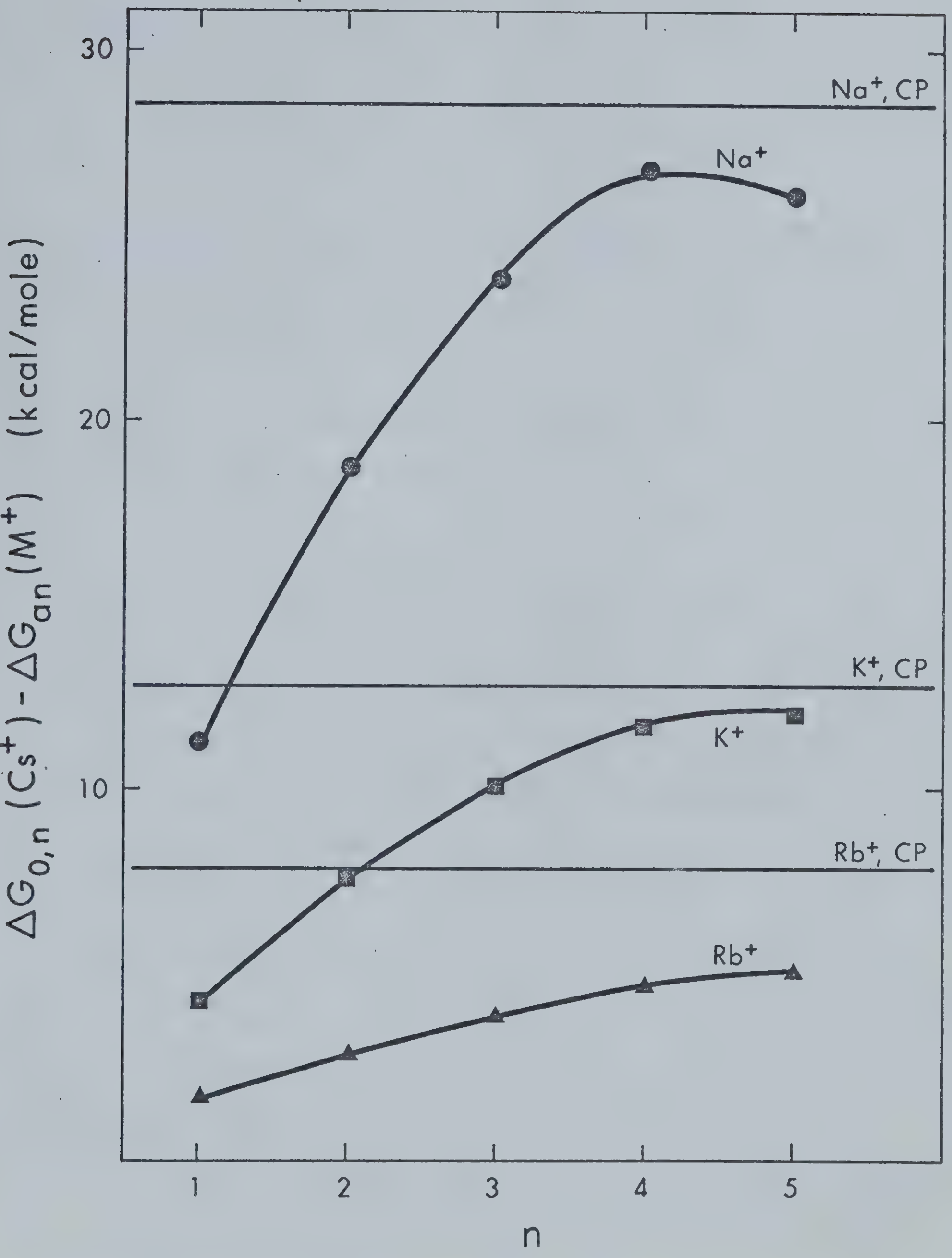

FIGURE 69 Comparison of Experimental Gas Phase Free Energies of Solvation with Total Single Ion Free Energies of Solvation in Acetonitrile Obtained by Case and Parsons (CP).

will reach the Case and Parson free energy difference. The sodium-cesium difference approaches a maximum when n equals 4 and then decreases. This again is a result of the highly unfavourable entropy of the sodium-acetonitrile 4,5 reaction.

## B Determination of Single Ion Free Energies of Solution in Acetonitrile from Gas Phase Data

For the alkali ions $Na^+$, $K^+$, $Rb^+$ and $Cs^+$, the gas phase free energy of clustering of five acetonitrile molecules has been obtained in this study:

$$\Delta G_{0,5} = \sum_{n=1}^{5} \Delta G_{n-1,n} \qquad 3.7$$

From the previous study on the solvation of the halide ions, $Cl^-$, $Br^-$ and $I^-$, and proper extrapolation, a similar $\Delta G_{0,5}$ may be obtained. Figure 70 shows the extrapolated plots of $\Delta G_{n-1,n}$ versus n used to obtain $\Delta G_{4,5}$ for $Cl^-$, $Br^-$ and $I^-$, and $\Delta G_{3,4}$ for $I^-$.

The differences $\Delta G_{o,n}(Cl^-) - \Delta G_{o,n}(M^+)$ are plotted versus n in Figure 71. For all the ion pairs this difference reaches a maximum at n equal to 4, and then falls off slightly at n equal to 5. If it is assumed that this difference will not change significantly at higher n, these values may be used to obtain single ion free energies of solution in acetonitrile. That is

$$\Delta G_{0,5}(X^-) - \Delta G_{0,5}(M^+) = \Delta G_s(X^-) - \Delta G_s(M^+).$$

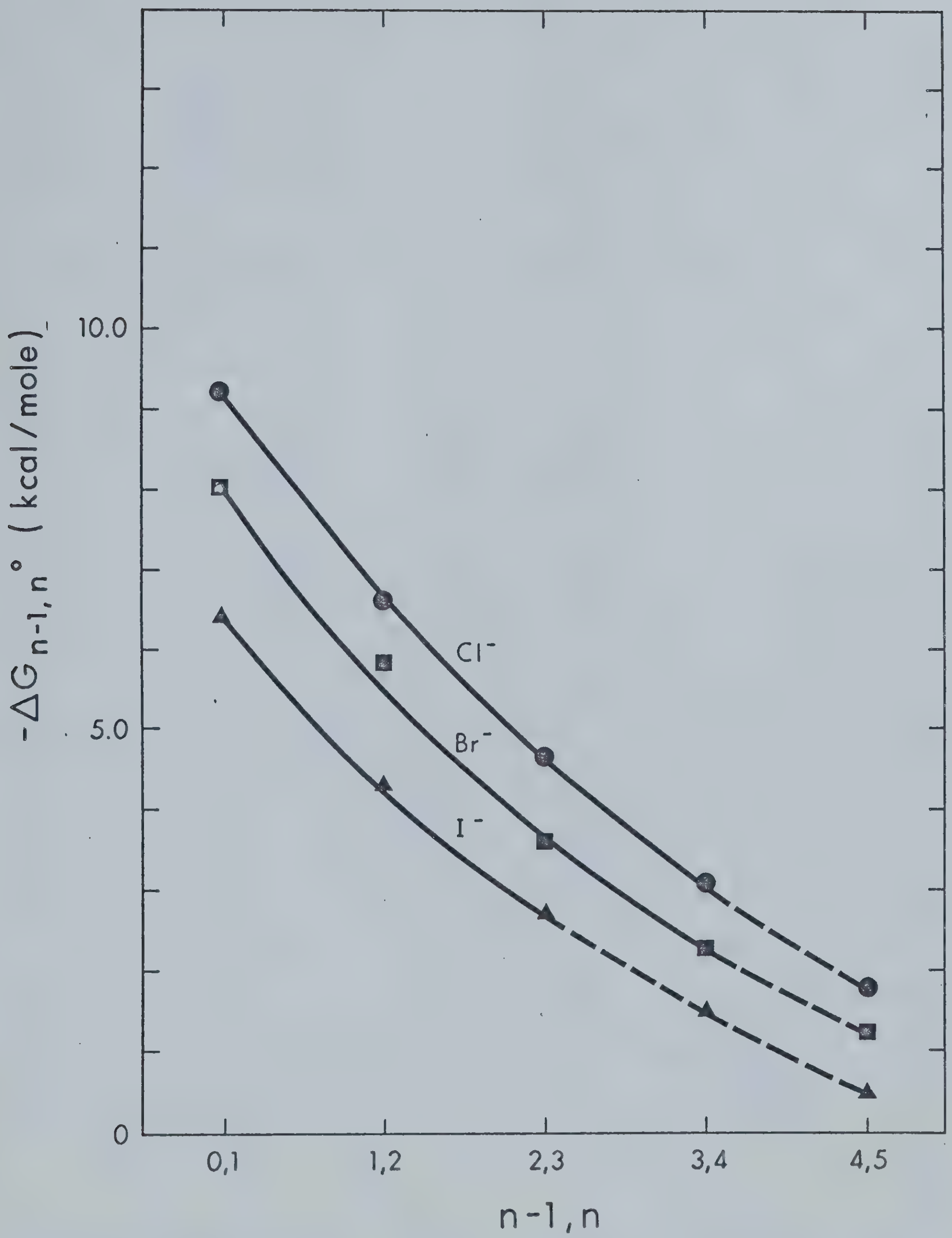

FIGURE 70 Extrapolation of - $\Delta G_{n-1,n}$ versus n-1,n Plots for the Gas Phase Solvation of Halide ions in Acetonitrile, in Order to Obtain Single Ion Free Energies of Solvation.

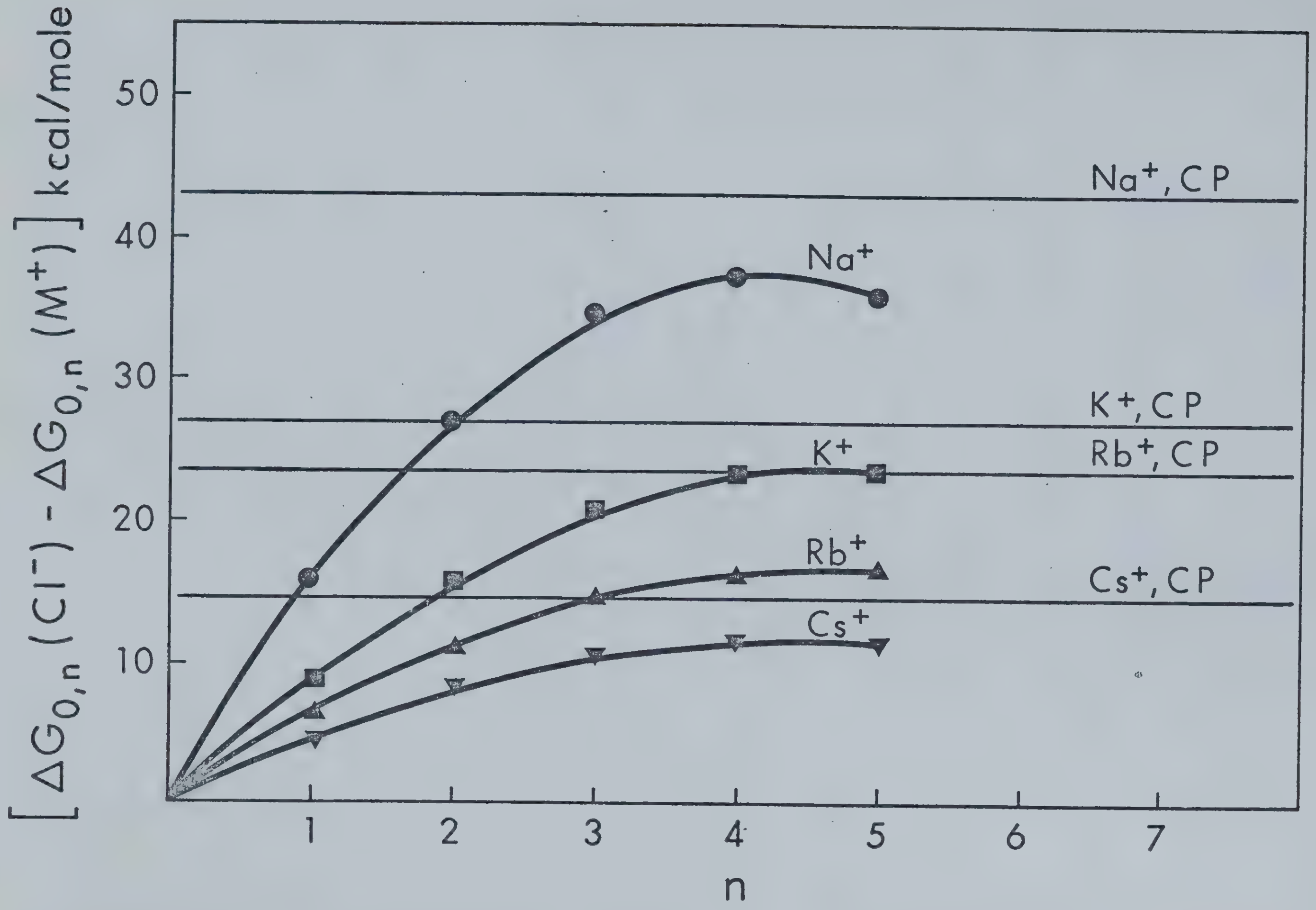

FIGURE 71 Comparison of the Experimental Difference in Gas Phase Free Energies of Solvation in Acetonitrile versus n to the Free Energy Differences of Case and Parsons (CP).

The total free energy of solvation of alkali halide salts have been given in a review by Padova (23). These are listed in Table 11. Thus, a series of equations results:

$$\Delta G_s(X^-) + \Delta G_s(M^+) = \Delta G_s(M^+X^-) \qquad 3.8$$

$$\Delta G_s(X^-) - \Delta G_s(M^+) = B \qquad 3.9$$

where B is the difference in free energies obtained in the gas phase, tabulated in Table 11. These equations may be solved for the various ion-pairs in order to obtain $\Delta G_s(X^-)$ and $\Delta G_s(M^+)$. These are shown in Table 12.

From the average value for each ion, values of the single ion free energy of solution in acetonitrile are thus obtained. These are essentially limiting values since it is likely (from Figure 71) that the difference $\Delta G_{o,n}(X^-) - \Delta G_{o,n}(M^+)$ will decrease at higher n. Thus for the alkali ions, the calculated $-\Delta G_s(M^+)$ will have a maximum limit and $-\Delta G_s(X^-)$ a minimum.

The ionic free energy of transfer, $\Delta G_t$, from water to acetonitrile can then be obtained using acceptable values of $\Delta G_h(M^+)$ or $\Delta G_h(X^-)$ in $H_2O$. The water values used are those of Randles (35). The free energies of transfer are compared with those obtained using other methods in Table 13. Where the single ion free energies were obtained in acetonitrile rather than by transfer techniques, the Randles values for $H_2O$ were used to obtain the free energies of transfer.

## TABLE 11

## Total Alkali Halide Solvation Free Energies in Acetonitrile and Experimental Differences in Free Energies Determined in the Gas Phase

| MX | $-\Delta G_s^o(M^+X^-)^{a,b}$ | $\Delta G_{0,5}(Cl^-) - \Delta G_{0,5}(M^+)^{a,c}$ |
|---|---|---|
| NaCl | 154.5 | 35.8 |
| NaBr | 153.0 | 40.1 |
| NaI | 148.0 | 45.7 |
| KCl | 139.0 | 22.9 |
| KBr | 137.5 | 27.2 |
| KI | 132.5 | 32.8 |
| RbCl | 134.5 | 16.1 |
| RbBr | 133.0 | 20.4 |
| RbI | 128.0 | 26.0 |
| CsCl | 125.5 | 11.0 |
| CsBr | 124.0 | 15.3 |
| CsI | 119.0 | 20.9 |

[a] Units of kcal/mole

[b] From Reference 23

[c] Standard state: 1 atmosphere; temperature 298° K

### TABLE 12

### Single Ion Free Energies[a] of Solvation in Acetonitrile

| $X^-$ / $M^+$ | $Cl^-$ | $Br^-$ | $I^-$ | Average $M^+$ | Case and Parsons[b] | Izmailov[c] |
|---|---|---|---|---|---|---|
| $Na^+$ | 59.35<br>95.15 | 56.45<br>96.55 | 51.15<br>96.85 | 96.2 | 98.8 | 90.5 |
| $K^{+}$+ | 58.05<br>80.95 | 55.15<br>82.35 | 49.85<br>82.65 | 82.0 | 83.0 | 75.0 |
| $Rb^+$ | 59.20<br>75.30 | 56.30<br>76.70 | 51.00<br>77.0 | 76.3 | 78.2 | 70.5 |
| $Cs^+$ | 57.25<br>68.25 | 54.35<br>69.65 | 49.05<br>69.95 | 69.3 | 70.3 | 61.5 |
| Average $X^-$ | 58.5 | 55.6 | 50.3 | | | |
| Case and Parsons[b] | 55.7 | 54.2 | 49.5 | | | |
| Izmailov[c] | 64.0 | 62.5 | 57.5 | | | |

---

[a] In units of kcal/mole

[b] Reference 37

[c] Reference 29

## TABLE 13

## Free Energies[a] of Transfer from Water to Acetonitrile

| | Izmailov[b] | Case and Parsons[c] | Coetzee and Campion[d] | Strehlow[e] | Abraham[f] | Parker[g] | Popovych[h] | This Work |
|---|---|---|---|---|---|---|---|---|
| $Na^+$ | 3.5 | -0.6 | 6.5 | | 4.0 | | | 2.0 |
| $K^+$ | 2.0 | -2.4 | 4.5 | | 2.4 | -0.1 | 0.8 | -1.4 |
| $Rb^+$ | 2.0 | -2.7 | 3.8 | -2.5 | 1.9 | | | -0.8 |
| $Cs^+$ | 1.5 | -2.5 | 3.3 | | 1.7 | 0.0 | | -1.8 |
| $Cl^-$ | 10.5 | 15.0 | 7.5 | | 9.9 | 11.4 | 10.0 | 12.2 |
| $Br^-$ | 6.5 | 10.7 | 4.9 | | 7.0 | 8.0 | 7.4 | 9.7 |
| $I^-$ | 3.0 | 8.2 | 1.8 | | 3.0 | 4.6 | 4.2 | 6.9 |

[a] kcal/mole

[b] Reference 29; $1/n^2$ extrapolation

[c] Reference 37; Volta potential

[d] Reference 28; Polarography, modified Born eq.

[e] Reference 31; Modified Born eq.

[f] Reference 91; reference electrolyte

[g] Reference 33; reference electrolyte

[h] Reference 34; reference electrolyte

The free energies of transfer determined from the gas phase results, agree quite well with those obtained in solution. Perhaps the most reliable results are those of Case and Parsons (37) since the single ion separation is not based directly on the radius of the ion (Born equation) or even indirectly on the radius ($1/n^2$ extrapolation and reference electrolyte), but rather on the assumption that the surface potential will be similar for acetonitrile and water.

Unfortunately, the errors in the gas phase studies are additive for the stepwise clustering reactions. Therefore, the values listed in Table 13 have a standard deviation of at least 2.5 kcal/mole. However, the results demonstrate that water and acetonitrile solvate cations to almost the same degree in solution and that anions are much less solvated than cations in acetonitrile.

## C Calculation of the Free Energy of Transfer from Water to Acetonitrile

Returning to the ion solvation cycle presented in the introduction and replacing the enthalpy with free energy we obtain the total free energy of solvation of an ion, i, as:

$$\Delta G_s(i) = n \times \Delta G_{evap} + (\Delta G_{i-s})_{o,n} + \Delta G_{BC} + \Sigma\Delta G_{SB} \qquad 3.10$$

Where n represents the number of ligands in the first solvation shell, $\Delta G_{evap}$ is the free energy of evaporation at

298° K, $(\Delta G_{i-s})_{0,n}$ is the experimentally determined free energy of ion-solvent molecule interactions obtained in the gas phase, $\Delta G_{BC}$ is the Born charging free energy representing the influence of the ion on the bulk solvent, and $\Sigma\Delta G_{SB}$ represents the free energy change due to the breaking of the solvent structure upon adding the ion.

For the free energy of transfer from water to acetonitrile:

$$\Delta G_t(i) = \Delta G_{an}(i) - \Delta G_w(i) \qquad 3.11$$

and by replacing the total solvation energies from Equation 3.10 the free energy of transfer may be represented by:

$$\begin{aligned}\Delta G_t(i) = \; & n_{an}\Delta G_{evap}(an) - n_w \Delta G_{evap}(w) \\ & + (\Delta G_{i-an})_{0,n_a} - (\Delta G_{i-w})_{0,n_w} \\ & + \Delta G_{BC}(an) - \Delta G_{BC}(w) \\ & + \Sigma\Delta G_{SB}(an) - \Sigma\Delta G_{SB}(w)\end{aligned} \qquad 3.12$$

The free energies of evaporation and the free energies of gas phase ion-solvent interactions are known from experimental data, but the other terms in Equation 3.12 are more speculative and based on assumptions. However, this

determination is not meant to be quantitative but rather to explain that effects other than close electrostatic interactions are responsible for the liquid phase experimental data which demonstrates that water is as good, or a better solvator of alkali ions as acetonitrile.

The first assumption that must be made is with respect to the number of solvent molecules in the solvation shell. One is tempted to set the coordination number of an alkali metal cation equal for all solvents, but from the gas phase solvation studies of water and acetonitrile, it is not obvious that this is the case. There is no indication in the alkali ion-water studies that a second shell is or is not formed, and thus these ions could be able to allow six water molecules in the first solvation shell. In the case of acetonitrile, the fifth ligand attaches with difficulty (from the free energy) and there was no indication that a sixth molecule would be allowed into the solvation shell due to the high entropy factors involved. Thus the first assumption is that the number of water molecules in the first solvation shell is between four and six, the number of acetonitrile molecules in the shell is either four or five and that $n_w \geq n_a$. From this assumption various values of the first two terms in Equation 3.12 as a function of $n_w$ and $n_a$ are determined for each ion and presented in Table 14.

The Born charging contribution is given by (15)

$$\Delta G_{BC} = -\frac{Z^2e^2}{2(r_i + 2r_s)}(1 - 1/D_s) \qquad 3.13$$

where Ze is the ionic charge, $r_i$ is the ionic radius, $r_s$ is the solvent radius (thus $r_i + 2r_s$ is the radius of the ion and its first solvation shell), and $D_s$ is the dielectric constant of the solvent. For water which is a somewhat spherical molecule, the generally accepted radius of 1.38 A (16) may be used. The ionic crystal radius may be used for $r_i$ since it has been postulated that in solution ions have their crystal radii (92). However, for acetonitrile which is not in the least spherical but rather cylindrical, a more complicated procedure is necessary to determine $r_a$. Since acetonitrile is not considered a structured liquid (93), it is possible to use the molecular volume as an estimate of its volume. From the van der Waal's radius of acetonitrile (94, 95), one can assume that the length of the molecule will be 3.4 times its width. The length ($l_a$) will be equal to ($2xr_a$) since the molecule is oriented lengthwise about the cation and:

$$l_a = \left(\frac{9.26 \times V_m}{\pi}\right)^{1/3} \qquad 3.14$$

where $V_m$ is the volume of one molecule determined from the density and molecular weight (96). This leads to a value of 6.40 for $l_a$ or 3.20 A for $r_a$. Although this value is determined in an awkward manner, it seems to be reasonable since one would expect from the bond lengths (see Chapter 4)

that acetonitrile would be ∿3 times longer than a water molecule. The dielectric constants used are 78.0 for water and 36.1 for acetonitrile (97). The resulting values of the Born-charging differences for acetonitrile and water are shown in Table 14.

The structure breaking term in Equation 3.9 is the most uncertain term in the entire equation. Since acetonitrile is not a structured liquid, one assumes that the energy lost due to adding an ion will be negligible (i.e. in the bulk liquid) and $\Delta G_{SB}(an) = 0$. However, water is a very structured liquid and there will be some loss of structure upon adding a cation (16). Eley and Evans (15) determined that in a tetrahedral case, that is four molecules in the solvation shell, that $\Delta G_{SB}(w) = 8$ kcal/mole. If we assume that this value is proportional to the number of molecules in the first shell, $\Delta G_{SB}$ will be equal to 10 for $n_w = 5$ and will be equal to 12 kcal/mole for $n_w = 6$.

The resulting $\Delta G_t$'s are shown in Table 15. Again it must be emphasized that this procedure involves too many unknowns and too many assumptions to be an acceptable quantitative determination of $\Delta G_t$. The coordination numbers of alkali ions have never been agreed upon experimentally (98), the Born charging equation involves ionic and molecular radii which are always suspect, and the structure breaking terms are essentially just guesses.

The $\Delta G_t$'s so determined are consistent in that the free energy of transfer for sodium is always more positive, i.e.

## TABLE 14

## Relevant Quantities to Predict Free Energy of Transfer[a]

| Ion | $Na^+$ | $K^+$ | $Rb^{+b}$ | $Cs^{+c}$ |
|---|---|---|---|---|
| $r_i$, $A^o$ | 0.95 | 1.33 | 1.48 | 1.69 |
| $(\Delta G_{BC})$ | -22.3 | 19.3 | 18.3 | 17.0 |
| $n_a = 4; n_w = 4$ | | | | |
| $\Delta(\Delta G_{evap})$ | 3.24 | 3.24 | 3.24 | 3.24 |
| $\Delta(\Sigma\Delta G_{SB})$ | -8.0 | -8.0 | -8.0 | -8.0 |
| $\Delta([\Delta G_{i-s}]_{o,n})$ | -15.1 | -15.6 | -14.4 | -14.1 |
| $\Delta G_t$ | 2.4 | -0.9 | -0.9 | -0.9 |
| $n_a = 4; n_w = 5$ | | | | |
| $\Delta(\Delta G_{evap})$ | 5.31 | 5.31 | 5.31 | 5.31 |
| $\Delta(\Sigma\Delta G_{SB})$ | -10.0 | -10.0 | -10.0 | -10.0 |
| $\Delta([\Delta G_{i-s}]_{o,n})$ | -11.2 | -12.4 | -11.4 | -11.6 |
| $\Delta G_t$ | 6.4 | 2.2 | 2.2 | 1.7 |
| $n_a = 4; n_w = 6$ | | | | |
| $\Delta(\Delta G_{evap})$ | 7.38 | 7.38 | 7.38 | 7.38 |
| $\Delta(\Sigma\Delta G_{SB})$ | -12.0 | -12.0 | -12.0 | -12.0 |
| $\Delta([\Delta G_{i-s}]_{o,n})$ | -8.3 | -10.1 | -10.0 | -10.1 |
| $\Delta G_t$ | 9.4 | 4.6 | 3.7 | 2.3 |

TABLE 14 (Continued)

| Ion | $Na^+$ | $K^+$ | $Rb^{+b}$ | $Cs^{+c}$ |
|---|---|---|---|---|
| $n_a = 5;\ n_w = 5$ | | | | |
| $\Delta(\Delta G_{evap})$ | 4.04 | 4.04 | 4.04 | 4.04 |
| $\Delta(\Sigma\Delta G_{SB})$ | -10.0 | -10.0 | -10.0 | -10.0 |
| $\Delta([\Delta G_{i-s}]_{o,n})$ | -11.6 | -13.8 | -13.0 | -12.7 |
| $\Delta G_t$ | 4.7 | -0.5 | -0.7 | -1.7 |
| $n_a = 5;\ n_w = 6$ | | | | |
| $\Delta(\Delta G_{evap})$ | 6.11 | 6.11 | 6.11 | 6.11 |
| $\Delta(\Sigma\Delta G_{SB})$ | -12.0 | -12.0 | -12.0 | -12.0 |
| $\Delta([\Delta G_{i-s}]_{o,n})$ | -8.7 | -11.5 | -11.4 | -11.2 |
| $\Delta G_t$ | 7.7 | 1.9 | 1.0 | -0.1 |

[a] All free energies in kcal/mole

[b] Water data for $(\Delta G_{i-w})_{o,n}$ extrapolated for n = 6

[c] Water data for $(\Delta G_{i-w})_{o,n}$ extrapolated for n = 5 and n = 6

# TABLE 15

## The Calculated Free Energies of Transfer as a Function of Coordinated Solvent Molecules

| | | | $\Delta G_t{}^a$ Calculated | | | |
|---|---|---|---|---|---|---|
| $n_a$ | $n_w$ | i = | $Na^+$ | $K^+$ | $Rb^+$ | $Cs^+$ |
| 4 | 4 | | 2.4 | -0.9 | -0.9 | -0.9 |
| 4 | 5 | | 6.4 | 2.2 | 2.2 | 1.7 |
| 4 | 6 | | 9.4 | 4.6 | 3.7 | 2.3 |
| 5 | 5 | | 4.7 | -0.5 | -0.7 | -1.7 |
| 5 | 6 | | 7.7 | 1.9 | 1.0 | -0.1 |

| | | | $\Delta G_t{}^a$ Experimental | | | |
|---|---|---|---|---|---|---|
| | | | -0.6 | -2.4 | -2.7 | -2.5[b] |
| | | | 6.5 | 4.5 | 3.8 | 3.3[c] |
| | | | 3.5 | 2.0 | 2.0 | 1.5[d] |
| | | | 4.0 | 2.4 | 1.9 | 1.7[e] |
| | | | | -0.1 | | 0.0[f] |
| | | | 2.0 | -1.4 | -0.8 | -1.8[g] |

[a] kcal/mole

[b] Reference 37

[c] Reference 28

[d] Reference 29

[e] Reference 91

[f] Reference 33

[g] This work

favouring water, than the other ions. This is also consistent with experimental data. Due to the tremendous discrepancy in experimental data, no conclusions can be made from our model with respect to how justifiable our assumptions are. However, when considering the difference between ions, the 4-water, 4-acetonitrile model is most consistent with the majority of the experimental determinations, including those in the present study.

This procedure has demonstrated that using only gas phase results is dangerous in predicting the relative solvation strengths of various solvents, in that reactions of the ion with the bulk liquid (Born-charging and the breaking of solvent structure) are ignored. However, they are of fundamental importance since they give intrinsic values for the close electrostatic interactions between an ion and the solvent molecules in the first solvation shell.

## 3.7 Summary

a) The equilibrium constants at various temperatures of the clustering of acetonitrile with alkali ions have been determined by high pressure mass spectrometry. From these constants, the corresponding thermodynamic functions $\Delta G^o$, $\Delta H^o$, and $\Delta S^o$ have been calculated.

b) From the unfavourable entropy values of the 4,5 reaction, the formation of a second shell of acetonitrile molecules about the alkali ion is not indicated.

c) The gas phase interactions between an alkali ion and acetonitrile are initially greater than between the ion and water, but the trend reverses as the number of ligands increases.

d) The interactions between an alkali ion and acetonitrile are much greater than between a halide ion and acetonitrile.

e) From the total alkali halide free energies of solvation and from the differences in alkali and halide, $\Delta G_{o,n}$'s, the single ion free energies of solvation in acetonitrile were determined. Using acceptable single ion free energies of hydration, the free energies of transfer for the alkali and halide ions from water to acetonitrile were obtained.

f) When effects of an alkali ion with bulk solvent are taken into account, the trend in the free energy of transfer of an ion from water to acetonitrile can be qualitatively predicted. The free energies so determined are consistent with experimentally determined values of the free energies of transfer.

## CHAPTER 4

# ION-SOLVENT ELECTROSTATIC CALCULATIONS

## 4.1 Introduction

In recent years, the calculation of the interaction energies of ion hydration and solvation has increased greatly. These include both classical electrostatic interactions (for example 3, 99 - 102) and quantum mechanical calculations (79, 103 - 108). The reasons for this growth in quantum mechanical calculations are probably twofold. One the one hand, M. O. methods using various approximations have developed to the point where they can give useful results for complicated systems such as ion hydration. On the other hand, experimental data on the gas phase hydration of ions now exists and thus can be compared with theoretical results.

In electrostatic calculations, the total energy is expressed as a sum of ion-dipole (and in some cases ion quadrople) energies, ion-induced dipole energies, ion-molecule dispersion forces and repulsion potentials. Although all the terms may be calculated according to different models, the various sets of calculations essentially fall into three groups, based on the methods used to obtain the repulsion potential. These groups may be classified as: 1) a hard sphere model in which the sum of the radius of the solvent molecule and the radius of the ion are used to obtain electronic repulsion energies (100, 102); 2) a semi-

empirical model in which the repulsion energy term is adjusted until the total energy agrees with experimental gas phase enthalpies (3, 99); and 3) a model in which the repulsion term is calculated from rare gas-atom repulsion potentials (3, 101). The present calculations are of the third type, since it was felt that the most unbiased results would thus be obtained.

In this chapter, an electrostatic model is presented which is quite general and could also be used for other protic and aprotic solvents. The model is believed especially useful for molecules in which one or both poles of the dipole are distributed over several atoms and for molecules with anisotropic polarizability.

## 4.2 The Electronic and Physical Structure of Acetonitrile

In order to understand the gas phase solvation of alkali metal ions in acetonitrile, it is first necessary to have an idea of the electronic structure of acetonitrile. The gas phase dipole moment of acetonitrile is 3.97 D (109). The carbon and nitrogen atoms in the cyano group are sp-hybridized, and the bonding consists of one central $\sigma$-bond and two $\pi$-bonds, giving a linear arrangement. The nitrogen lone pair is in a second sp-hybridized orbital and is colinear with the $C \equiv N$ axis. The lone pair is mainly responsible for the complexing of acetonitrile with electrophilic agents (for example, the proton, alkali metal ions, Lewis acids, etc.). However, weak complexes involving the $C \equiv N$ $\pi$-electrons

with $Cu^{+2}$ and $Ag^{+}$ are also thought to exist (87).

By using LCAO - SCF (linear combination of atomic orbitals - self consistent field) calculations fitted with gaussian type orbitals, Pople has determined the Mulliken gross electron population of the various atoms in acetonitrile (110). The net electron populations are shown in Table 16. However, the CNDO calculations are highly approximate and involve a certain amount of subjective parameterization, so the gaussian type orbital method appears more reliable (110).

A third set of theoretical electron density calculations were performed by Clementi (112) using a Hartree-Fock orbital approximation. These are compared with Pople's values in Table 16. According to Clementi, the hydrogen atoms act as σ and π donors to the methyl carbon, the methyl carbon acts as a σ and π acceptor as well as a charge carrier, the cyano carbon acts as a carrier as well as a σ and π donor to the nitrogen atom, which in turn is both a σ and π acceptor.

The bond lengths and angles in acetonitrile have been determined experimentally from microwave spectra (113). The resulting parameters are:

$d_{CH}$ = 1.112A

$d_{CC}$ = 1.458 A

$d_{CN}$ = 1.157 A

$\angle HCH = 109.3$

$\angle HCC = 109.7$

## TABLE 16

### Net Mulliken Electron Populations in Acetonitrile

$H_3 - {}_1C - {}_2C \equiv N$

| H | ${}_1C$ | ${}_2C$ | N | Reference |
|---|---|---|---|---|
| 0.034 | 0.021 | 0.062 | -0.185 | Pople (110) LCAO-GO |
| 0.032 | -0.024 | 0.087 | -0.159 | Pople (111) CNDO/2 |
| 0.247 | -0.657 | 0.085 | -0.174 | Clementi (112)<br>Hartree-Fock |
| 0.23 | -0.58 | -0.02 | -0.10 | Liskow et al (114)<br>Hartree-Fock |

The resulting structure of acetonitrile is pictured in Figure 72.

## 4.3 Interaction Energies

The total interaction energy, $E_t$, between a single solvent molecule and an ion is composed of ion-dipole and ion-induced dipole attraction, ion-molecule dispersion, and ion-ligand repulsive forces. It can be expressed as:

$$E_t = E_{dip} + E_{ind} + E_{dis} + E_{rep} \tag{4.1}$$

where $E_{dip}$ represents the dipole attraction energy between a solvent molecule and the central ion; $E_{ind}$, the induced dipole attraction energy; $E_{dis}$, the dispersion energy; and $E_{rep}$, the repulsive energy. To determine the total energy it is best to sum the individual energies treating ion-ligand distances as a variable parameter. The minimum value of E is then taken as the true value of $E_t$. This value can then be compared with the enthalpy of the reaction 4.2.

$$M^+ + S \rightleftarrows M^+S \tag{4.2}$$

### A Ion-Permanent Dipole Interactions ($E_{dip}$)

Although acetonitrile has a much larger dipole moment than water (3.97 D compared to 1.85 D), the individual point charge on the negative centre of the molecule is greater on the oxygen of water than on the acetonitrile nitrogen.

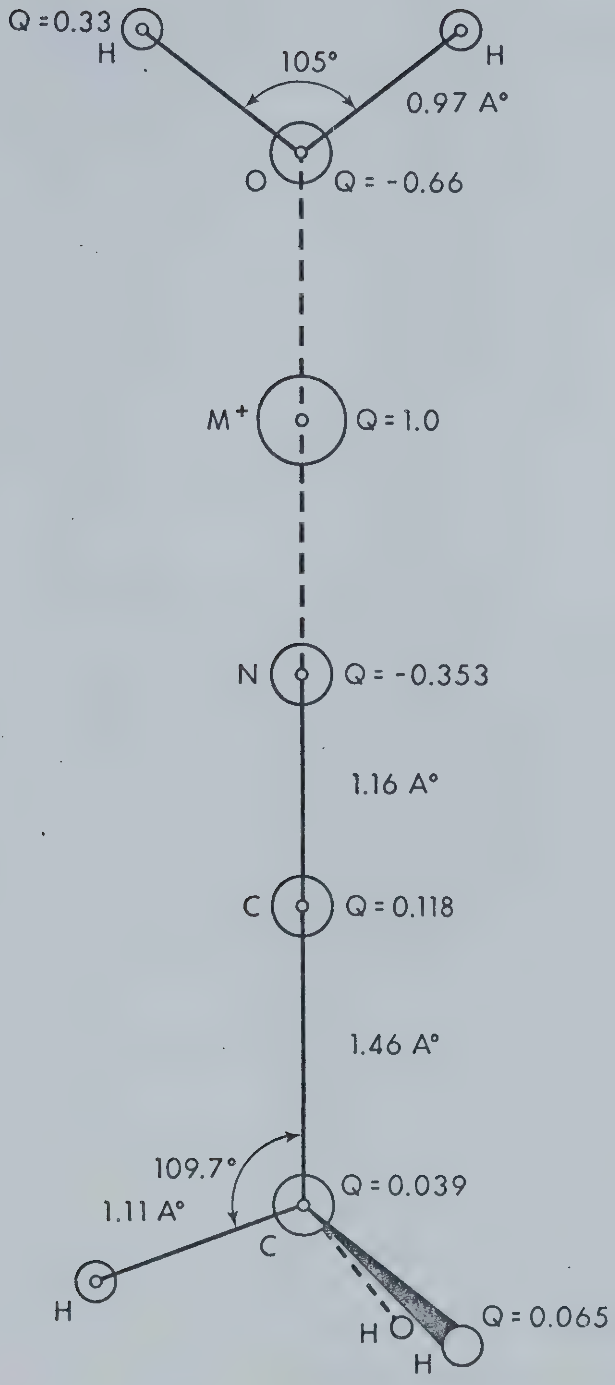
Q = 0.33
H
105°
H
0.97 A°
O
Q = -0.66
M+
Q = 1.0
N
Q = -0.353
1.16 A°
C
Q = 0.118
1.46 A°
109.7°
Q = 0.039
1.11 A°
C
H
H
Q = 0.065
H

FIGURE 72 Bond Distances, Angles, and Point Charge Distribution for Water and Acetonitrile .

If the net Mulliken electron population is used as the atomic point charge, the calculated dipole moment is much too low. For example, if Pople's electron distribution values (110) for water are taken (see Table 16), the resulting classical dipole moment will be 1.14 D. However, if the net Mulliken electron population is multiplied by 1.63, the true experimental moment of 1.85 results. This adjustment factor, 1.63, was found to also give the correct dipole moments for the methyl amines (Chapter 5). For acetonitrile, a higher adjustment factor of 1.91 was used to correlate the net electron populations with the experimental dipole moment. By using Pople's values for electron density (110) and adjusting them to give the correct dipole moment by means of the above factors, the point charges on the various atoms in both acetonitrile and water necessary for the electrostatic calculations may then be determined. These are shown together with bond angles and distances in Figure 72.

The ion-dipole attraction energy can be expressed as:

$$E_{dip} = 334 \sum_i Q_i/R_i \qquad 4.3$$

where $Q_i$ is the point charge on the $i^{th}$ atom of the solvent molecule, $R_i$ is the distance between the ion and the $i^{th}$ atom and 334 is a numerical value adjusted to give $E_{dip}$ in kcal/mole for values of $R_i$ in Angstroms and Q in atomic units.

## B Ion-Induced Dipole Interactions

The total polarizability of a molecule can be broken down into individual bond polarizabilities or even into individual atom polarizabilities. For acetonitrile and its highly polarizable $C \equiv N$ bond, it is best to use the bond polarizability approach. Each bond has a lateral and transverse polarizability tensor (115):

$$\alpha_b = 1/3\ (\alpha_l + 2\alpha_t) \qquad 4.4$$

where $\alpha_b$ is the bond polarizability, $\alpha_l$ the lateral polarizability or polarizability parallel to the bond and $\alpha_t$ is the transverse polarizability perpendicular to the bond. For an alkali metal ion the ion-induced dipole attraction energy can be expressed as (104):

$$E_{ind} = -167\,\Sigma\,(\alpha_l \cos^2\theta + \alpha_t \sin^2\theta\ )/R_{ij}^{\,4} \qquad 4.5$$

where ij represents the bond between atoms i and j, $\theta$ is the angle of this bond with respect to the ion (see Figure 73), and $R_{ij}$ is the distance between the ion and the polarizability centroid of the bond, and 167 is a numerical factor adjusted to give $E_{ind}$ in kcal/mole for values of $R_{ij}$ in angstroms and $\alpha$'s in angstroms$^3$.

The polarizability centroid of the bond is not easily obtainable. One method (104) is to take the mean atom polarizabilities of the two atoms in the bond ($\alpha_i$ and $\alpha_j$)

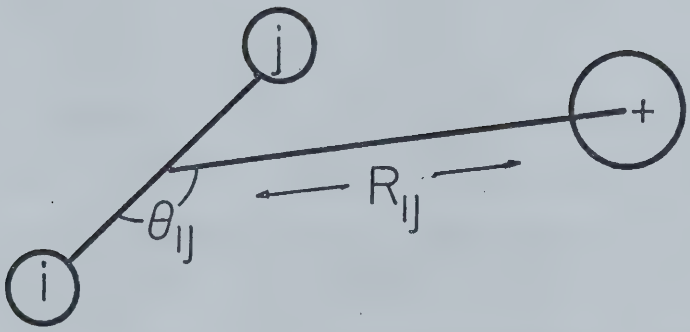
j
+
$R_{ij}$
$\theta_{ij}$
i

$$\alpha_{ij} = \alpha_{t_{ij}} \sin^2\theta_{ij} + \alpha_{l_{ij}} \cos^2\theta_{ij}$$

FIGURE 73 Representation of Bond Polarizabilities.

and then by using the lever principle:

$$\overline{ic} \times \alpha_i = \overline{jc} \times \alpha_j$$

where $\overline{ic}$ and $\overline{jc}$ are the atom-centroid distances. This leads to:

$$\overline{ic} = \overline{ij} \times \frac{\alpha_j}{\alpha_i + \alpha_j} \qquad 4.6$$

where $\overline{ij}$ is the bond length. Thus the location of the centroid may be obtained. In the case of acetonitrile, however, this is not sufficient. The electrons in the C ≡ N bond lie closer to the nitrogen than the carbon (112), and therefore the polarizability centroid should as well. However, the mean atomic polarizabilities predict that the centroid will lie slightly closer to the carbon. The same is true in the C--C bond. The electrons will lie closer to the sp cyano carbon since it is more electronegative than the $sp^3$ methyl carbon (116). The mean atomic polarizabilities would predict the centroid to be directly in the middle of the bond.

The method used in this work is to take Pople's electron populations of the various atoms and to determine the relative number of bonding electrons attributed to each atom. For example in the C ≡ N bond, the total number of electrons in the nitrogen is 7.185. Of these, two are inner shell, two

are lone pair directed away from the $C \equiv N$ bond and the others are involved in bonding with the carbon. From this we can say that the carbon end of the bond is deficient by .185 electrons. The centroid can then be set equal to

$$\frac{3.185}{2.815} = \frac{\overline{Cc}}{\overline{Nc}} \tag{4.7}$$

where $\overline{Cc}$ and $\overline{Nc}$ are the distances of the centroid from the carbon and nitrogen atoms. This method can then be used on the other bonds. The position of the polarizability centroids of the various bonds are shown in Table 17.

The values for the lateral and transverse bond polarizabilities are listed in Table 18 for acetonitrile. The C--C bond polarizability had to be adjusted since literature values are for $sp^3$-$sp^3$ bonds. This was done by vectorialy summing the bond polarizabilities for the C--H and $C \equiv N$ bonds and subtracting them from the total lateral and transverse components (117). The lateral value remains approximately the same, however, the transverse increases from the ordinary C--C bond. This is not too surprising since the C--C bond in acetonitrile is said to have some double bond character (116). In the present calculations due to the linearity of the molecule, only the lateral tensor is of importance.

The polarizability tensors of water have not been determined experimentally but have been estimated by Harrison (118). From his theoretical results, it can be assumed that

## TABLE 17

## Location of Polarizability Centroids

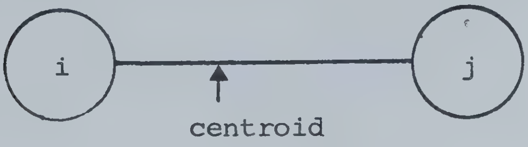

| i | j | Distance from Centroid to about i (In Angstrons) |
|---|---|---|
| N | C | 0.52 |
| C(sp) | C($sp_3$) | 0.58 |
| C | H | 0.53 |
| O | H | 0.32 |

## TABLE 18

## Bond and Molecular Polarizabilities[a]

---

### A. Bond Polarizabilities[b]

| Bond | $\alpha_l$ | $\alpha_t$ |
|---|---|---|
| C--H | 0.79 | 0.58 |
| C--C($sp_3$-$sp_3$) | 1.88 | 0.2 |
| C--C($sp$-$sp_3$)[c] | 1.88 | 0.76 |
| C ≡ N | 3.1 | 1.4 |
| O--H[d] | 0.72 | 0.72 |

### B. Molecular Polarizabilities

| Molecule | $\alpha_l$ | $\alpha_t$ |
|---|---|---|
| $CH_3CN$[e] | 5.56 | 3.67 |
| $H_2O$[d] | 1.44 | 1.44 |

---

[a] Units of $10^{-24}$ $cm^3$

[b] Reference 115, except where noted

[c] Derived from molecular polarizability

[d] Assuming near isotropic polarizability tensors, Reference 118

[e] Reference 117

the polarizability of each of the O - H bonds is approximately isotropic and not angle dependent. That is, it can be assumed that the lateral and transverse polarizability tensors are equal. The derived values are included in Table 18.

### C Dispersion Energy

The interaction energy due to the dispersion forces between an ion and a solvent molecule can be approximated by the modified London equation (119):

$$E_{dis} = -3/2 \frac{\alpha_I \alpha_S}{R_{IS}^6} \times \frac{I_I I_S}{I_I + I_S} \qquad 4.8$$

where $\alpha_I$ and $\alpha_S$ are the polarizabilities of the ion and solvent molecule, $I_I$ and $I_S$ are the ionization potentials for the ion and the solvent molecule and $R_{IS}$ is the distance between the centre of the ion and the geometric centre of the solvent molecule. Values for polarizabilities and ionization potentials for alkali ions are shown in Table 19.

It has been observed by Pitzer (120) that the London equation consistently gives results which are too low. Instead of using experimental ionization potentials, he suggested the use of "effective" ionization potentials, which are determined by multiplying the true potentials by a suitable coefficient, J. The J value of water and acetonitrile was taken as 2.5 (101) and those of the alkali metals were assumed similar to the corresponding noble-gas atoms and given the

## TABLE 19

### Ionization Potentials and Polarizabilities of Alkali Ions[a]

| Ion | Ionization Potential (eV) | Polarizability ($\mathring{A}^3$) |
|---|---|---|
| $Na^+$ | 47.1 | 0.24 |
| $K^+$ | 31.7 | 0.89 |
| $Rb^+$ | 27.4 | 1.81 |
| $Cs^+$ | 23.4 | 2.79 |

[a] Reference 119

value 2.25 (Pitzer's value for sp closed shells).

The London equation is isotropic. Since both acetonitrile and water are anisotropic, an angular term should be included. For water, this is not too serious (118), since the anisotropic part of the polarizability tensor is small. However, it is much larger for acetonitrile and should be taken into account. As was done in the case of ion-induced dipole energies, bond polarizability tensors can be used. Thus the London formula becomes:

$$E_{dis} = -34.56\frac{J_I I_I \times I_S J_S}{J_I I_I + J_S I_S} \times I_{ij}\frac{\alpha_t \sin^2 {}_{ij} + \alpha_l \cos^2 {}_{ij}}{R_{ij}^6}$$

where $_{ij}$, $\alpha_t$, $\alpha_l$ and $R_{ij}$ have the same definitions as in the equation for $E_{ind}$ (Equation 4.5). 34.56 is a numerical factor to give $E_{dis}$ in kcal/mole for values of I in eV, in $A^3$ and R in A.

## D Repulsion Energies

Various functional dependences of the repulsive potential have been used in electrostatic calculations. Of these, the $AR^{-12}$ Lennard-Jones potential has been applied most often. In the present work, the exponential form (Equation 4.10) was used.

$$E_{rep} = C_{Ij}e^{-a_{IS}r_{Ij}} \qquad 4.10$$

$C_{Ij}$ and $a_{Ij}$ are constants characteristic of the potential of the ion, I, and an atom, j, of the solvent molecule.

It has been found for rare gas potentials that the exponential form is more reliable than the $AR^{-12}$ form over large ion-neutral distances (121). The recent calculations of alkali and halide ion hydration made by Spears (99) and by Eleizer and Krindel (101) are in good agreement with experimental results. Both sets of calculations use an exponential form of the repulsive potential. However, Spears obtained the K - $H_2O$ repulsion potential from experimental enthalpies; and then from alkali-halide gas phase reactions and rare gas potentials obtained the values for the other alkali ion-water potentials. In the present case, it was felt that it would be valuable to calculate energies without using such experimental calibration since it is interesting to examine whether electrostatic calculations will predict that acetonitrile forms stronger complexes with alkali ions than water and that acetonitrile interacts more strongly with positive than with negative ions. Thus, the procedure of Eleizer and Krindel was used.

Various assumptions must be made when using the repulsive potential. The first assumption is that because of the strong radius dependence of the repulsive potential on the ion-atom distance, only the oxygen in water and the nitrogen in acetonitrile will have significant value. The second assumption was made necessary by lack of direct data on the O--ion and N--ion potentials. The repulsion potentials of O--O (122) and N--N (123) are available as well as the noble-gas atom pairs (124, 128). The repulsion potentials

of the alkali ion pair was assumed equal to the corresponding isoelectronic noble gas.

The constants $a_{Ij}$ and $C_{Ij}$ were then determined by the following combination rules (126):

$$a_{Ij} = (a_{II} + a_{jj})/2 \quad C_{Ij} = (C_{II}C_{jj})^{1/2} \qquad 4.11$$

The final values for a and C are summarized in Table 20.

The assumption that the repulsive potential of the alkali ion pair is approximately equal to the corresponding isoelectronic rare gas has been substantiated experimentally by Amdur (121, 127). Amdur's experiments involved elastic scattering of potassium ion beams by the rare gases (127) and other common molecules like $N_2$, $O_2$, etc. (121). The intermolecular potentials obtained in this manner were indistinguishable within experimental uncertainty for Ar-molecule potentials.

## E Total Energies

The final classical attractive and repulsive energies are presented in Table 21 along with the experimental ΔH. The total energies, $E_t$, agree remarkably well with the enthalpies for all the alkali ions with either acetonitrile or water.

The calculations predict that acetonitrile will react more strongly with an alkali ion than will water. This can be accounted for by the more favourable ion-dipole and ion-

## TABLE 20

### Parameters for the Exponential Form of the Repulsion Potential for Alkali Ions

| Pair (A-B) | $a_{AB}$[a] | $C_{AB}$[b] |
|---|---|---|
| O--O[c] | 3.565 | 1.87 |
| N--N[d] | 2.753 | 0.366 |
| H--H[e] | 3.01 | 0.0697 |
| Ne--Ne[f] | 4.78 | 28.0 |
| Ar--Ar[g] | 3.62 | 22.5 |
| Kr--Kr[g] | 3.03 | 14.2 |
| Xe--Xe[g] | 2.92 | 17.6 |
| $Na^+$--O | 4.17 | 7.24 |
| $Na^+$--N | 3.76 | 3.20 |
| $K^+$--O | 3.59 | 6.49 |
| $K^+$--N | 3.19 | 2.87 |
| $K^+$--H | 3.31 | 1.25 |
| $Rb^+$--O | 3.30 | 5.15 |
| $Rb^+$--N | 2.89 | 2.28 |
| $Cs^+$--O | 3.24 | 5.74 |
| $Cs^+$--N | 2.84 | 2.54 |

[a] Units of angstroms$^{-1}$

[b] Units of kcal/mole x $10^4$

[c] Reference 122

[d] Reference 123

[e] Reference 128

[f] Reference 124

[g] Reference 125

## TABLE 21

Electrostatic Potential Energies[a] for the Reactions:

$M^+ + H_2O \rightleftarrows M^+(H_2O)$ and $M^+ + CH_3CN \rightleftarrows M^+(CH_3CN)$

A. $H_2O$

| $M^+$ | $R_{M^+} - O$ [b] | $-E_{dip}$ | $-E_{ind}$ | $-E_{dis}$ | $E_{rep}$ | $-E_t$ | $-\Delta H$ [c] |
|---|---|---|---|---|---|---|---|
| $Na^+$ | 2.17 | 24.73 | 6.39 | 1.40 | 8.51 | 24.00 | 24.0 |
| $K^+$ | 2.59 | 17.79 | 3.36 | 1.72 | 5.95 | 16.92 | 17.9 (16.9)[d] |
| $Rb^+$ | 2.75 | 15.89 | 2.70 | 2.39 | 5.90 | 15.08 | 15.9 |
| $Cs^+$ | 2.84 | 14.95 | 2.40 | 2.96 | 5.98 | 14.46 | 13.7 |

B. $CH_3CN$

|  | $R_{M^+} - N$ [b] | $-E_{dip}$ | $-E_{ind}$ | $-E_{dis}$ | $E_{rep}$ | $-E_t$ | $-\Delta H$ [d] |
|---|---|---|---|---|---|---|---|
| $Na^+$ | 2.12 | 28.39 | 11.92 | 1.84 | 10.82 | 31.33 | (31) |
| $K^+$ | 2.57 | 21.31 | 6.56 | 2.46 | 7.90 | 22.43 | 24.4 |
| $Rb^+$ | 2.74 | 19.33 | 5.35 | 3.50 | 8.07 | 20.11 | 20.7 |
| $Cs^+$ | 2.84 | 18.30 | 4.77 | 4.28 | 7.98 | 19.38 | 19.2 |

[a] Energies in kcal/mole

[b] Units of angstroms

[c] Reference 3

[d] This work

induced dipole attraction terms in the acetonitrile-alkali ion interactions. The calculations also predict that the interaction energies will become less favourable as the size of the ion increases in agreement with the experimental results.

## 4.4 Rotation of the Ion-Ligand Bond

In the electrostatic calculations, it was assumed that the ion-ligand bond was directed along the dipole axis. To test whether or not this is predicted by electrostatic calculations, it is possible to rotate the acetonitrile and water molecules about the centre of the donor atom and find which configuration gives the most favourable energy of interaction. The rotation axes are pictured in Figure 74.

Because the hydrogens in water and the cyano carbon in acetonitrile come closer to the ion upon rotation, a repulsive potential must be added to account for electron repulsion. The H--H potential is known (Table 20) and thus by using the combination rules the values of $a_{H-ion}$ and $C_{H-ion}$ may be determined. Unfortunately the carbon potential is not known and it must be assumed that it will be similar to that of nitrogen.

Due to the linearity of the acetonitrile molecule (disregarding the methyl hydrogens) rotation about either the x or z axis will give the same results. With water, however, rotation about the x axis brings one hydrogen atom closer to the ion and moves one further away, i.e. the ion-

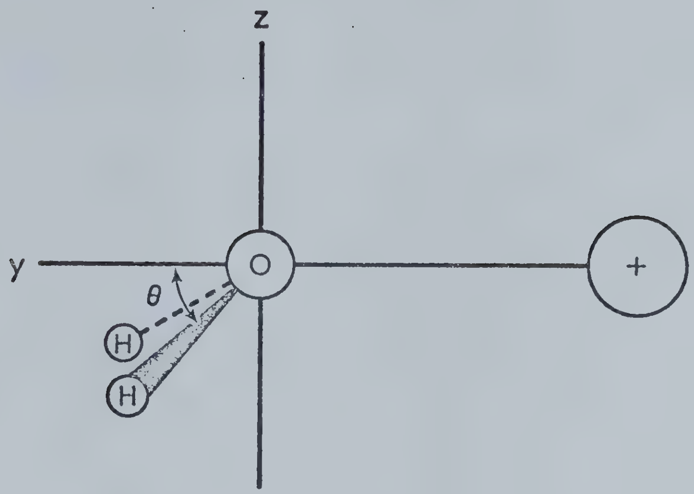

ROTATION ABOUT THE x AXIS

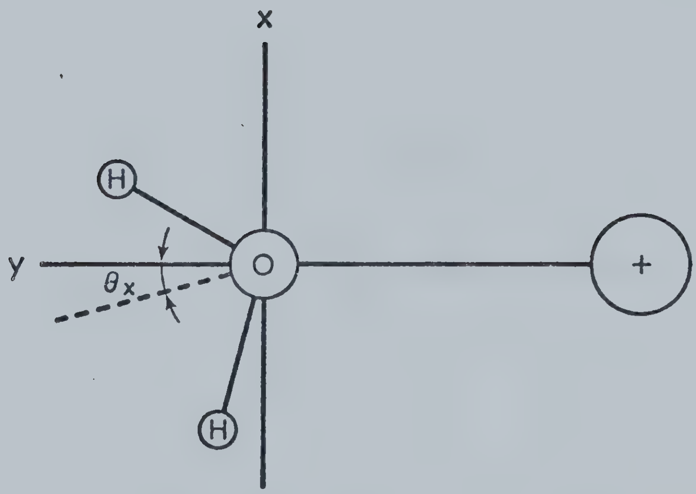

ROTATION ABOUT THE z AXIS

FIGURE 74 Rotation of the Ion--Ligand Bond.

ligand bond no longer lies on the plane of symmetry of the water molecule. Rotation about the z axis maintains the plane of symmetry and the atoms are kept equidistant from the ion.

The increase in energy upon rotation by an angle $\theta$ is presented in Table 22 for the potassium ion and the two solvents. The energy of the acetonitrile-ion interactions decreases much less rapidly than that of water upon rotation. This effectively means that the "bond" is more flexible than the water-ion bond. If this were the only feature affecting the entropy of the reaction, one would then expect that the entropy of the acetonitrile-potassium ion reaction would be slightly more favourable than the water-potassium ion reaction. But this is not the case; experimentally the water reaction has the more favourable entropy (-19.9 e.u. for water, compared to -21.5 e.u. for acetonitrile).

The directional character of the sp lone pair on the nitrogen in acetonitrile is not taken into account in these calculations. It has been postulated that it is this lone pair interaction with ions that results in complexing (87). With the present calculations, there is no method of incorporating the lone pair into the calculations.

For water, rotation about the x axis results in a rapid increase in energy, whereas rotation about the z axis is much more stable. This agrees very well with the results of Eleizer and Krindel (101) who used a similar treatment with alkali and halide ions with water.

## TABLE 22

## Effect of Rotation of the Solvent Molecule on Electrostatic Potential Energies[a]

| | Increase of Energy from Minimum | | |
|---|---|---|---|
| | $H_2O$ | | $CH_3CN$ |
| Angle[b] of Rotation | x-axis | z-axis | x or z axis |
| 0 | 0 | 0 | 0 |
| 10 | 0.26 | 0.13 | 0.08 |
| 20 | 1.25 | 0.53 | 0.33 |
| 30 | 2.40 | 1.21 | 0.75 |
| 40 | 4.59 | 2.16 | 1.35 |
| 50 | 7.66 | 3.42 | 2.17 |
| 60 | 12.03 | 4.99 | 3.23 |
| 70 | 18.26 | 6.90 | 4.58 |
| 80 | 27.06 | 9.18 | 6.28 |
| 90 | 39.00 | 11.89 | 8.49 |

[a] Energy in kcal/mole

[b] Angle in degrees

## 4.5 Electrostatic Calculations for Halide Ion-Acetonitrile Reactions

Using a model similar to the one used for calculating the classical electrostatic interaction potentials between alkali ions and an acetonitrile molecule, it is possible to calculate the interaction potentials between a halide ion and an acetonitrile molecule. The halide ion will most likely be orientated towards the methyl hydrogens, equidistant from each H atom.

The ion-dipole energy will be:

$$E_{ID} = -334 \sum^{i} Q_i/R_i \qquad 4.12$$

where $Q_i$ is the point charge on an atom i (Figure 72), and $R_i$ is the ion-atom distance. The numerical factor contains a minus sign, indicating the negative charge on the halide ion.

The bond polarizability tensors will be identical with those used for the positive ion calculations (Table 18). For the $C \equiv N$ and C--C bonds only the lateral tensors are needed since the halide ion will be on the $C{-}{-}C \equiv N$ axis. The ion-induced dipole interaction energy can again be expressed by Equation 4.5.

The modified London formula (Equation 4.9) can again be used to determine the ion-molecule dispersion energy. The value of J to "correct" the ionization potentials of the halide ions is 2.25, the same as for alkali ions (101).

The values of the ionization potentials and the polarizabilities of the halide ions used in the London formula are listed in Table 23.

The electronic repulsive term includes the ion-hydrogen atom repulsions, as well as the ion-carbon atom repulsions. The exponential form of the repulsion equation is again used:

$$E_{rep} = 3 \times C_{H-ion} \exp(-a_{H-ion} r_{H-ion}) + C_{C-ion} \exp(-a_{C-ion} r_{C-ion}) \qquad 4.13$$

The nitrogen-ion a and C values are used for carbon, since no such parameters have been obtained for C--C or C-ion electronic repulsions. The a and C values used in this calculation are shown in Table 24.

To obtain the total classical electrostatic potential, the distance between the halide ion and the methyl carbon was varied until a minimum occurred in the calculated energy. The total classical potentials are shown for $F^-$, $Cl^-$, $Br^-$ and $I^-$ in Table 25, along with the experimental enthalpies.

For the bromide and iodide ions, the calculated $E_t$'s agree extremely well with experimental enthalpies. However, the agreement is not as good for the chloride ion (1.5 kcal difference) and is even worse for the fluoride ion (4.5 kcal difference). The calculations demonstrate that halide ion-acetonitrile reactions will be much more unfavourable than alkali ion-acetonitrile reactions (comparing

## TABLE 23

### Ionization Potentials and Polarizabilities of Halide Ions[a]

| Ion | Ionization Potential (eV) | Polarizability ($A^{o3}$) |
|---|---|---|
| $F^-$ | 4.3 | 0.81 |
| $Cl^-$ | 4.0 | 2.98 |
| $Br^-$ | 3.8 | 4.24 |
| $I^-$ | 3.4 | 6.25 |

[a] Reference 119

## TABLE 24

### Parameters for the Exponential Form of the Repulsion Potential for Halide Ions and Acetonitrile

| Pair (A--B)[a] | $a_{AB}$ ($Å^{-1}$) | $C_{AB}$ (kcal/mole x $10^4$) |
|---|---|---|
| $F^-$--$C$[b] | 3.76 | 3.20 |
| $F^-$--H | 3.90 | 1.40 |
| $Cl^-$--C | 3.19 | 2.87 |
| $Cl^-$--H | 3.31 | 1.25 |
| $Br^-$--C | 2.89 | 2.28 |
| $Br^-$--H | 3.02 | 0.995 |
| $I^-$--C | 2.84 | 2.54 |
| $I^-$--H | 2.96 | 1.11 |

[a] From combination rules, Equation 4.11

[b] Carbon repulsion potential parameters considered the same as those for nitrogen

## TABLE 25

### Electrostatic Potential Energies[a] for the Reactions:

$$X^- + CH_3CN \rightleftarrows X^-(CH_3CN)$$

| $X^-$ | $R$[b] | $-E_{dip}$ | $-E_{ind}$ | $-E_{dis}$ | $E_{rep}$ | $-E_{tot}$ | $-\Delta H_{expt}$[c] |
|---|---|---|---|---|---|---|---|
| $F^-$ | 2.55 | 19.06 | 6.17 | .88 | 5.52 | 20.59 | 16.0 |
| $Cl^-$ | 3.10 | 14.51 | 3.21 | 1.06 | 3.86 | 14.93 | 13.4 |
| $Br^-$ | 3.37 | 12.84 | 2.43 | 0.93 | 3.36 | 12.84 | 12.9 |
| $I^-$ | 3.49 | 12.24 | 2.18 | 1.05 | 3.29 | 12.18 | 11.9 |

[a] Energies in kcal/mole

[b] R = distance from centre of ion to methyl carbon in angstroms

[c] Reference 2

Tables 21 and 25). This difference appears mainly to be due to the more favourable ion-dipole energies in the alkali ion-acetonitrile interaction.

## 4.6 Consistency of the Present Calculations with Other Electrostatic and Quantum Mechanical Calculations

As stated in Section 4.1, many authors have calculated interaction potentials for the hydration of an alkali ion. This provides an opportunity to compare the present results with those obtained using different methods.

In Table 26, the various terms in Equation 4.1 obtained in the present work are compared with those of Spears (101) for the reaction:

$$Na^+ + H_2O \rightleftarrows Na^+(H_2O) \qquad 4.14$$

Although each and every term of the equation was determined in a different manner, the final results are quite similar.

In Table 27 the total calculated interaction energies for reaction 4.14 are compared with those calculated by other authors. All are quite consistent with the experimental value and with the value calculated from the present model.

Also, the total electrostatic energy obtained in this study is compared with that of Green and Martin (102) in Table 27 for the chloride ion-acetonitrile reaction:

$$Cl^- + CH_3CN \rightleftarrows Cl^-(CH_3CN) \qquad 4.15$$

# TABLE 26

## Comparison of Electrostatic Potential Energies[a] Obtained in this Study with Those of Spears for the Reaction:

$$Na^+ + H_2O \rightleftarrows Na^+(H_2O)$$

| $R_{O-Na^+}$[b] | $-E_{dip}$ | $-E_{ind}$ | $-E_{dis}$ | $E_{rep}$ | $-E_{tot}$ |
|---|---|---|---|---|---|
| This work | | | | | |
| 2.17 | 24.7 | 6.4 | 1.4 | 8.5 | 24.0 |
| Spears (99) | | | | | |
| 2.25 | 24.8[c] | 8.4 | 1.5 | 10.1 | 24.6 |

[a] All energies in kcal/mole

[b] Units of angstroms

[c] Includes ion-dipole and ion quadrupole interactions.

## TABLE 27

## Comparison of Various Calculated Potential Energies

### A. $Na^+$--$H_2O$

| Reference | Calculated $-E_t$ (kcal/mole) | Experimental $-\Delta H_{o,1}$ (kcal/mole) |
|---|---|---|
| K. Spears (99) | | |
| Electrostatic | 24.6 | 24.0 |
| Eleizer and Krindel (101) | | |
| Electrostatic | 25.9-28.0 | |
| This work | 24.0 | |
| Kistenmacher, Popkie, and Clementi (79) | | |
| Hartree-Fock app. | 25.2 | |
| Diercksen and Kraemer (104) | | |
| SCF-MO-LCGO | 25.2 | |
| Burton and Daly (105) | | |
| CNDO/2 | 20.6 | |

### B. $Cl^-$--$CH_3CN$

| Reference | Calculated $-E_t$ (kcal/mole) | Experimental $-\Delta H_{o,1}$ (kcal/mole) |
|---|---|---|
| Green and Martin (102) | | |
| Electrostatic | 13.4 | 13.4 |
| This work | 14.9 | |

In their model they used a "hard sphere" approach in which the ion-acetonitrile radius was set equal to the sum of the atomic van der Waals' radii. This allowed them to ignore the dispersion and repulsion terms in Equation 4.1.

The present calculations thus seem quite consistent with those of other authors, but they provide a more universal method of calculating electrostatic potentials between an ion and a solvent molecule.

## 4.7 General Remarks on Electrostatic Calculations

The use of electrostatic calculations for the determination of reaction energies between an ion and solvent molecule is at best an approximate method. The dispersion and repulsion energies are very suspect since they involve many assumptions. With acetonitrile, the point charge distribution varies with the quantum mechanical method in which it is determined.

The present calculations correctly predict that an acetonitrile molecule will react with alkali ions more readily than a water molecule. They also predict that the order of ion-solvent interactions decrease with the size of the ion: $Na^+ > K^+ > Rb^+ > Cs^+$. The ion-ligand bond is also shown to lie in the direction of the dipole. The electrostatic calculations also predict that anions initially will be less solvated by acetonitrile than would cations.

## CHAPTER 5

# LEWIS BASICITIES WITH THE POTASSIUM ION AS A REFERENCE ACID

## 5.1 Introduction

A relative scale of basicities can be set up using the potassium ion as a reference Lewis acid and determining the thermodynamic functions of the reaction:

$$K^+ + B \rightleftarrows K^+B \qquad 5.1$$

where B represents any base. In the gas phase, intrinsic thermodynamic values of Reaction 5.1 may be obtained in the absence of solvation effects and further clustering of the base about the potassium ion.

Any alkali ion could be used as the reference acid; however, potassium proved to be the most useful. As was pointed out in a comparison of water and acetonitrile, the differences in base strength of various molecular bases decrease as the size of the ion increases. This means that lithium would provide the greatest difference in thermodynamic functions between various bases. However, the interactions between lithium or sodium and many of the "strong" bases studied are so strong that they require very high temperatures for the equilibrium determinations, which are beyond the capabilities of the present apparatus. The potassium ion seems to be ideal in this respect, since the $K_{0,1}$'s could be

measured accurately and there were significant differences in the interaction between bases and the ion, from which a basicity scale could be obtained.

## 5.2 Some Special Problems Encountered in Lewis' Basicities Determinations:

### Slow Clustering Reactions and Thermal Decomposition of the Base

The study of Reaction 5.1 proved to be difficult for many of the bases. The difficulties arose from cluster dissociation in the vacuum chamber and thermal decomposition of the gaseous base in the ion source due to the high temperatures of the potassium emitting filament (around $600^{\circ}$ C). For some bases, i.e. trimethylamine, high pressures of gas were required to bring the Reaction 5.1 to equilibrium; i.e., for some reason the clustering rate constants are low. Unfortunately, cluster dissociation (see Chapter 2) increases with pressure and is particularly serious for bulky molecules like trimethylamine. Therefore, an alternative method of determining the equilibrium constant for Reaction 5.1 was applied. The switching Reaction 5.2 is fast. Selecting a reference base $B_1$ which forms $K^+B_1$ rapidly, one finds that

$$K^+B_1 + B_2 \rightleftarrows K^+B_2 + B_1 \qquad 5.2$$

the ions $K^+B_1$ and $K^+B_2$ reach equilibrium at much lower pressure than that required for the clustering equilibrium

involving only $B_2$. The switching equilibrium constant, $K_S$, can be readily determined:

$$K_S = \frac{K^+B_2}{K^+B_1} \times \frac{P_{B_1}}{P_{B_2}} = \frac{K_2}{K_1} \qquad 5.3$$

As was pointed out in Chapter 1, $K_2$ will be equal to the product of the switching equilibrium and $K_1$. By using a well studied and easy to handle base, $B_1$, such as $H_2O$, the equilibrium constant $K_2$ can be obtained.

Problems caused by thermal decomposition of the bases were also encountered. Thus, in the study of the complexing of $K^+$ with primary aliphatic amines, the major ions found were not the $K^+$-amines, but ions of two or four mass units lower. As shown below, these ions were due to the thermal decomposition of the amine in the ion source by the high temperature filament and the clustering of the product with the potassium ion. Without knowing the degree of decomposition of the amine, it would be impossible to correctly determine the equilibrium constant for the $K^+$-amine reaction.

The following mechanism for the pyrolysis of a primary amine has been proposed (132, 133):

1) the primary breakdown of the amine with the formation of an aldimide

$$R\text{-}CH_2NH_2 \rightarrow RCH{=}NH + H_2 \qquad 5.4$$

where R represents H, $CH_3$, $CH_3CH_2$, etc.

2) the formation of a nitrile from the aldimide

$$RCH{=}NH \rightarrow RC{\equiv}N + H_2 \qquad 5.5$$

This mechanism is consistent with the products observed in the clustering reaction. For example, with methylamine, the products of pyrolysis are $CH_2{=}NH$ and $HC{\equiv}N$. When these products cluster with potassium, they yield ions which are lower by two and four mass units than the $K^+(CH_3NH_2)$ ion. Similarly, ethylamine yields $CH_3CH{=}NH$ and $CH_3CN$, and n-propylamine yields $CH_3CH_2CH{=}NH$ and $CH_3CH_2CN$.

The reaction mechanisms for the thermal decomposition of dimethyl and trimethylamine are slightly different (130). The pyrolysis of the tertiary amine may be represented as:

$$N(CH_3)_3 \rightarrow CH_3\cdot + N(CH_3)_2\cdot \qquad 5.6$$

$$CH_3\cdot + N(CH_3)_3 \rightarrow CH_4 + N(CH_3)_2.CH_2\cdot \qquad 5.7$$

$$N(CH_3)_2.CH_2\cdot \rightarrow CH_3\cdot + CH_3N{=}CH_2 \qquad 5.8$$

The main products being methane and methylmethyleneimine ($CH_3N{=}CH_2$). The pyrolysis of the secondary amine is a more complicated free radical process (130) and no mechanism has been proposed which fits the experimental products, which are methane, methylmethyleneimine and methylamine.

To determine the degree of dissociation of the amines two methods were used. Since acetonitrile is the major product in the decomposition of ethylamine, and since the $K_{0,1}$ for acetonitrile-potassium clustering had been determined, the amount of acetonitrile present could be determined from:

$$P_{CH_3CN} = \frac{K^+(CH_3CN)}{K_{0,1} \times K^+} \qquad 5.9$$

Because it appeared that acetonitrile was present in relatively small amounts, a time dependent study of the reaction was done at 297° C. A plot of the percentage total ionization of $K^+$ and $K^+(CH_3CN)$ is shown in Figure 75. The equilibrium constant for the 0,1 reaction of the potassium ion with acetonitrile at 297° determined from the Van't Hoff plot in Figure 57is 58.5. From Figure 75, the ratio of the ion intensities at equilibrium, $(K^+(CH_3CN)/K^+)$, is 0.81, leading to an acetonitrile pressure of 0.0138 torr. The total pressure was 0.23 torr, meaning that approximately 6% of the ethylamine had decomposed.

A second method, used to determine the degree of decomposition of propylamine, was analytical mass spectrometry. A liquid $N_2$ cooled trap was attached to the ion source to collect the condensable gases after passing through the ion source at 300° C. The mass spectrum of this sample was obtained and compared to the mass spectra of pure n-propylamine and propionitrile. A 3 $\mu\ell$ sample of propylamine

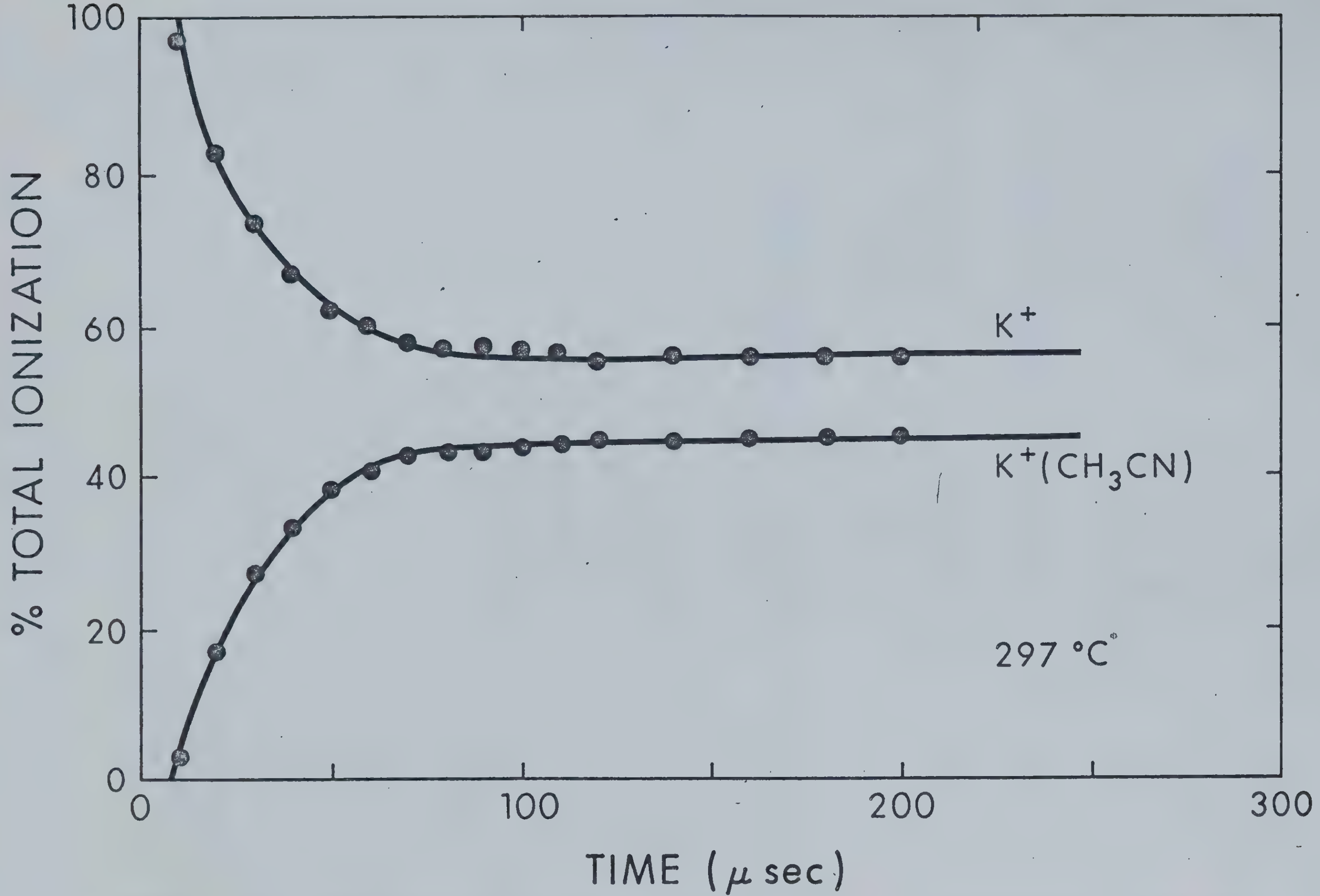

FIGURE 75 Time Dependence of Normalized Ion Intensities for the Determination of the Amount of Ethylamine Undergoing Thermal Decomposition.

yielded a m/e = 59 peak of 125.3 mm and a m/e = 54 peak of 6.9 mm. A similar 3 μℓ sample of propionitrile yielded no m/e = 59 peak and a m/e = 54 peak of 454 mm. Three μℓ of the collected sample yielded a 120.5 mm m/e = 59 peak and a 29.6 mm m/e = 54 peak. Of this mass 54 peak:

$$120.5 \times \frac{6.9}{123.5} = 6.7 \text{ mm}$$

can be attributed to the n-propylamine, leaving (29.6-6.7)=22.9 mm due to the propionitrile. Thus:

$$\frac{\text{Volume n-proplyamine}}{\text{Volume propionitrile}} = \frac{120.5/125.3}{22.9/454} = \frac{0.962}{0.0504}$$

which leads to 95% of propylamine and 5% propionitrile by volume in the sample collected from the ion source. No peaks were observed in the spectrum of the mixture which could not be accounted for by n-propylamine or propionitrile. From this method, it appeared that only 5% of the amine decomposed at 300° C.

Thus, the equilibrium constants for the aliphatic amines appear to be in error by 5 - 6%. Since pyrolysis only becomes serious at temperatures above 450° C (129, 130 , the ion source temperature will not lead to decomposition of the amines and thus the enthalpies of the reactions will not be affected.

A 5 - 6% error in the equilibrium constants will only lead to an error of approximately -0.1 e.u. in the entropy,

which compared to the error in least square fitting (usually around 1 e.u.) is not serious. Therefore, the effects of the pyrolysis were neglected in the evaluation of the equilibrium constants.

## 5.3 Presentation of Results - Amines

The equilibrium constants of Reaction 5.1 were determined at various temperatures for B = ammonia, dimethylamine, n-propylamine, aniline, pyridine, and ethylenediamine; (the data on ethylenediamine is presented in Chapter 6). In Figures 76 to 80, the resulting equilibrium constants, $K_{0,1}$, are plotted as a function of the pressure of the base. The resulting plots remain constant over the pressure ranges studied, indicating that equilibrium has been achieved. In Figure 81 the switching equilibrium constant for the reaction:

$$K^+(H_2O) + CH_3NH_2 \rightleftarrows K^+(CH_3NH_2) + H_2O \qquad 5.10$$

is plotted as a function of the ratio of the two bases (i.e. $P_{H_2O}/P_{CH_3NH_2}$. Only representative temperatures are shown in the plot since all the $K_s$'s lie in somewhat the same range. Although there is considerable scatter, the switching equilibrium does not seem to vary as a function of the pressure ratio of the bases. In Figure 82 the switching equilibrium constant for the reaction:

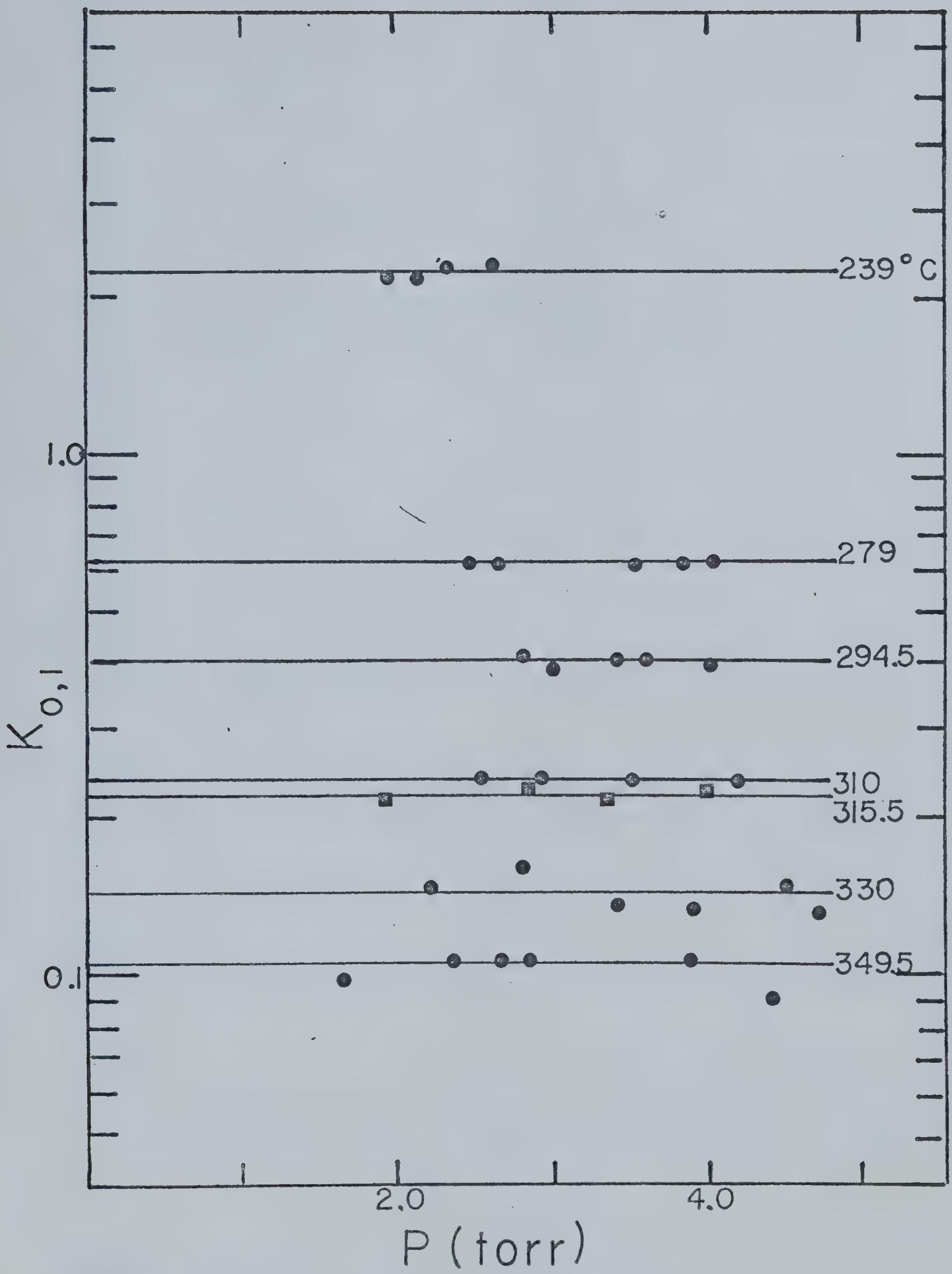

FIGURE 76 Equilibrium Constants versus Pressure at Various Temperatures for the Reaction:

$$K^+ + NH_3 = K^+(NH_3) .$$

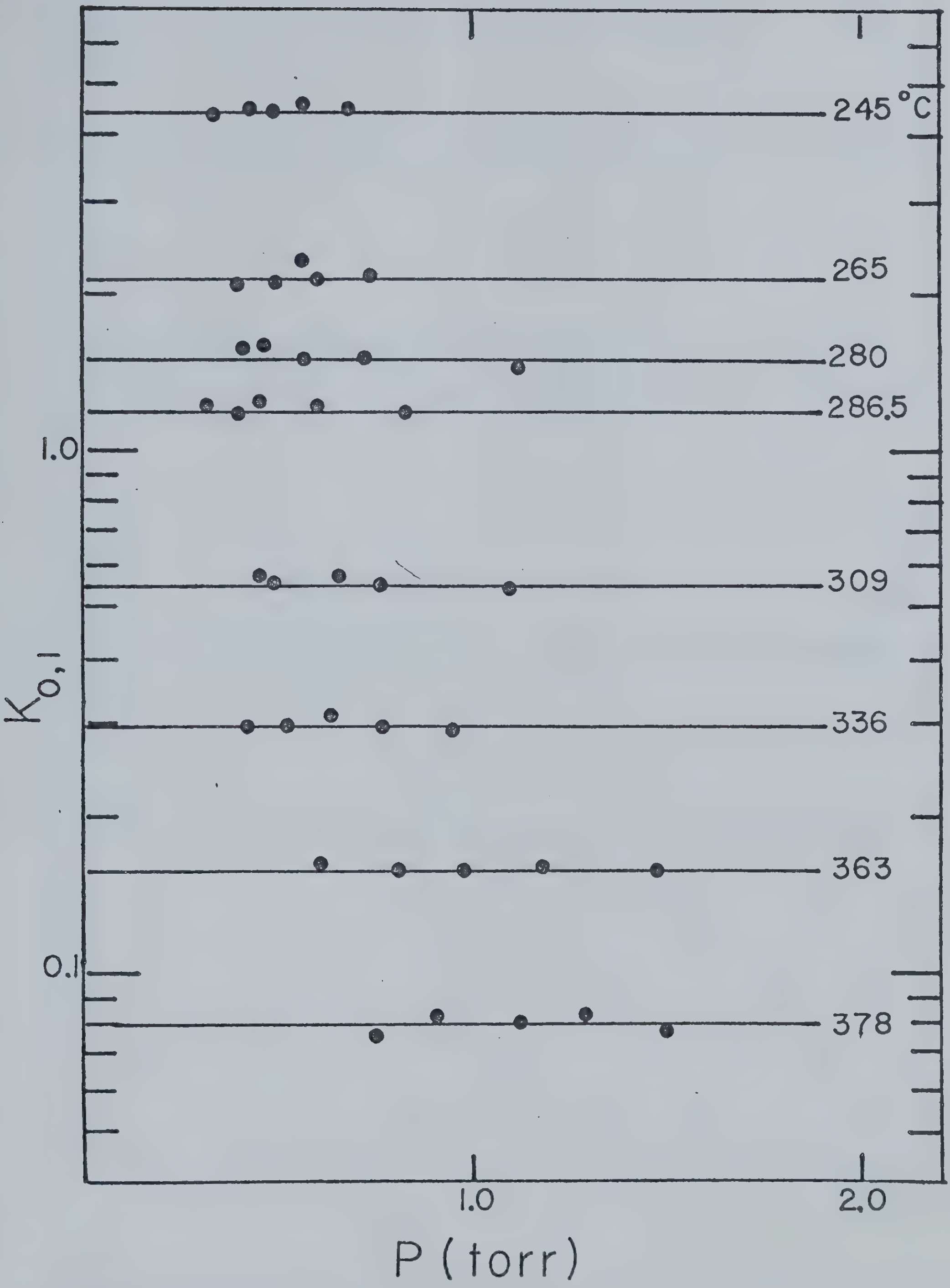

FIGURE 77 Equilibrium Constants versus Pressure at Various Temperatures for the Reaction:

$$K^+ + (CH_3)_2NH = K^+[(CH_3)_2NH] .$$

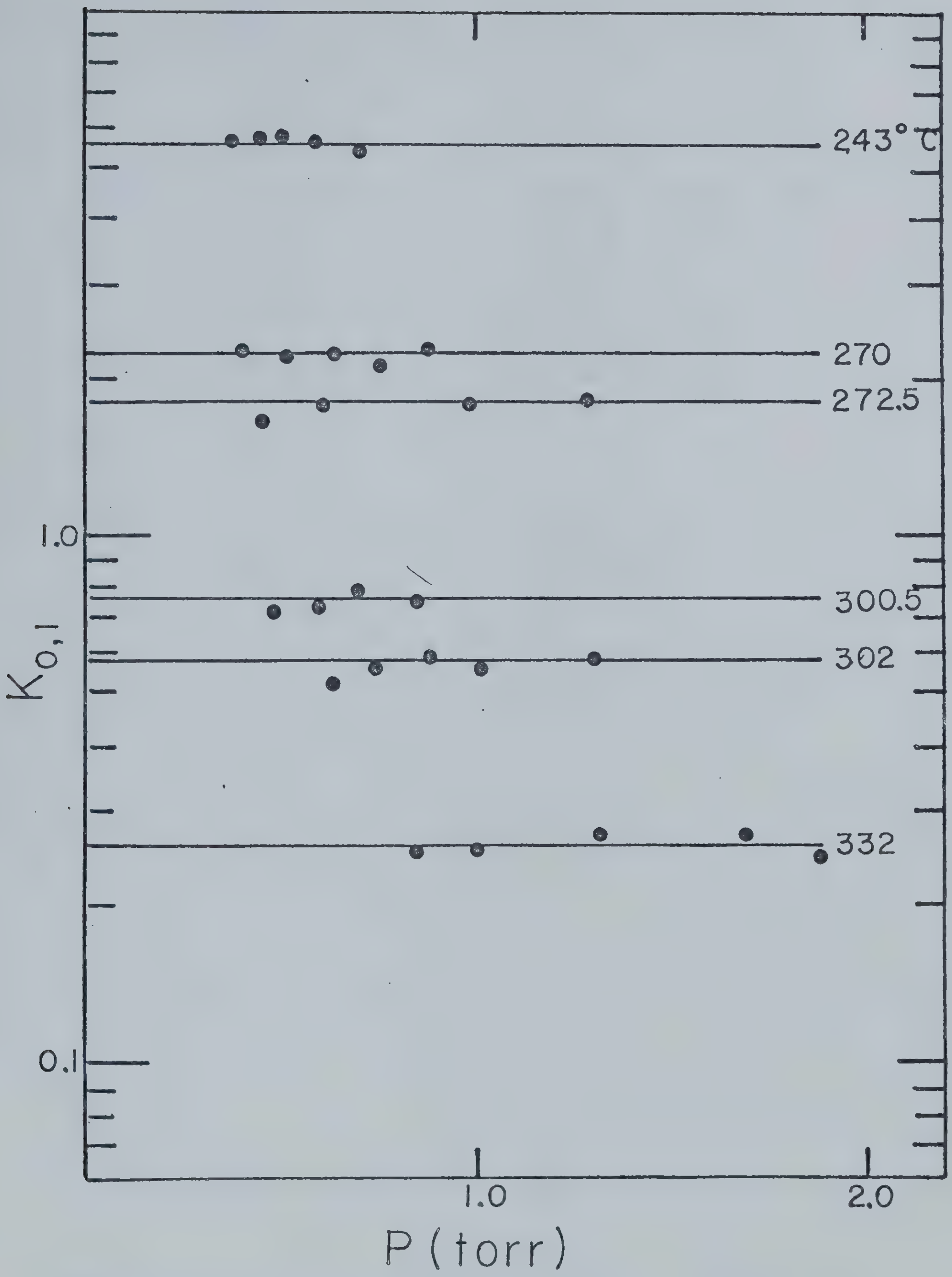

FIGURE 78 Equilibrium Constants versus Pressure at Various Temperatures for the Reaction:

$$K^+ + CH_3CH_2CH_2NH_2 = K^+(CH_3CH_2CH_2NH_2) .$$

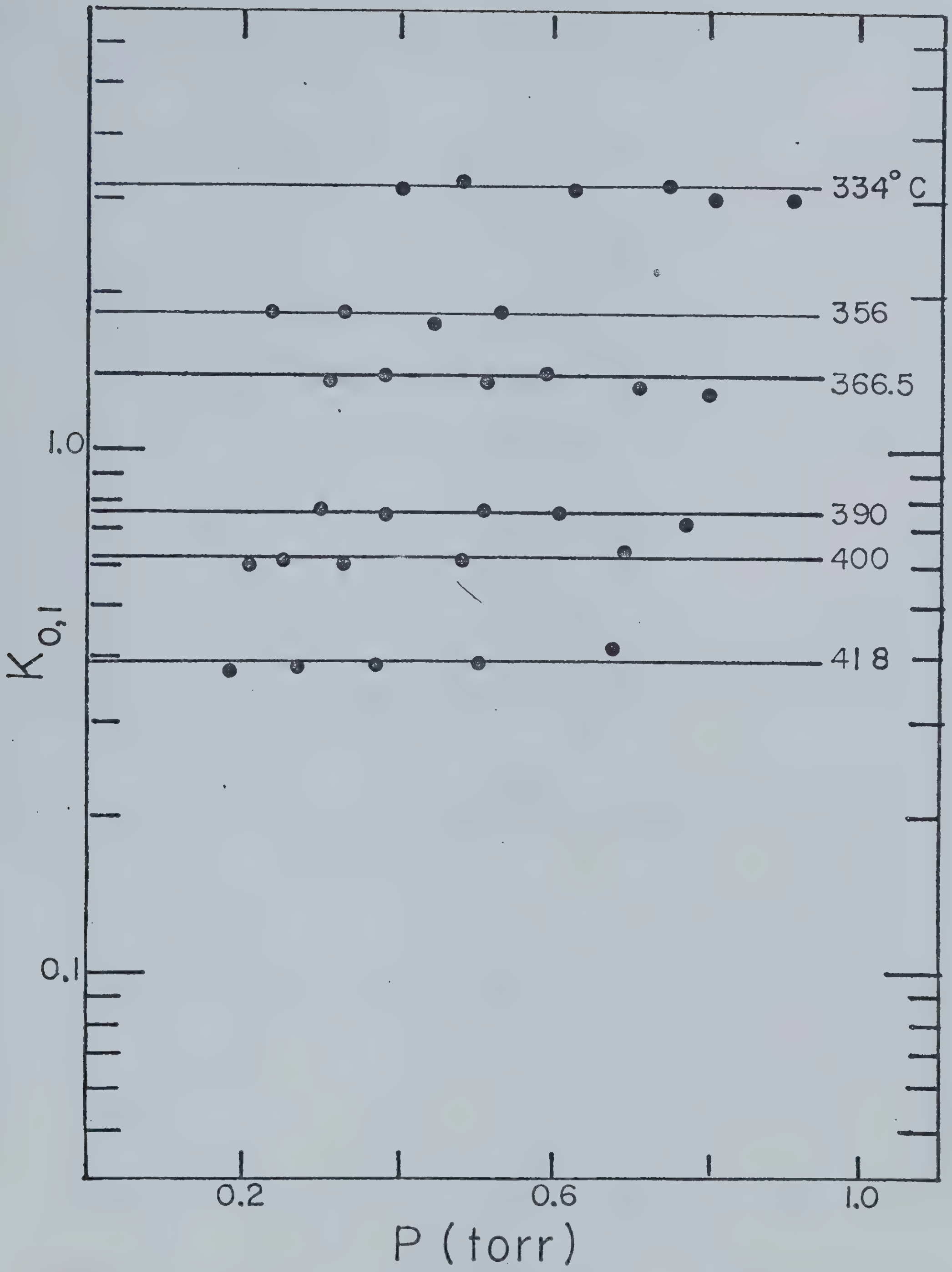

FIGURE 79 Equilibrium Constants versus Pressure at Various Temperatures for the Reaction:

$$K^+ + \text{pyridine} = K^+(\text{pyridine})\ .$$

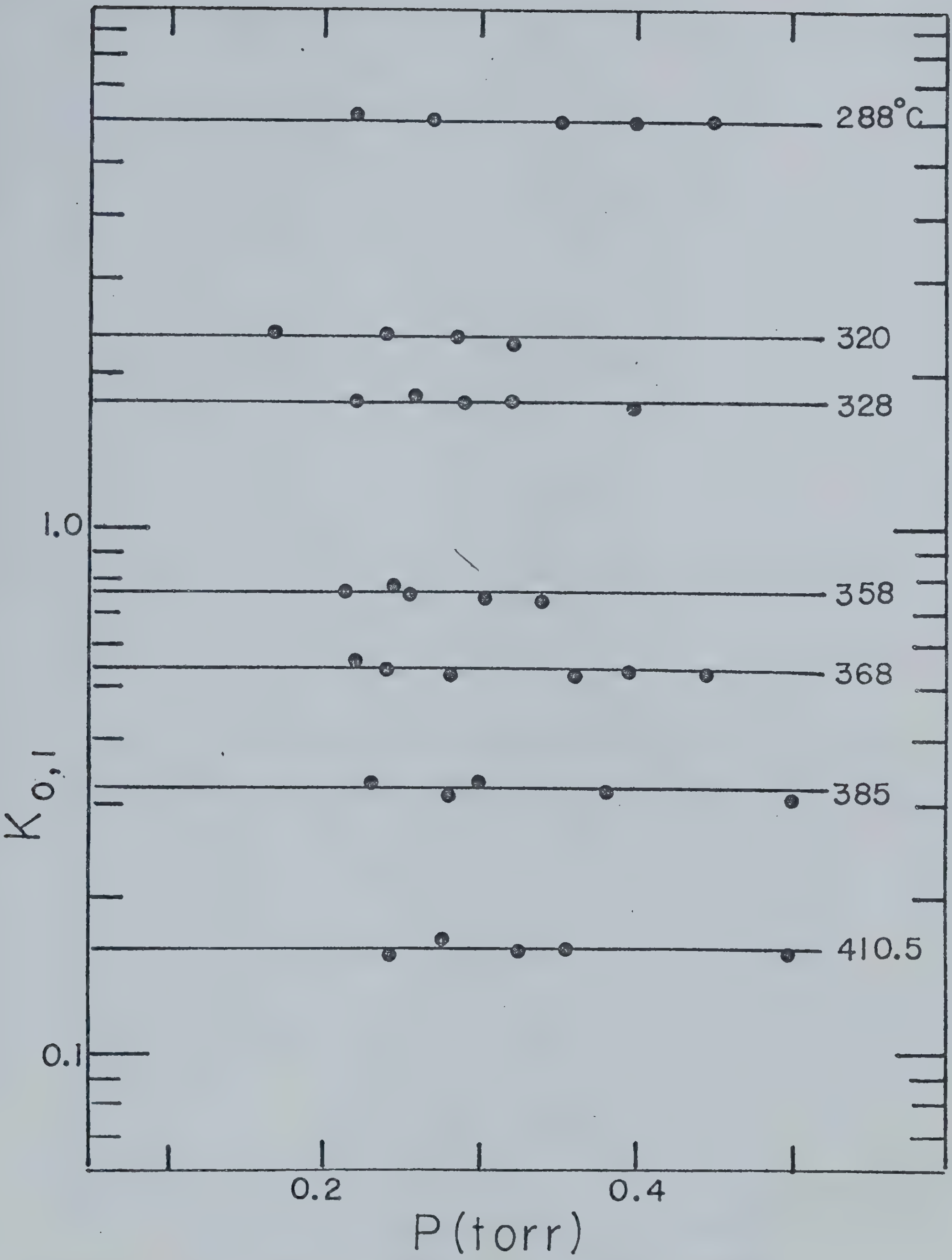

FIGURE 80 Equilibrium Constants versus Pressure at Various Temperatures for the Reaction:

$$K^+ + \text{aniline} = K^+(\text{aniline}) .$$

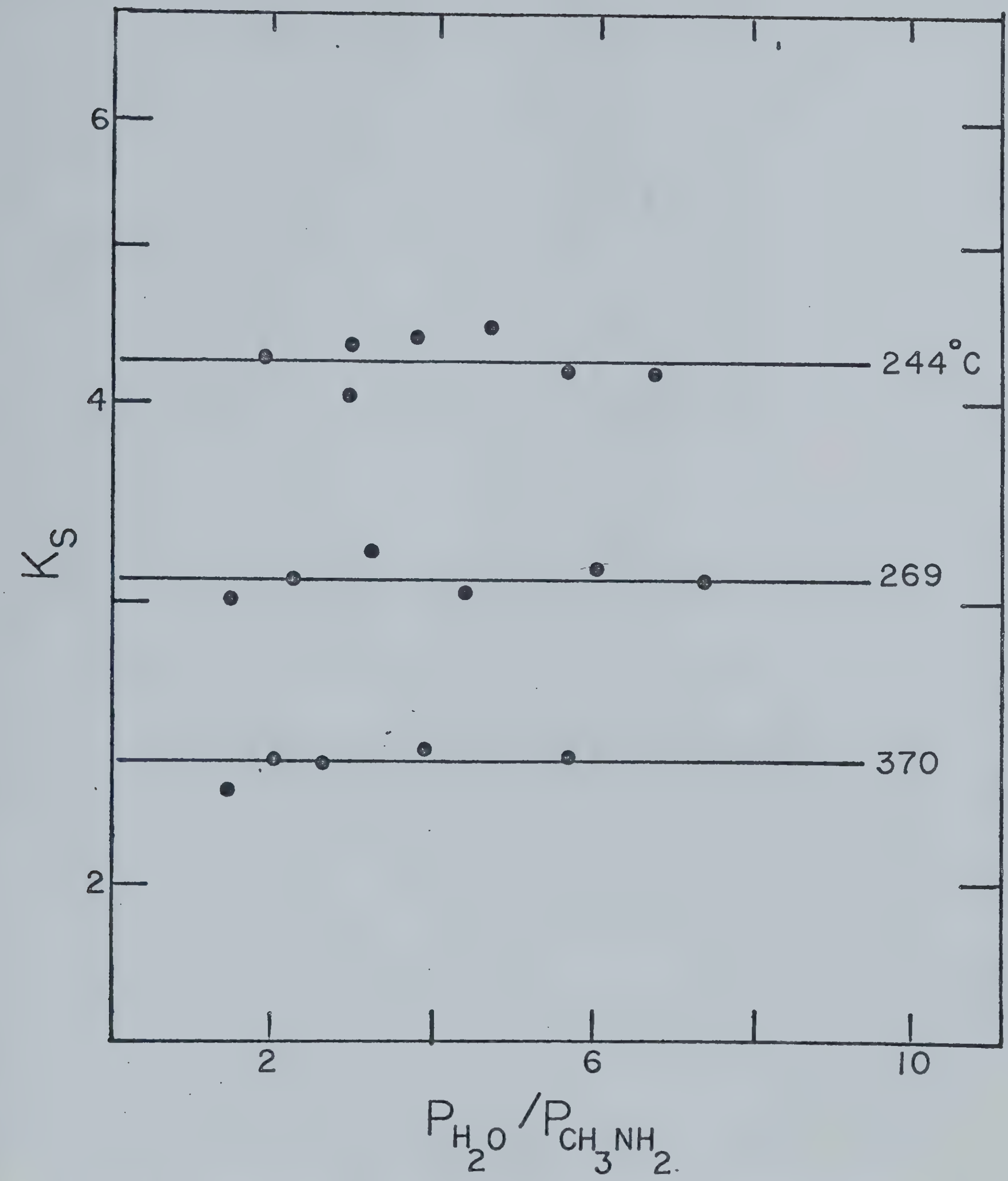

FIGURE 81 Switching Equilibrium Constants versus Pressure Ratio at Representative Temperatures for the Reaction:

$K^+(H_2O) + CH_3NH_2 = K^+(CH_3NH_2) + H_2O$ .

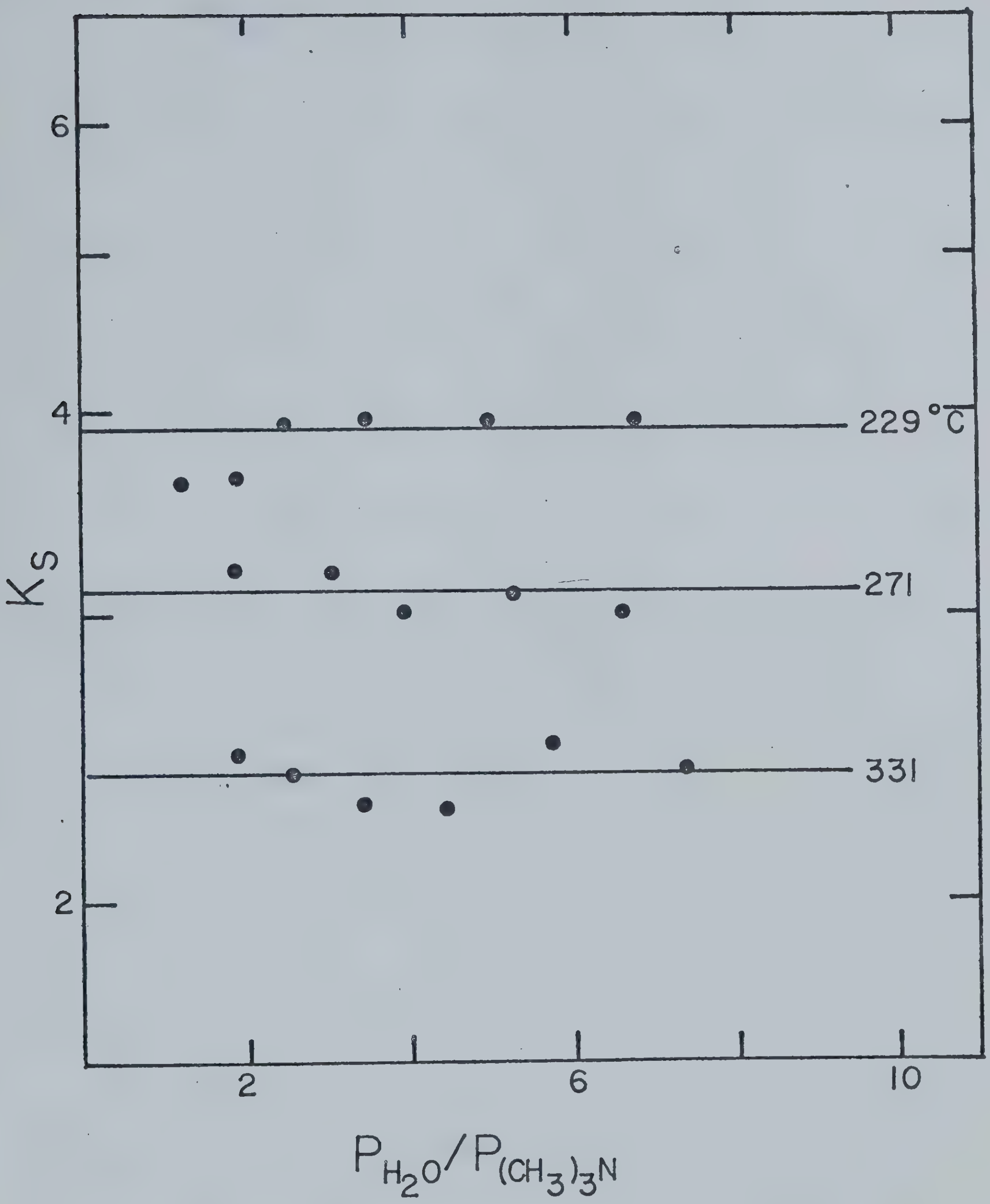

FIGURE 82 Switching Equilibrium Constants versus Pressure Ratio at Representative Temperatures for the Reaction:

$$K^+(H_2O) + (CH_3)_3N = K^+((CH_3)_3N) + H_2O \; .$$

$$K^+(H_2O) + (CH_3)_3N \rightleftarrows K^+[(CH_3)_3N] + H_2O \qquad 5.11$$

is similarly plotted at representative temperature values over the range of temperatures studied.

The switching equilibrium constants can then be plotted as a function of 1/T to determine the thermodynamic values $\Delta H^o{}_s$, $\Delta G^o{}_s$ and $\Delta S^o{}_s$ from a Van't Hoff type plot (Figure 83). By using the thermodynamic functions for the reaction:

$$K^+ + H_2O \rightleftarrows K^+(H_2O) \qquad 5.12$$

the thermodynamic values for Reaction 5.1 for monomethyl- and trimethylamine are thus determined by simple addition:

$$\Delta f^o{}_{amine} = \Delta f^o{}_S + \Delta f^o{}_{H_2O} \qquad 5.13$$

where $\Delta f$ represents any thermodynamic function: $\Delta G$, $\Delta H$, or $\Delta S$. The values for the water-potassium ion reaction are $\Delta H^o = -16.9$ kcal/mole, $\Delta S^o = -19.9$ e.u. and $\Delta G^o = -11.0$ kcal/mole.

The Van't Hoff type plots for Reaction 5.1 for ammonia, monomethylamine, n-propylamine, aniline and pyridine are shown in Figure 84 and similar plots for ammonia and the methylamines are shown in Figure 85. The thermodynamic functions derived from the plots are tabulated in Table 28.

To demonstrate that the Van't Hoff plots obtained by the switching reaction are reasonable, three points (open

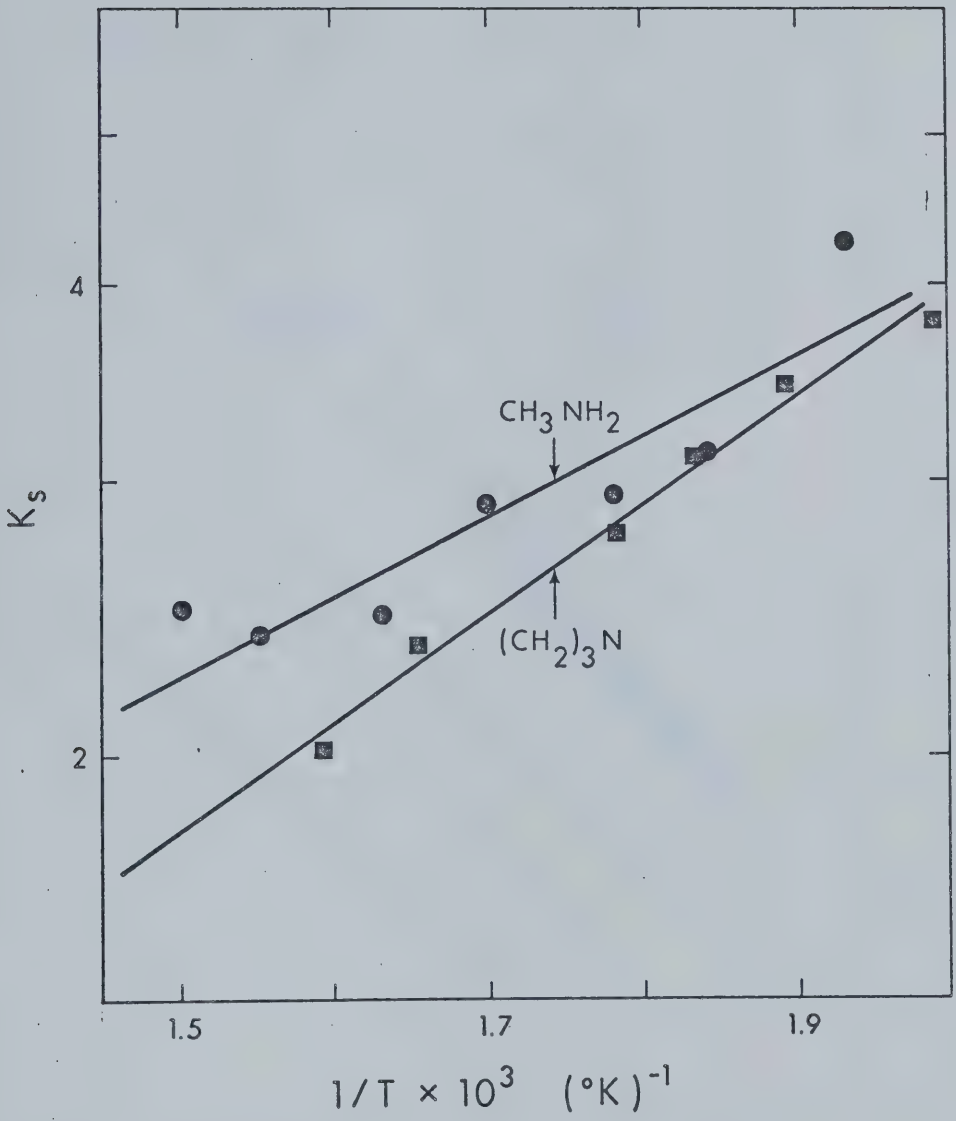

FIGURE 83 Van't Hoff Type Plots of Switching Equilibrium for the Reactions:

$$K^+(H_2O) + B = K^+B + H_2O \ .$$

B = $CH_3NH_2$ and $(CH_3)N$ .

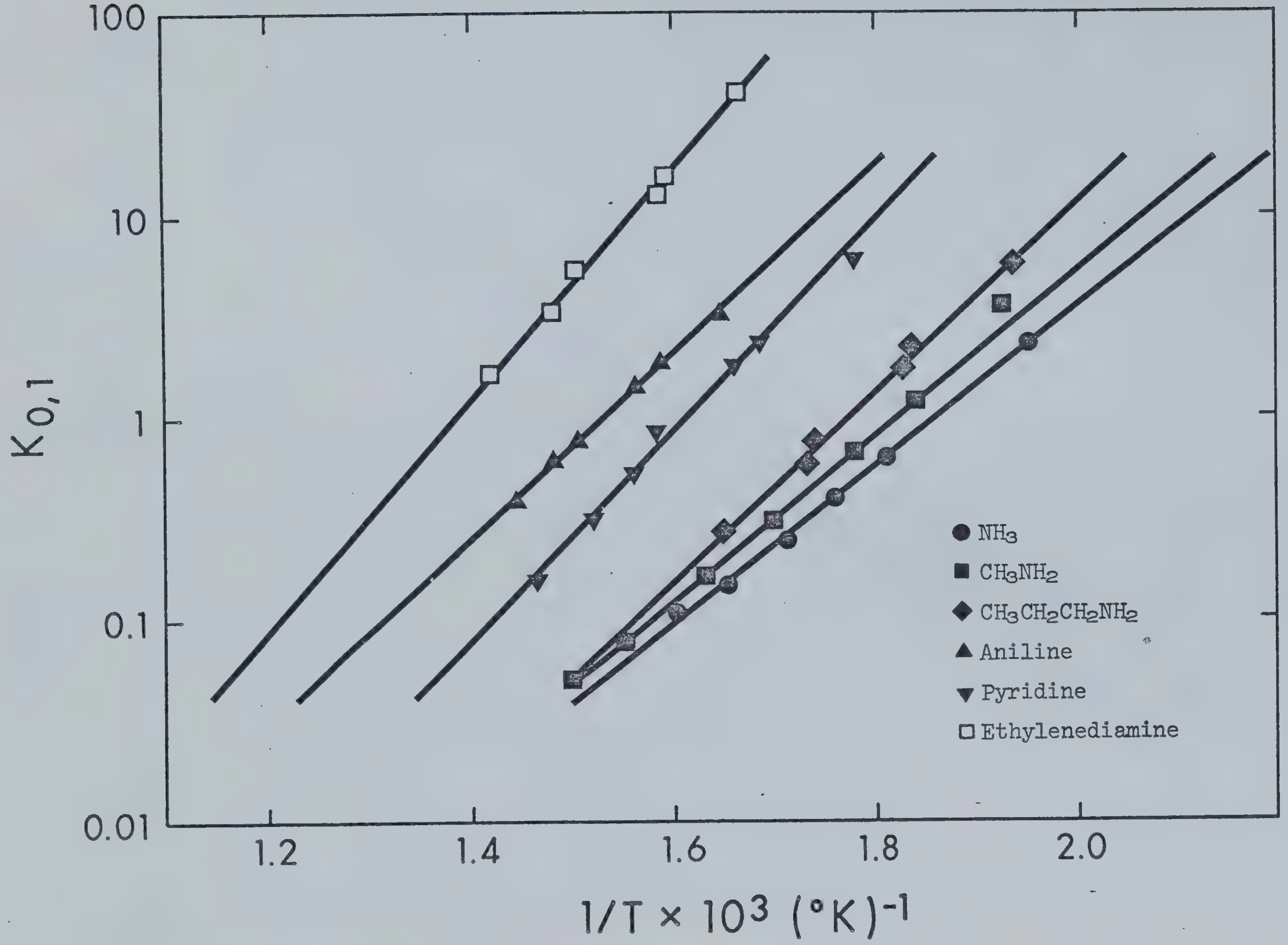

FIGURE 84 Van't Hoff Type Plots for Various Amines Reacting with the Potassium Ion.

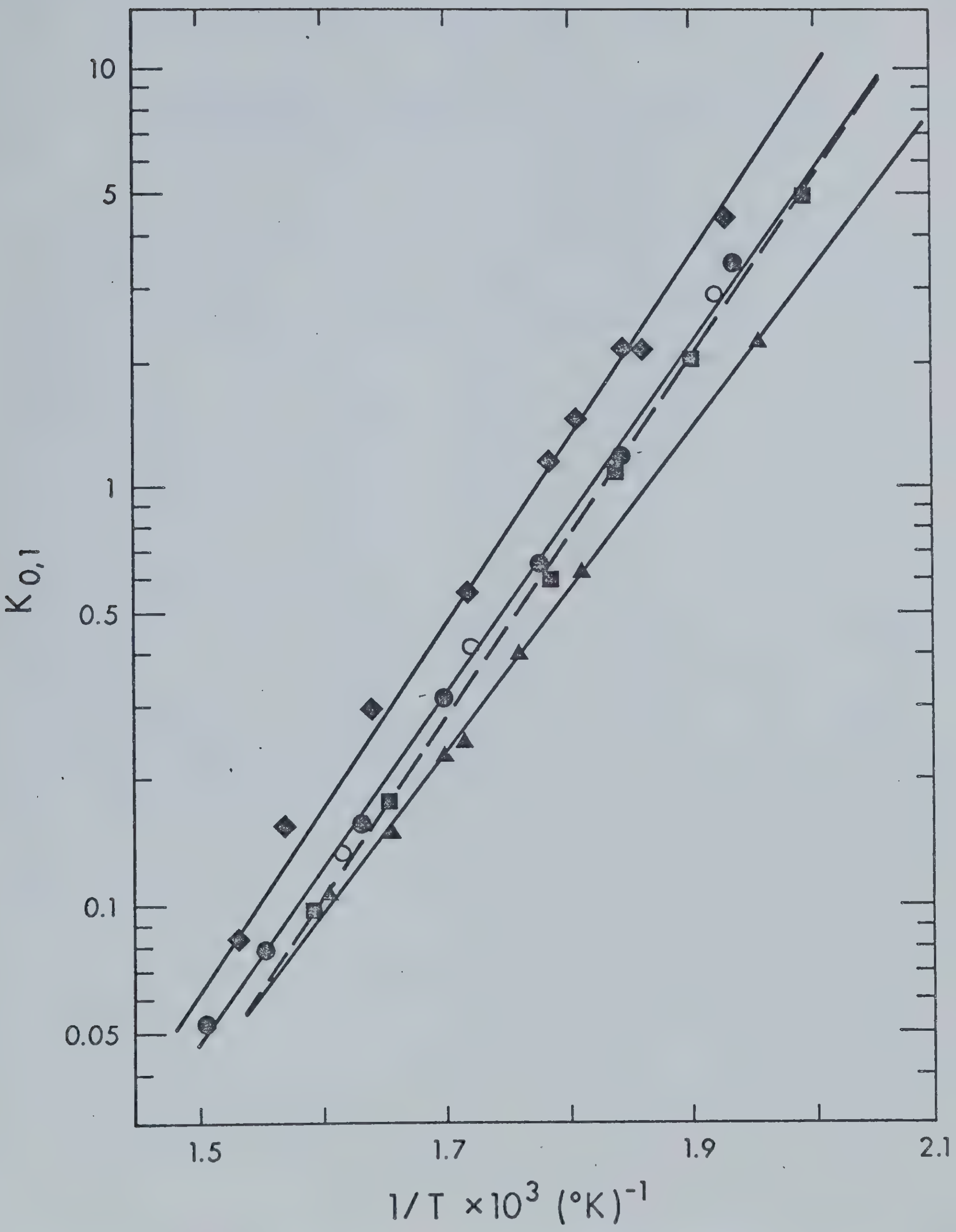

FIGURE 85 Van't Hoff Type Plots for the Methyl Amines Reacting with the Potassium Ion.

▲ $NH_3$

● $CH_3NH_2$

◆ $(CH_3)_2NH$

■ $(CH_3)_3N$

○ Methylamine from normal clustering reactions.

# TABLE 28

Thermodynamic Functions for the Reactions:

$K^+ + \text{Amine} \rightleftarrows K^+(\text{Amine})$

| Amine | $-\Delta H^o$ | $-\Delta S^o$ [a] | $-\Delta G^o_{298}$ [a] | $-\Delta G^o_{600}$ [a] |
|---|---|---|---|---|
| Ammonia | 17.8 | 20.0 | 11.8 | 5.79 |
| Methylamine | 19.1 | 21.8 | 12.7 | 6.16 |
| Dimethylamine | 19.5 | 21.4 | 13.1 | 6.65 |
| Trimethylamine | 20.0 | 23.4 | 13.0 | 5.96 |
| n-Propylamine | 21.8 | 25.5 | 14.2 | 6.47 |
| Aniline | 22.8 | 23.7 | 15.8 | 8.60 |
| Pyridine | 20.7 | 18.6 | 15.2 | 9.56 |
| Ethylendiamine | 25.7 | 22.3 | 19.04 | 12.31 |

[a] SS = 1 atm.

circles) determined for the reaction:

$$K^+ + CH_3NH_2 \rightleftarrows K^+(CH_3NH_2) \qquad 5.14$$

are included in Figure 85. Although these points are suspect since they were determined under the adverse conditions described in Section 5.2, they fall close enough to the Van't Hoff plot obtained by the switching reaction to rule out any serious errors which might occur by using the ligand interchange or switching method.

## 5.4 Basicity Scales

When comparing the results of gas phase amine basicity with the potassium ion as a reference acid to the basicity when the proton or trimethylboron are the Lewis acids, it is best to use both the enthalpy data and the standard free energy at 298° K. The free energy comparison takes into account the entropy, which in the case of the proton is similar for all the amines, but with $K^+$ or $B(CH_3)_3$ there are considerable entropy differences between the amines.

In Table 29 the experimentally determined $\Delta H$'s and $\Delta G$'s for the reactions:

$$A + :B \rightleftarrows A:B \qquad 5.15$$

where A represents the reference acid, are presented. The data for the proton reactions are from Yamdagni and Kebarle

## TABLE 29

A Comparison of Thermodynamic Properties of the Gas Phase Reactions:

$A + :B \rightleftarrows A:B$

| A | $K^{+}$ [b] | | $H^{+}$ [c] | | $B(CH_3)_3$ [d] | |
|---|---|---|---|---|---|---|
| B | $-\Delta H^{o}$ | $-\Delta G^{o}_{298}$ | $-\Delta H^{o}$ [f] | $-\Delta G^{o}_{298}$ | $-\Delta H^{o}$ | $-\Delta G^{o}_{298}$ |
| $NH_3$ | 17.9 | 11.8 | 207 | 198 | 13.75 | 1.86 |
| $CH_3NH_2$ | 19.1 | 12.7 | 217.8 | 208.8 | 17.14 | 5.54 |
| $(CH_3)_2NH$ | 19.5 | 13.1 | 225.3 | 216.3 | 19.26 | 6.27 |
| $(CH_3)_3N$ | 20.0 | 13.0 | 230.3 | 221.3 | 17.62 | 4.00 |
| $CH_3CH_2CH_2NH_2$ | 21.8 | 14.2 | 222.7[e] | 213.7[e] | 18.14 | 5.33 |
| $NH_2CH_2CH_2NH_2$ | 25.7 | 19.0 | 234.9 | 222.1 | | |
| Pyridine | 20.7 | 15.2 | 225.6 | 216.6 | 17.0 | 4.13 |
| Aniline | 22.8 | 15.8 | 215.9 | 206.9 | | |

[a] In kcal/mole

[b] This work

[c] Reference 57, except where noted

[d] References 67 - 71

[e] Reference 65

[f] Assuming negligible proton transfer entropy except for ethylenediamine

(57) or Aue, Webb, and Bowers (65), and the trimethyl boron data are from Brown (67 - 71).

In the following sections reference will often be made to this Table in order to explain differences in the basicity orders with the various reference Lewis acids.

## 5.5 Discussion of Gas Phase Amine Basicity Order with Potassium Ion as a Reference Acid

From Table 28, it can be seen that the relative order of free energies of the various amines differs at 298° K and in the middle of the experimental range, 600°K. Similarly, the enthalpy order differs from the free energy order. The question then arises, which is the best thermodynamic value to use as an order of basicity. With the proton as a reference acid, this problem does not arise, since the entropy of proton transfer is very low or negligible. However, with potassium this is not the case, and there are distinct differences in the entropy of the various reactions.

Without a doubt the most accurate thermodynamic value is the free energy of the reaction in the experimental range, since no extrapolation is necessary. Thus at 600° K, the order of basicity of the amines studied is:

$$NH_3 < (CH_3)_3N < CH_3NH_2 < CH_3CH_2CH_2NH_2 < (CH_3)_2NH$$

$$< C_6H_5NH_2 < C_5H_5N < NH_2CH_2CH_2NH_2$$

It would be advantageous to break this discussion down to the various groups: methyl amines, primary aliphatic amines, aromatic amines, and bidentate amines.

A Methyl Amines

The free energy of reaction 5.1 at 600° K increases in an anomolous order with methyl substitution:

$$NH_3 < (CH_3)_3N < CH_3NH_3 < (CH_3)_2NH$$

This is in agreement with the order determined by Brown (67) using the bulky $B(CH_3)_3$ as a reference Lewis acid. The enthalpies of the reaction, however, increase steadily with methyl substitution:

$$NH_3 < CH_3NH_2 < (CH_3)_2NH < (CH_3)_3N$$

which is in agreement with the gas phase proton affinities of methyl amines. The major difference in the two orders must be attributed to the unfavourable entropy of the reaction:

$$K^+ + (CH_3)_3N \rightleftarrows K^+ [(CH_3)_3N]$$

Pople has done theoretical calculations of the Mulliken electron populations of the various atoms in ammonia and the methyl amines (110). These are shown in Figure 86. Unlike other bases, the gas phase Bronsted basicity increases with

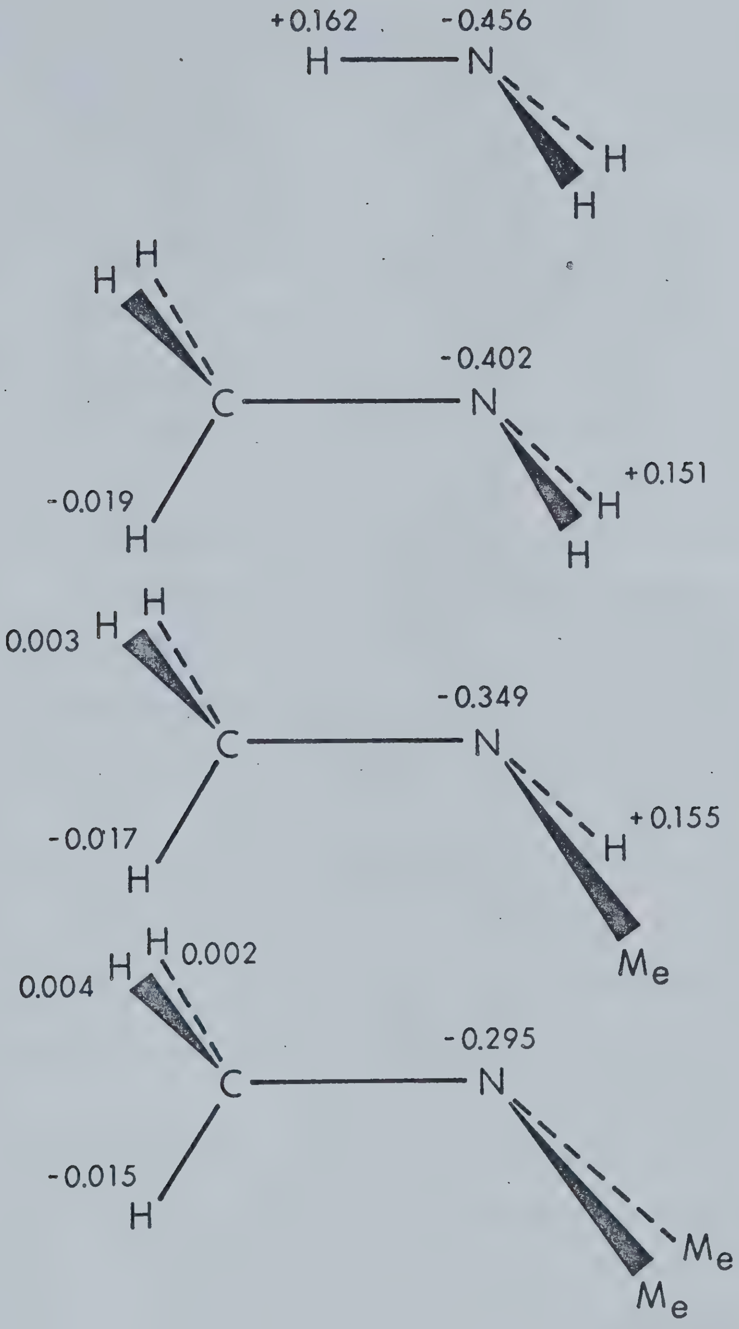
+0.162
-0.456
H
N
H
H
H
H
-0.402
C
N
-0.019
H
+0.151
H
H
0.003
H
H
-0.349
C
N
-0.017
H
+0.155
H
Me
0.004
H
H
0.002
-0.295
C
N
-0.015
H
Me
Me

FIGURE 86 Net Electron Populations on the Various Atoms in the Methyl Amines from Pople (reference 110).

a decrease in the electron population of the donor atom (i.e. nitrogen). With oxygen as the donor, methyl substitution increases the electron population of the oxygen atom (110), as well as the basicity.

Using a simple electrostatic model as was done in Chapter 4 and "normalizing" the electron populations to fit dipole moments, it is possible to predict a classical order of interaction energy which should correspond to the enthalpy order.

Due to the lack of knowledge of C--N bond polarizabilities, a simplified atom polarizability approach is necessary to determine the ion-induced dipole energies. The mean atom polarizabilities can be determined from the total molecular polarizabilities of the methyl amines, i.e.:

$$\alpha_{\text{amine}} = \sum_i \bar{\alpha}_i \qquad 5.16$$

where $\bar{\alpha}_i$ represents the mean atom polarizabilities. The molecular and resulting atom polarizabilities are listed in Table 30.

For the dispersion energy equation, i.e., the London formula, the radius $R_0$ was taken as the distance between the geometric centre of the amine and the centre of the ion.

The total repulsion energy must include hydrogen atom-ion terms as well as carbon atom-ion terms. As was done in Chapter 4, the carbon potential was assumed similar to the nitrogen atom potential.

## TABLE 30

### Atomic and Molecular Polarizabilities and Ionization Potentials of the Methyl Amines

| Amine | Ionization Potentials (ev)[a] | Polarizability ($A^{o3}$)[b] |
|---|---|---|
| $NH_3$ | 10.15 | 2.34 |
| $CH_3NH_2$ | 9.41 | 4.18 |
| $(CH_3)_2NH$ | 8.93 | 5.92 |
| $(CH_3)_3N$ | 7.82 | 7.92 |

| Mean Atomic Polarizabilities[c] ($A^{o3}$) | |
|---|---|
| N | 0.98 |
| C | 1.00 |
| H | 0.44 |

[a] Reference 131

[b] Reference 132

[c] from molecular polarizabilities

The total energy, $E_t$, is then:

$$E_t = E_{dip} + E_{ind} + E_{dis} + E_{rep} \qquad 5.17$$

where

$$E_{dip} = 334 \sum_i Q_i/R_i \qquad 5.18$$

$$E_{ind} = -167 \sum_i \bar{\alpha}_i/R_i^4 \qquad 5.19$$

$$E_{dis} = -34.56 \frac{I_A I_{K^+}}{I_A + I_{K^+}} \frac{\alpha_A \alpha_{K^+}}{R_0^6} \qquad 5.20$$

$$E_{rep} = \sum_i C_{K^+-i} \exp(-a_{K^+-i} R_i) \qquad 5.21$$

where $Q_i$ is the charge on the atom, $R_i$ is the atom-ion distance, $\alpha_A$ is the molecular polarizability of the amine, $\alpha_{K^+}$ is the potassium ion polarizability, $\bar{\alpha}_i$ is the mean polarizability of the atom, $I_A$ and $I_{K^+}$ are the ionization potentials of the amine and the potassium ion respectively, $C_{K^+-i}$ and $a_{K^+-i}$ are the atom-potassium ion repulsion potential parameters described in Chapter 4. As was done in the previous chapter for the electrostatic calculations, the ionization potentials of the amines and the potassium ion were "corrected" by multiplying $I_A$ by 2.5 and $I_{K^+}$ by 2.25 (101). The new values of the ionization potentials were then substituted into the dispersion equation.

The coordinates of the various atoms in the amines were

determined from the bond lengths and angles (133-5). These are listed in Table 31 for trimethylamine and ammonia. Monomethylamine and dimethylamine coordinates were determined by replacement of the hydrogens of ammonia by methyl groups. From these coordinates the ion-atom distances, $R_i$, could easily be obtained.

From the resulting interaction potential energies (Table 32), it can be seen that the ion-dipole term is substantially larger for ammonia than for the other amines. However, the ion-induced dipole and dispersion terms increase with methyl substitution, which results in trimethylamine being the most stable of the methyl amines in its interaction with the reference acid, $K^+$.

The electrostatic calculations correctly predict the order of the interaction of the amine with the reference acid, but the relative differences between amines are quite different from the experimental enthalpies of the reaction.

These calculations demonstrate that in addition to the electron density on the donor atom, polarizability and dispersion forces are important in determining the basicity order of amines.

## B Primary Aliphatic Amines

Only two primary aliphatic amines were studied: monomethylamine and n-propylamine. Ethylamine was attempted but due to thermal decomposition and the high efficiency of the reaction:

## TABLE 31

## Coordinates[a] for the Atoms in Trimethylamine and Ammonia

| Trimethylamine[b] | | | |
|---|---|---|---|
| Atom | x | y | z |
| N | 0 | 0 | 0 |
| $C_1$ | 0 | 1.36 | 0.52 |
| $H_1$ (trans) | 0 | 1.15 | 1.58 |
| $H_{11}$ | 0.88 | 1.97 | 0.42 |
| $H_{12}$ | -0.88 | 1.97 | 0.42 |
| $C_2$ | 1.18 | -0.68 | 0.52 |
| $H_2$ (trans) | 0.995 | -5.75 | 1.58 |
| $H_{21}$ | 1.28 | -1.74 | 0.42 |
| $H_{22}$ | 2.15 | -0.13 | 0.42 |
| $C_3$ | -1.18 | -0.68 | 0.52 |
| $H_3$ (trans) | -0.995 | -5.75 | 1.58 |
| $H_{31}$ | -2.15 | -0.13 | 0.42 |
| $H_{32}$ | -1.28 | -1.74 | 0.42 |

## TABLE 31 (Continued)

| Ammonia[c] | | | |
|---|---|---|---|
| Atom | x | y | z |
| N | 0 | 0 | 0 |
| $H_1$ | 0 | 0.94 | 0.385 |
| $H_2$ | 0.81 | -0.47 | 0.385 |
| $H_3$ | -0.81 | -0.47 | 0.385 |

[a] in angstroms

[b] Reference 135

[c] Reference 133

## TABLE 32

## Calculated Electrostatic Potentials[a] for the Reactions:

$K^+ + \text{Amine} \rightleftarrows K^+(\text{Amine})$

|  | $R_{K^+ -- N}$[b] | $-E_{dip}$ | $-E_{ind}$ | $-E_{dis}$ | $E_{rep}$ | $-E_T$ | $-\Delta H$ Experimental |
|---|---|---|---|---|---|---|---|
| $NH_3$ | 2.58 | 17.48 | 6.05 | 2.97 | 8.98 | 17.53 | 17.9 |
| $CH_3NH_2$ | 2.52 | 16.06 | 8.16 | 5.23 | 11.19 | 18.26 | 19.0 |
| $(CH_3)_2NH$ | 2.46 | 15.96 | 10.51 | 7.56 | 13.90 | 20.12 | 19.5 |
| $(CH_3)_3N$ | 2.43 | 16.08 | 12.62 | 8.90 | 15.68 | 21.89 | 20.0 |

[a] In kcal/mole

[b] Potassium-nitrogen distance in angstroms

$$K^+(CH_3CH_2NH_2) + CH_3CN \rightleftharpoons K^+(CH_3CN) + CH_3CH_2NH_2 \qquad 5.22$$

the intensity of the $K^+$-ethylamine ion was too small to measure accurately.

From the two primary amines studied, it appears evident that increased chain length favours the stability of the potassium ion-amine complex. Both the enthalpies and free energies at 600° agree with this finding. At higher temperatures though, it is possible that the more unfavourable entropy of the propylamine complex will make it less stable.

With trimethyl boron as a reference acid, the same result occurs; that is, the enthalpy of the complexing of $B(CH_3)_3$ with propylamine is more favourable than with monomethylamine (69). The proton affinity of primary amines is also known to increase with an increase in alkyl chain length (65).

## C Ethylenediamine-bidentate Ligands

This subject is covered extensively in the next chapter. It is obvious that the two nitrogen electron donors make the ethylenediamine-potassium ion complex much more stable than monodentate amine-potassium ion complexes.

## D Aromatic Amines

In the complexing of aromatic amines, the greatest differences between the potassium ion and the other gas phase reference Lewis acids, the proton and trimethyl

boron, emerge.

(i) Pyridine

The unshared electron pair on the nitrogen in pyridine is present in an $sp^2$ orbital in the plane of the aromatic ring. Because of this orientation, these electrons cannot be delocalized by interaction with the aromatic $\pi$ electrons. The $\pi$ electron density is greater at the nitrogen than at the carbon atoms. Therefore, it is reasonable to expect that the total electron density ($\pi + \sigma$) at the nitrogen should make pyridine at least as strong a base as the methylamines (136).

In solution this is not the case ($K_b$(pyridine) = $1.71 \times 10^{-9}$; $K_b$(methylamine) = $4.38 \times 10^{-4}$) (96). Wheland (137) has suggested that this is due to the increased electronegativity of the nitrogen in pyridine. An increase in electronegativity would mean that the electrons on the nitrogen would be less available for donation to the electrophilic acid. This increase is brought about because atoms joined in multiple linkages supposedly have greater electronegativity. Another way of looking at it is that a nitrogen in an $sp^2$ configuration will have a higher electronegativity than one in an $sp^3$ configuration. The same argument was used in the discussion of the dipole moment of the C—C bond in acetonitrile (page 176).

In the gas phase, pyridine has approximately the same proton affinity as dimethylamine. However, if compared

to a secondary amine of approximately the same polarizability such as piperidine, pyridine is considerably less basic (by 5 kcal). Thus it appears with respect to the proton as a reference acid that in solution the low basicity is a combination of solution effects as well as the high nitrogen electronegativity.

The present study demonstrates that pyridine is a stronger base than all the methylamines. The reason for this difference from the gas phase proton affinities is not obvious. The $-\Delta S$ of the potassium ion-pyridine clustering reaction is quite low (Table 28), indicating a smaller loss of freedom in the formation of the cluster than is normal. Whether this is due to a greater freedom for rotation about the $K^+$-N bond since pyridine is planar, or whether this is due to some statistical factor based on interaction with the electrons in the aromatic ring is difficult to say from this work. However, it has been suggested (136) that the ion-molecule bond most likely occurs through the nitrogen lone pair. Further study on pyridine and its derivatives (such as 2,6-dialkyl pyridines) would help provide information on bonding sites. If the lone pair is involved in the ion molecule bond, then the addition of bulky alkyl groups should sterically affect the clustering reaction.

### (ii) Aniline

In solution aniline is a much poorer base than monomethyl amine. Pauling (95) has suggested that this is due to the delocalization of the unshared electron pair on the nitrogen through the various resonance structures:

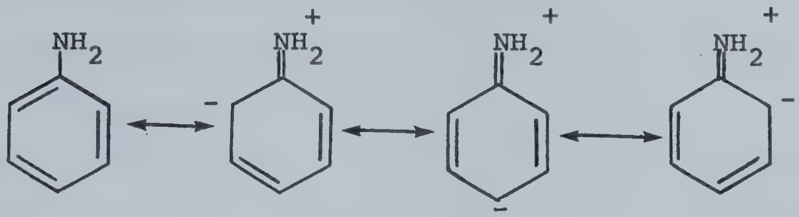

as well as the stability of the unionized molecule over the phenylammonium ion which has no similar resonance structures. In the gas phase the proton affinity of aniline is ~2 kcal/mole lower than methylamine, which would be expected from the above hypothesis.

The potassium ion reactions would at first be expected to show the same result. However, the enthalpy and free energies of the $K^+$-aniline reaction are considerably greater than the corresponding $K^+$-methylamine reaction. The following theory could explain this difference.

In quantum mechanical calculations (138), Pople has shown that the N--C bond in aniline has some double bond character. Furthermore, the Mulliken electron density calculations demonstrate that there is $\pi$-charge donation from the nitrogen to the ring as well as $\sigma$-charge withdrawal from the ring to the nitrogen atom. The resulting dipole moment may be represented as:

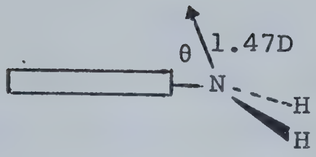

where the angle θ has the value 43° experimentally (139) or 67° when determined theoretically (132).

The potassium ion will most likely lie on the axis of the resulting dipole vector and thus be oriented towards the ring. In arene-silver coordination compounds (140), the major type of bonding is a σ-type bond involving the π-electrons of the carbons and the empty 5s orbital of the silver ion (141):

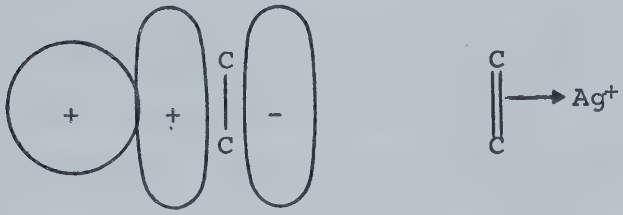

This could occur with the 4s orbital of the potassium ion as well. Thus in the case of aniline-$K^+$, the complex could be stabilized by interaction with the ring as well as with the donor atom, nitrogen. Not only is the higher relative enthalpy (i.e. more negative) of the reaction:

$$K^+ + C_6H_5NH_2 \rightleftarrows K^+(C_6H_5NH_2) \qquad 5.23$$

over the corresponding methylamine reaction predicted but also the more unfavourable entropy due to the greater

restriction of the potassium ion. Due to the small size of the proton, such an interaction with the ring would probably not occur and there would be no stabilization of the complex.

## 5.6 Correlation of Gas Phase Lewis Acid-Amine Reactions

It would be advantageous to be able to correlate the gas phase Lewis acid-base interactions. Drago (142, 143) has suggested the use of a four paramater equation (Equation 5.24) to predict the enthalpy of such interactions:

$$E_AE_B + C_AC_B = -\Delta H \qquad 5.24$$

$E_A$ and $E_B$ were originally interpreted as the susceptibility of the acid and base, respectively, to undergo electrostatic interactions, and $C_A$ and $C_B$ as the susceptibility of the acid and base to form covalent bonds. The equation may also be rewritten in matrix notation by assigning the acid parameters to a vector $X_A$ and the base parameters to a vector $Y_A$:

$$X_A = \begin{bmatrix} E_A \\ C_A \end{bmatrix} \quad \text{and} \quad Y_B = \begin{bmatrix} E_B \\ C_B \end{bmatrix}$$

The enthalpy will then be a scalar function of the vector:

$$-\Delta H = Y_B{}^T X_A = [E_BC_B] \begin{bmatrix} E_A \\ C_A \end{bmatrix} = E_BE_A + C_BC_A \qquad 5.25$$

Equations 5.24 and 5.25 have an infinite number of solutions for each of the parameters.

Drago has taken enthalpy data for 280 Lewis acid-base reactions and obtained a "best-fit" solution for the parameters $E_B$, $E_A$, $C_B$, and $C_A$ for 43 bases and 31 acids (143). In order to do this, the values $E_A = 1.0$ and $C_A = 1.0$ were arbitrarily assigned to iodine, and the parameters $E_B = b \times \mu$ and $C_B = a \times R_D$ (where $\mu$ is the ground state dipole moment, $R_D$ is the total distortion polarizability of the amine, and a and b are proportionality constants) for the series of ammonia and the methyl amines. Then by studying the iodine-amine enthalpies, the proportionality terms a and b were determined and initial values of $E_B$ and $C_B$ were then obtained. These values could then be used to determine parameters of another acid and so on. The best fit solution was then obtained by a least square method through the variation of the various E and C parameters, always maintaining iodine's $E_A = C_A = 1.0$.

This is a very empirical approach, but it does have predictive power. However, most of the enthalpies used by Drago were determined in weakly solvating media (cyclohexane or carbon tetrachloride) and not in the gas phase. Arhland (144) has pointed out that solution effects are important even in weakly solvating liquids. This is further shown by Drago's values for boron trifluoride. In the gas phase, completely different values are obtained for $E_A$ and $C_A$ than in solution. As predicted by Arhland, the E/C ratio is

higher in the gas phase than in solution. In solution acetonitrile has much lower parameters than ammonia. But gas phase reactions involving the potassium ion show acetonitrile to react more strongly than ammonia. Thus gas phase interactions cannot be readily predicted with the use of solution enthalpies. Perhaps it would be better to use a six-parameter equation in which solution effects, $S_A$ and $S_B$, are included:

$$E_AE_B + C_AC_B + S_AS_B = -\Delta H \qquad 5.26$$

With the available gas phase acid-base reactions, it is then possible, using a similar method to Drago's to determine values for the Lewis acid-base parameters: $E_A$, $E_B$, $C_A$ and $C_B$.

### Method I

The potassium ion is chosen as a reference gas phase acid. Considering Pearson's softness parameter (145) of potassium (0.238) as somewhat equivalent to the ratio C/E (144), the parameters $E_A$ and $C_A$ can be set equal to 4.0 and 1.0 respectively. In the same manner as used by Drago, the electrostatic portion of the methyl amines can be set proportional to their dipole moment and the covalent portion can be set proportional to the total distortion polarization of the amine. Thus:

$$E_{K^+}E_B + C_{K^+}C_B = -\Delta H(K\ \text{-amine})$$

or

$$4b\mu_{\text{amine}} + aR_{D_{\text{amine}}} = -\Delta H(K^+\text{-amine}) \qquad 5.27$$

The dipole moments, total polarization and experimental enthalpies for the potassium ion-methyl amine reactions are listed in Table 33. The following equations result:

$$(4 \times b \times 1.45) + (a \times 5.9) = 17.8$$

$$(4 \times b \times 1.28) + (a \times 10.58) = 19.1$$

$$(4 \times b \times 1.02) + (a \times 14.96) = 19.5$$

$$(4 \times b \times 0.64) + (a \times 20.01) = 20.0$$

These equations are then mutually solved for a and b in a least squares manner. The best values of a and b are thus obtained: $a = 0.672$ and $b = 2.375$. The observed and calculated enthalpies are compared in Table 34 along with the values of $E_B$ and $C_B$ for the methyl amines.

The E and C parameters are then determined for the proton and for trimethylboron in a least squares best fit manner, using the amine parameters and the experimental proton affinities of the amines and ΔH values for the boron

## TABLE 33

## Dipole Moments and Total Polarization of Methyl Amines and Experimental Enthalpies for the Reaction:

$$K^+ + :B \rightleftarrows K^+:B$$

| Amine | Dipole Moment[a] (Debyes) | Total Distortion Polarization[b] (cc/mole) | -ΔH for Potassium Ion-Amine Reaction[c] (kcal/mole) |
|---|---|---|---|
| $NH_3$ | 1.45 | 5.90 | 17.8 |
| $CH_3NH_2$ | 1.28 | 10.58 | 19.1 |
| $(CH_3)_2NH$ | 1.02 | 14.96 | 19.5 |
| $(CH_3)_3N$ | 0.64 | 20.01 | 20.0 |

[a] Reference 109

[b] Reference 132

[c] This work

## TABLE 34

### Calculated and Experimental Enthalpies for Potassium Adducts with Methyl Amines

| Amine | $E_B$ | $C_B$ | $-\Delta H$ Calc.[a] | $-\Delta H$ Exp.[a] |
|---|---|---|---|---|
| $NH_3$ | 3.44 | 3.96 | 17.7 | 17.8 |
| $CH_3NH_2$ | 3.04 | 7.11 | 19.3 | 19.1 |
| $(CH_3)_2NH$ | 2.42 | 10.05 | 19.7 | 19.5 |
| $(CH_3)_3N$ | 1.52 | 13.45 | 19.5 | 20.0 |

[a] in units of kcal/mole

-amine complexes. The only other base whose enthalpy of complex formation has been studied with the three reference acids is pyridine. Its parameters are then determined from the acid E and C parameters.

All the parameters are then put in a computer program and redetermined until a "best-fit" solution is obtained, at all times keeping the potassium ion's $E_A = 4.0$ and $C_A = 1.0$. The final E and C values for the acids and bases are listed in Table 35. The only major change from the initial values in Table 34 is in trimethylamine. This anomaly is likely due to steric effects (142) which are in some manner incorporated into the E and C parameters. The enthalpies calculated from Equation 5.1 are compared with experimental values in Table 36. In all cases, the calculated enthalpies are within 2.5% of the experimental values.

### Method II

The values of $E_B$ and $C_B$ for the amines are originally taken as those determined by Drago (Table 37). From these in a best fit manner, $E_A$ and $C_A$ values are obtained for the acids: $K^+$, $H^+$, and $B(CH_3)_3$. The base parameters are then altered as in Method I until a best fit solution is determined. The resulting final parameters and calculated enthalpies are shown in Table 37 and Table 38 respectively.

The ratio C/E has been used to depict the relative softness or hardness of an acid or base by Klopman (146).

## TABLE 35

### Best Fit Gas Phase E and C Parameters

Acids

| Lewis Acid | $E_A$ | | $C_A$ | | $C_A/E_A$ |
|---|---|---|---|---|---|
| $K^+$ | 4.0 | | 1.0 | | 0.25 |
| $H^+$ | 46.73 | 0.07 | 10.77 | 0.04 | 0.231 |
| $B(CH_3)_3$ | 2.21 | 0.01 | 1.56 | 0.01 | 0.706 |

Bases

| | $E_B$ | | $C_B$ | | $C_B/E_B$ |
|---|---|---|---|---|---|
| $NH_3$ | 3.53 | 0.01 | 3.82 | 0.02 | 1.08 |
| $CH_3NH_2$ | 3.03 | 0.01 | 7.03 | 0.01 | 2.31 |
| $(CH_3)_2NH$ | 2.86 | 0.01 | 8.29 | 0.04 | 2.89 |
| $(CH_3)_3N$ | 3.41 | 0.01 | 6.47 | 0.02 | 1.89 |
| Pyridine | 3.57 | 0.02 | 5.92 | 0.10 | 1.66 |

# TABLE 36

## Calculated and Experimental Enthalpies for Various Gas Phase Lewis Acid-Base Reactions

| Acid | Base | $-\Delta H$ Calc. (kcal/mole) | $-\Delta H$ Expt. (kcal/mole) |
|---|---|---|---|
| $K^+$ | | | |
| | $NH_3$ | 17.9 | 17.8 |
| | $CH_3NH_2$ | 19.1 | 19.1 |
| | $(CH_3)_2NH$ | 19.7 | 19.5 |
| | $(CH_3)_3N$ | 20.1 | 20.0 |
| | Pyridine | 20.2 | 20.7 |
| $H^+$ | | | |
| | $NH_3$ | 205.8 | 207.0 |
| | $CH_3NH_2$ | 217.3 | 217.8 |
| | $(CH_3)_2NH$ | 223.0 | 225.3 |
| | $(CH_3)_3N$ | 229.2 | 230.3 |
| | Pyridine | 230.4 | 225.6 |
| $B(CH_3)_3$ | | | |
| | $NH_3$ | 13.7 | 13.7 |
| | $CH_3NH_2$ | 17.6 | 17.6 |
| | $(CH_3)_2NH$ | 19.2 | 19.3 |
| | $(CH_3)_3N$ | 17.6 | 17.6 |
| | Pyridine | 17.1 | 17.0 |

# TABLE 37

## E and C Parameters for Various Lewis Acids and Bases Using Drago's Amine Parameters

| Bases | | | |
|---|---|---|---|
| From Drago[a] | | | |
| | $E_B$ | $C_B$ | C/E |
| $NH_3$ | 1.36 | 3.46 | 2.54 |
| $CH_3NH_2$ | 1.30 | 5.88 | 4.52 |
| $(CH_3)_2NH$ | 1.09 | 8.73 | 8.01 |
| $(CH_3)_3N$ | .808 | 11.54 | 14.28 |
| Pyridine | 1.17 | 6.40 | 5.47 |
| Corrected to Best Fit | | | |
| $NH_3$ | 1.43 | 2.68 | 1.87 |
| $CH_3NH_2$ | 1.00 | 8.42 | 8.41 |
| $(CH_3)_2NH$ | .847 | 10.63 | 12.55 |
| $(CH_3)_3N$ | 1.217 | 7.11 | 5.84 |
| Pyridine | 1.315 | 6.13 | 4.66 |

| Acids | | | |
|---|---|---|---|
| | $E_A$ | $C_A$ | C/E |
| $K^+$ | 10.55 | 1.02 | 0.0967 |
| $H^+$ | 123.56 | 11.06 | 0.0895 |
| $B(CH_3)_3$ | 7.31 | 1.223 | 0.1673 |

[a] Reference 143

## TABLE 38

## Calculated and Experimental Enthalpies for Various Lewis Acid-Base Reactions Using Drago's[a] Base Parameters

| Acid | Base | $-\Delta H$ Calc.(kcal/mole) Drago's | Corrected | $-\Delta H$ Exp. (kcal/mole) |
|---|---|---|---|---|
| $K^+$ | | | | |
| | $NH_3$ | 17.9 | 17.8 | 17.8 |
| | $CH_3NH_2$ | 19.8 | 19.1 | 19.1 |
| | $(CH_3)_2NH$ | 20.5 | 19.8 | 19.5 |
| | $(CH_3)_3N$ | 20.4 | 20.1 | 20.0 |
| | Pyridine | 18.9 | 20.1 | 20.7 |
| $H^+$ | | | | |
| | $NH_3$ | 206.3 | 206.5 | 207.0 |
| | $CH_3NH_2$ | 225.7 | 216.8 | 217.8 |
| | $(CH_3)_2NH$ | 231.2 | 222.2 | 225.3 |
| | $(CH_3)_3N$ | 227.5 | 229.0 | 230.3 |
| | Pyridine | 215.3 | 230.3 | 225.6 |
| $B(CH_3)_3$ | | | | |
| | $NH_3$ | 14.2 | 13.7 | 13.7 |
| | $CH_3NH_2$ | 16.7 | 17.6 | 17.6 |
| | $(CH_3)_2NH$ | 18.6 | 19.2 | 19.3 |
| | $(CH_3)_3N$ | 20.0 | 17.6 | 17.6 |
| | Pyridine | 16.3 | 17.1 | 17.0 |

[a] Reference 143

A large C/E means a "soft" acid or base. From both methods used in this study the ratios C/E vary in the same manner (although since the reference in one case was $K^+$ and in the other iodine, the ratios are not numerically the same). From Table 37 the "corrected best fit" order of hardness of the acids will be $H^+ > K^+ > B(CH_3)_3$. The order of hardness of the bases will be $NH_3$ > pyridine $> (CH_3)_3N > (CH_3)NH_2 > (CH_3)_2NH$. These orders are similar to the qualitative classification by Pearson (54). That is, the proton and potassium are hard acids; trimethyl boron is borderline; ammonia is a hard base; pyridine, dimethyl- and trimethylamine are borderline or soft. Only monomethylamine seems out of place, since it has been classified by Pearson as hard.

Drago has pointed out (143) that the procedures used by Pearson to determine hardness and softness do not give the same results as the C/E ratio because the magnitudes of the C and E numbers are lost in the ratio. This can best be demonstrated by comparing the values for the proton with those of potassium. The ratios of C/E are very similar (.23 for the proton, .25 for the potassium ion); however the magnitude of the values are 10 times greater for the proton. Thus, even though the proton is the "hardest" acid, the high C terms means that it will interact with "soft" bases to a larger degree than $K^+$ or even the much "softer" trimethylboron. Therefore, the magnitude of the C and E parameters are more important in determining the

enthalpy of an acid-base reaction than is their ratio.

## 5.7 Limitations of the Drago Four Parameter Equation

When using the four parameter equation to obtain the E and C parameters for a base, the ratio $E_A/C_A$ should be quite different in order to obtain accurate parameters (143). If reaction enthalpy data is available from only two acids, it is imperative that the $E_A/C_A$ ratio be substantially different. Equation 5.24 may be rewritten in the following manner:

$$(E_A/C_A)E_B + C_B = -\Delta H/C_A \qquad 5.28$$

When solving this equation for two acid-base reactions, (in which the base remains the same), all accuracy will be lost if the ratios $E_A/C_A$ are similar. As a result, this correlation fails drastically when considering bases such as water or acetonitrile, for in order to determine the $E_B$ and $C_B$ parameters, it is first necessary to use only the acid parameters of the proton and the potassium ion, since no other data exists in the gas phase. Due to the similarity in the ratios $E_A/C_A$, this is dangerous and the results predict very wild values of $E_B$ and $C_B$ (i.e. for acetonitrile: $E_B = -18.7$, $C_B = 99.2$ and for water: $E_B = -3.68$ and $C_B = 31.5$).

If it is assumed that the $E_B$ water parameter is proportional to its dipole moment and the $C_B$ parameter is

proportional to the total distortion polarization, the resulting parameters ($E_B = 4.3$, $C_B = 2.4$; Method I) lead to a $\Delta H = -19.6$ for the potassium ion-water reaction, and a proton affinity of 226, both of which are considerably higher than experimental values (Table 29).

Thus, this method of gas phase Lewis acid-base correlation seems limited to systems which are alike in their acid-base interactions. That is, it would only work if an acid interacts with each of the bases in the same manner. For example, with aniline the potassium ion may interact with the aromatic ring as well as with the nitrogen, yet the proton would not. This would not be predicted from the present correlation system.

## 5.8 Gas Phase Lewis Basicity of Ethers with $K^+$ as a Reference Acid

Due to the unshared pairs of electrons on the oxygen atom, ethers undergo complexing reactions with Lewis or Bronsted acids. This complexing ability is central to much of the chemistry of ethers (147). The solvation of cations in ethers plays an important role in many organic reactions, (for example, the Grignard reaction). Thus it was felt that the study of the interaction between the potassium ion and various ethers would provide useful thermodynamic results.

In the present study, equilibrium constants were determined as a function of temperature for the two reactions:

$$K^+ + CH_3OCH_3 \rightleftarrows K^+(CH_3OCH_3) \qquad 5.29$$

$$K^+ + C_2H_5OC_2H_5 \rightleftarrows K^+(C_2H_5OC_2H_5) \qquad 5.30$$

The equilibrium constants remained constant as a function of pressure as is demonstrated in Figures 87 and 88. The thermodynamic functions $-\Delta H^o$, $\Delta G^o{}_{298}$, $\Delta G^o{}_{600}$ and $\Delta S^o$ for the above reactions were obtained from Van't Hoff plots (Figure 89). These thermodynamic values are listed in Table 39.

From the Van't Hoff plots and Table 39, it can be seen that dimethyl ether is less basic than diethyl ether when $K^+$ is a reference Lewis acid. This is in agreement with proton affinity measurements (148) but in conflict with the gas phase basicity when the bulky Lewis acid $BF_3$ is used as the reference acid (149). A comparison of the enthalpies for Reactions 5.29 and 5.30 using $K^+$, $H^+$, and $BF_3$ as the reference acids is given in Table 40.

In solution it has been commonly supposed that water is more basic than the ethers. This anti-inductive order has been attributed to steric strains. However, the present data and proton affinity measurements demonstrate that both dimethyl ether and diethyl ether are much more basic than water. Thus, as was the case in the methyl amine basicities, this anomolous order is likely due to a solvation effect.

The Van't Hoff plot of the reaction between the potassium ion and dimethylamine is included in Figure 89

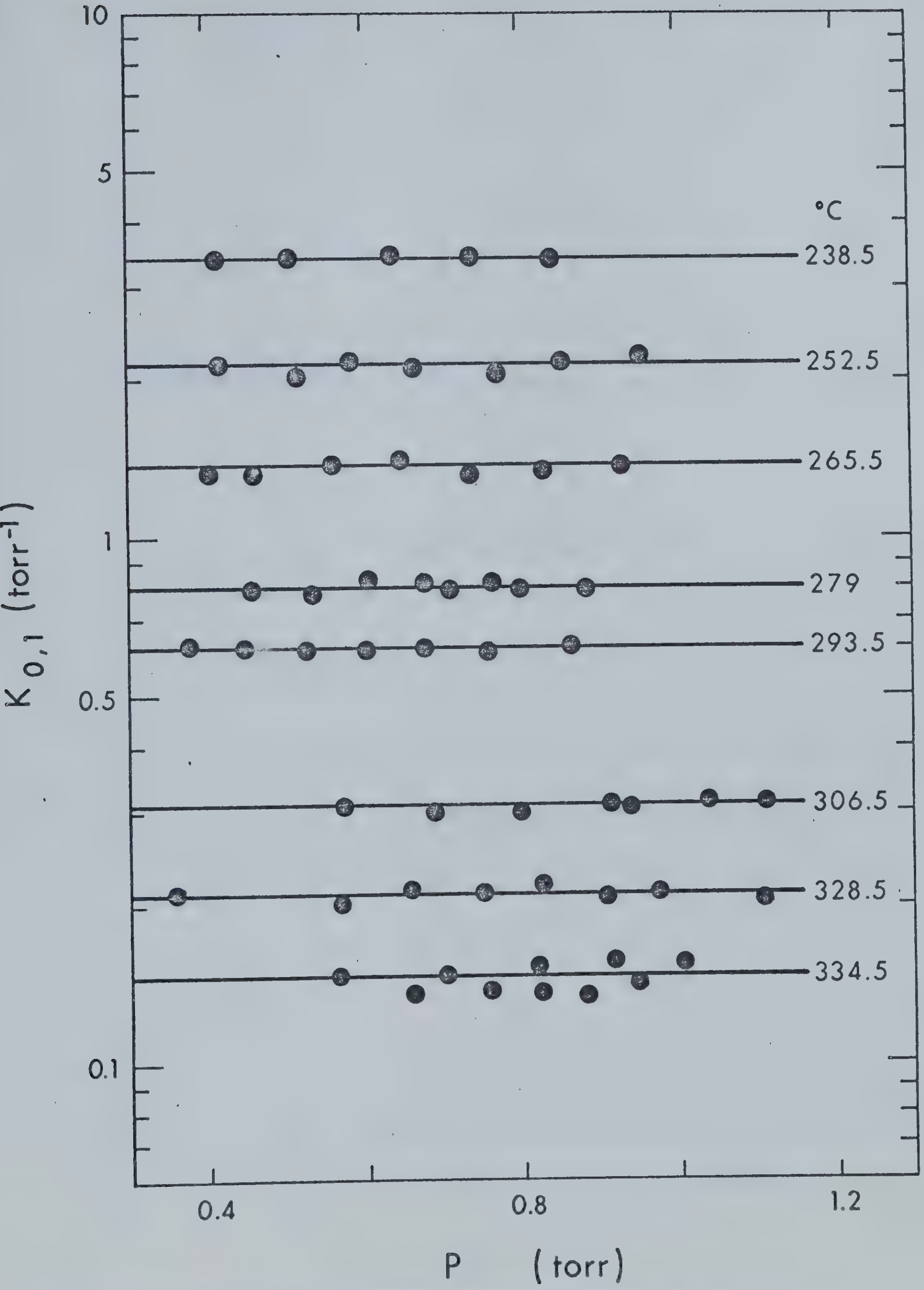

FIGURE 87 Equilibrium Constants versus Pressure at Various Temperatures for the Reaction:

$$K^+ + (CH_3)_2O = K^+((CH_3)_2O) .$$

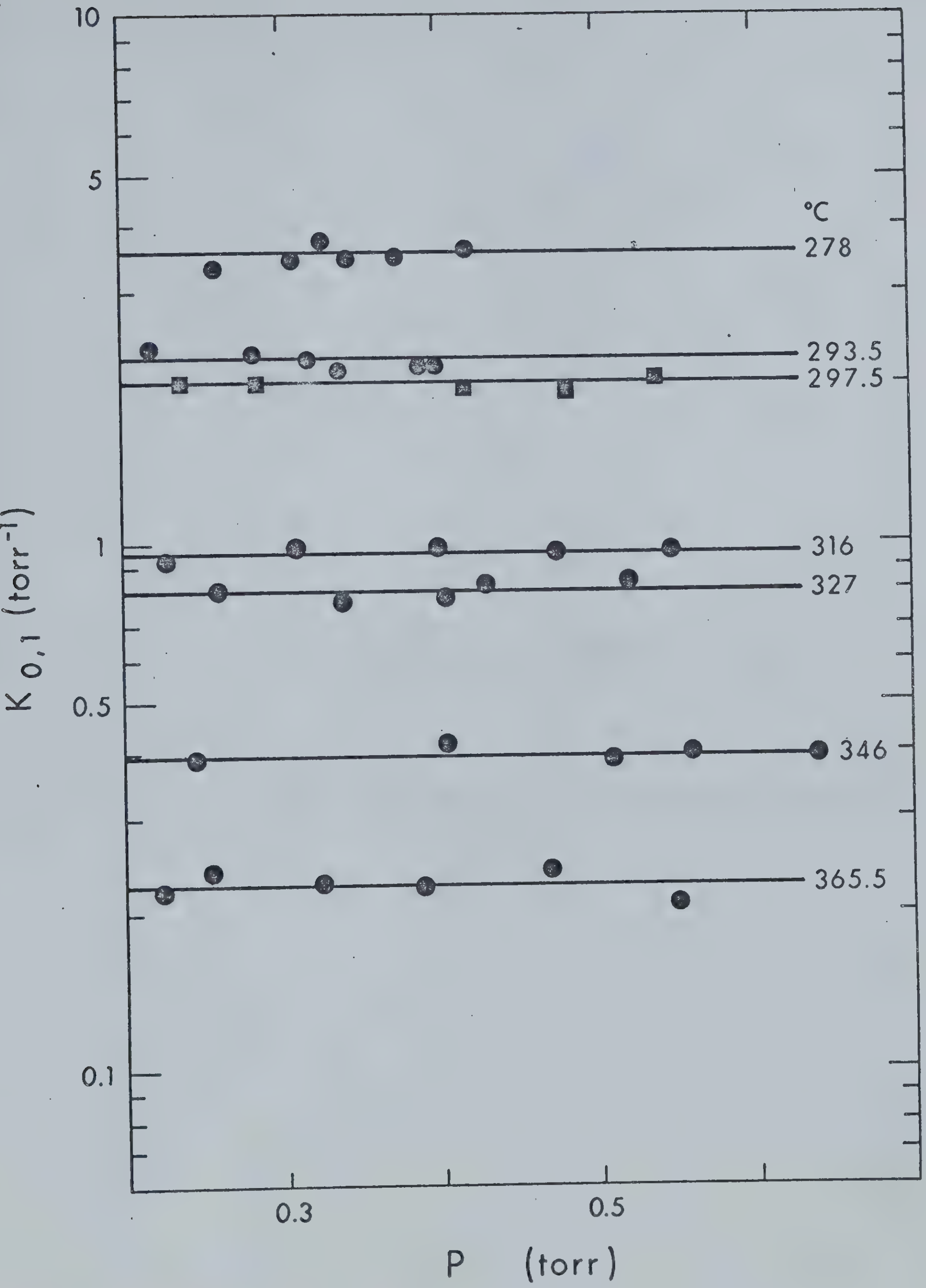

FIGURE 88 Equilibrium Constants versus Pressure at Various Temperatures for the Reaction:

$$K^+ + (C_2H_5)_2O = K^+((C_2H_5)_2O) .$$

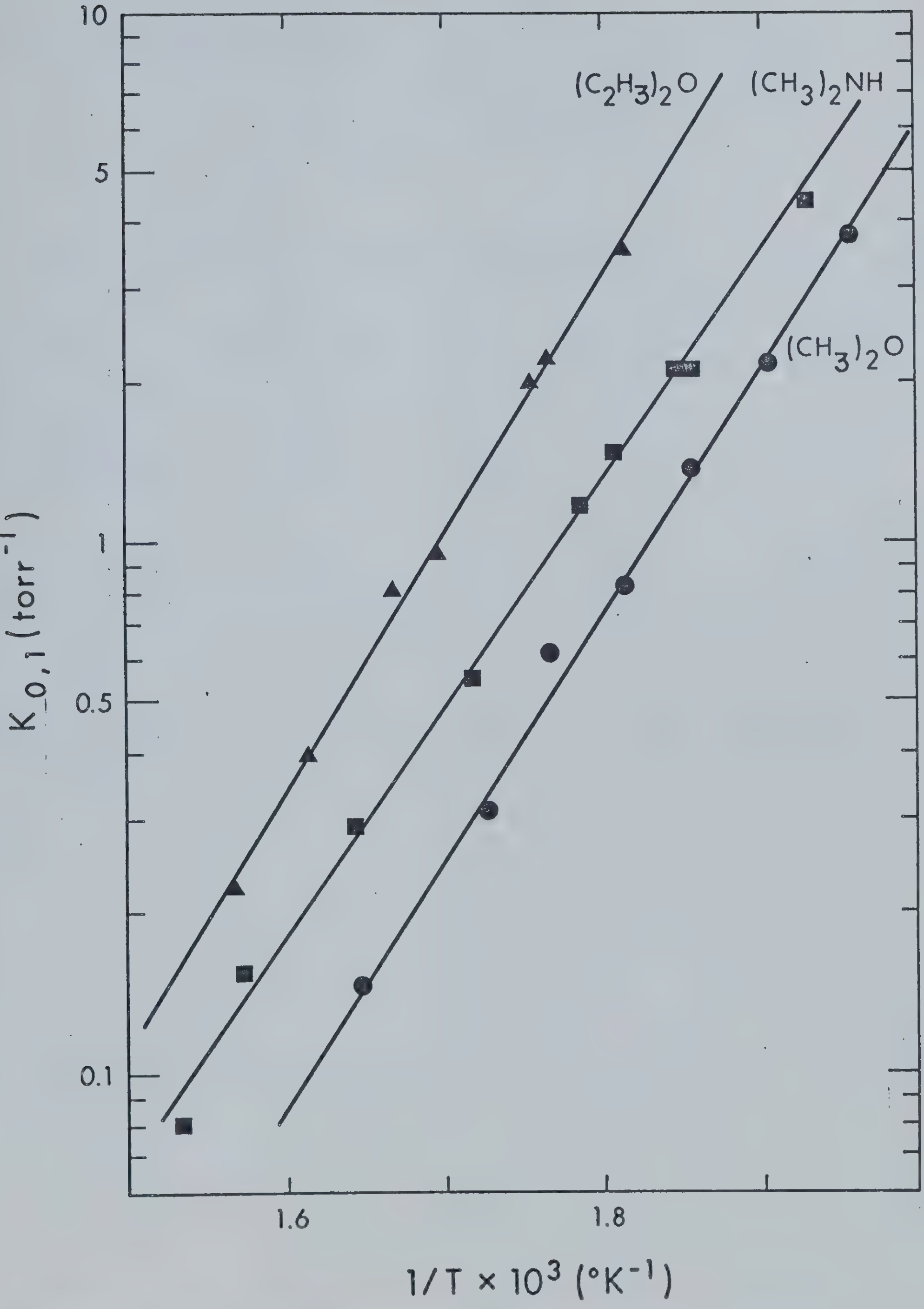

FIGURE 89 Van't Hoff Type Plots of the Interaction Between Dimethyl- and Diethyl Ethers and the Potassium Ion.

# TABLE 39

## Thermodynamic Functions for the Reactions:

## $K^+ + \text{Ether} \rightleftarrows K^+(\text{Ether})$

| Ether | $-\Delta H^\circ$ (kcal/mole) | $-\Delta S^\circ$ (e.u.) | $-\Delta G^\circ_{298}$ (kcal/mole) | $-\Delta G^\circ_{600}$ (kcal/mole) |
|---|---|---|---|---|
| $CH_3OCH_3$ | 20.8 | 24.8 | 13.4 | 5.89 |
| $C_2H_5OC_2H_5$ | 22.3 | 24.7 | 14.9 | 7.51 |
| $(CH_3)_2NH$ | 19.5 | 21.4 | 13.1 | 6.65 |

## TABLE 40

### Enthalpy[a] and Free Energy[a] at 298° C for the Reactions:

Acid + Ether ⇄ Complex

| | $CH_3OCH_3$ | $C_2H_5OC_2H_5$ |
|---|---|---|
| $K^+$[b] | | |
| $-\Delta H^o$ | 20.8 | 22.3 |
| $-\Delta G^o_{298}$ | 13.4 | 14.9 |
| $H^+$[c] | | |
| $-\Delta H^o$ | 186 | 199 |
| $-\Delta G^o_{298}$[d] | 179 | 192 |
| $BF_3$[e] | | |
| $-\Delta H^o$ | 13.3 | 10.9 |
| $-\Delta G^o_{298}$ | 3.7 | 3.6 |

[a] in kcal/mole

[b] This work

[c] Reference 148

[d] Assuming $-\Delta S$ approximately 30 e.u.

[e] Reference 149

and the thermodynamic values are compared with the ether values in Table 39. From the Van't Hoff plots and the standard free energy at 600° K, the centre of the experimental range, it can be seen that dimethylamine is more basic than dimethyl ether. This is in agreement with proton affinity measurements ( $PA(CH_3O_2CH_3) = 186$; $PA((CH_3)_2NH) = 225$). The $-\Delta H^o$ value for the $K^+-(CH_3)_2NH$ reaction is lower than the corresponding $-\Delta H^o$ value for Reaction 5.29. However, as was mentioned earlier in this chapter, the order of basicity is best given by the more accurate $-\Delta G^o_{600}$ value.

Thus, it would appear that diethyl ether is more basic than dimethyl ether, which in turn is more basic than water when $K^+$ is the reference acid. Also, it seems that dimethylamine is slightly more basic than dimethyl ether. Both of these results are in agreement with gas phase Bronsted basicity results. Further research on ether basicity and gas phase solvation of cations in ethers is currently underway in this laboratory.

## 5.9 Other Bases

### A Water

Water is less basic in the gas phase than ammonia when $K^+$ or $H^+$ is the reference Lewis acid. For the potassium ion reaction with either base, the electrostatic calculations carried out in Chapter 4 for water and in this chapter for

ammonia predict this due to the higher polarizability of ammonia. From the Pearson hard and soft acid-base theory, it could then be said that water is a "harder" base than ammonia.

## B Acetonitrile

Acetonitrile is more basic than ammonia when the potassium ion is the reference Lewis acid, yet less basic when the proton is the reference acid. If it is assumed that the proton is a "harder" acid than the potassium ion, then it seems reasonable that acetonitrile will be a "softer" base than ammonia.

A summary of the gas phase Lewis basicities of the bases used in this study is given in Table 41.

## TABLE 41

### Standard Free Energies at 600° K and Enthalpies for the Reactions:

$K^+(\text{Base}) \rightleftarrows K^+ + \text{Base}$

| Base | $\Delta G^o_{600}$ [a] (kcal/mole) | $\Delta H^o$ (kcal/mole) |
|---|---|---|
| $NH_3$ | 5.79 | 17.8 |
| $CH_3NH_2$ | 6.16 | 19.1 |
| $(CH_3)_2NH$ | 6.65 | 19.5 |
| $(CH_3)_3N$ | 5.96 | 20.0 |
| $n\text{-}C_3H_7NH_2$ | 6.47 | 21.8 |
| $C_6H_5NH_2$ | 8.60 | 22.8 |
| $C_5H_5N$ | 9.56 | 20.7 |
| $NH_2CH_2CH_2NH_2$ | 12.31 | 25.7 |
| $CH_3OCH_3$ | 5.89 | 20.8 |
| $C_2H_5OC_2H_5$ | 7.51 | 22.3 |
| $CH_3OC_2H_4OCH_3$ | 14.72 | 30.8 |
| $H_2O$ | 4.96 | 16.9 |
| $CH_3CN$ | 11.50 | 24.4 |

[a] Standard state = 1 atm.

# CHAPTER 6

# MULTIDENTATE LIGANDS

## 6.1 Introduction

Very few complexes of alkali metals have been reported and those that have are mainly formed from multidentate ligands containing the "hard" donor atoms nitrogen and oxygen (150). Besides the fact that alkali ions form very weak complexes compared to transition metals (in most cases the complexes are referred to as solvates for alkali metals), lack of spectroscopic transitions and magnetic properties in alkali metals accounts for their coordination chemistry receiving less attention than that of metals with partly filled d- or f- orbitals.

The recent interest in the coordination chemistry of alkali ions, and in particular sodium and potassium, originated with the synthesis of cyclic polyethers (crown ethers) which are cation selective, and act as reasonable models for the transport of sodium and potassium ions across membranes (for example, 151 - 155). Other research groups (150) are interested in alkali ion coordination because of their importance to the metabolism of plants. Although solvation effects play an important role in such complexes, intrinsic thermodynamic data from the gas phase study of interactions between the potassium ion and various polyethers and polyamines could provide important background information.

By beginning with the simplest polyethers and amines -

1,2-dimethoxyethane and ethylenediamine - certain trends in the complexing of $K^+$ with these polydentate ligands should become evident. Experimental results involving such systems will be presented and discussed in the present chapter.

## 6.2 Presentation of Results - Ethylenediamine

Ethylenediamine (abbreviated en, and represented by structure I) is a very common bidentate ligand in the complexing of transition metals. The lone pairs on the two nitrogen atoms are readily donated to the electrophilic metal ion.

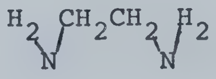

In the present study, the equilibrium constants of the following reactions were determined:

$$K^+ + en \rightleftarrows K^+(en) \tag{6.1}$$

$$K^+(en) + en \rightleftarrows K^+(en)_2 \tag{6.2}$$

$$K^+(en)_2 + en \rightleftarrows K^+(en)_3 \tag{6.3}$$

The equilibrium constants for the three reactions are plotted as a function of pressure at various temperatures in Figures 90 - 92 respectively. The Van't Hoff type plots of the reactions are shown in Figure 93, and the thermodynamic

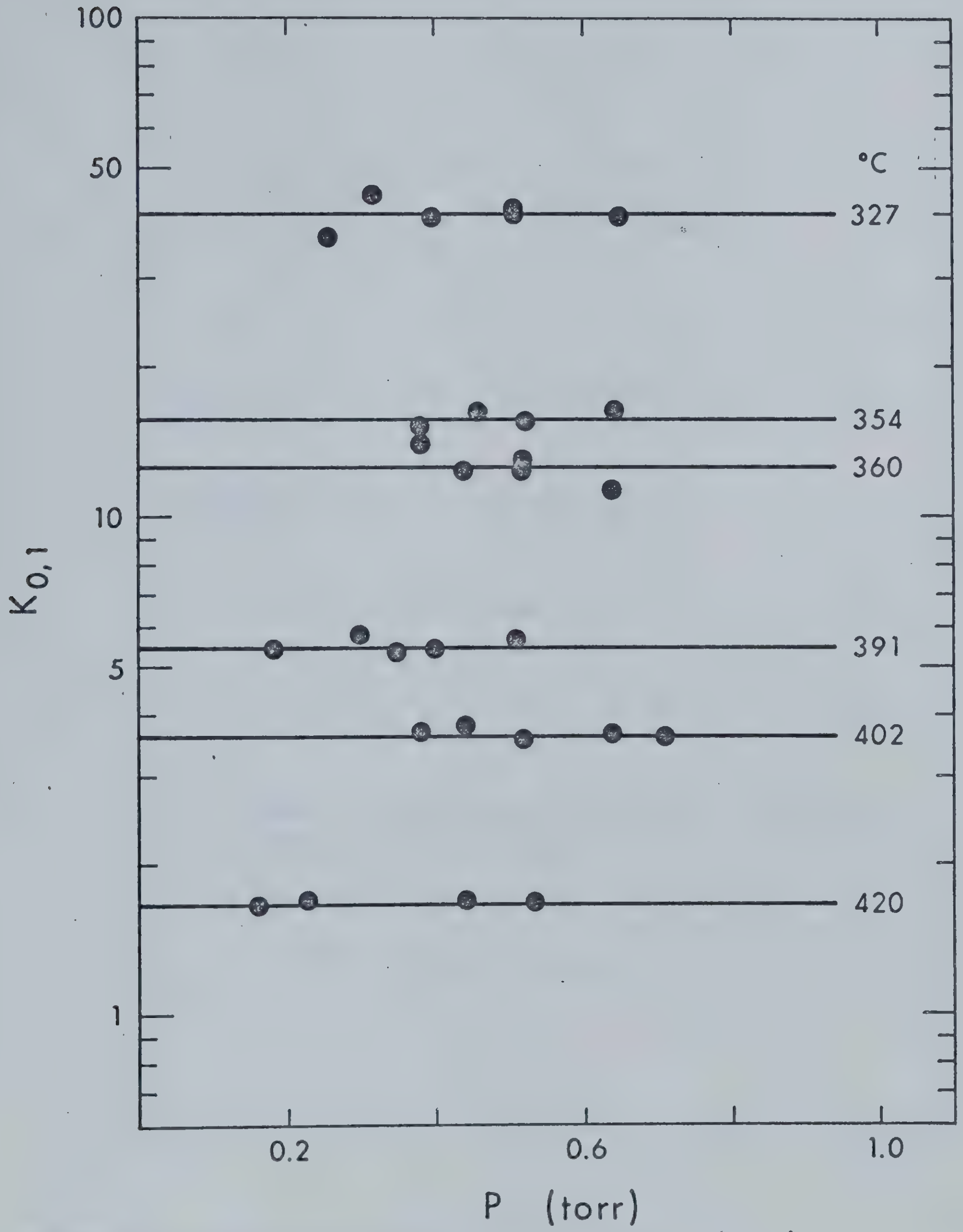

FIGURE 90 Equilibrium Constants versus Pressure at Various Temperatures for the Reaction:

$$K^+ + en = K^+(en) .$$

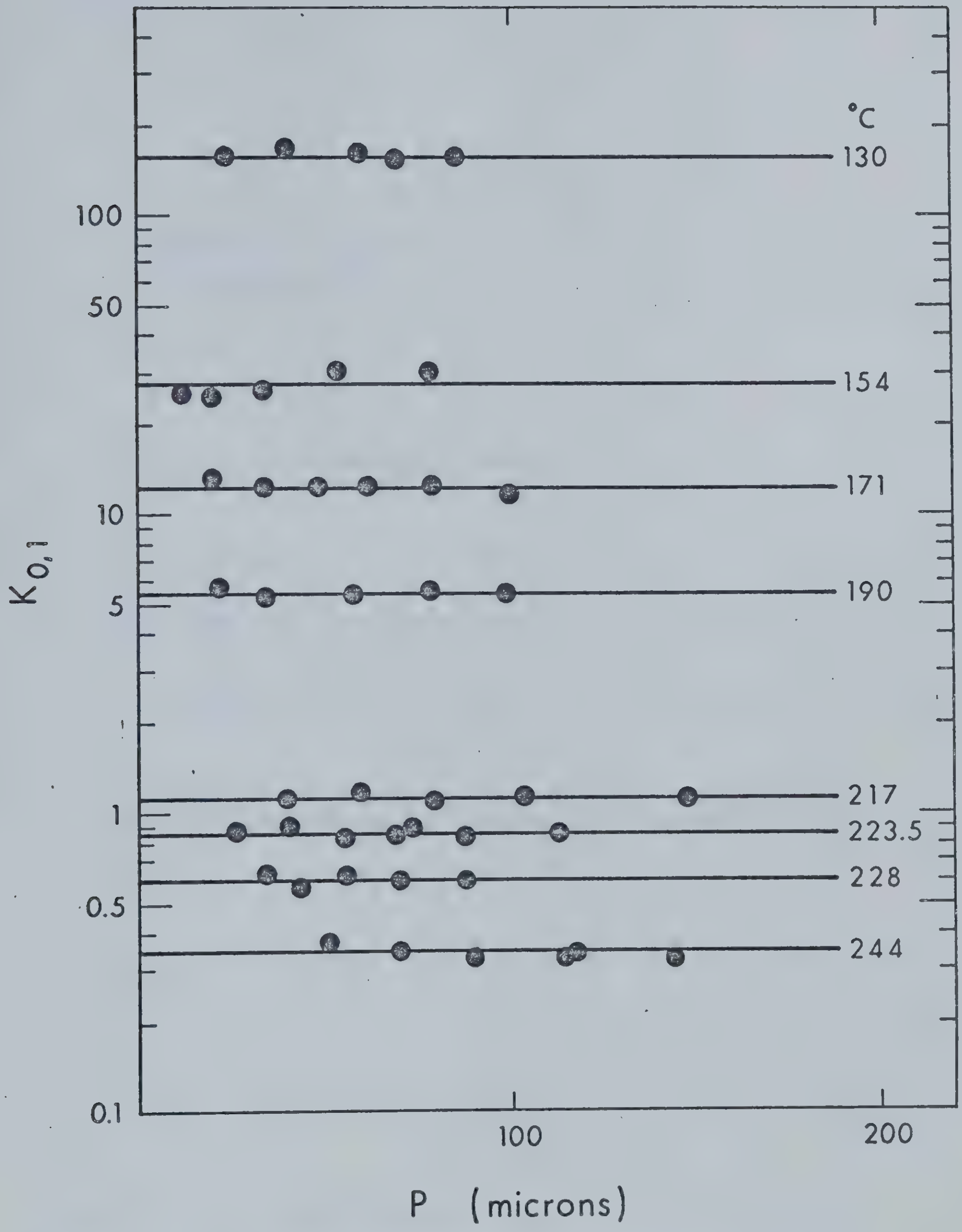

FIGURE 91 Equilibrium Constants versus Pressure at Various Temperatures for the Reaction:

$$K^+(en) + en = K^+(en)_2 .$$

$N_2$ used as a third body.

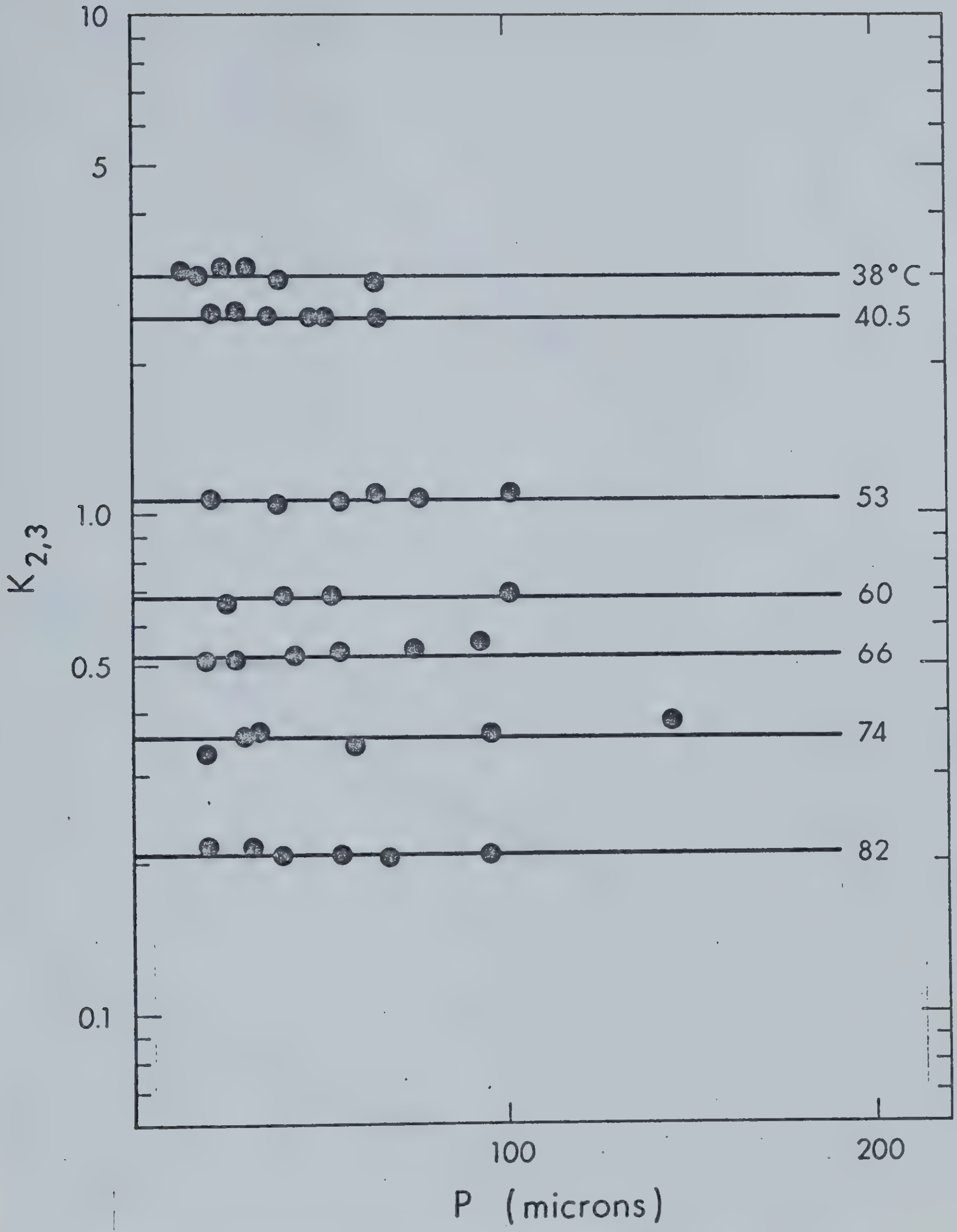

FIGURE 92 Equilibrium Constants versus Pressure of Ethylenediamine at Various Temperatures for the Reaction:

$$K^+(en)_2 + en = K^+(en)_3 .$$

$N_2$ used as a third body.

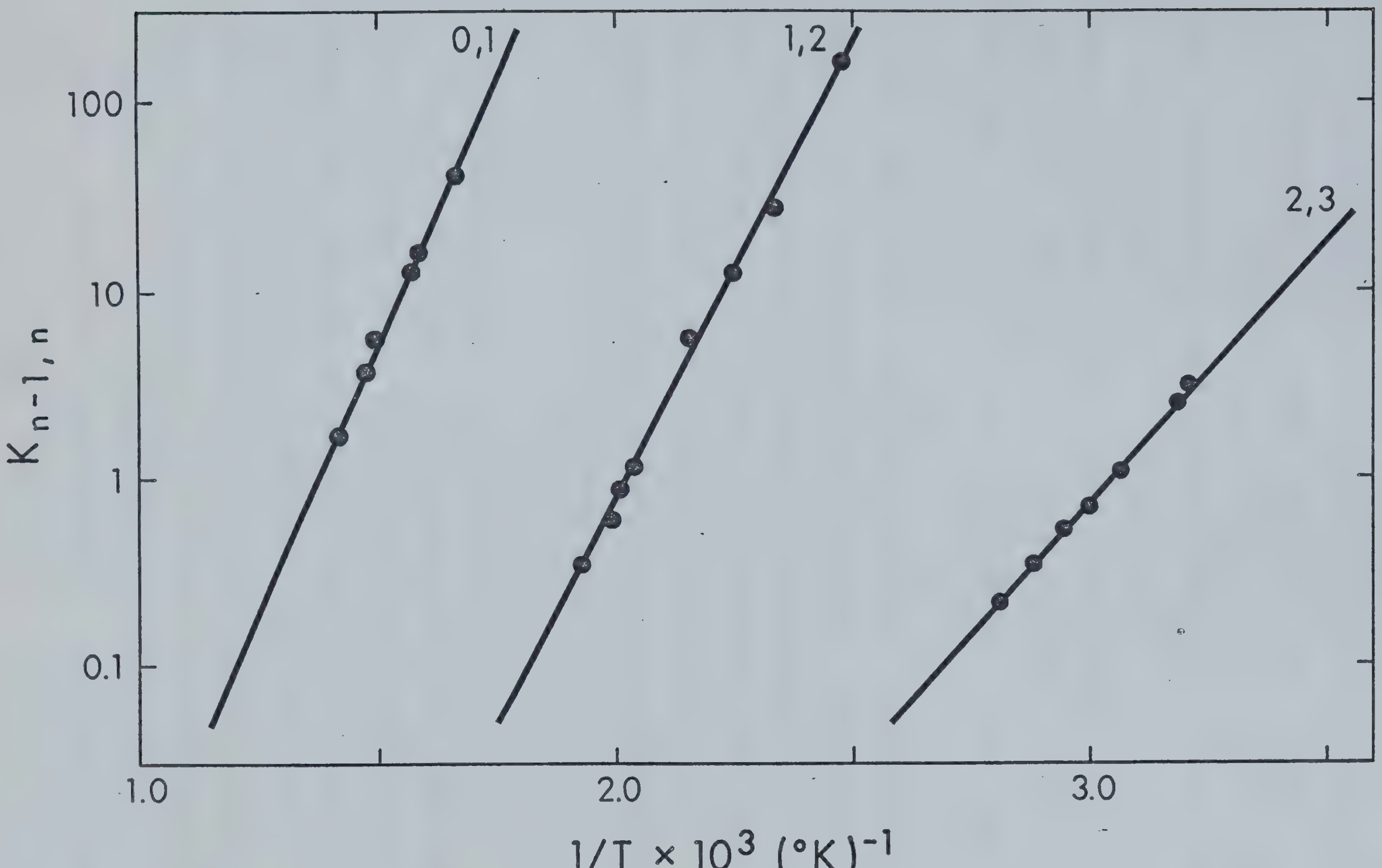

FIGURE 93 Van't Hoff Type Plots for the Reactions: $K^+(en)_{n-1} + en = K^+(en)_n$ .

values obtained from the plots are listed in Table 42.

For Reactions 6.2 and 6.3, the "stripping" phenomenon described in Chapter 2 became very serious and it was difficult to measure the equilibrium constants accurately since the maximum pressure was approximately 0.3 torr before the constants began to drop with pressure. In order to expand the pressure range, a third body, nitrogen, was added to the system, and the pressure of ethylenediamine was lowered to 10-100 microns. The method in which this was done is given in Section 2.5.

The same method could not be used when studying the $K_{0,1}$ equilibrium (Reaction 6.1), since much higher pressures of ethylenediamine are required to achieve equilibrium. This is demonstrated in Figure 94. Therefore, the standard method, using pure ethylenediamine and measuring the pressure directly on the manometer, was employed for obtaining the equilibrium constants for Reaction 6.1.

## 6.3 General Discussion - Ethylenediamine

From the Van't Hoff plots for the gas phase complexing of ethylenediamine by potassium (Figure 93) and the thermodynamic values determined from them (Table 42), several observations may be made. There is a slight decrease in $\Delta H$ from the 0,1-reaction to the 1,2-reaction of 3.5 kcal/mole; however the decrease between the 1,2 and 2,3-reactions is 9.3 kcal/mole, much more substantial than in any previous clustering reaction with alkali metals. The entropy becomes

## TABLE 42

## Thermodynamic Functions for the Reactions:

$$K^{+}(en)_{n-1} + en \rightleftarrows K^{+}(en)_{n}$$

| Reaction | $-\Delta H^{o}$ (kcal/mole) | $-\Delta G^{o\,a}$ (kcal/mole) | $-\Delta S^{a}$ (e.u.) |
|---|---|---|---|
| 0,1 | 25.7 ± 0.5 | 19.0 ± 0.5 | 22.3 ± 0.8 |
| 1,2 | 22.2 ± 0.5 | 12.7 ± 0.6 | 32.0 ± 1.1 |
| 2,3 | 12.9 ± 0.3 | 5.1 ± 0.4 | 26.3 ± 0.9 |

[a] Standard State = 1 atm; 298° K

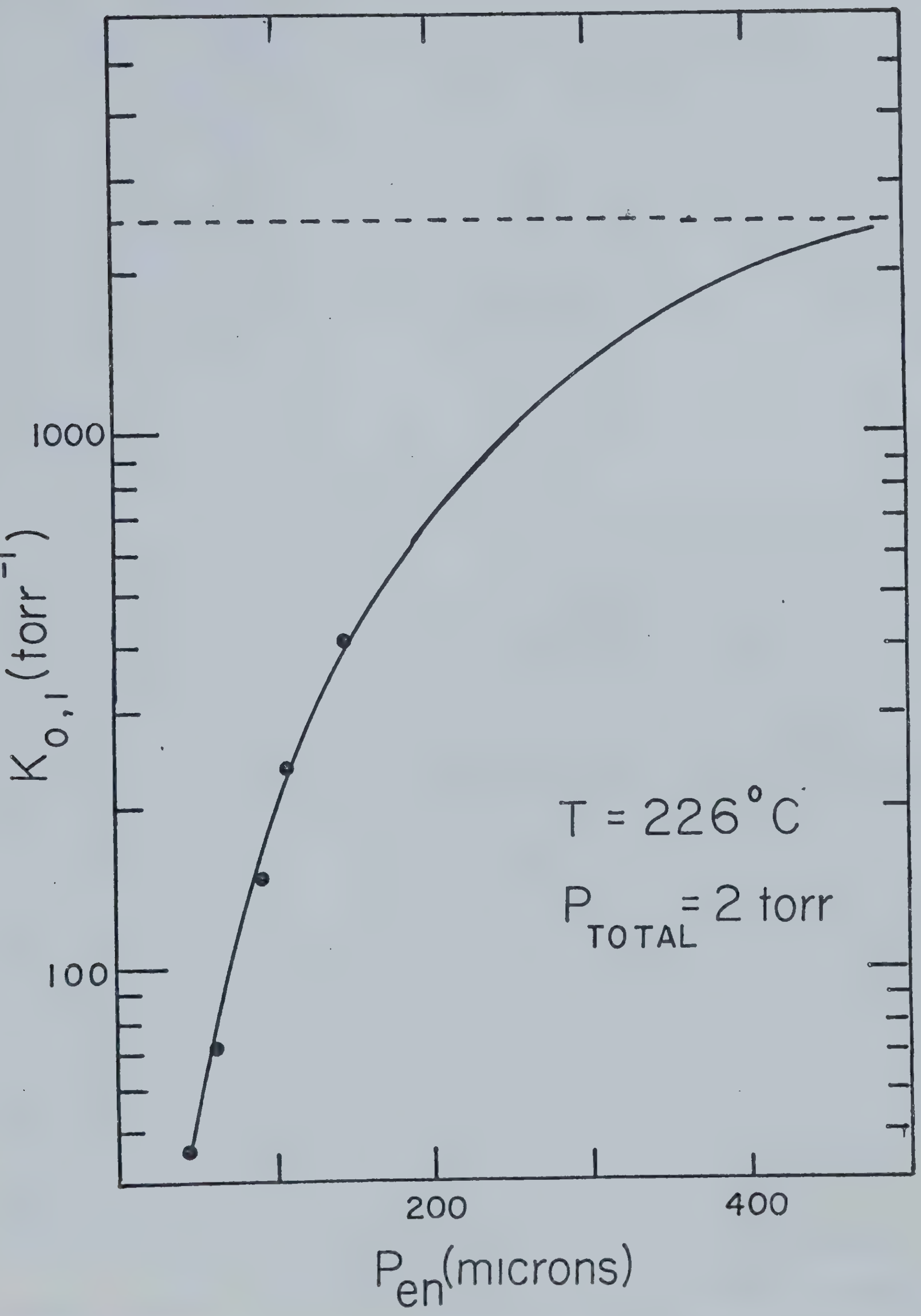

FIGURE 94 Plot of $K_{0,1}$ for the Complexing of $K^+$ with Ethylenediamine versus Pressure of en, Demonstrating Non-equilibrium. Dashed line represents value from Van'Hoff Plot.

much less favourable for the 1,2-reaction compared to the 0,1. This is expected due to much more hindered rotation and the more geometrically specific orientation of two bidentate molecules compared to one. One would therefore expect (from the same argument) that the third ethylenediamine ligand would have an even less favourable entropy, and the change in $\Delta S$ would be greater than between the 1,2 and 0,1 reactions. However, this is not the case. The entropy becomes more favourable (less negative) upon the addition of the third bidentate ligand.

There are many possibilities for this occurrence, all of which are quite plausible. The first is that the third ethylenediamine molecule "attaches" itself to the potassium ion in such a way that only one nitrogen is oriented towards the ion. The value of $\Delta H_{2,3}$ should then be similar to $\Delta H_{4,5}$ for the clustering of methylamine. Although $\Delta H_{4,5}$ for methylamine has not been determined, it would appear from the acetonitrile and water studies that the $-\Delta H_{4,5}$ would likely be lower than $-\Delta H_{2,3}$(en). Another possibility is that the addition of the third ligand forces one of the previously doubly attached ligands to become monodentate due to dipole-dipole repulsions. The more favourable entropy would then be expected. A third possibility is that the third molecule attaches in bidentate fashion, but the dipole-dipole repulsions force the ligands much farther from the molecule and thus are more loosely bound. A final possibility is that the third ligand becomes hydrogen

bonded to one of the previously attached ligands - thus forming a second shell. The more favourable entropy supports this idea, but again the enthalpy value appears too high, unless the second, non-hydrogen bonded nitrogen is oriented towards the ion, or is itself hydrogen bonded. It is difficult to predict which of these models, if any, will result upon the addition of a third ethylenediamine molecule. The important finding is that the third en molecule is much more weakly held than the first two. Thus tetracoordination is indicated.

The Van't Hoff plot for the clustering of n-propylamine with potassium can be compared with that for Reaction 6.1 as a qualitative proof of chelation. This is done in Figure 95. If only one end of the ethylenediamine molecule were interacting with the potassium ion, it would be expected that the enthalpy of the reaction would be in the same range as the aliphatic amines, and especially that of n-propylamine. From the Van't Hoff plots, it can be seen that there is a tremendous difference between ethylenediamine and propylamine, indicative of the chelation of the potassium ion by the bidentate ligand.

One would expect that chelation would cause a greater restriction on the freedom of motion of a molecule and the entropy of a chelation reaction would be much more unfavourable than the entropy of a monodentate clustering reaction. However, from Tables 28 and 42, it can be seen that the $\Delta S_{0,1}$ for the clustering of a bidentate ligand is in the

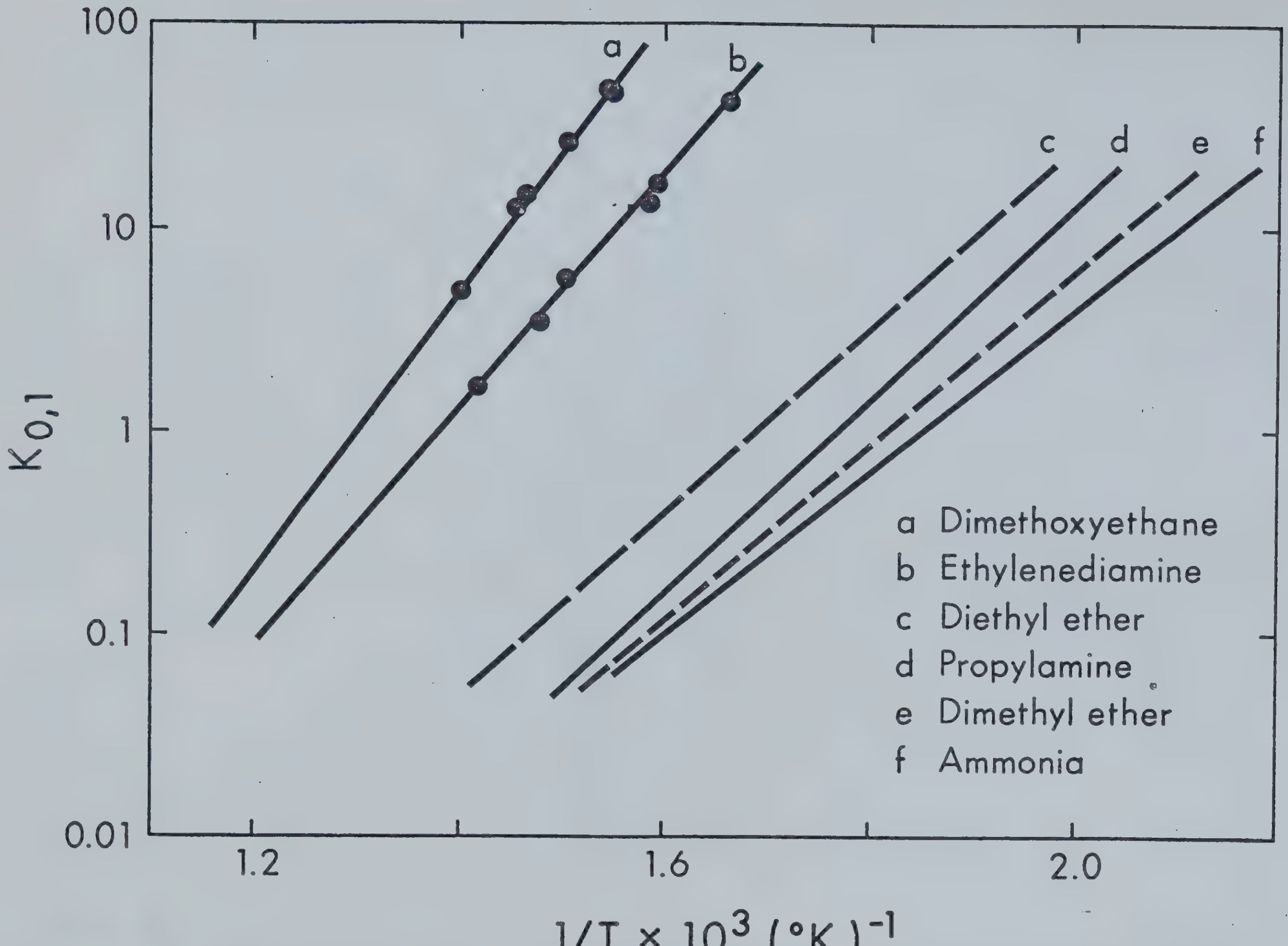

FIGURE 95 Van't Hoff Type Plots of the Various Complexing Reactions Between $K^+$ and Bases.

same range as the $\Delta S_{0,1}$ for the clustering of a monodentate ligand to the potassium ion. This would seem to indicate the loss of freedom due to the chelation of ethylenediamine is small. When a monodentate ligand, such as n-propylamine, interacts with the potassium ion, the methylene and methyl groups tend to be directed away from the ion due to ion-dipole repulsions. Thus both the monodentate and bidentate ligands will have a preferred orientation when they form a complex with the potassium ion and both ligands will have restricted rotational freedom. Therefore, the entropies of single molecule clustering reactions need not be too different.

## 6.4 Stability Constants - the Chelation Effect

The equilibrium constants, $K_{n-1,n}$, for Reactions 6.1 to 6.3 may also be referred to as stepwise stability constants. The overall stability constant, $\beta_n$, will then be the equilibrium constant for the reaction:

$$K^+ + n(\text{en}) \rightleftarrows K^+\text{en}_n \qquad 6.4$$

and

$$\beta_n = \prod_{i=1}^{n} K_{i-1,i} \qquad 6.5$$

Thus from the gas phase interactions, intrinsic stability constants can be readily determined. In Table 43 the

## TABLE 43

Stability Constants for the Reactions:

$$K^+(en)_{n-1} + en \rightleftarrows K^+(en)_n$$

| n | log $K_{n-1,n}$ [a] | log $\beta_n$ [a] |
|---|---|---|
| 1 | 13.9 | 13.9 |
| 2 | 9.3 | 23.2 |
| 3 | 3.7 | 26.9 |

[a] SS = 1 atm; 298° K

stepwise stability constants and overall stability constant (for n up to 3) for the reaction between ethylenediamine and the potassium ion are shown (standard state one atmosphere, 298° K).

In solution, the stepwise stability constant, $K_{0,1}$, for a bidentate ligand is always greater than the product of the stability constants, $K_{0,1}K_{1,2}$, for two monodentate ligands which are similar to the bidentate ligand. For example in the complexing of nickel (II) by ammonia and ethylenediamine (156):

$$Ni^{+2} + 2NH_3 \rightleftarrows [Ni(NH_3)_2]^{+2} \quad \beta = 10^5 \qquad 6.6$$

$$Ni^{+2} + en \rightleftarrows [Ni(en)]^{+2} \quad \beta = 10^{7.5} \qquad 6.7$$

This overall stability of the complex containing a chelate ring over one which does not is referred to as the "chelate effect". The chelate effect is said to be due to the favourable entropy of the chelation reaction in solution (156). This may be interpreted in a qualitative way. When atoms of the ligand enter the coordination sphere of an ion, water molecules are necessarily displaced. In a nonchelate system, each water molecule is displaced by one ligand molecule and the total number of molecules in the system remains constant. However, in a chelation reaction, one ligand molecule displaces two or more water molecules and the net number of free molecules increases. As a result,

the disorder or entropy of the system increases. Another way to look at the problem is to imagine a bidentate ligand with one end attached to an ion. This means that the second end cannot be too far away and the probability of it interacting with the metal ion is much greater than that of an independent ligand somewhere in the bulk solution.

In the gas phase a somewhat similar entropy effect will be noticed since the order of the system will increase with the addition of two ligands compared to only adding one bidentate ligand. The translational entropy term is very important in the gas phase. With two monodentate ligands this translational entropy term will be counted only once. Thus, the bidentate ligand should be relatively more stable from an entropy point of view.

It can be assumed from previous studies on alkali ion solvation that the free energy of Reaction 6.8 will be about

$$K^+(CH_3NH_2) + CH_3NH_2 \rightleftarrows K^+(CH_3NH_2)_2 \qquad 6.8$$

-10 kcal/mole. Combining this with the $\Delta G_{0,1}$ for the reaction between the potassium ion and methylamine (Table 28, Chapter 5) gives a total $\Delta G_{0,2}$ of -22.7 kcal/mole or a $\beta_2$ of $10^{16.6}$ for Reaction 6.9. The standard free energy of Reaction 6.10

$$K^+ + 2CH_3NH_2 \rightleftarrows K^+(CH_3NH_2)_2 \qquad 6.9$$

$$K^+ + en \rightleftarrows K^+(en) \qquad 6.10$$

is -19.0 kcal/mole ( $\beta = 10^{13.9}$), which means that the potassium ion complex with two methylamine ligands is more stable than the ethylenediamine complex. This is in direct conflict with the chelate effect which would predict the opposite, that is, that the ethylenediamine-potassium ion complex would be more stable.

This difference in stabilities can be attributed to the enthalpies of the reactions. Assuming the enthalpy of Reaction 6.8 to be about -16 kcal/mole, the total enthalpy of Reaction 6.9 will then be about -35 kcal/mole. For the ethylenediamine reaction, the enthalpy is -25.7 kcal/mole, which means from an enthalpy point of view it is much less stable. This large difference in enthalpies can be looked at in two ways. The two methylamine molecules can approach the potassium ion from opposite sides. This means that the dipole-dipole repulsions will be minimized. However, the two negative poles on the ethylenediamine molecule will be relatively close together and there will be a lowering of the interaction energy due to a dipole-dipole repulsion. In addition, when one end of the ethylenediamine molecule attaches to the potassium ion, a slight positive charge will be induced on the nitrogen atom. Due to the field effect (157), some of this induced charge will be transferred

to the second nitrogen, lowering its negative point charge, i.e. its basicity will be lowered. Thus, from an electrostatic viewpoint, two monodentate ligands should interact more strongly with the potassium ion than one bidentate ligand.

From the free energies given above for the two reactions, it is obvious that the favourable entropy of the bidentate ligand reaction is overridden by the more favourable enthalpy of the monodentate reaction. In solution this is not the case and the entropy differences become more important in determining the stabilities of the complexes. One possible explanation is that in solution the field effect does not play as important a role as it does in the gas phase. This is due to the field effect being inversely proportional to the dielectric constant of the solvent (157). Thus, in solution the basicity of the second donor atom in a bidentate ligand will not be lowered and the overall enthalpy of the bidentate ligand-ion reaction will be relatively more stable than it would be in the gas phase.

## 6.5 1:1 Complex of Potassium and Dimethoxyethane

Dimethoxyethane (II) is the methyl ether of ethylene glycol

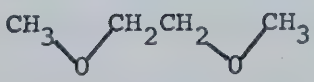

(II)

and is often simply referred to as "glyme" (glycol methyl ether). It has two donor oxygen atoms and thus it would be expected to form a chelate type complex with the potassium ion. In organic reactions, it is often used as a solvent for reactions involving alkali metals due to the high solubility of the alkali metal in it.

The equilibrium constant for the reaction

$$K^{+} + \text{glyme} \rightleftharpoons K^{+}(\text{glyme}) \qquad 6.11$$

was studied as a function of temperature. The plot of $K_{0,1}$ versus pressure at various temperatures is shown in Figure 96. The Van't Hoff plot is included in Figure 95, along with ethylenediamine. The thermodynamic values obtained from the plot are compared with those of ethylenediamine in Table 44. Chelation is demonstrated by comparing the monodentate ethers, dimethyl and diethyl ether, and noting the large differences between the Van't Hoff plots (Figure 95).

The interaction between dimethoxyethane and the potassium ion is much stronger than that between ethylenediamine and $K^{+}$. Potassium has been found to complex more readily to oxygen than to nitrogen in the study of cyclic crown complexes (158), and the gas phase results agree with this for bidentate ligands. A more suitable comparison would be between dimethoxyethane and N,N', dimethylenediamine ($CH_3$-NH-$CH_2CH_2$-NH-$CH_3$); however, the latter compound

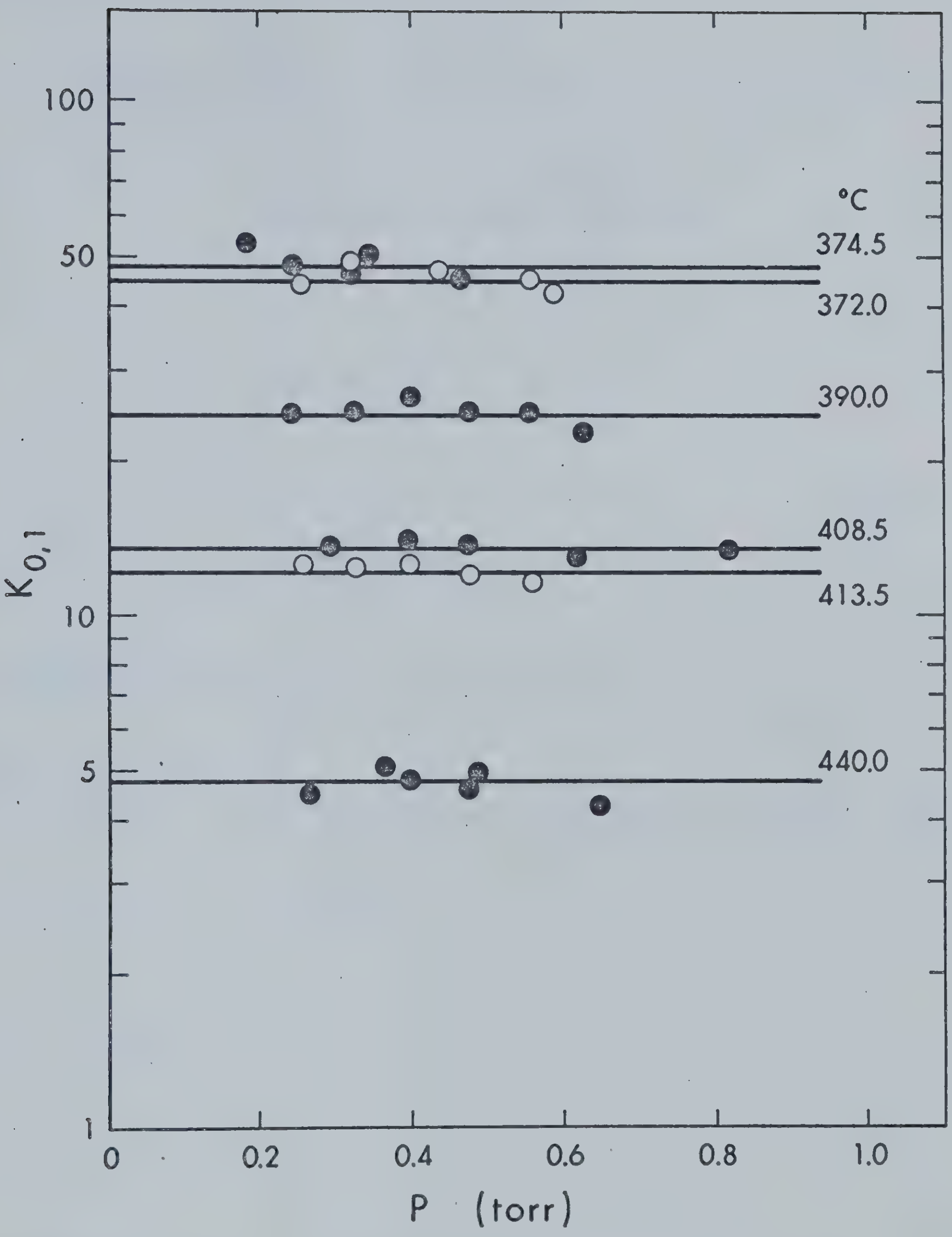

FIGURE 96 Equilibrium Constants versus Pressure at Various Temperatures for the Reaction:

$$K^+ + \text{glyme} = K^+(\text{glyme}) .$$

## TABLE 44

### The Thermodynamic Relationships for the Reaction:

$$K^+ + \text{glyme} \rightleftarrows K^+(\text{glyme})$$

### Compared with the Reaction:

$$K^+ + \text{en} \rightleftarrows K^+(\text{en})$$

| Compound | $-\Delta H$ (kcal/mole) | $-\Delta S^a$ (e.u.) | $-\Delta G^a$ (kcal/mole) |
|---|---|---|---|
| Dimethoxyethane (glyme) | 30.8 ± 1.1 | 26.8 ± 1.6 | 22.8 ± 1.2 |
| Ethylenediamine (en) | 25.7 ± 0.5 | 22.3 ± 0.7 | 19.0 ± 0.5 |

[a] SS = 1 atm; 298° K

has not yet been studied. It would be expected from the monoamines that N,N',dimethylenediamine would interact more strongly than ethylenediamine but probably by no more than one or two kcal/mole (comparing monomethyl- and dimethylamine).

## 6.6 Summary

This study gives preliminary data on the interaction between the potassium ion and multidentate ligands. The overall and stepwise gas phase stability constant of the reactions:

$$K^+(en)_{n-1} + en \rightleftarrows K^+(en)_n$$

were obtained up to n equals 3, as well as the thermodynamic functions for the above reactions and the reaction:

$$K^+ + glyme \rightleftarrows K^+(glyme)$$

The following conclusions can be stated:

1) Chelation occurs between the potassium ion and the bidentate ligands ethylenediamine and dimethoxyethane.

2) The interactions between diethers and the potassium ion are stronger than between similar amines and the potassium ion.

3) Although interactions between the bidentate ligands are much stronger than monodentate ligands, no

"chelation effect" is noted in the gas phase.

For higher polyethers and amines, a different experimental technique will be necessary. Since the ion source was at its maximum temperature for the study of the bidentate ligands, and since the tridentate ligands will interact more strongly, the equilibrium:

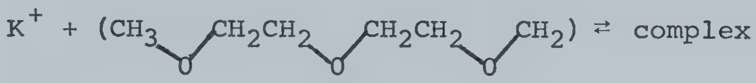

$$K^+ + (CH_3OCH_2CH_2OCH_2CH_2OCH_2) \rightleftarrows \text{complex}$$

diglyme

will require much higher temperatures in order that the equilibrium constants be accurately determined. A switching equilibrium experiment of the type:

$$K^+(\text{glyme}) + \text{diglyme} \rightleftarrows K^+(\text{diglyme}) + \text{glyme}$$

would probably be the most efficient method.

## CHAPTER 7

## SUGGESTIONS FOR FURTHER RESEARCH

### 7.1 Complexes Involving the Silver Ion

The study of the complexing of the monovalent silver ion with various conjugated systems would prove interesting. From the potassium ion complexes with aniline and acetonitrile, the possibility that the π electrons of the base interact with the empty 4s orbital of the ion exists. With silver this is even more likely, due to back donation of electrons from the d-orbitals in a π-type bond. For example, for arene-silver reactions the following two types of bonds would exist (141):

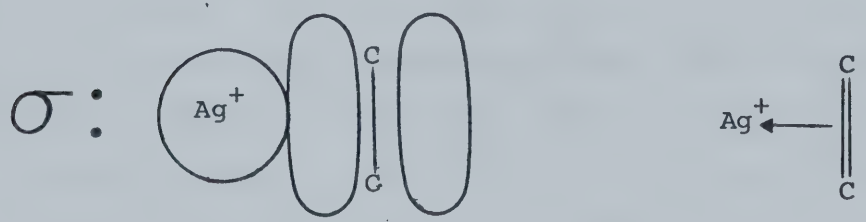

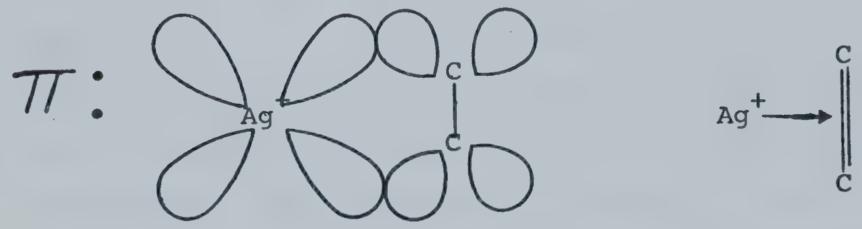

The σ-type bond is expected to be stronger than the π-bond (140).

With this idea in mind, the complexing of various conjugated compounds with the silver ion can be studied in

a systematic manner: alkenes, alkynes, cycloalkenes, benzene, substituted benzenes, and heterocyclic aromatic compounds.

Silver (I) in most cases forms 2:1 complexes with various ligands. When higher complexes are formed the stability constants, $K_3$ and $K_4$ are relatively small compared to $K_1$ and $K_2$. Thus, in the step-by-step clustering of a ligand on the silver ion, it is likely that there would be a severe break in the enthalpy and free energy upon the addition of the third ligand. As a guess, one would expect that the first two ligands would join at an enthalpy much greater than with the potassium ion and the next few ligands would have thermodynamic properties very close to the clustering of the ligands with potassium (since potassium and silver are about the same size).

Experimentally, it does not appear that the silver ion would be that hard to produce. The ionization potential of silver is relatively low (7.5 ev) and a thermionic ion source such as was used with the alkali ions would likely work.

Gas phase silver ion complexes and their thermodynamic functions would be of great interest to the field of organometallic and coordination chemistry as well as to electrochemistry where the silver-silver ion electrode is often used.

## 7.2 Alkali Ion Complexes with Crown Ethers

As was pointed out in the last chapter, the study of cyclic polyethers has developed remarkably in the last few years. In 1967, C. J. Pedersen (152) presented a paper describing the synthesis and ion selectivity of over thirty such "crown" compounds. Since then, the thermodynamics of ion-crown ether complexing reactions in various solvents have been studied extensively by calorimetric (154), NMR (159), ultraviolet (160) and potentiometric (161) techniques. This interest developed because cyclic polyethers can be used as a model for biological activity as related to ion transport, photosynthesis and oxidative phosphorylation (154).

Crown ethers are cyclic polyethers which have a lipophilic exterior and hydrophilic centre cavity ringed with electron donor atoms (oxygens). In the presence of a metal ion, the ether assumes a highly specific conformation. A Courtald model of one of the most common crown ethers, dibenzo-18-crown-6 is shown in Figure 97. The crown ethers are usually described in an abbreviated manner. The first number in the name describes the total number of atoms in the ring and the second number represents the number of oxygen atoms in the ring. The substituents (if there are more than one) are usually, although not always, placed symmetrically. The structures of a few common crown ethers are shown in Figure 98.

The question then arises: why would high pressure

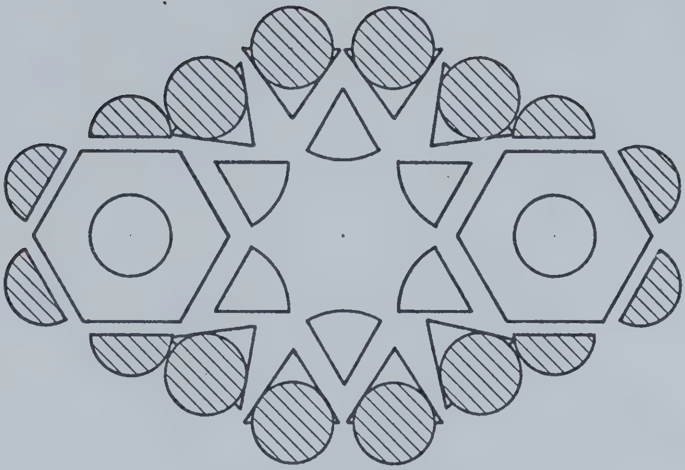

COURTALD MODEL

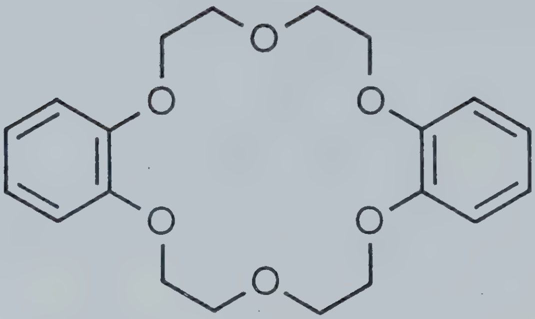

STRUCTURAL FORMULA

FIGURE 97 Courtald[a] and Structural Models of Dibenzo-18-crown-6.

a) taken from reference 152

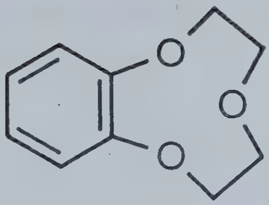

BENZO - 9 - CROWN - 3

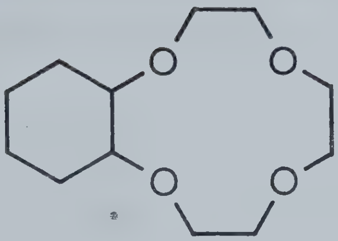

CYCLOHEXYL - 12 - CROWN - 4

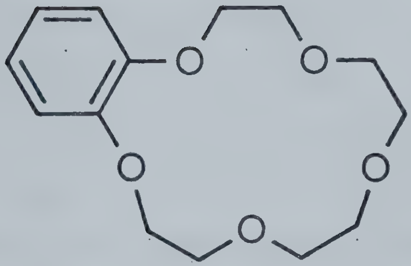

BENZO - 15 - CROWN - 5

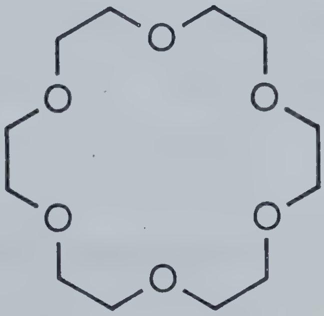

18 - CROWN - 6

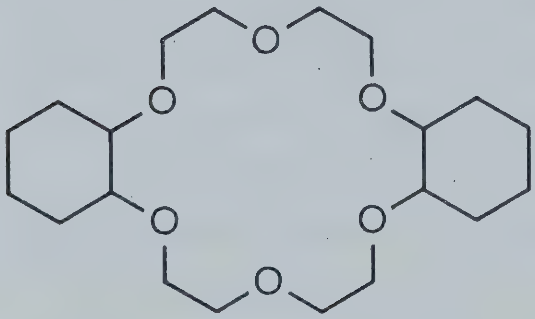

DICYCLOHEXYL - 18 - CROWN - 6

FIGURE 98 Some Common Cyclic Polyethers.

mass spectrometry be useful in studying such complexes? In the determination of the thermodynamic properties of the reaction 7.1

$$M^{+} + Cr \rightleftharpoons M^{+}Cr \qquad 7.1$$

in solution, it is difficult to obtain the single ion thermodynamics since the metal ion must be introduced as a salt (usually a chloride, iodide or most often a thiocynate). In the gas phase, this problem is eliminated. The solution studies have shown that the ion selectivity of these compounds is highly solvent dependent (159, 160, 162). With the high pressure mass spectrometer, there are no solvent effects and intrinsic thermodynamic values for Reaction 7.1 may be obtained.

Crown ethers are known to form complexes of more than a 1:1 ratio with a cation (153). This is dependent on the size of the ring cavity compared to the diameter of the ion. If an ion is small enough to fit into the cavity, it will form very stable 1:1 complexes. But if it is much smaller than the hole, no stable complex will form, and the feature of ion selectivity enters. If the ion is much larger than the cavity, then it will tend to form 2:1 or 3:2 complexes which are referred to (153) as "sandwich" or "club-sandwich" complexes respectively (Figure 99). The hole diameters of some complexes are compared with the alkali diameters in Table 45 and the resulting complexes

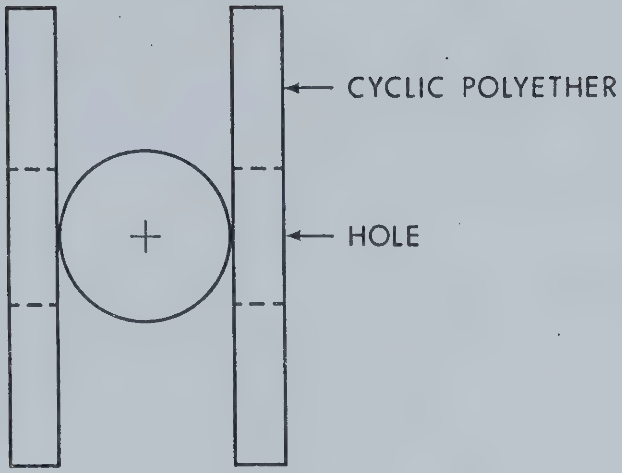
CYCLIC POLYETHER
HOLE
+

"SANDWICH" COMPLEX

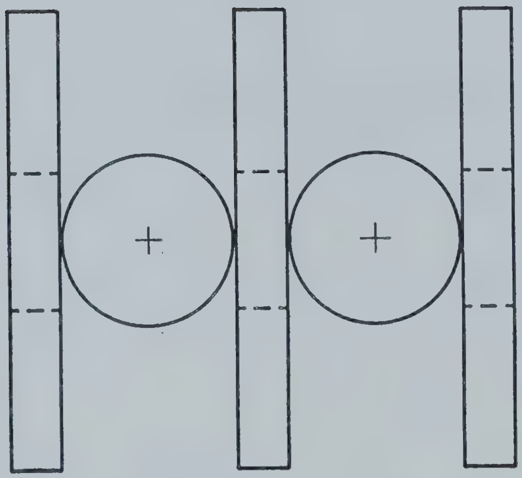

"CLUB SANDWICH" COMPLEX

FIGURE 99 Rough Approximation of Alkali Ion--Crown Ether Complexes. From Reference 153.

## TABLE 45

### Stable Complexes between Alkali Ions and Some Crown Ethers

| Crown Ether (Hole Cavity, A°)[a] | $M^+$ (Ionic Diameter, A°)[b] | | | | |
|---|---|---|---|---|---|
| | $Li^+$ (1.56) | $Na^+$ (1.96) | $K^+$ (2.66) | $Rb^+$ (2.98) | $Cs^+$ (3.30) |
| Dibenzo-14-crown-4 (1.2 - 1.5) | 1:1 | | | | |
| Benzo-15-crown-5 (1.7 - 2.2) | | 1:1 | 2:1[c] | 2:1 | 2:1 |
| Dibenzo-18-crown-6 (2.6 - 3.2) | | | 1:1 | 1:1<br>2:1 | 2:1<br>3:2 |

[a] Reference 153

[b] Goldschmidt ionic diameters

[c] 2 moles crown ether to 1 mole $K^+$

are listed. By using a mass spectrometer, the study of such complexing is easily achieved, since the masses of the complexes are readily determined - a difficult feature in the crystal study of crown ether complexes at this time (153). Thus, the study of alkali ion-crown ether complexing in the gas phase would provide valuable information to the present research on the ion selectivity of crown ethers.

Since most of the crown ethers are solids at room temperature, a more sophisticated gas handling plant must be used. However, with the present system, crown ethers with low melting points (i.e. below $100^{\circ}$ C) could be studied if care were taken to maintain the system at high temperatures to prevent condensation of the ether vapours. The melting points of some common cyclic polyethers which would be of interest to study are listed in Table 46. Vapour pressure data is not yet available for these compounds.

The complexing of the crown ethers with alkali ions may be difficult to measure directly since the reaction is expected to be very exothermic from the present study of potassium and dimethoxyethane. The addition of electron withdrawing substituents such as the nitro group to the aromatic ring (if there is one) of a crown ether will decrease the basicity of the adjacent oxygens (159). By using this idea and the use of switching reaction such as 7.2

$$M^{+}Cr_{1} + Cr_{2} \rightleftharpoons M^{+}Cr_{2} + Cr_{1} \qquad 7.2$$

## TABLE 46

## Melting Points of Some Crown Ethers[a]

| Crown Ether | Melting Point ($^{o}C$) |
|---|---|
| Benzo-9-crown-3 | 67 - 69 |
| Benzo-12-crown-4 | 44 - 45.5 |
| Cyclohexyl-12-crown-4 | below 26 |
| Benzo-15-crown-5 | 79 - 79.5 |
| Cyclohexyl-15-crown-5 | below 26 |
| 18-crown-6 | 39 - 40 |
| Benzo-18-crown-6 | 43 - 44 |
| Cyclohexyl-18-crown-6 | below 26 |
| Dicyclohexyl-18-crown-6 | between 36 and 56 (isomers) |
| Dicyclohexyl-21-crown-7 | below 26 |

[a] From references 152 and 153

or similar reactions, the relative stabilities of the complexes could then be determined. To obtain the thermodynamic properties of Reaction 7.1 would require the use of available data. The best system would likely be $K^+$-glyme:

$$K^+ \text{ glyme} + \text{Cr} \rightleftarrows K^+\text{Cr} + \text{glyme} \qquad 7.3$$

The gas phase study of the complexing of crown ethers with alkali ions thus seems possible. The results of such a study would provide interesting and valuable information to biological systems.

# REFERENCES

1. M. Arshadi, R. Yamdagni, and P. Kebarle, J. Phys. Chem. 74, 1475 (1970).
2. R. Yamdagni and P. Kebarle, J. Am. Chem. Soc. 94, 2940 (1972).
3. I. Dzidic and P. Kebarle, J. Phys. Chem. 74, 1466 (1970).
4. S. K. Searles and P. Kebarle, Can. J. Chem. 47, 2619 (1969).
5. W. C. Gardiner, Jr., "Rates and Mechanisms of Chemical Reactions", W. A. Benjamin, Inc., New York (1969), Chapter 6.
6. J. D. Payzant, Ph. D. Thesis, University of Alberta (1973).
7. N. G. Adams, D. K. Bohme, D. B. Dunkin, F. C. Fehsenfeld, and E. E. Ferguson, J. Chem. Phys. 52, 3133 (1970).
8. L. J. Puckett and M. W. Teague, J. Chem. Phys. 54, 2564 (1971).
9. G. E. Keller and F. E. Niles, Chem. Phys. Lett. 10, 526 (1971).
10. M. Szwarc, in "Ions and Ion Pairs in Organic Reactions", edited by M. Szwarc, Wiley-Interscience, New York (1972).
11. D. N. Bhattacharyva, C. L. Lee, J. Smid, and M. Szwarc, J. Phys. Chem. 69, 608 (1965).
12. M. Born, Z. Physik 1, 45 (1920).
13. B. E. Conway and J. O'M. Bockris, in "Modern Aspects of Electrochemistry", Vol. 1, edited by B. E. Conway and J. O'M. Bockris, Academic Press, New York (1964).
14. J. D. Bernal and R. H. Fowler, J. Chem. Phys. 1, 515 (1933).

15. D. D. Eley and M. G. Evans, Trans. Faraday Soc. 34, 1093 (1938).

16. H. S. Frank and W. Y. Wen, Discuss. Faraday Soc. 24, 133 (1957).

17. J. O'M. Bockris and A. K. N. Reddy, "Modern Electrochemistry", Vol. 1, Plenum Publishing Co., New York (1970).

18. J. O'M. Bockris and P. P. S. Saluja, J. Phys. Chem. 76, 2296 (1972).

19. A. J. Parker, Quart. Rev. (London) 16, 163 (1962).

20. A. J. Parker, J. Chem. Soc., 1328 (1961).

21. G. J. Janz and S. S. Danyluk, Chem. Rev. 60, 209 (1960).

22. I. M. Kolthoff, S. Bruckenstein, and M. K. Chantooni, J. Am. Chem. Soc. 83, 3927 (1961).

23. J. I. Padova, in "Modern Aspects of Electrochemistry", Vol. 7, edited by B. E. Conway and J. O'M. Bockris, Butterworth and Co., London (1972).

24. O. Popovich, CRC Critical Reviews in Anal. Chem. 1, 73 (1970).

25. W. M. Latimer, K. S. Pitzer, and C. M. Slanski, J. Chem. Phys. 7, 108 (1939).

26. H. M. Koepp, H. Wendt, and H. Strehlow, Z. Elektrochem. 64, 483 (1960).

27. J. F. Coetzee and J. J. Campion, J. Am. Chem. Soc. 89 2513 (1967).

28. N. A. Izmaylov, Dokl. Akad. Nauk. SSSR 149, 884 (1963).

29. V. A. Pleskov, Ups. Khim. 16, 254 (1947).

30. H. Strehlow, in "The Chemistry of Non-Aqueous Solvents", edited by J. J. Lagowski, Academic Press, New York (1966), Chapter 4.

31. E. Grunwald, G. Baughman, and G. Kohnstom, J. Am. Chem. Soc. 82, 5801 (1960).

32. R. Alexander and A. J. Parker, J. Am. Chem. Soc. 89, 5549 (1967).

33. O. Popovych, Anal. Chem. 38, 558 (1966).

34. D. A. Owensby, A. J. Parker and J. W. Diggle, J. Am. Chem. Soc. 96, 2682 (1974).

35. J. E. Desnoyer and C. Jolicoeur, in "Modern Aspects of Electrochemistry", Vol. 5, edited by J. O'M. Bockris and B. E. Conway, Plenum Press, New York (1969).

36. J. E. B. Randles, Trans. Faraday Soc. 52, 1573 (1956).

37. B. Casé and R. Parsons, Trans. Faraday Soc. 63, 1224 (1967).

38. B. Case, N. S. Hush, R. Parsons, and M. E. Peover, J. Electroanal. Chem. 10, 360 (1965).

39. I. Dzidic, Ph. D. Thesis, University of Alberta (1970).

40. P. Kebarle, S. K. Searles, A. Zolla, J. Scarborough, and M. Arshadi, J. Am. Chem. Soc. 89, 6393 (1967).

41. A. J. Cunningham, J. D. Payzant, and P. Kebarle, J. Am. Chem. Soc. 94, 7627 (1972).

42. A. Good, D. A. Durden, and P. Kebarle, J. Chem. Phys. 52, 212 (1970).

43. A. M. Hogg and P. Kebarle, J. Chem. Phys. 43, 449 (1965).

44. A. M. Hogg, R. M. Haynes, and P. Kebarle, J. Am. Chem. Soc. 88, 28 (1966).

45. S. K. Searles and P. Kebarle, J. Phys. Chem. 72, 742 (1968).

46. J. D. Payzant, A. J. Cunningham and P. Kebarle, Can. J. Chem. 51, 3242 (1973).

47. E. P. Grimsrud and P. Kebarle, J. Am. Chem. Soc. 95, 7939 (1973).

48. K. Hiraoka, E. P. Grimsrud, and P. Kebarle, J. Am. Chem. Soc. 96, 3359 (1974).

49. L. G. McKnight and J. M. Sawina, J. Chem. Phys. 57, 5156 (1972).

50. I. N. Tang and A. W. Castleman, Jr., J. Chem. Phys. 57, 3638 (1972).

51. G. N. Lewis, J. Franklin Inst. 226, 293 (1938).

52. S. Ahrland,J. Chatt, and N. R. Davies, Quart. Rev. (London) 12, 265 (1958).

53. R. G. Pearson, J. Am. Chem. Soc. 85, 3533 (1963).

54. R. G. Pearson, J. Chem. Ed. 45, 581,463 (1968).

55. R. G. Pearson, Science 151, 172 (1966).

56. R. S. Mulliken, J. Phys. Chem. 56, 801 (1952).

57. R. Yamdagni and P. Kebarle, J. Am. Chem. Soc. 95, 3504 (1973).

58. M. S. B. Munson, J. Am. Chem. Soc. 87, 2332 (1965).

59. J. P. Briggs, R. Yamdagni, and P. Kebarle, J. Am. Chem. Soc. 94, 5128 (1972).

60. I. Dzidic, J. Am. Chem. Soc. 94, 8333 (1972).

61. J. I. Brauman, J. M. Riveros, and L. K. Blair, J. Am. Chem. Soc. 93, 3914 (1971).

62. E. M. Arnett, F. M. Jones III, M. Taagepera, W. G. Henerson, D. Holtz, J. L. Beauchamp, and R. W. Taft, J. Am. Chem. Soc. 94, 4724 (1972).

63. W. G. Henerson, M. Taagerpera, D. Holtz, R. T. McIver, Jr., J. L. Beauchamp, and R. W. Taft, J. Am. Chem. Soc. 94, 471 (1972).

64. M. T. Bowers, D. H. Aue, H. M. Webb, and R. T. McIver, Jr., J. Am. Chem. Soc. 93, 4314 (1971).

65. D. H. Aue, H. M. Webb, and M. T. Bowers, J. Am. Chem. Soc. 94, 4726 (1972).

66. E. L. Muetterties, in "The Chemistry of Boron and its Compounds", edited by E. L. Muetterties, Wiley and Sons, New York (1967).

67. H. C. Brown, H. Bartholomay, Jr., and M. D. Taylor, J. Am. Chem. Soc. 66, 435 (1944).

68. H. C. Brown and M. D. Taylor, J. Am. Chem. Soc. 69, 1332 (1947).

69. H. C. Brown, M. D. Taylor, and S. Sujishi, J. Am. Chem. Soc. 73, 2464 (1951).

70. H. C. Brown and G. Barbaras, J. Am. Chem. Soc. 69, 1137 (1947).

71. H. C. Brown and G. Barbaras, J. Am. Chem. Soc. 75, 6 (1953).

72. H. C. Brown, J. Chem. Soc., 1248 (1956).

73. J. G. Collins, Ph. D. Thesis, University of Alberta (1968).

74. S. K. Searles, Ph. D. Thesis, University of Alberta (1970).

75. R. O. Jenkins and W. G. Trodden, "Electron and Ion Emmission from Solids", Routlege and Kegan Paul Ltd., London (1965), Chapter 7.

76. J. R. Blewett and E. J. Jones, Phys. Rev. 50, 464 (1936).

77. S. Dushman, "Scientific Foundation of Vacuum Technique", Wiley and Sons, New York (1949).

78. W. E. Potter and K. Mauersberger, Rev. Sci. Instrum. 43, 1327 (1972).

79. H. Kistenmacher, H. Popkie and E. Clementi, J. Chem. Phys. 58, 1689 (1973).

80. R. Johnsen, H. L. Brown, and M. A. Biondi, J. Chem. Phys. 55, 186 (1971).

81. R. M. Snuggs, Ph. D. Thesis, Georgia Institute of Technology (1970).

82. E. W. McDaniel, "Collision Phenomena in Ionized Gases", Wiley and Sons Inc., New York (1964), Chapter 9.

83. G. E. Keller, R. A. Beyer, and L. M. Colonna-Romano, Phys. Rev. A8, 1446 (1973).

84. A. M. Tyndall, "The Mobility of Positive Ions in Gases", Cambridge University Press, Cambridge (1938).

85. G. H. Wannier, Phys. Rev. 83, 648 (1966).

86. R. J. Varney, J. Chem. Phys. 31, 1314 (1959).

87. J. Grundles and P. Klaboe, in "The Chemistry of the Cyano Group", edited by Z. Rappoport, Interscience Publishers, New York (1970).

88. J. D. Lambert, G. A. Roberts, J. S. Rowlinson and V. J. Wilkinson, Proc. Roy. Soc. (London) Ser. A 196, 113 (1949).

89. F. E. Murray and W. G. Schneider, Can. J. Chem. 33, 797 (1955).

90. A. D. Buckingham and R. E. Raab, J. Chem. Soc., 5511 (1961).

91. M. H. Abraham, J. C. S. Faraday I 69, 1375 (1973).

92. R. H. Stokes, J. Am. Chem. Soc. 86, 979 (1964).

93. D. Feakins and K. G. Lawrence, J. Chem. Soc. A, 212 (1966).

94. W. A. Sheppard, in "The Chemistry of the Cyano Group", edited by Z. Rappoport, Interscience Publishers, New York (1970).

95. L. Pauling, "The Nature of the Chemical Bond", 3rd ed., Cornell University Press, Ithaca, New York (1960).

96. "Handbook of Chemistry and Physics", 47th ed., edited by R. C. Weast, Chemical Rubber Co., Cleveland (1966).

97. D. S. Berns and R. M. Fuoss, J. Am. Chem. Soc. 83, 1321 (1961).

98. J. F. Hinton and E. S. Amis, Chem. Rev. 71, 627 (1971).

99. K. Spears, J. Chem. Phys. 57, 1850 (1972).

100. S. Goldman and R. G. Bates, J. Am. Chem. Soc. 94, 1476 (1972).

101. I. Eliezer and P. Krindel, J. Chem. Phys. 57, 1884 (1972).

102. R. D. Green and J. S. Martin, J. Am. Chem. Soc. 90, 3659 (1968).

103. E. Clementi and H. Popkie, J. Chem. Phys. 57, 1077 (1972).

104. G. H. F. Diercksen and W. P. Kraemer, Theoret. chim. Acta 23, 387,393 (1972).

105. R. E. Burton and J. Daly, Trans. Faraday Soc. 66, 1281 (1970); 67, 1219 (1971).

106. K. G. Breitschwerdt and H. Kistenmacher, Chem. Phys. Lett. 14, 288 (1972).

107. H. Lischka, T. Plesser, and P. Schuster, Chem. Phys. Lett. 6, 263 (1970).

108. P. Russegger, H. Kischka, and P. Schuster, Theoret. chim. Acta 24, 191 (1972).

109. A. L. McClennan, "Tables of Experimental Dipole Moments", W. H. Freeman and Co. San Francisco (1963).

110. W. J. Hehre and J. A. Pople, J. Am. Chem. Soc. 92, 2191 (1970).

111. J. A. Pople and M. S. Gordon, J. Am. Chem. Soc. 89, 4253 (1967).

112. E. Clementi and D. Klint, J. Chem. Phys. 50, 4899 (1969).

113. L. F. Thomas, E. I. Sheppard, and J. Sheridan, Trans. Faraday Soc. 51, 619 (1955).

114. D. H. Liskow, C. F. Bender, H. F. Schaefer III, J. Am. Chem. Soc. 94, 5178 (1972).

115. H. Denbigh, Trans. Faraday Soc. 36, 936 (1940).

116. W. J. Orville-Thomas, "The Structure of Small Molecules", Elsevier Publishing Co., Amsterdam (1966), page 129.

117. R. J. W. LeFevre, R. J. Orr, and G. L. D. Ritchie, J. Chem. Soc., 2499 (1965).

118. J. F. Harrison, J. Chem. Phys. 49, 3321 (1968).

119. J. S. Muirhead-Gould and K. J. Laidler, Trans. Faraday Soc. 63, 944 (1967).

120. K. S. Pitzer, Advan. Chem. Phys. 2, 59 (1959).

121. I. Amdur, J. E. Jordan, L. W.-M. Fung, L. J. F. Hermans, S. E. Johnson, and R. L. Hance, J. Chem. Phys. 59, 5329 (1973).

122. J. T. Vanderslice, E. A. Mason, and W. G. Maisch, J. Chem. Phys. 32, 515 (1960).

123. J. T. Vanderslice, E. A. Mason, and E. H. Lippincott, J. Chem. Phys. 30, 129 (1959).

124. W. E. Bleick and J. E. Mayer, J. Chem. Phys. 2, 252 (1934).

125. E. A. Mason and W. E. Rice, J. Chem. Phys. 22, 843 (1954).

126. E. A. Mason, J. Chem. Phys. 22, 49 (1955).

127. I. Amdur, J. E. Jordan, K.-R. Chien, L. W.-M. Fung, R. L. Hance, E. Hulpke, and S. E. Johnson, J. Chem. Phys. 57, 2117 (1972).

128. J. T. Vanderslice and E. A. Mason, J. Chem. Phys. 33, 492 (1960).

129. H. A. Taylor and H. E. Achilles, J. Phys. Chem. 35, 2658 (1931).

130. A. G. Carter, P. A. Bosanquet, C. G. Silcocks, M. W. Travers, and A. F. Whilshire, J. Chem. Soc., 459 (1939).

131. V. I. Vedeneyev, L. V. Gurvich, V. N. Kondratiev, V. A. Medvedev, and Ye. L. Frankevich, "Bond Energies, Ionization Potentials and Electron Affinities", Edward Arnold Ltd., London (1962).

132. R. J. W. LeFevre and P. Russel, Trans. Faraday Soc. 43, 374 (1967).

133. A. Almenningen and O. Bastiansen, Acta Chem. Scan. 9, 815 (1955).

134. T. Nishikawa, T. Itoh, and K. Shimoda, J. Chem. Phys. 23, 1735 (1955).

135. V. Schomaker, Acta Cryst. 3, 46 (1950).

136. R. A. Barnes, in "Pyridine and Its Derivatives, Part One", edited by E. Klingberd, Interscience Publishers, New York (1960).

137. G. W. Wheland, "Resonance in Organic Chemistry", Wiley and Sons, New York (1955), page 357.

138. W. J. Hehre, L. Radom, and J. A. Pople, J. Am. Chem. Soc. 94, 1496 (1972).

139. M. J. Aroney, R. J. W. LeFevre, L. Radom, and G. D. L. Ritchie, J. Chem. Soc. B, 507 (1968).

140. C. D. M. Beverwijk, G. J. M. VanDerKerk, A. J. Lewsink, and J. G. Noltes, Organomet. Chem. Rev. A5, 215 (1970).

141. M. J. S. Dewar, Bull. Soc. Chim. France 18, 79 (1951).

142. R. S. Drago and B. B. Wayland, J. Am. Chem. Soc. 87, 3571 (1965).

143. R. S. Drago, G. C. Vogel, and T. E. Needham, J. Am. Chem. Soc. 93, 6014 (1971).

144. S. Arhland, Structure and Bonding 5, 118 (1968).

145. R. G. Pearson and R. J. Mawby, "Halogen Chemistry", Vol. 3, edited by V. Gutmann, Academic Press, New York (1967).

146. G. Klopman, J. Am. Chem. Soc. 90, 223 (1968).

147. S. Searles, Jr., and M. Tamres, in "The Chemistry of the Ether Linkage", edited by S. Patai, Interscience Publishers, London (1967).

148. J. L. Beauchamp, Ann. Rev. Phys. Chem. 22, 527 (1971).

149. H. C. Brown and R. M. Adams, J. Am. Chem. Soc. 64, 2557 (1942).

150. A. K. Banerjee, A. J. Layton, R. S. Nyholm, and M. R. Truter, J. Chem. Soc. A, 2536 (1969).

151. H. Lehn, Structure and Bonding 16, 1 (1973).

152. C. J. Pedersen, J. Am. Chem. Soc. 89, 7017 (1967).

153. C. J. Pedersen, J. Am. Chem. Soc. 92, 386 (1970).

154. R. M. Izatt, D. P. Nelson, J. H. Rytting, B. L. Haymore, and J. J. Christensen, J. Am. Chem. Soc. 93, 1619 (1971).

155. H. K. Frensdorff, J. Am. Chem. Soc. 93, 4684 (1971).

156. F. A. Cotton and G. Wilkinson, "Advanced Inorganic Chemistry", 2nd edition, Interscience Publishers, New York (1966), page 156.

157. C. K. Ingold, "Structure and Mechanism in Organic Chemistry", 2nd edition, Cornell University Press, Ithaca (1969), page 1108.

158. M. R. Truter, Structure and Bonding 16, 71 (1973).

159. E. Shchori, J. Jagur-Grodzinski, and M. Shporer, J. Am. Chem. Soc. 95, 3842 (1973).

160. A. T. Tsatas, R. W. Steams, and W. M. Risen, Jr., J. Am. Chem. Soc. 94, 5247 (1972).

161. H. K. Frensdorff, J. Am. Chem. Soc. 93, 600 (1971).

162. E. M. Arnett and T. C. Moriarity, J. Am. Chem. Soc. 93, 4908 (1971).

B30117